

Cofactors and H₂ metabolism at the origin of life

Inaugural dissertation

For the attainment of the title of Doctor of Philosophy (Ph.D.)
in the Faculty of Mathematics and Natural Sciences
at the Heinrich Heine University Düsseldorf

Presented by

Delfina Patrícia Henriques Pereira, M.Sc.

From Nadadouro, Portugal

2024

From the Institute of Molecular Evolution
at the Heinrich Heine University

Published by permission of the
Faculty of Mathematics and Natural Sciences at
Heinrich Heine University Düsseldorf

Supervisor: *Prof. Dr. William F. Martin*

Co-supervisor: *Dr. Martina Preiner*

Date of the oral examination: 14/11/2024

Statement of declaration

I hereby declare that this dissertation is the result of my own work. No other person's work has been used without due acknowledgement. This dissertation has not been submitted in the same or similar form to other institutions. I have not previously failed a doctoral examination procedure.

Düsseldorf, 11th September

Delfina P. Henriques Pereira



*Adapted painting from Delfina P. Henriques Pereira
to those who dedicate their life to
finding LUCA*

Acknowledgements

First and foremost, the making of this thesis would have not been possible if not for the contributions of my supervisors: William F. Martin and Martina Preiner. Bill welcomed me in his lab as a master student in 2019 and gave me a peak into his “secret project” with Martina. Under the wings of Andrey Viera, I completed my master thesis still hungry for more and started drawing plans for a doctorate in this freshly made chemistry group at the Institute of Molecular Evolution. I was lucky to start a new project, of Martina’s creation, in Düsseldorf, which eventually lead me to move with her to Marburg where I completed the thesis. To my two supervisors and Andrey, I thank them for their scientific advice, for guiding me through this project and supporting me through many changes. During this trip, I also had the great opportunity to meet Carlo Kleineremanns and Filipa Sousa which only showed me support and gave me great career and scientific advice.

For my time in Düsseldorf, I thank Verena Zimorski, and Renate Bode for helping me move into a new country and manage German bureaucracy with much care and patience, and Margarete Stracke for helping to manage and organize the labs. Nils Kapust for organizing social events for everyone, keeping the energy in the Institute up and always making a positive impact. Andrey, Max, Natalia, Loraine, Maria, Carolina and Falk were impactful in making every week in Düsseldorf worth remembering, by sharing their scientific knowledge, time, culture, laughs and support, in and out of the office. During this period, I also had the pleasure to visit Dr. Harun Tüysüz’s laboratory and collaborate with Tuğçe Beyazay and Kendra Belthle for a week in Mülheim. While on a personal trip to Vienna I also had the pleasure to visit Filipa’s laboratory. I thank them all for their hospitality and for showing me how different laboratories and work groups can be. Finally, I must thank the entire NMR department in Dusseldorf for working tirelessly to measure every sample, even when we kept sending above the limit number of samples.

In Marburg, I thank Ina Leiker, Daniela England and Dušica Radoš for helping me settle in Marburg and assisting with bureaucracy. Without Dr. Xiulan Xie, at the front of the NMR department, the continuation of the project in Marburg would not be possible. I thank her for the professionalism, dedication and kindness. The continuation of this project would have also not been possible without Martina, not just

as a supervisor, she guided me through work and personal problems with immeasurable care and patience. Joining her new group, I had the unique experience of working alongside her to build a lab from ground up, to which Giuseppe and Oskari joined half a year later. I cherish the many insightful discussions, jokes, and sense of community we built in the lab.

Through the years, I also had the pleasure to supervise and work alongside Janna, Zainab, Quynh, Carla, and Mahiob, who tolerated me with much grace and helped push this project forward in the lab and through helpful discussions.

I have nothing but gratitude for the company and support Luca gave me during our time together. Thank you.

Aos meus amigos na Holanda, que trouxeram Portugal para mais perto, agradeço por manterem as saudades de casa sob controlo. Para a minha família em Portugal, mae, pai, Vanessa, Ricardo, Noah e Rio, obrigada por serem tão pacientes, e por me apoiarem incondicionalmente à dor que vos causo por estar longe.

Last but not least, thank you to my supervisors, Natalia, and Filipa again, for proof-reading this thesis. To all people mentioned above and some more, I owe all my scientific growth and much of my personal growth, necessary to complete this thesis as is. Thank you!

Publications in this thesis

- I. **Henriques Pereira, D.P.**, Leethaus, J., Beyazay, T., Do Nascimento Vieira, A., Kleinermanns, K., Tüysüz, H., Martin, W.F., Preiner, M., 2022. Role of geochemical protoenzymes (geozymes) in primordial metabolism: specific abiotic hydride transfer by metals to the biological redox cofactor NAD⁺. FEBS J. 289, 3148–3162. <https://doi.org/10.1111/febs.16329>
- II. **Henriques Pereira, D.P.**, Xie, X., Beyazay, T., Nicole, P., Subrati, Z., Belz, J., Volz, K., Tüysüz, H., Preiner, M., 2024. A possible pre-enzymatic role of the “non-functional” tail of NAD: specific reduction on mineral surfaces. In revision for: Proc. Natl. Acad. Sci.
- III. **Brabender, M., Henriques Pereira, D.P., Mrnjavac, N.**, Schlikker, M.L., Kimura, Z.-I., Sucharitakul, J., Kleinermanns, K., Tüysüz, H., Buckel, W., Preiner, M., Martin, W.F., 2024. Ferredoxin reduction by hydrogen with iron functions as an evolutionary precursor of flavin-based electron bifurcation. Proc. Natl. Acad. Sci. 121, e2318969121. <https://doi.org/10.1073/pnas.2318969121>

Table of contents

Abstract	9
Zusammenfassung	10
Aim of the thesis	11
Introduction	12
I. Hadean Earth	12
Connection to the Last Universal Common Ancestor	12
Serpentinization and hydrothermal vents	13
Life mirrors serpentinization	15
II. Transition metals	15
Inorganic cofactors	15
H ₂ activation and redox potential in vivo	18
H ₂ activation "in metallum"	19
III. Organic cofactors	20
Clues to their antiquity	23
Nicotinamide Adenine Dinucleotide	24
Shared structure of prebiotic origins	24
Past and future considerations	25
Prospects	28
Publications	30
Publication I – Role of geochemical protoenzymes (geozymes) in primordial metabolism: Specific abiotic hydride transfer by metals to the biological redox cofactor NAD ⁺	30
Publication II – The dinucleotide structure of the cofactor NAD enables its specific reduction on mineral surfaces	31
Publication III – Ferredoxin reduction by hydrogen with iron functions as an evolutionary precursor of flavin-based electron bifurcation	32
Conclusion and Outlook	33
References	35

Abstract

Serpentinizing systems are a likely location for the origin of life. These underwater structures are rich in minerals, harbour pH and temperature gradients, dissolved carbon sources such as CO₂, and a stable source of electrons from geochemically produced H₂. Central to the hypothesis built around these geochemical systems are minerals as precursors of enzymes, e.g. catalysing the reduction of CO₂ with the electrons from H₂ to organic matter. Analyses of ancient metabolic networks place organic cofactors as central to the establishment of autocatalytic chemical networks as a step between abiotic and biotic chemistry. This work explores potential prebiotic functions of cofactors, considering H₂ as the energy source, natural minerals as primary catalysts, and conditions approaching those of hydrothermal systems.

This work studies both organic (NAD) and protein-bound inorganic cofactors (iron-sulphur clusters in ferredoxin), focusing on their stability under hydrothermal conditions and functional interactions with H₂ and hydrothermal minerals. Experimental results from the first and second publications show that NAD⁺ is reduced with Ni⁰, Fe⁰, Ni/Fe alloys and Co⁰ in the presence of H₂ (5 bar, anoxic, pH 8.5, 40 °C). Publication II also highlights the importance of the AMP moiety in the function of NAD in environments with different mineral compositions. In addition, this work demonstrates the functionality of these cofactors in hydrothermal environments in the presence of high metal and water activity. Finally, the third publication shows that *Clostridium pasteurianum* ferredoxin requires H₂ and Fe⁰ to be reduced under the same conditions.

The results show that complex enzyme functions can sometimes be substituted by metal and water alone, in certain cases not even requiring exogenous H₂. Overall, this work provides fundamental experimental insights into how cofactors may have contributed to the origin of life.

Zusammenfassung

Serpentinisierende Systeme sind eine mögliche Umgebung für die Entstehung des Lebens. Diese porösen Unterwasserstrukturen sind reich an Mineralien, beherbergen pH und Temperaturgradienten, gelöste Kohlenstoffquellen wie CO_2 und eine stabile Energie- und Elektronenquelle aus geochemisch erzeugtem H_2 . Im Mittelpunkt der Hypothese, die sich auf diese geochemischen Systeme stützt, stehen Mineralien als Vorläufer von Enzymen, die z. B. die Reduktion von CO_2 mit den Elektronen aus H_2 zu organischem Material katalysieren. Bioinformatische Analysen konservierter Stoffwechselwege zeigen, dass organische Cofaktoren eine zentrale Rolle bei der Etablierung autokatalytischer chemischer Netzwerke spielen, die einen Schritt zwischen abiotischer und biotischer Chemie darstellen. In dieser Arbeit werden mögliche präbiotische Funktionen von Cofaktoren untersucht, wobei H_2 als Energiequelle, natürliche Mineralien als erste Katalysatoren und Bedingungen, die denen von hydrothermalen Systemen ähneln, berücksichtigt werden.

In dieser Arbeit werden sowohl organische (NAD) als auch proteingebundene anorganische Cofaktoren (Ferredoxin) untersucht, wobei der Schwerpunkt auf ihrer Stabilität unter hydrothermalen Bedingungen und funktionellen Wechselwirkungen mit H_2 und hydrothermalen Mineralien liegt. Experimentelle Ergebnisse aus Publikation I und II zeigen, dass NAD^+ mit Ni^0 , Fe^0 , Ni/Fe-Legierungen und Co^0 in Gegenwart von H_2 (5 bar, anaerob, pH 8.5, 40°C) reduziert. Publikation II unterstreicht zudem auch die Bedeutung der AMP-Komponente für die Funktion von NAD. Darüber hinaus wird in dieser Arbeit die Funktionalität dieser Cofaktoren in hydrothermalen Umgebungen in Gegenwart hoher Metall- und Wasseraktivität nachgewiesen. In Publikation III konnte gezeigt werden, dass Ferredoxin (isoliert aus *Clostridium pasteurianum*), im Gegensatz zu NAD weniger flexible in puncto Metallwahl ist und H_2 und Fe^0 benötigt, um unter den gleichen Bedingungen reduziert zu werden.

Die Ergebnisse zeigen, dass komplexe Enzymfunktionen allein durch Metall und Wasser ersetzt werden können, wobei in bestimmten Fällen nicht einmal exogenes H_2 erforderlich ist. Insgesamt liefert diese Arbeit grundlegende Experimente, um festzustellen, wie Cofaktoren zur Entstehung des Lebens beigetragen haben könnten.

Aim of the thesis

This research aims to contribute to the ongoing search for the origin of life and help to describe the prebiotic autocatalytic network that produced the building blocks of life. One goal is to experimentally replicate the conditions found in hydrothermal vents. These underwater structures can be studied on Earth today, and they likely existed on Hadean Earth, as they did in Mars. They generate gradients of pH, temperature, and dissolved nutrients; mineral catalysts are available, and H_2 is naturally produced in the crust during serpentinization – a geochemical process in which hot water hydrolysis ferromagnesian minerals to serpentine. This is interesting to study in the context of the origin of life because life also generates gradients to stay far from equilibrium, requires metals for enzymatic activity, liquid water and, hydrogen (H_2) is necessary for the oldest known biological form of carbon fixation – the linear acetyl-CoA pathway. Because hydrogen probably played a crucial role as an energy and electron source in early metabolic processes, it is important to understand the activation of the generally inert H_2 gas under geochemical conditions. In modern H_2 -dependent microbes (hydrogenotrophs), the activation of H_2 and the distribution of protons and electrons through metabolism requires cofactors in addition to a complex enzymatic machinery. The main goal here is to identify prebiotic precursors of these biological processes that could have been instrumental in the evolution of biological networks in serpentine systems.

At the basis of this project are theories that resurfaced with new metabolomic and structural data analysis, suggesting that cofactors are older than life and were instrumental in establishing an autocatalytic system. In order to critically evaluate these theories, this dissertation will specifically address several key research questions: Are redox cofactors stable under the alkaline hydrothermal conditions specific to serpentinizing systems? Can inorganic catalysts present in these environments, especially transition metals, facilitate the transfer of electrons and hydrides from hydrogen (H_2) to redox cofactors? In addition, how do these metals interact with cofactors – do they stabilize them, are they toxic to their integrity, or neither? By answering these questions, the research is designed to provide an experimental foundation for cofactor-based theories of prebiotic evolution and contributes to the field of origin of life research.

Introduction

It is human nature to assign meaning to things, and life is no exception. Biologists, chemists, philosophers, and religious people have tried to define it in a variety of subjective ways, but when searching for its definition, one cannot find an agreed-upon answer (Gayon *et al.*, 2010). The same goes for the researchers working to discover its origin, who are also interdisciplinary and have long been working towards an undefined goal. This changed in the 1990s when it was discovered that all living things can be traced back to a single identity called the Last Universal Common Ancestor (LUCA) (Dyson, 1999; Penny and Poole, 1999). Defined from a top-down approach, LUCA is a concept made up of traits from different extant species, well preserved over eons, that together describe the oldest creature or colony from which all known life originated. Top-down inferences of LUCA's physiology were helpful in extrapolating the characteristics of its habitat, and they were essential to establish an entity that all disciplines could continue trying to uncover by a bottom-up approach (Martin *et al.*, 2016; Penny and Poole, 1999; Weiss *et al.*, 2016; Wimmer *et al.*, 2021; Woese and Fox, 1977). In attempting to bridge the "impassable abyss (that) existed between the living and the dead" (Oparin, 1938), we must first understand what exactly that abyss is.

I. Hadean Earth

Connection to the Last Universal Common Ancestor

LUCA and its direct relatives are the furthest we can travel back in life's timeline, but life could have emerged millions of years before that. Investigation of the isotopic composition of Eoarchean rocks in the Saglek block revealed biogenic graphite dating to 3.95 billion years ago (Ga) (Tashiro *et al.*, 2017), and a recent phylogenetic study proposed that LUCA existed as early as 4.09–4.32 Ga (Moody *et al.*, 2024). Assuming that life emerged after the Moon-forming impact (4.48 Ga) (Bottke *et al.*, 2015; Hartmann and Davis, 1975; Mrnjavac *et al.*, 2023), this leaves a not-so-long interval of 200–500 million years for the Earth's surface to cool, for liquid water to rain down, and for life to evolve from inorganic matter to a protocell (LUCA).

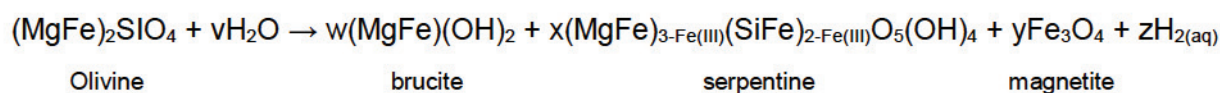
For metabolism to exist, energy is required. For this effect, LUCA was an autotrophic anaerobe (Martin *et al.*, 2016; Moody *et al.*, 2024; Weiss *et al.*, 2016) and used, at least in part, the linear acetyl-CoA pathway for H₂-dependent carbon (CO₂) fixation (Ljungdhal, 1986; Martin, 2020; Moody *et al.*, 2024; Weiss *et al.*, 2016; Wood *et al.*, 1986). To activate molecular hydrogen (H₂), it needed hydrogenases, other metalloenzymes and cofactors, some of which oxygen sensitive, in its central metabolic pathways (Weiss *et al.*, 2016). Thus, to live, LUCA needed an anoxic environment with available transition metals, CO₂, and a natural source of H₂.

Earth was anoxic during the Archean and Hadean eon, before the Great Oxygenation Event 2.45 Ga (Bekker *et al.*, 2004; Holland, 1999) CO₂ was abundant during the Hadean eon, both in the atmosphere and dissolved in the ocean (Liu, 2004; Ueda and Shibuya, 2021). H₂ was scarcer but was naturally made available by serpentinizing hydrothermal vents – a geochemical process that produces H₂ from hydrolysed rock, described in detail in the chapter below. Serpentinizing vents had transition metals readily available as well, mostly as minerals, making these underwater structures likely hosts for LUCA and the origin of life (Baross and Hoffman, 1985; Corliss *et al.*, 1981; Weiss *et al.*, 2016). Evidence from a Martian meteorite shows us that serpentinization occurred on Mars around the time of the Moon-forming impact, about 4 billion years ago (Ga) (Steele *et al.*, 2022). There is also evidence that it occurs on several other celestial bodies, which speaks to the universality of this geochemical formation (Holm *et al.*, 2015; Sleep *et al.*, 2004; Vance and Melwani Daswani, 2020).

Serpentinization and hydrothermal vents

On Earth, serpentinization occurs mostly near mid-ocean ridges, where plate activity is higher, and fissures can form. At spreading zones, molten lava rises from magma chambers to the seafloor, forming black smokers. In these structures, direct contact with magma causes water to reach temperatures in excess of 400 °C and releases large amounts of magmatic CO₂ (4–215 mmol/kg) and H₂S (3–110 mmol/kg) (Kelley *et al.*, 2002; Rona *et al.*, 1986). A few kilometres away from the ridge, fissures can still form, and cold, acidic water falls in contact with hot rock. Off-ridge systems are not in direct contact with magmatic rocks and therefore have a very different composition and lower temperatures (< 200 °C) (Kelley *et al.*, 2005, 2001).

In both cases, when serpentinization occurs, hot water-rock interactions hydrolyse ultramafic rocks (ferromagnesian minerals), most commonly olivine, for the production of serpentine and up to 15 mmol H₂/kg (Charlou *et al.*, 2002; Klein *et al.*, 2013). The general reaction can be described as follows (Klein *et al.*, 2013; McCollom and Bach, 2009):



To make H₂, the electrons come from the oxidation of ferrous iron (Fe²⁺) with water, to ferric iron (Fe³⁺) (Sleep *et al.*, 2011). This can generate sufficient reduction potential to reduce iron (Fe) and nickel (Ni) oxides to form Ni/Fe alloys, such as awaruite (Ni₃Fe) (Foustoukos *et al.*, 2015; Klein and Bach, 2009) or even native metals (Ni⁰ and Fe⁰) in very special cases (Dekov, 2006; Kanellopoulos *et al.*, 2018; Kepezhinskis *et al.*, 2020). Off-ridge systems have a lower silica content and a higher ultramafic rock content, which results in more serpentinization and thus more hydroxides, making it alkaline (pH 8–12) and more H₂ producing (Kelley *et al.* 2001, 2005; Seyfried *et al.* 2015). This is very different from serpentinizing black smokers, which tend to be very acidic (pH 2–5) and have a lot of dissolved sulphides (Charlou *et al.*, 2002).

The circulating serpentinizing water in the crust picks up dissolved minerals and gases from the surrounding rock, further enriching the water. As it returns to the surface, it mixes with the ocean (2 °C, pH 7.5–8), forming all kinds of gradients of temperature, pH, and dissolved molecules across the structure (Schwander *et al.*, 2023). This occurred especially during the Hadean eon, when seawater was acidic and steeper gradients formed with the alkaline off-ridge vents where seawater and hydrothermal fluids mixed (Holland, 1984). Eventually, the minerals become insoluble and precipitate on the seafloor to form complex nano- and microporous mineral-rich hydrothermal vents that tower over the serpentinizing system (Baross and Hoffman 1985). The far from equilibrium conditions over the vents, in a system that produces constant heat and H₂, make serpentinization a process worth studying in the context of the origin of life (Martin *et al.*, 2008; Martin and Russell, 2003; Preiner *et al.*, 2018; Schwander *et al.*, 2023).

Life mirrors serpentinization

Serpentine systems are now home to hundreds of animal species and many more microbes, with new species being discovered every year. Most of them live on the sides and around the vents. In the warm waters of the vents, thermophilic anaerobes feed on CO₂ or other small reduced carbon compounds (Zeng *et al.*, 2021). LUCA's successors (Moody *et al.*, 2024; Weiss *et al.*, 2016) – methanogenic archaea and acetogenic bacteria – that live on H₂ and CO₂ still today also inhabit hydrothermal systems (Kelley *et al.*, 2005; Zeng *et al.*, 2021). Allegorically, the vents themselves perform H₂-dependent CO₂ fixation. Under hydrothermal conditions in the laboratory (100 °C, 25 bar CO₂/H₂), the fixation of CO₂ can be catalysed by natural minerals such as Fe₃O₄ and Ni₃Fe to produce up to 200 mM of formate overnight and less than 0.1 mM acetate, pyruvate, methanol and methane – the same intermediates and products of the reductive acetyl-CoA pathway (Beyazay *et al.*, 2023a, 2023c, 2023b; Preiner *et al.*, 2020). Olivine-rich vents contain about 1–3 mmol/kg methane of abiotic origin (Grozeva *et al.*, 2020; Proskurowski *et al.*, 2008; Schwander *et al.*, 2023) formate, ethane, propane, and butane have also been detected in smaller amounts (Etiope and Sherwood Lollar, 2013; Holm and Charlou, 2001; Lang *et al.*, 2010; McDermott *et al.*, 2015; Suda *et al.*, 2017). In other words, hydrothermal vents are inorganic systems that harbour minerals capable of producing organic metabolites, reminiscent of a proto-metabolism.

II. Transition metals

Since the discovery of hydrothermal vents, researchers have noticed connections between life and natural geochemical reactions. It is not only the reaction reagents and products that are the same in hydrothermal and biological systems: they put at the driving wheel the same transition metals to achieve product selectivity and overcome energy barriers (Russell and Martin, 2004).

Inorganic cofactors

Inorganic cofactors are metal ions and iron sulphide (FeS) clusters that can provide catalytic activity to the enzymes that use them, act as electron conduits, help mediate folding, stabilize negative charges, and help position and stabilize the substrate (Loutet *et al.*, 2015). Their presence is noticed throughout life and is relevant

to the function of at least 40% of all crystallized enzymes (Guengerich, 2016). Metals accelerate certain reactions over others, preserving the unique profile of the species (Loutet *et al.*, 2015).

FeS clusters are ubiquitous in life and essential for single electron transfer in redox reactions, forming the functional and sometimes structural part of proteins often involved in respiration. Magnesium (Mg), iron, zinc (Zn), copper (Cu), nickel, cobalt (Co), and molybdenum (Mo) are the most common metal cofactors found in various oxidation states. Depending on the organism and its metabolism, different amounts of each metal are required for survival (Loutet *et al.*, 2015; Valdez *et al.*, 2014). For example, copper and zinc have become more available after the great oxidation event, while nickel and cobalt are most relevant to anaerobic metabolism, especially methanogens (Hawco *et al.*, 2020; Saito *et al.*, 2003).

The incorporation of carbon and hydrogen into anaerobic metabolism is done by metalloenzymes. For the activation of H₂ specifically, [Ni,Fe]-hydrogenases are likely the most ancient enzymes (Greening *et al.*, 2016; Moody *et al.*, 2024). As for CO₂, the most ancient pathway of CO₂ fixation via the acetyl-CoA pathway whereby CO₂ is converted to CO in the [NiFe₄S₄] cluster of carbon monoxide dehydrogenase (CODH). In addition, another CO₂ molecule enters a separate branch with its own metalloenzymes and (de)hydrogenases to make a methyl group (Ragsdale and Pierce, 2008; Shima *et al.*, 2002). Ultimately, a corrinoid iron-sulphur protein (CFeSP) within the Acetyl-CoA Synthase (ACS) transfers the methyl group to a Ni–Ni active site, bridged by cysteine thiol to a [Fe₄S₄] cluster. Here, the methyl group transferred by CFeSP and the CO group derived from CODH, join and by thiolysis of the acetyl group, acetyl-CoA is formed for the rest of the carbon metabolism to unfold (Cohen *et al.*, 2020; Ragsdale and Kumar, 1996). The metals mentioned above are part of the active centre of these enzymes, but for the electrons to reach them, chains of FeS clusters exist within the protein to carry the electrons to and from the active centre to and from other (co)factors (Ragsdale and Pierce, 2008; Shima *et al.*, 2002; Sousa and Martin, 2014). The structures of these enzymes' active centres are represented in **Figure 1**, below.

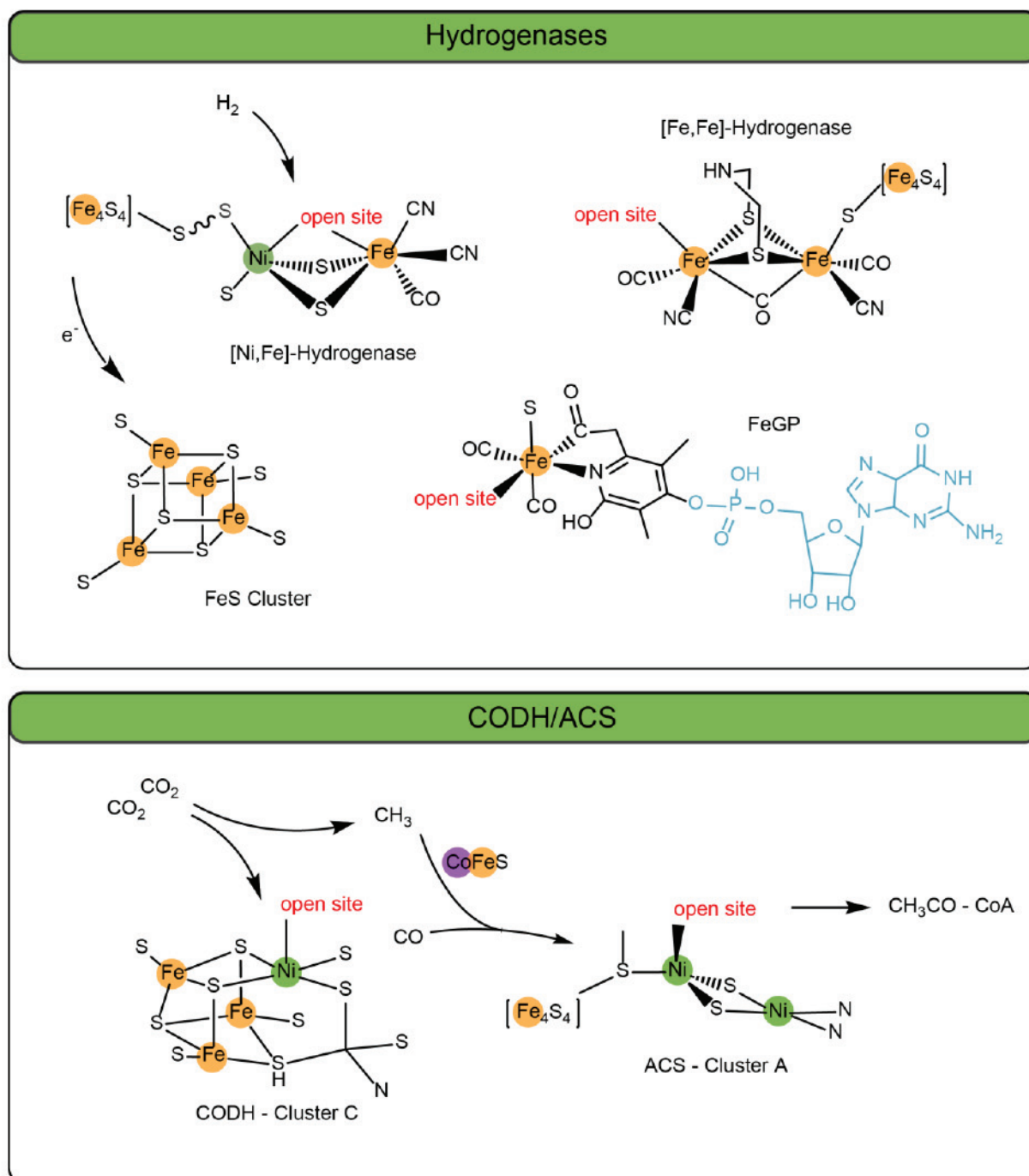
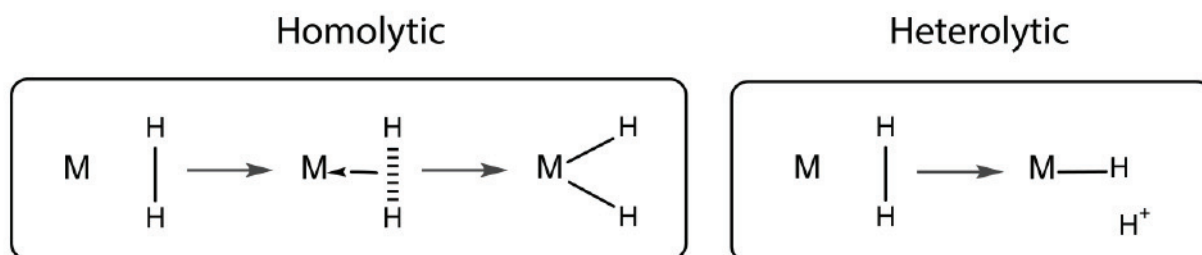


Figure 1 The metal centres of [Ni,Fe] (Ogata *et al.* 2005), [Fe,Fe] (Nicolet *et al.* 1999) and [Fe]-Hydrogenases (Huang *et al.* 2019) are represented above. [Ni,Fe] and [Fe,Fe] clusters are closely positioned to FeS clusters (Fe_4S_4), which carry electrons to and from the centre, while [Fe]-Hydrogenase's cofactor – iron-guanylylpyridinol (FeGP) – directly transfers the electrons to the substrate. The nucleotide guanosine monophosphate in FeGP is highlighted in blue. A scheme of a $[Fe_4S_4]$ cluster is represented below the hydrogenases. Underneath are depicted the structures of the complex carbon monoxide dehydrogenase/acetyl-CoA Synthase (CODH/ACS). Cluster A of ACS: a Ni-Ni active site bridged by cysteine thiol to a $[Fe_4S_4]$ cluster, (Cohen *et al.* 2020); and cluster C of CODH: a [Ni-4Fe-5S] cluster (Dobbek *et al.* 2001). The complex was drawn in the context of a simplified acetyl-CoA pathway, where the methyl branch is reduced to an arrow. In reality, this branch is also rich in metalloenzymes, such as (de)hydrogenases, culminating in the corrinoid iron-sulphur protein (CFeSP), before joining the CO branch to make acetyl-CoA. Fe – Orange; Ni – Green; Cobalt – Purple; “open site” indicates where the substrate binds to the cluster.

H₂ activation and redox potential in vivo

Although H₂ is a widely used source of electrons for hydrogenation in industrial, geochemical, and biological processes, it is also very unreactive without a strong energy source or a catalyst. The H–H bond can be cleaved into two H atoms (H[•]), a reaction described by homolytic cleavage, or into a hydride ion (H[−]) and a proton (H⁺), by heterolytic cleavage (+200 kJ mol^{−1}) (**Scheme 1**). In all cases, transition metals are often used as catalysts to activate H₂ (Kubas, 2007).



Scheme 1 Represented on the left is the homolytic cleavage of H₂, resulting in an unstable dihydride metal complex. On the right is the heterolytic cleavage which makes a metal-bound hydride and a free proton. M = Metal. Redrawn and adapted from Kubas (2007).

Life as we know it was probably H₂ dependent at its origin (Moody *et al.*, 2024; Weiss *et al.*, 2016; Wimmer *et al.*, 2021). In hydrogenotrophs' metabolisms, the activation of H₂ and the further processing of its electrons can be done by [NiFe], [FeFe] and [Fe] hydrogenases (Thauer, 2011). H₂ diffuses through hydrophobic channels of the enzymes until it reaches the active site, where heterolytic cleavage occurs by various mechanisms. The details of this reaction have been described in detail by Lubitz *et al.* (2014) and Shima *et al.* (2020). Notably, metal-bound hydrides on the iron guanylyl pyridinol (FeGP) cofactor of [Fe] hydrogenases are transferred directly to the substrate: methenyl-tetrahydromethanopterin (Arriaza-Gallardo *et al.* 2023; Huang *et al.* 2020); whereas the other two hydrogenases require FeS centres and hydrophobic channels to transport electrons and H⁺, respectively. This is an enzymatic step that can also go the opposite direction if the organism needs to produce H₂ to dispose of electrons.

The electrons are often transferred to carriers such as coenzyme F₄₂₀, nicotinamide adenine dinucleotide (NAD), and ferredoxin. The latter is a small ubiquitous non-enzymatic protein (6–12 kDa) responsible for electron transfer with the relevant redox couple being Fe²⁺/Fe³⁺ (FeS cluster) (Tagawa and Arnon, 1962). The clusters of different ferredoxins can be [2Fe–2S], [3Fe–3S] or [4Fe–4S], but the latter is said to be the oldest, and represented in **Figure 1** (Fitch and Bruschi, 1987). The

reduction of Fd (standard redox potential (E°) = -450 mV) by H_2 is essential to keep the metabolism thermodynamically afloat in H_2 -growing microorganisms, allowing electrons to flow downhill, but involves a more complex mechanism by hydrogenases: flavin-based electron bifurcation. Due to the low redox potential of Fd, its reduction by H_2 is not favourable (E° = -414 mV) under physiological conditions. However, when coupled to the reduction of a high potential electron acceptor, a trick employed by bifurcating hydrogenases, the reaction becomes overall exergonic while producing two reduced cofactors (Buckel and Thauer, 2018, 2013).

Flavin-based electron bifurcation begins after H_2 is activated by hydrogenases. The electrons produced are transferred to a flavin-containing enzyme complex. Flavins have three different oxidation states (0, -1 , -2) with different midpoint redox potentials, the average of which is more positive than H_2 and thus favours reduction (E° = -300 mV). The electrons can then leave the flavin in two different directions. The endergonic branch uses the first electron from the flavin redox pair $-1/-2$ with an extremely high midpoint potential ($E_{-1/-2} \geq -910$ mV), making the one-electron reduction of Fd possible. In the exergonic branch, the reduction of high-potential carriers, such as NAD (E° = -320 mV), with the pair $0/-1$ ($E_{0/-1} \leq +360$ mV) seems to have a thermodynamic barrier. However, individual electron transfer steps can make positive changes in potential in an overall thermodynamically favourable reaction, maintain this branch exergonic (Buckel and Thauer, 2018; Lubner *et al.*, 2017; Nitschke and Russell, 2012; Page *et al.*, 1999).

To maintain H_2 -dependent metabolism, inorganic cofactors (Ni, Fe, FeS; and organic cofactors like flavins and others) are indispensable. Although modern hydrogenases do not always require Ni, its metal-bound hydride is more stable than in Ni-free hydrogenases (Lubitz *et al.* 2014). Regardless, every hydrogenase requires transition metals in its active centre. While proteins are rather complex molecules, transition metals have always been available on Earth, essential for LUCA's metabolism and probably the origin of life.

H_2 activation “in metallum”

Transition metals are particularly well suited for hydrogenation in industrial processes (Aireddy and Ding, 2022). Although H_2 can be absorbed onto metal surfaces relatively quickly by physisorption, the weakly stabilized van der Waals

interactions cannot cleave the H–H bond. To be chemically activated, hydrogen must be chemisorbed, which heterolytically cleaves the H–H bond to produce a single hydride on the metal surface, forming a sigma (σ) bond (**Scheme 1**) (Aireddy and Ding, 2022; Kubas, 2007)

The same transition metals that carry out the fixation of carbon and hydrogen in biology are used as catalysts in industrial-scale reactions. Nickel activates hydrogen to produce methane (CH_4) through CO_2 methanation reaction (Sabatier process) (Wang *et al.*, 2022). The same process can be reversed to produce H_2 from methane and steam, which can then be activated by iron or magnetite (Fe_3O_4) to hydrogenate nitrogen to ammonia (Haber-Bosch process) (Ertl, 1983; Kandemir *et al.*, 2013; Leigh, 2004). Fe is also used in the Fischer-Tropsch process to convert the CO_2/H_2 pair into liquid hydrocarbons that can be used for fuel production (Heveling, 2012). The same mechanism can be extrapolated to mineral surfaces, allowing the inorganic reduction of the CO_2/H_2 pair in hydrothermal vents, as discussed throughout chapter I.

Transition metals are effective catalysts in both homogeneous and heterogeneous catalysis. We find them in biology, chemistry and geology. During the Hadean eon, minerals and reducing conditions in hydrothermal systems would be sufficient to sustain a proto-metabolism (Wimmer *et al.*, 2021).

III. Organic cofactors

The abyss between prebiotic chemistry and life

Metabolites or precursors thereof could have been formed in hydrothermal vents (Baross and Hoffman, 1985; Corliss *et al.*, 1981; Martin *et al.*, 2008; Schwander *et al.*, 2023), a different location on earth (Damer and Deamer, 2020; Maruyama *et al.*, 2019; Pearce *et al.*, 2017) or meteorites that carry products from an extra-terrestrial system (Zeichner *et al.*, 2023). Starting from undirected abiogenesis, it possibly took a long time until the surface-based network chemically evolved into a self-sustaining network (Nghe *et al.*, 2015).

In a study from 2020, Xavier *et al.* computationally identified self-sustaining networks within methanogens and acetogens and concluded that they were maintained when there was a constant source of small-molecule catalysts, mostly cofactors, but not when provided with bases or amino acids. Proteins and RNA

macromolecules are end-products and non-essential to sustain the network, but cofactors are. They identified nucleotide-derived cofactors to be the most prevalent of cofactors and necessary for the network (Xavier *et al.*, 2020). Another study compared several phylogenetic analyses of LUCA and reached the same conclusion that nucleotide-cofactors are particularly ancient (Crapitto *et al.*, 2022).

The prebiotic network contains inorganic cofactors in the form of metal ions and possibly even FeS clusters, but as suggested by Xavier *et al.* (2020), organic cofactors would be necessary to establish more complex and directed autocatalytic networks. This is theoretically possible as there are many proposed mechanisms for the inorganic synthesis of nucleotide cofactors (Copley *et al.*, 2007; Fontecilla-Camps, 2019; Harrison and Lane, 2018; Kim and Benner, 2018; Kirschning, 2021a; Miller and Schlesinger, 1993). The idea that nucleotide cofactors are fossils of earlier metabolic networks is not new (White, 1976). Because nucleotides are also the monomers of genetic polymers, they were mostly discussed in the context of the RNA world. Proponents of this theory argue that first self-replicating systems were driven by self-replicating catalytic RNA molecules, before DNA genomes and protein-driven metabolism emerged (Crick, 1968; Fine and Pearlman, 2023; Gilbert, 1986; Orgel, 1968; Woese, 1965). For it, it is often argued that small nucleotide-like molecules could have established a pre-RNA world, which would gradually evolve into the RNA world (Cafferty *et al.*, 2018; Copley *et al.*, 2007; Goldman and Kacar, 2021; Kirschning, 2021b; White, 1976). However, there is no reason to believe that a nucleotide-world inevitably leads to an RNA-world, as nucleotides, and cofactors in general, are also strongly associated to protein metabolism (Fried *et al.*, 2022; Sanchez-Rocha *et al.*, 2024; Xavier *et al.*, 2020). Most proteins in ancient pathways are apoenzymes (inactive) and catalytic active only when metals and/or organic cofactors bind to their active centre (Ragsdale and Pierce 2008; Shima *et al.* 2002). Additionally, NADH can mediate reductive amination of α -ketoacids with ammonia to produce the building blocks of proteins (Nogal *et al.*, 2024). Regardless of what proceeded small nucleotides, these small cofactors are always discussed as essential pillars to origin of life theories.

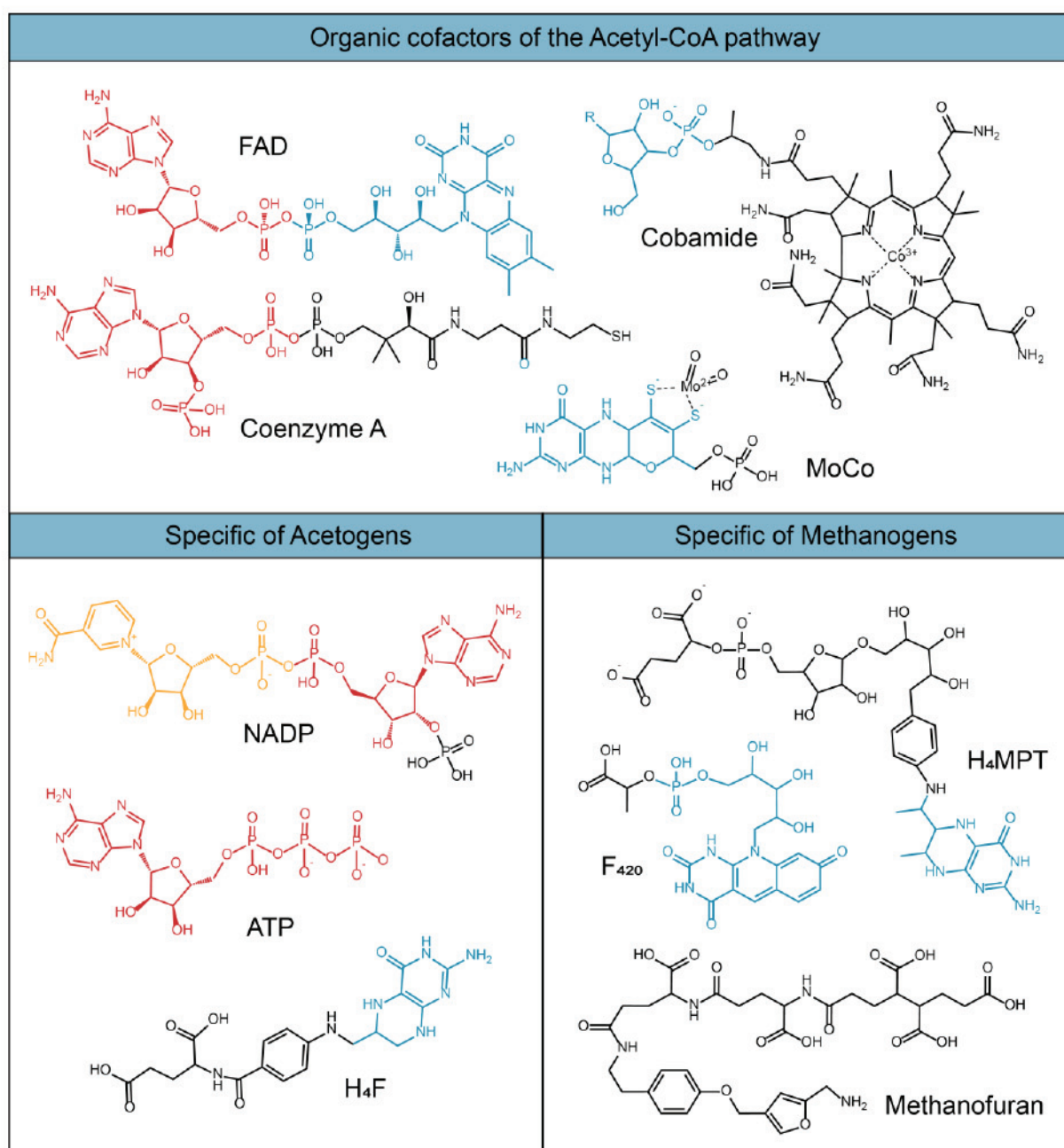


Figure 2 The linear acetyl-coA pathway entails a variety of nucleotide-derived cofactors (Fuchs 2011; Martin 2020). The first step always requires molybdenum cofactor (MoCo), and a flavin for flavin-based bifurcation. The intermediate steps require different cofactors for the methyl branch in acetogens and methanogens, ultimately converging again in the last step where coenzyme A (CoA) is required. **Blue** are structures of cobamide, which –R can be a nucleobase or not, methylene tetrahydrofolate (H₄F), tetrahydromethanopterin (H₄MPT), 8-hydroxy-5-deazaflavin (F₄₂₀), MoCo and flavin adenine dinucleotide (FAD), which derive from nucleotides in their biosynthesis (Graham and White 2002; Schwarz and Mendel 2006; Shin *et al.* 2016). Highlighted in **red** is AMP(PP) and in **yellow** nicotinamide mononucleotide (NMN). Another cofactor the acetyl-CoA may also require is FeGP, when Ni is scarce and [Fe]-hydrogenases are produced instead of [Ni,Fe] -hydrogenases. The FeGP structure is represented in **Figure 1** (Huang *et al.*, 2019).

Formed from inorganic resources (and smaller metabolites of abiotic origin), soluble organic cofactors could have been instrumental in the evolution of metal-dependent networks. These smaller catalytic components would form the basis of a proto-metabolism (Copley *et al.* 2007; Fontecilla-Camps 2019; Harrison and Lane 2018; Kim and Benner 2018; Kirschning 2021b; Miller and Schlesinger 1993) from which genetic information and complex proteins could evolve (Copley *et al.* 2007; Fontecilla-Camps 2019; Fried *et al.* 2022; Goldford *et al.* 2024; Kirschning 2021b; Martínez Giménez and Tabares Seisdedos 2022; Tremmel *et al.* 2019). These ideas fuelled the need to investigate ancient cofactors in a prebiotic context, which eventually inspired all three publications in this thesis (Brabender *et al.*, 2024; Henriques Pereira *et al.*, 2025, 2022).

Clues to their antiquity

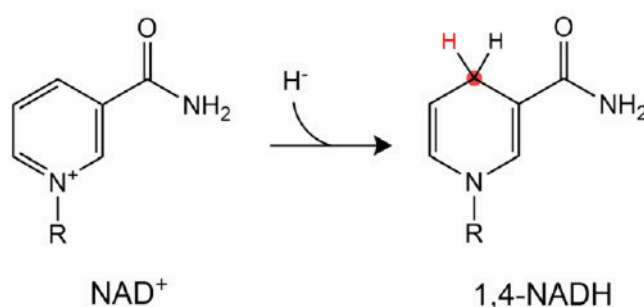
Organic cofactors are essential for a variety of enzymatic functions, but are most commonly found in oxidoreductases and transferases (Fischer *et al.*, 2010). They bind to relatively simple but ancient folds (e.g. P-loop NTPases, TIM beta/alpha-barrels, OB and Rossmann folds), which are composed exclusively of prebiotically available amino acids (Sanchez-Rocha *et al.*, 2024). Many ancient cofactors such as flavins, pterins, and folates are sensitive to oxygen and light degradation. They are also often universal, conserved across all domains of life, as in the case of Coenzyme A (CoA), S-adenosyl-methionine (SAM), NAD(P), and others. To this argument is also the fact that in addition to NADH, flavins (Argueta *et al.*, 2015), pyridoxal 5'-phosphate (Metzler and Snell, 1952; Zabinski and Toney, 2001), S-adenosylmethionine (SAM) (Barrows and Magee, 1982), CoA (Wagner and Payne, 2013), and other cofactors (Bazhenova *et al.* 2000; Benkovic 1978; Mizuhara and Handler 1954), can also promote reactions without any other catalysts.

The pathway to produce acetyl-CoA requires six different organic cofactors in methanogens and seven in acetogens, which are involved in all but one step of each pathway (**Figure 2**) (Fuchs, 2011; Martin, 2020). Of these, only one organic cofactor in methanogenic bacteria (methanofuran) is not a nucleotide or, in their biosynthesis, nucleotide-derived (Graham and White, 2002; Schwarz and Mendel, 2006; Sousa and Martin, 2014). The predominance of cofactor-dependent enzymes in these organisms is strongly related to H₂ metabolism: more than 80% of all oxidoreductases use at least

one organic cofactor in their active site (Fischer *et al.*, 2010) of which 90% is a nicotinamide cofactor (NAD(P)) (Wu *et al.*, 2013).

Nicotinamide Adenine Dinucleotide

The first organic cofactor discovered was NAD, which was named "cozymase" by British biochemists Arthur Harden and William John Young in 1906 (Harden and Young, 1906). 30 years later, in 1936, Otto Heinrich Warburg discovered that "cozymases" transfer a hydride from one molecule to another (Warburg and Christian, 1936). Today, we know that NAD(P)s are required for more than 1500 enzymatic reactions in microorganisms (Förster *et al.*, 2003). They are essential for energy management and help kick-start all major autocatalytic metabolic networks. ATP, on the other hand, famously called the energy currency of the cell, is an essential intermediate, but is not needed to start autocatalytic networks (Xavier *et al.*, 2020). NAD(P)s participate in redox reactions as electron carriers by undergoing nucleophilic addition of a hydride at the C4 of the pyridinium moiety of nicotinamide (**Scheme 2**). Overall, they are particularly primordial and relevant cofactors, commercially available, and easy to handle during experiments due to their stability towards O₂ and light. From both a theoretical and practical point of view, this dinucleotide was the best candidate to initiate a new research effort on ancient nucleotide cofactors. The first two publications in this thesis reflect the interest and impact of studying NAD, and consider how the results might apply to other nucleotide cofactors (Henriques Pereira *et al.*, 2025, 2022).



Scheme 2 The reduction of NAD⁺ in biology is mediated by enzymes. In this case the C4 (marked in red) of the nicotinamide ring is initially reduced by transfer of two electrons and a proton (H), resulting in the production of 1,4-NADH.

Shared structure of prebiotic origins

Most cofactors have an adenosine monophosphate (AMP) moiety in their structure (**Figure 2**, in red). However, it's never their chemically active group, with the exception of adenosine triphosphate (ATP). NAD has an additional active nucleotide

attached to AMP, forming a dinucleotide structure. Others have different molecules attached to AMP, such as 4'-phosphopantetheine, which carries the acetyl group in acetyl-CoA, or a flavin (FAD). Finally, some contain cyclic nitrogenous bases that are nucleotide-derived in their biosynthesis but do not carry a nucleotide within their structure, such as SAM, which has an adenine nucleoside and folates or pterins which stem from GTP but do not show nucleotidic features anymore (Graham and White, 2002; Schwarz and Mendel, 2006; Shin et al., 2016). The AMP or AMP-like structures of these cofactors mostly provide a structural "handle" for enzymatic binding (Denessiouk *et al.*, 2001; Sanchez-Rocha *et al.*, 2024) leading to theories of late addition of the AMP moiety to prebiotic active proto-cofactors (Goldman and Kacar 2021; Kirschning 2021b, 2021a). Although protein domains that bind to AMP cofactors are among the oldest, they are also very diverse, suggesting that they were selected to recognize these cofactors and not the other way around (Ji *et al.*, 2007). The implications of a prebiotic origin to the AMP moiety are many and thus motivated an experimental test, presented in Publication II (Henriques Pereira *et al.*, 2025).

Past and future considerations

If some organic cofactors are indeed ancient, they should be able to survive certain hydrothermal conditions, and through reactions with geochemical hydrides on mineral surfaces, transfer protons and electrons from H₂ and other transfer groups from available resources. At present, we know that mild hydrothermal temperatures (at least ≤ 100 °C) are required to mitigate hydrolysis of most ancient organic cofactors, while pH stability varies widely (Anderson and Anderson, 1963; Buyske *et al.*, 1954; Hemmerich *et al.*, 1965; Kaplan *et al.*, 1951; Matos and Wong, 1987; Oey *et al.*, 2003; Tyagi *et al.*, 2009).

Because of their role in metabolism, organic cofactors have become purchasable supplements, increasing the need for pharmaceutical companies to find problem as it seeks to engineer cofactor-dependent enzymes such as oxidoreductases. NAD(P) being such a central cofactor, it is often examined in such studies. A recurring method is the regeneration of electron carriers using electrodes (Chenault, Simon, and Whitesides 1988). However, other methods from enzymatic, chemical, electrochemical, and photochemical regeneration can be applied (Wu *et al.*, 2013). Canivet, Süss-Fink and Štěpnička (2007) have developed organometallic complexes of rhodium, iridium, and ruthenium to catalyse the 1,4-regioselective

reduction of NAD^+ to NADH in aqueous solution with sodium formate as hydride donor (60 °C and pH 7). Another iridium-aqua complex can produce protons and NADH from the H_2 with NAD^+ and also the reverse process under atmospheric pressure at room temperature (Maenaka *et al.*, 2012). These metals and platinum-group metals are most often used for hydrogenation due to the stable hydrides that can form on the surface of their complexes (Noffke *et al.*, 2012). However, these metals, and most certainly the synthetic organometallic complexes, are not easy to find in nature. Without the optimized synthetic complex, it is also uncertain if the reduction of NAD^+ will be stereoselective, or efficient and further investigation on the reduction of NAD under abiotic conditions is necessary. The stereoselectivity of different metals was investigated and discussed in publication 1 and 2, but the latter work also investigated how the dinucleotide structure of NAD might influence this (Henriques Pereira *et al.*, 2025, 2022).

An example of natural organometallic complexes are FeS clusters. They resemble the mineral structure of greigite (Fe_3S_4), which occurs in off-ridge hydrothermal systems (White *et al.*, 2015). The transfer of electrons from FeS to NAD^+ is thermodynamically favoured, but NAD requires a hydride to be reduced. According to the work of Weber *et al.* (2022) FeS minerals could have driven NAD^+ reduction (initial pH about 6.5, anoxic, 70°C), but this reaction is slow (2% yield after 72h with 10 equiv), and degradation of the substrate to cyclic NAD and adenosine diphosphate ribose in acidic water (Mayer and Moran, 2024), degradation of NADH to nicotinamide and ADP at 70°C (Hachisuka *et al.*, 2017), as well as NADH oxidation under acidic conditions, accumulate faster. Alternatively, H_2 is a better hydride donor. Not only can it be cleaved on mineral surfaces to form hydrides, it is also accessible (10–15 mmol/kg) in serpentinizing systems (Charlou *et al.*, 2002; Kelley *et al.*, 2002) and the main abiotic electron source for anaerobic respiration. Whether heterolytic cleavage of the H_2 bond and hydride transfer to the cofactor is possible at low temperatures with non-optimized catalysts was unknown prior to all three publications presented in this thesis. Since anaerobic microbes and serpentinizing systems are particularly rich in Ni and Fe , it made the most sense to test them rather than others. Publications I and II use native metals and oxides (Fe^0 , Ni^0 , Co^0 , FeO , NiO , etc.) (Brabender *et al.*, 2024; Henriques Pereira *et al.*, 2022), and Publications II and III use serpentinizing minerals

(Fe₃O₄, Ni₃Fe, etc.) (Brabender *et al.*, 2024; Henriques Pereira *et al.*, 2025) covering a wide range of available Ni and Fe minerals and redox states.

Instead of studying FeS clusters as catalysts for the reduction of other electron carriers, it would be most valuable to study them as they are used in biology: for electron transfer. Unlike organic cofactors, which are free in the cytosol, FeS clusters are always bound to proteins, usually through cysteine. It so happens that these clusters can spontaneously form inorganic Fe²⁺/Fe³⁺ and S²⁻ with micromolar concentrations of cysteine under alkaline hydrothermal conditions (Jordan *et al.* 2021). However, the reduction of ferredoxin is not favoured by H₂ except by flavin-based electron bifurcation. In the prebiotic context, the energetic gap between the different oxidation states of free flavins (0, -1, -2) is much smaller than the difference in prosthetic flavins, and is also unlikely to promote Fd reduction (Anderson 1983; Buckel and Thauer 2018). In other words, the potential generated by the reduction of a high potential cofactor would not cover the cost of the low potential cofactor, leaving Fd oxidized. In this scenario, it is possible that flavins were prosthetic to a small protein, but first we should rule out that minerals alone are sufficient to catalyse this reaction under prebiotic conditions (Sousa *et al.*, 2018), which we aimed to do in publication 3 (Brabender *et al.*, 2024).

The problem of H₂ activation under mild hydrothermal conditions, as well as the distribution of the obtained resources, whether that is through electron (e.g. Fd) or hydride (e.g. NAD) carriers, is most important for understanding the evolution of autocatalytic networks in a prebiotic world. However, little is known about how cofactors could have contributed to this fact. This gap of knowledge was a good starting point for the experimental work done all throughout the development of this thesis (Brabender *et al.*, 2024; Henriques Pereira *et al.*, 2025, 2022).

Prospects

As stated in the *Introduction*, cofactors are essential to establish any kind of biological network, however rudimentary its machinery may be (Xavier *et al.*, 2020), and thus a valuable subject of study for the field of origin of life research. However, very little experimental work has been done to integrate cofactors in prebiotically relevant environments, and it is uncertain whether their reduction is possible and efficient using naturally available catalysts (Weber *et al.*, 2022). Considering the characteristic temperature and pH gradients, catalytic minerals, and dissolved gases of serpentinizing hydrothermal vents (Martin *et al.*, 2008; Preiner *et al.*, 2018; Schwander *et al.*, 2023), in addition to the similar metabolic characteristics of the LUCA (Martin *et al.* 2016; Moody *et al.* 2024; Weiss *et al.* 2016), discussed in chapter I – Hadean Earth, this work aims to fill the knowledge gap on the stability of inorganic and organic cofactors under mild hydrothermal conditions and their ability to metabolize H₂. In doing so, the experimental work provides prebiotic alternatives to complex enzymatic processes such as electron bifurcation and H₂ activation. All three publications address these issues, but as foundation to the following work, Publication I is particularly insightful to the interactions between water, an organic cofactor (NAD), and native Ni, Fe, and Co (Henriques Pereira *et al.* 2022). Publication II expands on the same topic by testing a variety of NiFe alloys ((Henriques Pereira *et al.*, 2025)). Publication III applies the same knowledge to a different kind of electron carrier – *Clostridium pasteurianum* ferredoxin – which harbours two [4Fe–4S] clusters (Brabender *et al.*, 2024). By testing very different cofactors – high and low potential cofactors, nucleotide and protein, electron and hydride carrier, organic and inorganic cofactor – the goal is to test a variety of characteristics that are essential to any metabolism and thus understand H₂ proto-metabolism better.

Pondering on the shared nucleotide structure of ancient organic cofactors (**Figure 2**), and the evolution of protein-cofactor domains discussed in chapter III – Organic cofactors, it is striking that there is no known evolutionary purpose for the shared moiety. Perhaps, if modern cofactors or precursors thereof existed before life in a proto-metabolism, the function of the “AMP-handle” lies in a prebiotic context, to fulfil prebiotic functions. This hypothesis motivated the experimental work conducted in Publication III, comparing the reduction, oxidation and stability of NAD under

hydrothermal conditions to its “AMP-less” metabolite: nicotinamide mononucleotide (NMN) (**Figure 2**, in yellow) (Henriques Pereira *et al.*, 2025).

Publications

Publication I – Role of geochemical protoenzymes (geozymes) in primordial metabolism: Specific abiotic hydride transfer by metals to the biological redox cofactor NAD⁺.

Year: 2022

Authors: Delfina P. Henriques Pereira, Jana Leethaus, Tuğçe Beyazay, Andrey Do Nascimento Vieira, Karl Kleinermanns, Harun Tüysüz, William F. Martin, and Martina Preiner.

Contribution: First author.







Involved in planning all experiments. Directly performed all experiments with NAD and metal, supervised all experiments about NAD's stability, and prepared the samples for surface analysis. Analysed and discussed the data obtained. Responsible for organizing the Supplementary Information and assisting with writing and making figures for the main text.

Published in: The Federation of European Biochemical Societies (FEBS) Journal

DOI: 10.1111/febs.16329

Summary: This project provides a detail analysis of H₂-Metal-NAD⁺ interactions under mild alkaline (pH 8.5) hydrothermal conditions (40 °C), proposing a different mechanism for each metal studied (Ni, Fe and Co). Using deuterated water (²H₂O) confirmed that Fe⁰ can form hydrides from water at 40 °C, resulting in the observed 1,4-NAD²H molecule. The results are particularly striking because the hydride transfer with pure metal is 1,4-regioselective, a function we usually attribute to organometallic complexes, such as in enzymes.

Role of geochemical protoenzymes (geozymes) in primordial metabolism: specific abiotic hydride transfer by metals to the biological redox cofactor NAD⁺

Delfina P. Henriques Pereira¹ , Jana Leethaus¹, Tugce Beyazay² ,
 Andrey do Nascimento Vieira¹ , Karl Kleinermanns³, Harun Tüysüz² , William F. Martin¹ 
 and Martina Preiner^{4,5} 

¹ Institute for Molecular Evolution, Heinrich Heine University, Düsseldorf, Germany

² Max-Planck-Institut für Kohlenforschung, Mülheim an der Ruhr, Germany

³ Institute for Physical Chemistry, Heinrich Heine University, Düsseldorf, Germany

⁴ Department of Ocean Systems, Royal Netherlands Institute for Sea Research, Den Burg, The Netherlands

⁵ Department of Earth Sciences, Utrecht University, The Netherlands

Keywords

cofactors; electron donors; hydrogen;
 hydrogenase; NADH; origin of life;
 reduction; serpentinizing systems

Correspondence

M. Preiner, Department of Ocean Systems,
 Royal Netherlands Institute for Sea
 Research, 1790 AB Den Burg and
 Department of Earth Sciences, Utrecht
 University, 3584 CD Utrecht,
 The Netherlands
 Tel: +31 30 253 1409
 E-mail: martina.preiner@nioz.nl

(Received 18 November 2021, revised 9
 December 2021, accepted 17 December
 2021)

doi:10.1111/febs.16329

Hydrogen gas, H₂, is generated in serpentinizing hydrothermal systems, where it has supplied electrons and energy for microbial communities since there was liquid water on Earth. In modern metabolism, H₂ is converted by hydrogenases into organically bound hydrides (H[−]), for example, the cofactor NADH. It transfers hydrides among molecules, serving as an activated and biologically harnessed form of H₂. In serpentinizing systems, minerals can also bind hydrides and could, in principle, have acted as inorganic hydride donors—possibly as a geochemical protoenzyme, a ‘geozyme’—at the origin of metabolism. To test this idea, we investigated the ability of H₂ to reduce NAD⁺ in the presence of iron (Fe), cobalt (Co) and nickel (Ni), metals that occur in serpentinizing systems. In the presence of H₂, all three metals specifically reduce NAD⁺ to the biologically relevant form, 1,4-NADH, with up to 100% conversion rates within a few hours under alkaline aqueous conditions at 40 °C. Using Henry’s law, the partial pressure of H₂ in our reactions corresponds to 3.6 mM, a concentration observed in many modern serpentinizing systems. While the reduction of NAD⁺ by Ni is strictly H₂-dependent, experiments in heavy water (²H₂O) indicate that native Fe can reduce NAD⁺ both with and without H₂. The results establish a mechanistic connection between abiotic and biotic hydride donors, indicating that geochemically catalysed, H₂-dependent NAD⁺ reduction could have preceded the hydrogenase-dependent reaction in evolution.

Introduction

Hydrogen (H₂) is the main source of electrons for chemoautotrophic, industrial, and geochemical CO₂ fixation [1–3]. There are two main sources of naturally

occurring H₂: abiotic geochemical production (serpentinization) and biotic biochemical production via hydrogenases in fermentations. Today, anaerobic autotrophs

Abbreviations

¹H-NMR, proton nuclear magnetic resonance, an analytical method to characterise and quantify hydrogen-containing molecules; Co, cobalt; Fd_{ox}/Fd_{red}, oxidised/reduced ferredoxins; Fe, iron; LUCA, the last universal common ancestor, a theoretical cell based on phylogenetic reconstructions of the most conserved genetic setup between bacteria and archaea; NAD⁺/NADH, oxidised and reduced form of nicotinamide adenine dinucleotide; Ni, nickel.

such as methanogens grow mainly from H₂ of biotic origin, approximately 150 million tons of H₂ per year are produced by microorganisms and consumed by methanogens [4,5]. Only a small fraction of primary production is attributable to chemolithoautotrophy from H₂ geochemically generated during serpentinization in hydrothermal systems [5]. When the first microbial lineages evolved, however, abiotic H₂ was probably the major source of electrons for primary production in ancient ecosystems and metabolism [5–8].

Making the electrons of H₂ accessible

In the absence of effective catalysts, hydrogen is a surprisingly unreactive gas. It can only become chemically or biochemically useful when it is activated, that is, when its covalent bond is broken and the two H-atoms are separated [9]. The homolytic cleavage of gas-phase H₂ that breaks the H–H bond into two H atoms (H·) is endergonic by +436 kJ·mol^{−1} [5,10]. The heterolytic cleavage into a hydride ion (H[−]) and a proton (H⁺) is less endergonic [5,10] but still requires +200 kJ mol^{−1}.

Metal and mineral surfaces can adsorb H₂ both as a molecule by physisorption and as H-atoms by dissociative chemisorption [11–14]. Physisorption of H₂ usually requires very little energy (3–5 kJ·mol^{−1}) so it is most easily observed at low temperature in the range of liquid helium [14]. For chemisorption, hydrogen has to overcome the activation barrier and thus higher temperatures are usually required to form the metal-bound hydride, depending on the material. If the kinetic energy of the H₂ molecule is high enough, it can be dissociated directly on the surface of a suitable catalyst. But indirect chemisorption starting from the transient physisorbed state is also possible; physisorbed H₂ molecules can diffuse quickly on catalyst surfaces and then dissociate when the right catalytic site is met [3,14–16].

Microbes solved the problem of H₂ activation and cleavage about 4 billion years ago with the origin of hydrogenases, enzymes that dissociate H₂ into two protons and two electrons. H₂ was the source of electrons for primary production before photosynthesis emerged [8] and hydrogenases were already present in the last universal common ancestor (LUCA) [17]. All hydrogenases known catalyse a reversible reaction such that they can either use H₂ as an electron source or dispose of leftover electrons as H₂. There are three different kinds of hydrogenases, all of them holding transition metals coordinated by varying ligands in their active sites: [NiFe], [FeFe] and [Fe] [4,18–20]. Most of the reaction intermediates in the active site of hydrogenases have been determined [20]. All three perform a heterolytic cleavage of H₂, but do so in mechanistically

different ways; the same applies to the reverse reaction, the formation of H₂. The bond is polarised at an open metal site, such that a proton (H⁺) is accepted by a nearby base ligand, while the hydride (H[−]) remains bound to the metal, transiently altering its oxidation state. In the case of [FeFe] hydrogenases, H[−] is bound end-on to one of the two Fe atoms [9,20,21]. In [NiFe] hydrogenases, H[−] binds to both Ni and Fe (with help of an extra electron coming from Ni), making the hydride more stable than the one in [FeFe] hydrogenases [9,20,21]. The mechanism of [Fe] hydrogenases involves a direct hydride transfer from H₂ to an organic substrate, in contrast to the other two hydrogenases which need the assistance of FeS centres for this procedure [22].

Hydride carriers in biology

Though the reaction mechanisms of hydrogenases differ, their result is similar: Electrons from H₂ are transferred to soluble electron acceptors such as NAD⁺, F₄₂₀, or iron-sulfur clusters of oxidised ferredoxins (Fd_{ox}) for entry into metabolism [23]. While NAD and F₄₂₀ donate and accept electron pairs as hydrides (two-electron reactions), ferredoxin donates and accepts single electrons (one-electron reactions). In this paper, we focus on NAD and the H[−]-transfer reaction that reduces its oxidised form, NAD⁺, to its reduced form NADH [24,25]. NADH is a universal redox cofactor present in all cells, it is one of the most central molecules of metabolism, being essential in autocatalytic metabolic networks, meaning that without NADH metabolism cannot take place [26].

While hydrogenases make the electrons of H₂ accessible in modern cells [1,5,27], at the emergence of metabolism, before the existence of enzymes, electrons from H₂ that participated in CO₂ reduction and organic synthesis must have been activated by inorganic means such as mineral and metal surfaces [28–31]. Minerals could have served as prebiotic protohydrogenases ('geozymes') producing surface-bound hydrides (e.g. Fe–H) from dissociated H₂ which, in turn, are a prebiotic version of NADH. That this abiotic catalysis works for the reduction of CO₂ was shown previously [32,33]. Here our question was whether geochemical hydrides can reduce NAD⁺ to NADH which could have served as a soluble electron carrier at the origin of metabolic pathways. The existence of soluble electron carriers at origins is of interest for early metabolic evolution because catalytically active sites on minerals are immobile, whereas soluble organic hydride carriers such as NADH can transport activated H to mineral surfaces that might, for

example, catalyse organic redox reactions but not H₂ activation *in situ*.

Connecting geochemical with biological hydride carriers

To address possible transition points between abiotic and biotic hydride donation and the question of why NAD⁺/NADH became one of the universal hydride donors and acceptors in metabolism, we investigated geochemical conditions under which NAD⁺/NADH can (a) accept (and donate) hydrides and (b) remain stable. From earlier studies, it is known that NAD⁺ can be reduced heterogeneously on industrial catalysts [34,35] at neutral to slightly alkaline pH, so an approach under more rugged and natural conditions seemed possible. In a prebiotic context, this would entail a constant supply of environmental H₂ and accessible mineral surfaces. Serpentinizing systems harbour geochemical sites that reduce H₂O to H₂ via the oxidation of Fe(II)-containing minerals and thus provide these conditions [36,37]. Most but not all of these systems are alkaline because of the accumulation of metal hydroxides during serpentinization reactions [36,38]. Some microbes inhabiting such environments appear to lack hydrogenase enzymes [39], suggesting that even today, there might be alternative (abiotic?) and probably metal-based entry points for H₂ into metabolism.

To reduce NAD⁺ with H₂, we investigated three different metals as potential H₂ activating agents: Fe, Co and Ni. We started with native metals to keep the reactions as simple as possible. Both Fe and Ni are employed in the active centres of hydrogenases, but are also found in serpentinizing systems in oxidised and reduced forms [40,41]. We included Co because it is a crucial transition metal in autotrophic CO₂ fixation [1] and it is assumed to have been abundant in the Archean anoxic ocean [42]. In addition, Co complexes are being tested for its properties as artificial hydrogenases [43]. The hydrides of all three metals are known to have approximately the same hydricity (tendency to transfer hydrides) [44] as NADH and are ultimately direct neighbours in the periodic system of elements, so this choice of metals would also allow us to set their experimental behaviour in relation to their electrochemical potential.

Results

NAD⁺ reduction with H₂ and transition metals under alkaline conditions

We used conditions approximating those found in alkaline serpentinizing systems (starting pH 8.5, 5 bar

H₂ atmosphere, 40 °C), with metals Fe, Ni and Co [40,45] in powdered form, (1 M). The resulting aqueous H₂ concentration of 3.6 mM (calculated using Henry's law, s. Equation S1) is comparable to that found in hydrothermal effluent [38,40]. Under these conditions, the reduction of 3 mM NAD⁺ to NADH was facile (Fig. 1A,B). Fe, Ni and Co also play important catalytic roles in autotrophic metabolism [46–48]. That all three metals promote the reaction between NAD⁺ and H₂ to NADH was observed with ¹H-NMR, enabling us to make a detailed structural determination of our products as various prospective hydride acceptor sites exist on the NAD⁺ molecule and also degradation products such as nicotine amide are possible [49,50]. Our results show that indeed the biological form of NADH, 1,4-NADH, was the main product. We also observe some degradation products (mainly nicotinamide), but in low concentrations under the reaction conditions tested.

In order to probe the nature of H₂–metal interactions in these reactions, we performed four different experiments with each metal (for visual overview s. Fig. S1). In two reactions, we first pretreated the metal powders in a dry state with H₂ gas for 16 h at 50 °C before adding a buffer/NAD⁺ solution. Chemisorption and dissociation of H₂ is feasible at these temperatures [51–53]. This approximates the situation in serpentinizing systems, where H₂ is being produced continuously, such that the minerals could be constantly hydrogenated (i.e. organic redox cofactors and not hydrogenated minerals would be rate-limiting in the geochemical reaction). In addition, and in accordance with previous industrial investigations of heterogeneous NAD⁺ reduction [35], a thermal (> 350 °C) pretreatment of the catalyst with H₂ increased the yield of reduced NADH due to more or less saturating hydrogenation of the catalyst. Pretreated and non-pretreated metal powders were mixed with the phosphate buffer/NAD⁺ solution and reactions from 0.5 to 4 h were performed either under 5 bar of Ar or H₂ at 40 °C. In the Ar experiments, NAD⁺ reduction can be attributed to the activity of preformed hydrides on the metal surface. Controls without metals were conducted in each run, showing that metals are needed for the reduction of NAD⁺. All experiments were repeated at least three times. All the corresponding spectra can be found in Fig. S2.

The results summarised in Fig. 2 show how each metal responds to the different experiments over a 4-h course. The corresponding table with all individual measurements and standard deviation values can be found in the supplementary information (Table S1). Pretreating the metals with H₂ has a positive effect on

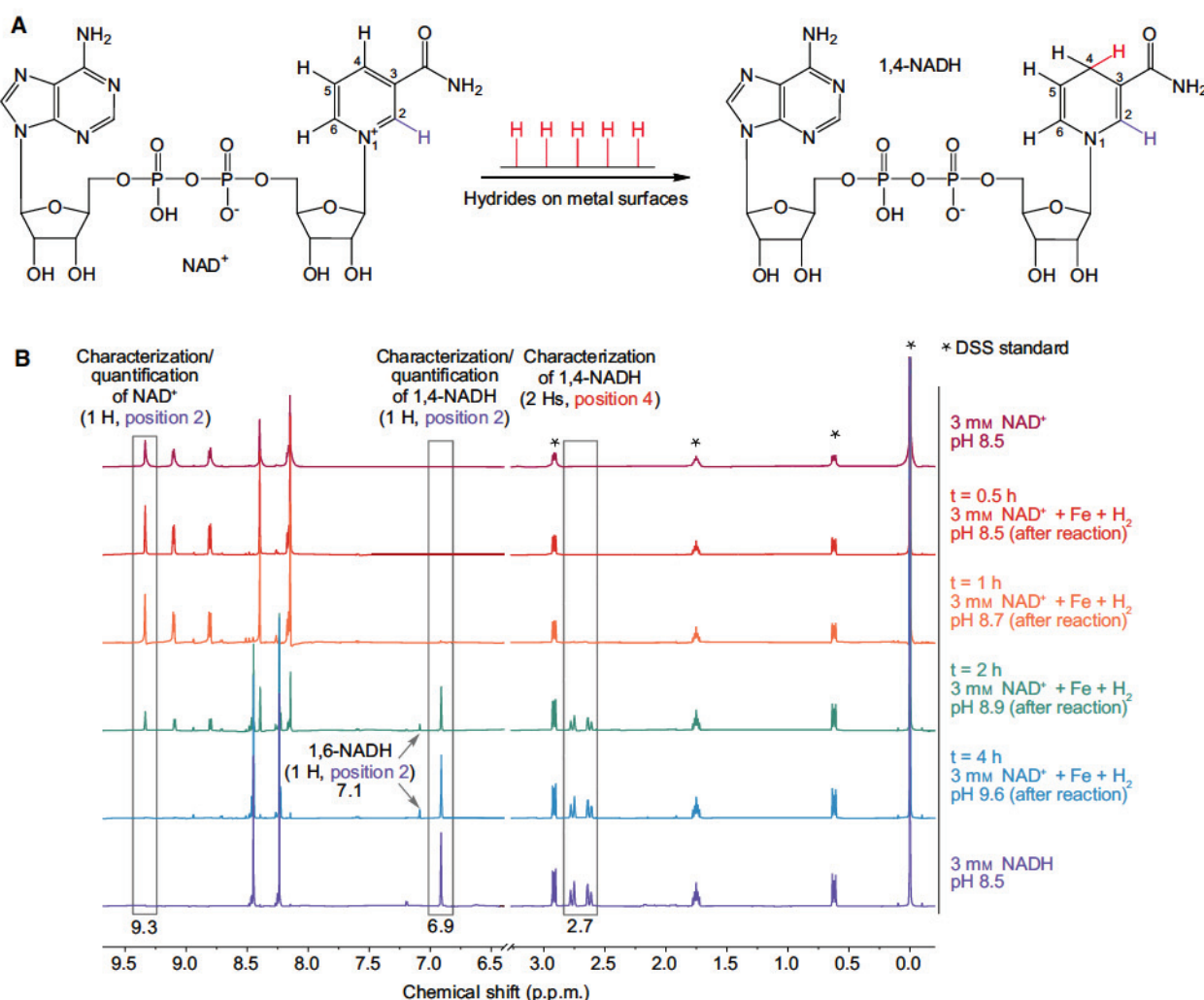


Fig. 1. Reduction of NAD⁺ with H₂ and Fe powder over time. (A) NAD⁺ is reduced to 1,4-NADH, the naturally occurring reduced form of nicotinamide adenine dinucleotide (NAD). This means a hydride is added to the carbon in position 4 of the aromatic cycle of NAD⁺. NAD⁺ can also be reduced at two further positions, the second and the sixth, thus leading to 1,2-NADH and 1,6-NADH respectively [84]. (B) Within 4 h, NAD⁺ is reduced to 1,4-NADH as monitored via ¹H-NMR. A pH shift from 8.5 to 9.6 is observed, probably due to the oxidation of Fe powder coupled to the reduction of H₂O to hydrides/H₂ (accumulation of OH⁻). The peaks of the used NMR standard sodium trimethylsilylpropanesulfonate (DSS) are marked with asterisks.

the NAD reducing activity of all three metals: Fe reaches high NADH yields quickly (Fig. 2A), as does Co (Fig. 2B), but the clearest effect can be seen with Ni, where only with H₂-pretreatment NADH yields approaching 50% can be reached. With both Fe and Co nearly 100% conversion from NAD⁺ to NADH is observed, but with one important difference: while Co clearly needs H₂ gas during the reaction to reach a high yield of NADH, Fe shows almost identical results under Ar as it does under H₂. Under Ar, Co can still convert almost 50% of NAD⁺ to NADH. The amount of metal used in comparison to NAD⁺ is very high (1 M of metal to 3 mM NAD⁺, so 333 : 1), but

experiments with a ratio of 20 : 1 (62.5 mM to 3 mM NAD⁺) and 10 : 1 (62.5 mM to 6 mM NAD⁺) (Fig. S3) showed that all three metals still yield NADH at the lower ratios. While Fe yields about 40% NADH at 10 : 1, Ni only reaches 0.6% at the same metal to NAD⁺ ratio.

We also observed a significant pH increase (s. Fig. S4) during the Fe and Co reactions and the development of coloured colloids (Fe: dark green, Co: pink; s. Fig. S5), especially when there was no H₂ gas added to the reaction or when not pretreated with H₂, while the pH remained stable and the solution colloid free (though coloured yellow) during the Ni reactions. The

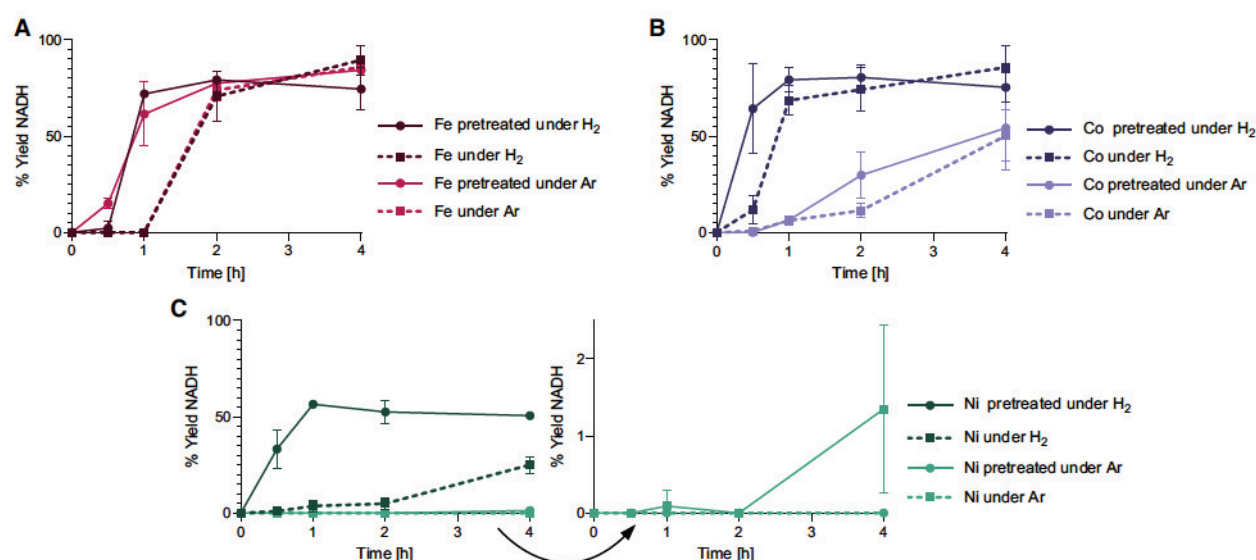


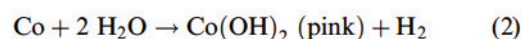
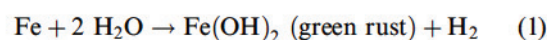
Fig. 2. NADH synthesis with Fe, Co and Ni under four different settings. In the experiments, the three metal powders were either pretreated with H₂ gas overnight at 50 °C before the reactions under 5 bar H₂ or Ar between 0.5 and 4 h (solid lines and circles), or the reactions took place without the pretreatment (dashed lines and squares). Data points shown are mean \pm SD. (A) Fe does not need an external H₂ source under the given conditions, NADH synthesis is equally efficient in both cases. Pretreated Fe reduces NAD⁺ faster but does not lead to a higher yield overall. Repetitions from 0.5 h to 4 h: n(pretreated, H₂) = 3, 3, 4, 3; n(H₂) = 3, 4, 4, 6; n(pretreated, Ar) = 2, 3, 2, 3; n(Ar) = 1, 4, 3, 3. (B) Co can reduce up to roughly 50% of NAD⁺ without an external H₂ source, but the presence of H₂ gas improved the yield and accelerated the conversion immensely. Pretreatment with H₂ also decreased the reaction time of the conversion visibly as long as there is an H₂ source during the reaction. Repetitions from 0.5 h to 4 h: n(pretreated, H₂) = 4, 4, 4, 4; n(H₂) = 4, 4, 4, 5; n(pretreated, Ar) = 2, 5, 4, 6; n(Ar) = 4, 4, 4, 4. (C) Ni powder cannot reduce NAD⁺ under the absence of H₂ as an electron source. Pretreated with H₂, Ni shows a 50% yield of NADH. Pretreated Ni can convert a very small amount of NAD⁺ to NADH under Ar, suggesting that hydrides are covering the surface of the metals after the pretreatment. Repetitions from 0.5 h to 4 h: n(pretreated, H₂) = 4, 3, 3, 4; n(H₂) = 4, 4, 4, 6; n(pretreated, Ar) = 2, 5, 4, 6; n(Ar) = 0, 4, 4, 4.

pH shift observed was also the reason we chose to work with a 1 M phosphate buffer. With buffers of lower concentrations, the pH of the Fe and Co samples shifted far into the alkaline range (> pH 10 and > pH 9 respectively), conditions under which NAD⁺ is unstable and decomposes [54] (s. Figs. S6, S7A). NADH, however, is far more stable under alkaline conditions, as we were able to determine in additional experiments, the results of which are summarised in Fig. S7B. The phosphate buffer can, however, lead to a degradation of NADH [55], which can explain minor losses we observed in NAD⁺ conversion (Table S1).

These observations led us to the conclusion that while Ni clearly catalysed the dissociation of H₂ gas and is thus making electrons from H₂ accessible to NAD⁺, both Fe and Co themselves can serve as the electron source instead of H₂ gas and are being oxidised (directly connected to the developing colouration), especially during the experiments without external H₂ source (under Ar). We undertook additional experiments to further investigate the role of Fe and Co as reductants.

Probing the role of metals with ²H: H₂ activation, H₂ synthesis, both or something else?

The observed pH shifts and colouration were a hint for following redox reactions taking place (the hydroxides generated are partly soluble [56] and lead to an pH increase):



Fe and Co powder are able to produce nascent H₂: freshly synthesised H₂ from two hydrogen atoms. The intermediates of this reaction are surface-bound hydrides [57] which could, in theory, be directly transferred to NAD⁺. It is also known that Fe readily produces H₂ from water under mild alkaline conditions [58]. To clarify the present mechanisms, Fourier-transform infrared spectroscopy (FTIR) was performed on all three metals (Fe, Co and Ni) before and after the reaction under Ar (expecting the highest

oxidation rate in these experiments in contrast to the ones under H₂ gas and hence more reducing conditions). The respective FTIR spectra (s. Fig. S8) show the differences between the metals very clearly, in line with our other results. Ni does not show any visible changes, Co does, but not clearly enough to specify the nature of the change. The spectrum of Fe after the reaction shows a new Fe-O bond (in the region of 500–600 cm⁻¹) as well as stretching and bending bands of -OH groups located around 3200 and 950 cm⁻¹ respectively, which indicates transformation of metallic iron into iron hydroxides such as Fe(OH)₂, confirmed by the dark green colouration of the Fe samples ('green rust').

To further probe the mechanisms of NAD⁺ reduction, we replaced H₂O in the solvent with heavy water (²H₂O, D₂O) to determine the source of the hydrides added to NAD⁺. There were two reasonable options: either protons from H₂O and metal electrons (formed

to surface-bound hydrides) or surface-bound hydrides from H₂ gas. Previous work on reducing NAD⁺ and ²H sources [59,60] provided us with mechanistic details and reference ¹H-NMR spectra for NAD²H species, the presence of which can be monitored via the duplet of duplet at 2.7 p.p.m. (position 4 as shown in Fig. 1). In our case, we would expect the formation of NAD²H instead of NADH if the hydride comes from ²H⁺ in ²H₂O plus electrons from metal, while NADH should be formed if the H₂ gas is the prevalent hydride source. Three 2-hour NAD⁺ reduction experiments with Fe, Co and Ni were performed in ²H₂O (otherwise using the same conditions as described above): metals under Argon, H₂-pretreated metals under Argon and metals under H₂. The results are shown in Fig. 3 with a focus on the 2.7 p.p.m. peaks described above (s. Fig. S2 to see the full range of the shown spectra). When no (under Argon Fig. 3A) or only little H₂ (pretreated and reaction under Argon, Fig. S9 and

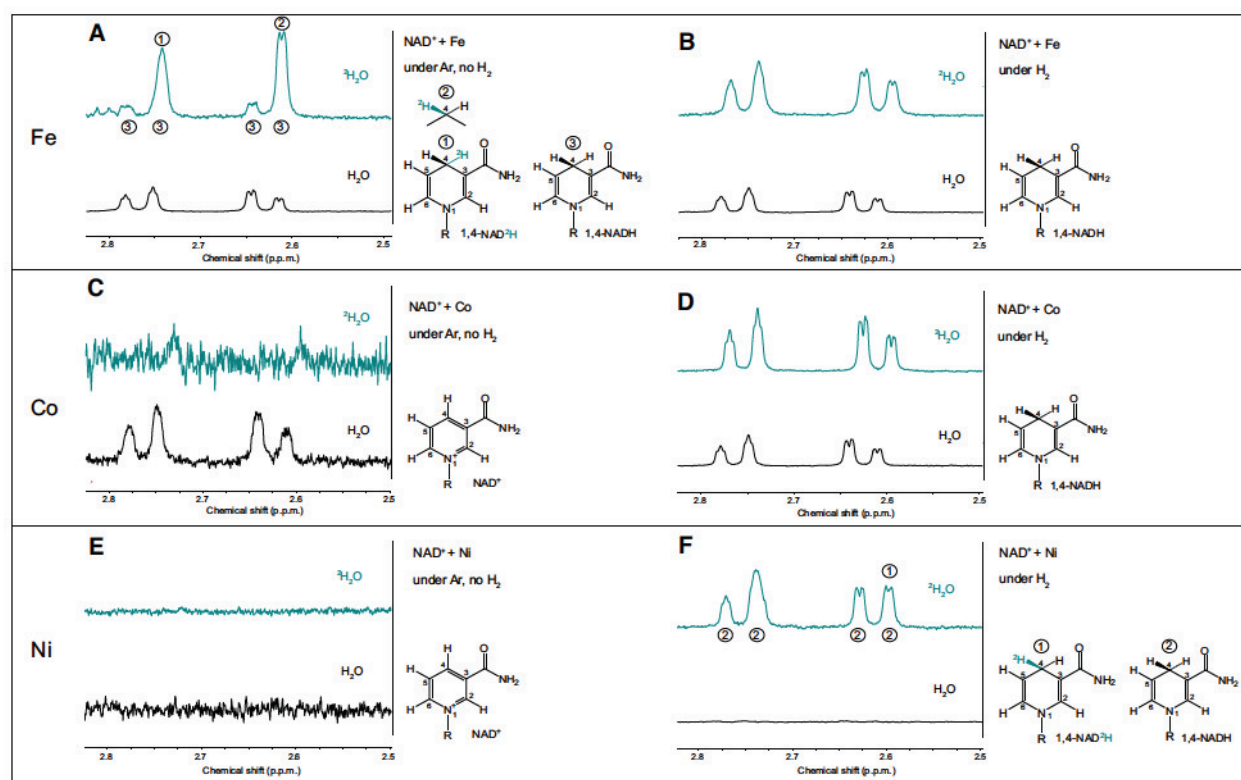


Fig. 3. Two-hour experiments in ²H₂O to determine the source of the H⁻ reducing NAD⁺. (A) When there is no external H₂ source, Fe delivers the electrons to form ²H⁻ from ²H₂O which is transferred to NAD⁺. The Deuterium (²H) at position 4 in the nicotinamide ring of NADH changes the proton coupling visibly. (B) The mechanism for NADH formation apparently changes when H₂ is added to the reaction. NADH becomes the main product, suggesting that H₂ is catalytically activated by Fe. (C) Co does not produce NAD²H (or NADH) over the detection limit under Ar gas in ²H₂O. (D) When H₂ is added to the reaction, Co promotes NADH formation. (E) Ni does not produce NAD²H (or NADH) over the detection limit under Ar gas in ²H₂O (or ¹H₂O). (F) In contrast to the ¹H₂O experiments, Ni highly promotes NADH formation in ²H₂O under H₂ after 2 h. Note that (C) and (E) are more vertically zoomed in than the rest of the panels as the product concentration was significantly lower.

Table S1) is in the experimental system, NAD²H is the prevalent product of the reactions with Fe. This indicates that Fe reduces ²H₂O to ²H[−] which then is transferred to NAD⁺. When the reaction is performed under ¹H₂ atmosphere (Fig. 3B), however, the product does not contain any measurable amount of ²H, suggesting that ¹H₂ is the hydride source in this case. We confirmed these observations additionally by integrating the duplet of duplet at 2.7 p.p.m. in both the Ar and the H₂ experiments (the peak integrals correspond to the number of associated ¹H; ²H is not detected). The integral values were compared to those of the singlet at 6.9 (1 ¹H-proton), ultimately showing that in ²H₂O and under Ar only one ¹H-proton is detected at position 4 of NADH (Table S2). In combination with the other findings above, the reaction path involving Fe-dependent reduction of water (or ²H₂O) to metal-bound hydride (or ²H[−]) appears reasonable. Fe seems to employ both described mechanisms, depending on the conditions. The positive effect of Fe pretreatment with H₂ is not explained by the present results. However, it is worth to mention that the overall yield of NADH with Fe under Ar is substantially lower and variable in ²H₂O (0–50%, Table S1) than it is in ¹H₂O (60–70%), while pretreatment increases the yield of NAD²H in the ²H₂O experiments (~80%, Table S1). We still registered a pH shift and slight green colouration suggesting the formation of Fe(OH)₂ (Figs. S4, S5). We will return to this observation shortly.

Cobalt does not deliver a picture as clear as that obtained for Fe. H₂ was necessary during the Co catalysed reaction to detect NADH formation in the ²H₂O experiments. Co reduces NAD⁺ to NADH under Ar, without H₂ and with ¹H₂O as proton source (Fig. 3C, lower trace), although with a far lower yield than Fe (Fig. 2B or Table S1). In the ²H₂O experiments however, H₂ was necessary for NADH formation. We could not observe any NAD²H formation after 2 h (Fig. 3D). Performing the same experiment for 4 h yielded detectable amounts of NADH, but not enough to investigate the peak at 2.7 p.p.m. (Table S1) and thus the status of deuteration.

In the case of Ni, the experiments under Ar confirm the conclusion from the previous experiments (no NADH formation). Nevertheless, a surprising effect of ²H₂O was observed: while only very little NADH formation was observed after 2 h in H₂O under H₂, almost all NAD⁺ is converted to NADH in ²H₂O (Fig. 3F) and there seems to be a very small amount of NAD²H formed. We have no thorough explanation for this puzzling observation, but it is possible that H₂O absorbing on the Ni surface occupies sites needed for H₂ dissociation—while ²H₂O does not as easily

[61–63]. The formation of NAD²H is probably the result of an exchange between H⁺ and ²H⁺ as the peak distribution is by far not as clear as in the case of Fe (Fig. 3A).

Overall, we were able to derive some valuable conclusions from the experiments performed under ²H₂O, but there are also some observations (e.g. yield loss with Fe and Co) that we cannot properly explain so far and are most likely the result of isotopic effects.

Being aware that metal ions are going into solution during our experiments, we also tried to exclude these dissolved species as being the true catalysts in our reactions. Therefore, we performed a ‘hot filtration test’ for all metals, that is, we separated the solid from the liquid phase after a 1 h reaction under H₂ (so we could test whether hydride-bearing, soluble complexes are being formed), added a new NAD⁺/buffer solution onto the solid phase and resumed the reaction under 5 bar for both parts for another 1 h and compared the NADH yields (Fig. S10). The separated liquid phase did not show any additional NADH formation for any of the metals, while the separated solid phase was still able to promote a very high NAD⁺ → NADH transformation yield (95% for Fe, 81% for Co, 35% for Ni after 1 h of reaction time). This indicates that the solid metals are the (far) more crucial species for NAD⁺ reduction in our experiments.

In addition, we also observed that the reaction with fresh NAD⁺ and ‘used’ metal powders (powders that had already been used in a previous H₂ reaction) yielded more NADH in 1 h than pristine metal powder would in that time (Fig. S11). The same experimental order, but with the first step under Ar instead of H₂ lead to similar results. This could mean one of several things. On one hand, it is possible that the oxidised forms of the metals (Equations 1 and 2) are better catalysts for the hydrogenation reaction than the native metal forms. We performed additional experiments (16 h pretreatment with H₂, 4 h reaction time under H₂) with magnetite (Fe₃O₄), cobalt(II,III)oxide (Co₃O₄) and nickel(II)oxide (NiO) using the same amount of metal atoms per mol to test their ability to promote NAD⁺ reduction. In this case, however, no oxide yielded any NADH (Fig. S12). On the other hand, it is also possible that the 1 h reaction served as a pretreatment step (e.g. hydride formation on metal surfaces from either H₂ gas or oxidation of the metals), resulting in the observed higher yield of NADH after 1 h of reaction.

Discussion

We tested Fe, Co and Ni for their ability to reduce NAD⁺ with H₂ gas to establish a connection between

a biotic H[−] donor (NADH) and an abiotic donor (metal hydride). The reduction was performed by all three metals, which however showed differences in their reactivity and response to H₂-pretreatment. The detailed effects of H₂-pretreatment on each of the metals under the present conditions will be investigated further. In this publication, we were able to collect some insights concerning the possible mechanisms in the performed experiments.

Mechanisms: where do the hydrides come from?

Of all three metals, Ni produced the lowest (but still substantial) NADH yields with around 50% after H₂ pretreatment (Fig. 2C), but it employs the most straightforward hydrogenation mechanism, additionally backed up by the results of the experiments with heavy water. Known to enable the dissociation of H₂ [15,64–67], Ni was able to reduce NAD⁺ under H₂ gas and showed the strongest positive response to pretreatment with H₂ gas out of the three metals. This suggests that Ni-bound hydrides are transferred to NAD⁺ to produce mainly 1,4-NADH (s. Fig. 4A). The redox potentials calculated for the experimental conditions (40 °C, 5 bar H₂, pH 8.5) back up the observations (Equation S2) [68,69]: the potential of Ni(OH)₂ + 2 e[−] + 2 H⁺ ↔ Ni⁰ + 2 H₂O (E = −390 mV) is not reducing enough to enable 2 H₂O + 2 e[−] ↔ H₂ + 2 OH[−] (E = −510 mV).

Iron also dissociates H₂ to metal-bound hydrides, but can also produce fresh H₂ from water via metal-

bound hydrides under mild hydrothermal conditions [57,58,70]. This is consistent with the midpoint potential calculated for the experimental conditions: Fe(OH)₂ + 2 e[−] + 2 H⁺ ↔ Fe⁰ + 2 H₂O (E = −550 mV) [68], which is more negative than the redox potential for H₂ formation from H₂O (E = −510 mV). In our experiments, 100% NAD⁺ reduction was reached under all conditions after 4 h with Fe (Fig. 2A). The Fe reactions also benefit from pretreatment with H₂ gas, reaching high NADH yields in shorter times. The mechanistic effect of pretreatment, however, could not be determined. Through further experiments in heavy water (²H₂O) we were able to confirm that the reaction depends on the abundance of ¹H₂ gas: if the reactions take place under a 5 bar ¹H₂ atmosphere, surface dissociation of ¹H₂ seems to be the main pathway, while under Ar atmosphere freshly produced hydrides are apparently transferred from the metal surface (Fig. 4B). Fe is still visibly oxidised (formation of green rust Fe(OH)₂; Fig. S5) under the reducing H₂ atmosphere, but much less so than under Ar. We cannot exclude at this point that these oxidised forms of iron catalytically enhance the reaction with H₂ gas, but experiments we conducted with metal oxides as a proxy suggest they cannot promote NAD⁺ reduction by themselves (Fig. S12).

Following our preliminary report of metal-dependent NAD⁺ reduction with H₂ [71], it was recently reported [72] that iron sulfides can reduce small amounts of NAD⁺, but without an external

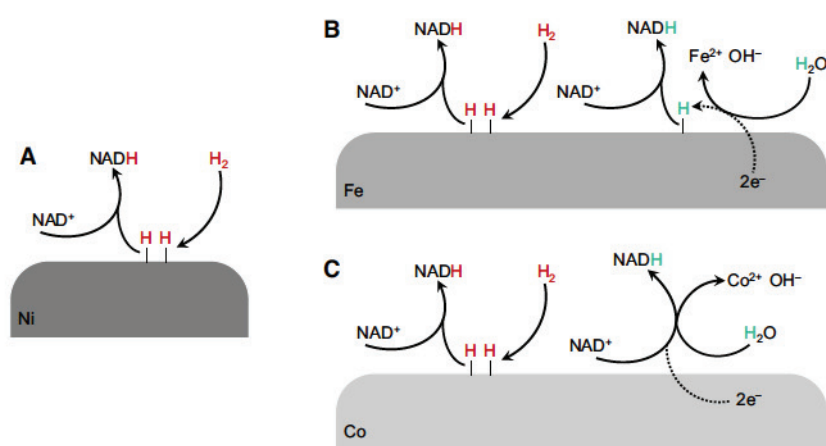


Fig. 4. Proposed mechanisms for NAD⁺ reduction depending on the used metal. (A) H₂ dissociates on the Ni surface. The metal-bound hydrides can then directly reduce NAD⁺ to NADH. (B) Fe employs two different mechanisms, depending on the availability of H₂ gas in the atmosphere. Without H₂, Fe itself delivers the electrons for hydride formation on its surface, the necessary proton comes from H₂O. With H₂ around, Fe is able to assist H₂ dissociation like Ni. (C) Co also is able to activate H₂ to transfer the hydride to NAD⁺. But without H₂ gas in the atmosphere, Co seems to employ a different mechanism than iron. Judging from the electrochemical potentials, it is able to reduce NAD⁺ directly without hydride formation. Note that the absorption of water molecules and/or hydroxides on the metal surfaces are not considered in these depictions.

electron source such as H₂, so the combination of both oxidised iron compounds such as iron sulfides, iron hydroxides or iron oxides and H₂ gas as electron donor has to be investigated further. In the conditions of serpentinizing hydrothermal vents, H₂ is abundant and ubiquitous [38,73], hence it is not clear what kinds of prebiotic environments such reactions in the absence [72] of H₂ would be modelling. In the presence of H₂ under the conditions reported here, NAD⁺ reduction is complete, rapid, and facile. Our experiments were performed under an excess of metal (1 M of metal to 3 mM NAD⁺, so 333 : 1), but lowering the amount of metal in relation to NAD⁺ (20 : 1 and 10 : 1, Fig. S3) did not automatically decrease the NADH yield by the same magnitude—at least for Fe and Co. This either means that the amount of metal does not directly influence the yield, underlining the catalytic character of the metals or that the NAD⁺ concentration is the limiting factor in our 333 : 1 experiments. Nickel is not spent during the reaction and depends on the abundance of H₂ to reduce NAD⁺ which strongly suggests that Ni is acting as a catalyst—an inorganic precursor of an enzyme, a geozyme—for the biochemical reaction. This made the drop of NADH yield between the 333 : 1 (50%) and 20 : 1 (1%) experiments surprising and suggests that the area of the hydrogenated Ni surface has to be quite large to efficiently reduce NAD⁺. As we also observed that Ni yields substantially more NADH under H₂ gas when the reactions take place in ²H₂O instead of H₂O (Fig. 3F), we posit that water molecules quickly cover Ni's surface and thus block the catalytic sites needed for H₂ dissociation. This also could explain why Ni is performing better when pretreated with H₂ before adding the aqueous NAD⁺/buffer: here, metal-bound hydrides can form before the binding sites are blocked by water molecules. Once NADH is being formed, these sites can be taken by water molecules again, which would explain why experiments with Ni do not exceed a 50% yield of NADH. Under geochemical conditions with lower water activity (also found in serpentinizing systems [74,75]), this process might be less of an issue than in the aqueous solutions investigated in our experiments.

Judging from our time-course experiments, we assumed that Co is also able to both dissociate H₂ and produce H₂ *in situ*, as pretreated Co gave the highest yield of 1,4-NADH in the shortest amount of time (Fig. 2B). Co is visibly far more dependent upon the presence of H₂ gas to attain higher NADH yields than Fe. But there is a third mechanism to be considered here, looking at the following midpoint potentials (calculated for the given experimental conditions)

[68,69,76]: although $\text{Co(OH)}_2 + 2\text{e}^- + 2\text{H}^+ \leftrightarrow \text{Co}^0 + 2\text{H}_2\text{O}$ ($E = -407\text{ mV}$) cannot directly enable $2\text{H}_2\text{O} + 2\text{e}^- \leftrightarrow \text{H}_2 + 2\text{OH}^-$ ($E = -510\text{ mV}$), it would be able to reduce $\text{NAD}^+ + 2\text{e}^- + \text{H}^+ \leftrightarrow \text{NADH}$ ($E = -390\text{ mV}$) directly. This might explain why we were not able to demonstrate both mechanisms for Co with the heavy water experiments as we could with Fe. Without H₂, Co did not show any reduction during the 2 h ²H₂O experiments. The data thus indicate that Co is able to dissociate H₂ [77] and transfer electrons to NAD⁺ (either in hydride form or directly), but the results concerning the possibility of a nascent H₂ pathway for Co are not conclusive (Figs. 3C,4C). In case Co is indeed directly transferring electrons to NAD⁺, there might be a kinetic inhibition in the ²H₂O experiments due to slower proton transfer [78].

In a geochemical context, it should be mentioned that in serpentinizing systems we can expect both abiotic hydride donor mechanisms to take place if the electron acceptor will permit: H₂ is constantly produced from H₂O on mineral surfaces (bound hydride intermediate) and dissolved H₂ gas (as a source for freshly chemisorbed hydride) is present in the hydrothermal effluent.

By separating the liquid and the solid phase mid-experiment we were trying to exclude homogeneous catalytic mechanisms (catalysis by metal ions in solution), which are known for hydrogenation reactions [9]. Our results indicate that reactions of the divalent metals do not play a major role in the present reactions. For Ni, this is in line with the role of Ni⁰ in the reaction mechanism of CODH proposed by Ragsdale (2009) [46], although in that reaction, electrons stem from ferredoxin rather than directly from H₂. We explicitly are not excluding colloidal hydroxides as potential catalysts for Fe and Co as we were not able to reliably separate them from the solid phase without changing the rest of the solid phase. However, experiments with Fe₃O₄, Co₃O₄ and NiO under H₂ atmosphere as a proxy for oxidised phases show that they do not promote NADH synthesis at all (Fig. S12).

NAD stability under alkaline conditions and the possibility for reversible reactions

In order to have been useful at life's emergence, NAD had to serve as both hydride donor and hydride acceptor. That means the oxidation/reduction reaction has to be able to proceed in both directions under the given environmental conditions. Very small pH fluctuations could bear upon this issue. From the present data (Fig. S7) we observe that NADH is more stable under (very) alkaline conditions than NAD⁺ which will degrade within a few hours under alkaline

conditions [54]. Also in our reduction experiments (at pH 8.5, usually increasing during the reaction), we observe a loss of NAD⁺ in reactions in which it is not quickly converted to substantial amounts of NADH (Table S1). Under slightly acidic conditions, however (pH < 7), NADH will be oxidised quite quickly. Thus, in an environment in which pH can slightly vacillate around neutral pH, both reduction and oxidation of NAD are possible. Mineral catalysts could probably direct the reversibility at even smaller pH ranges. In serpentinizing systems, local pH microenvironments have an influence on serpentinization rates [79], which might mean serpentinization rates could also have an influence on pH. Depending on the exact mineral composition of a serpentinizing system, pH depends on the buffering characteristics of mineral compounds, such that pH is not a static parameter. Under specific rock compositions, there are even a few acidic serpentinizing systems on modern Earth [38], although the chemical reactions of serpentinization are bound to ultimately make a hydrothermal system alkaline.

Abiotic and biotic hydride donors

Our study shows that metal surfaces can serve as abiotic hydrogenases (or 'geozymes') that can transfer the electrons from H₂ directly to an organic cofactor. This direct transfer of two electrons from H₂ to an organic cofactor, without intervention of one-electron transfer through FeS centres, has only been recently observed for a hydrogenase, namely the F₄₂₀ reducing [Fe] hydrogenase of methanogens and some anaerobic bacteria [22]. Metal hydrides could not only have served as abiotic hydride donors for biological molecules in early evolution, but also bring into focus a possible transition point from abiotic to biotic hydride donors in a prebiotic context. Prior to the origin of hydrogenases, early metabolic systems [6,26,80] were possibly still dependent upon metal hydrides from their geochemical surroundings but at some point an organic molecule that was able to integrate the hydride and transfer it to acceptors such as CO₂ under the given environmental conditions and made the protocell independent of metal hydrides. Though this is a strong hypothesis in need of testing, we note that there are cells living in H₂-rich environments today that appear to lack hydrogenases [39]. Our findings suggest that early redox cofactors might have interacted with H₂ rich environments in a far more complex manner than previously suspected. Our findings also show that in the case of Ni, an essential element of acetogens and methanogens [46], there exists a direct, rapid, and facile reaction between NAD⁺ and metal hydrides. Overall, H₂ gas is able to convert an organic molecule (NAD⁺) to an

organic hydride carrier (NADH) in the absence of enzymes [81], in the presence of native metals [41] under the conditions of H₂ rich hydrothermal vents, which naturally deposit native Ni (and Fe) in the form of the mineral awaruite (Ni₃Fe) [40,82,83].

Materials and methods

Samples with pretreatment

4 mmol of iron powder (Fe⁰; 99.9+ % metals basis, particle size < 10 µm, Alfa Aesar, Thermo Fisher Scientific, Lancashire, UK), cobalt powder (Co⁰; metal basis, particle size 1.6 µm, Alfa Aesar) and nickel powder (Ni⁰; metal basis, particle size 3–7 µm, Alfa Aesar) were placed in reaction glass vials, closed with a PTFE-membrane bearing crimp cap, equipped with a syringe needle for gas exchange, and lastly exposed to 5 bars of H₂ overnight (16 h, 400 r.p.m. and 50 °C) in a stainless-steel high-pressure reactor (BR-300, Berghof Products + Instruments GmbH, Eningen, Germany). Afterwards, for NAD⁺ reduction, a solution of 12 µmol of NAD⁺ (free acid, Merck Millipore, Darmstadt, Germany) in 4 mL of 1 M phosphate buffer (pH 8.5; potassium phosphate monobasic and sodium phosphate dibasic, Honeywell Fluka, Fisher Scientific, Schwerte, Germany; in HPLC-grade water) was prepared and added via a disposable syringe through the needle in the membrane, leading to an overall concentration of 1 M metal. As an experimental control, one additional sample was prepared for every reaction without any metal powder. The samples were reintroduced in the reactor, which was closed tightly and pressurised again with either 5 bar of Ar or 5 bar of H₂, depending on the experiment. For the controls with metal oxides (Fe₃O₄, 50–100 nm, 97% trace metals; Co₃O₄, < 10 µm; NiO, > 99.995% trace metals; Sigma-Aldrich, Taufkirchen, Germany) we used 1 M worth of metal atoms according to each oxide (0.333 M for Co₃O₄ and Fe₃O₄ and 1 M for NiO).

Samples without pretreatment

4 mmol of each metal powder were placed in 5 mL glass vials (beaded rim) with a polytetrafluoroethylene (PTFE)-coated stirring bar. The described NAD⁺ solution in phosphate buffer was pipetted on top, and sealed with a crimp cap with a PTFE-coated membrane. One sample was prepared without metal powder to work as a control. To allow gas exchange between the interior and the exterior of the glass vial, a syringe needle was placed through the crimp cap membrane before the vials were placed in the high-pressure reactor.

Reaction

After pressurising the reactor with either 5 bar of Ar gas (99.998%, Air Liquide, Paris, France) or 5 bar of H₂ gas (99.999%, Air Liquide), the reactions were started and regulated by a temperature controller (BTC-3000, Berghof

Products + Instruments GmbH). Reactions were performed from 0.5 h to 4 h at 40 °C. After the reaction, the reactor was depressurised and the samples (metal powders and solution) were transferred to 2 mL Eppendorf tubes and centrifuged for 15 min at 16 000 *g*. (Biofuge fresco, Heraeus, Hanau, Germany). The supernatants (NAD⁺/NADH) and pellets (metal powders) were subjected to different analyses which are described below.

Separation of metal and supernatant to check for the active catalytic species

To study the liquid and solid phases separately, we separated them after a 1-h reaction with NAD⁺ (5 bar H₂, 40 °C) through hot filtration. The liquid phase was pipetted to a new glass vial with a new PTFE-coated stirring bar and sealed. The solid phase also went into a new glass vial but with a fresh NAD⁺ stock solution. Then, all-glass vials were re-introduced to the reactor to perform another 1-h reaction.

²H₂O controls

Three control experiments were made for Fe and Co: one for pretreatment under Ar, one for reactions with H₂, and another under Ar. Our controls contained ²H₂O instead of the corresponding volume of HPLC-grade water with all other parameters and analytic procedures maintained.

Measurement of pH

The pH after the reaction was measured for all samples containing inorganic catalysts using a Lab 875 Multiparameter Benchtop Meter (SI Analytics, Xylem, Mainz, Germany) and a pH electrode (SI Analytics).

Quantitative ¹H-NMR analysis

To detect and quantify the formation of NADH and side products such as nicotinamide and the decrease of NAD⁺ we used an existing protocol for quantitative proton nuclear magnetic resonance (¹H-NMR) [32,33]. The internal standard was a 7-mm solution of sodium 3-(trimethylsilyl)-1-propanesulfonate (97%, Sigma-Aldrich) in deuterium oxide (CH₃ peak at 0 p.p.m.; ²H₂O or D₂O, D₂O 99.9 atom % D, Sigma-Aldrich), mixed 1:6 with the supernatant of our samples. qNMR spectra were obtained on a Bruker (Billerica, MA, USA) Avance III 600 using a ZGESGP pulse program. Thirty-two scans were made for each sample with a relaxation delay of 40 s (600 MHz) and a spectral width of 12 315 p.p.m. (600 MHz). Analysis and integration were performed using MESTRENOVA (v.10.0.2) software.

UV-Vis Spectroscopy analysis

UV-Vis Spectroscopy was performed in some experiments as a complementary analysis to ¹H-NMR with an Agilent

Technologies (Santa Clara, CA, USA) Cary 300 UV-Vis Compact Peltier spectrometer. Two UV-Quartz cuvettes were used for each measurement, one containing the supernatant of a sample and the other 1 M phosphate buffer (pH 8.5) as a reference value. Analysis was made using the Cary UV Workstation.

Fourier Transform Infrared (FTIR) Measurements

The metals from a 4 h reaction under Ar in ¹H₂O were collected from their glass vials and individually washed with Milli-Q water through suction filtration. Then, the metal samples were dried using a vacuum desiccator overnight and homogenised with a mortar and pestle for analysis. FTIR spectra of the metal powders before and after the reaction were obtained on Perkin Elmer-Spectrum Two (Perkin Elmer, Waltham, USA) utilising an Attenuated Total Reflectance (ATR) geometry with a LaTiO₃ detector. For each measurement, the dry powder was directly measured on the surface of the ATR crystal at room temperature without any pretreatment. Each spectrum was collected with the resolution of 4 cm⁻¹ with 32 scans in the range of 400–4000 cm⁻¹.

Acknowledgements

MP thanks Kamila B. Muchowska, Joseph Moran, and Joana C. Xavier for discussions. MP, DPHP, JL and WFM thank the CeMSA@HHU (Center for Molecular and Structural Analytics @Heinrich Heine University) for recording the NMR-spectroscopic data. WFM and HT thank the Volkswagen Foundation (96_742) and the German Research Foundation (MA-1426/21-1 / TU-315/8-1). HT thanks the Max Planck Society for the basic funding. WFM thanks the European Research Council for funding (Advanced Grant EcolMetabOrigin 101018894).

Conflict of interest

The authors declare no conflict of interest.

Author contributions

MP and DPHP planned experiments; DPHP, TB, and JL performed experiments; MP and DPHP analysed data; MP and DPHP wrote the paper, WFM and KK edited the manuscript; WFM, KK, HT, AV provided supervision of the lab work.

Peer review

The peer review history for this article is available at <https://publons.com/publon/10.1111/febs.16329>.

Data availability statement

The authors confirm that the data supporting the findings of this study are available within the article and its supplementary materials. Original data files (¹H-NMR and FTIR spectra) are available on request from the corresponding author, MP.

References

- Fuchs G. Alternative pathways of carbon dioxide fixation: Insights into the early evolution of life? *Annu Rev Microbiol.* 2011;65:631–58.
- Sleep NH, Meibom A, Fridriksson T, Coleman RG, Bird DK. H₂-rich fluids from serpentinization: geochemical and biotic implications. *Proc Natl Acad Sci USA.* 2004;101:12818–23.
- Porosoff MD, Yan B, Chen JG. Catalytic reduction of CO₂ by H₂ for synthesis of CO, methanol and hydrocarbons: Challenges and opportunities. *Energy Environ Sci.* 2016;9:62–73.
- Thauer RK, Kaster AK, Seedorf H, Buckel W, Hedderich R. Methanogenic archaea: ecologically relevant differences in energy conservation. *Nat Rev Microbiol.* 2008;6:579–91.
- Thauer RK, Kaster A, Goenrich M, Schick M, Hiromoto T, Shima S. Hydrogenases from methanogenic archaea, nickel, a novel cofactor, and H₂ storage. *Annu Rev Biochem.* 2010;79:507–36.
- Weiss MC, Sousa FL, Mrnjavac N, Neukirchen S, Roettger M, Nelson-Sathi S, et al. The physiology and habitat of the last universal common ancestor. *Nat Microbiol.* 2016;1:1–8.
- Sleep NH, Bird DK, Pope EC. Serpentinite and the dawn of life. *Philos Trans R Soc B Biol Sci.* 2011;366:2857–69.
- Martin WF, Bryant DA, Beatty JT. A physiological perspective on the origin and evolution of photosynthesis. *FEMS Microbiol Rev.* 2018;42:205–31.
- Kubas GJ. Fundamentals of H₂ binding and reactivity on transition metals underlying hydrogenase function and H₂ production and storage. *Chem Rev.* 2007;107:4152–205.
- Kubas GJ. Molecular hydrogen complexes: coordination of a σ bond to transition metals bond. *Acc Chem Res.* 1988;21:120–8.
- Ertl G. Primary steps in catalytic synthesis of ammonia. *J Vac Sci Technol.* 1983;1:1247–53.
- Leigh GJ. Haber–Bosch and other industrial processes. In: Smith BE, Richards RL, Newton WE, editors. Catalysts for nitrogen fixation: nitrogenases, relevant chemical models, and commercial processes. Dordrecht: Springer; 2004. p. 33–54.
- Kandemir T, Schuster ME, Senyshyn A, Behrens M, Schlögl R. The Haber-Bosch process revisited: on the real structure and stability of “ammonia iron” under working conditions. *Angew Chemie - Int Ed.* 2013;52:12723–6.
- Pisarev AA. Hydrogen adsorption on the surface of metals. In: Gangloff RP, Somerday BP, editors. Gaseous Hydrogen Embrittlement of Materials in Energy Technologies Part 1. Woodhead Publishing Limited; 2012. p. 3–26.
- Harris J, Andersson S. H₂ dissociation at metal surfaces. *Phys Rev Lett.* 1985;55:1583–6.
- Harris J. Dissociation of H₂ on metal surfaces. *Langmuir.* 1991;7:2528–33.
- Weiss MC, Sousa FL, Mrnjavac N, Neukirchen S, Roettger M, Nelson-Sathi S, et al. The physiology and habitat of the last universal common ancestor. *Nat Microbiol.* 2016;1:16116.
- Thauer RK. Hydrogenases and the global H₂ cycle. *Eur J Inorg Chem.* 2011;7:919–21.
- Fontecilla-Camps JC, Ragsdale SW. Nickel-iron-sulfur active sites: Hydrogenase and CO dehydrogenase. *Adv Inorg Chem.* 1999;47:283–333.
- Lubitz W, Ogata H, Ru O, Reiherse E. Hydrogenases. *Chem Rev.* 2014;114:4081–148.
- Siegbahn PEM, Tye JW, Hall MB. Computational studies of [NiFe] and [FeFe] hydrogenases. *Chem Rev.* 2007;107:4414–35.
- Huang G, Wagner T, Ermler U, Shima S. Methanogenesis involves direct hydride transfer from H₂ to an organic substrate. *Nat Rev Chem.* 2020;4:213–21.
- Buckel W, Thauer RK. Flavin-based electron bifurcation, ferredoxin, flavodoxin, and anaerobic respiration with protons (Ech) or NAD⁺(Rnf) as electron acceptors: A historical review. *Front Microbiol.* 2018;9:401.
- Kurz LC, Frieden C. Anomalous equilibrium and kinetic α-Deuterium secondary isotope effects accompanying hydride transfer from reduced nicotinamide adenine dinucleotide. *J Am Chem Soc.* 1980;102:4198–203.
- Klinman JP. The mechanism of enzyme-catalyzed reduced nicotinamide adenine dinucleotide-dependent reductions. Substituent and isotope effects in the yeast alcohol dehydrogenase reaction. *J Biol Chem.* 1972;247:7977–87.
- Xavier JC, Hordijk W, Kauffman S, Steel M, Martin WF. Autocatalytic chemical networks at the origin of metabolism. *Proc R Soc B Biol Sci.* 2020;287:20192377.
- Buckel W, Thauer RK. Energy conservation via electron bifurcating ferredoxin reduction and proton/Na⁺ translocating ferredoxin oxidation. *Biochim Biophys Acta - Bioenerg.* 2013;1827:94–113.
- Fontecilla-Camps JC. Geochemical continuity and catalyst/cofactor replacement in the emergence and evolution of life. *Angew Chemie - Int Ed.* 2019;58:42–8.

- 29 Camprubi E, Jordan SF, Vasiliadou R, Lane N. Iron catalysis at the origin of life. *IUBMB Life*. 2017;69:373–81.
- 30 Preiner M, Xavier JC, Sousa FL, Zimorski V, Neubeck A, Lang SQ, et al. Serpentinization: Connecting geochemistry, ancient metabolism and industrial hydrogenation. *Life*. 2018;8:41.
- 31 McGlynn SE, Glass JB, Johnson-Finn K, Klein F, Sanden SA, Schrenk MO, et al. Hydrogenation reactions of carbon on Earth: Linking methane, margarine, and life. *Am Mineral*. 2020;105:599–608.
- 32 Preiner M, Igarashi K, Muchowska K, Yu M, Varma SJ, Kleinermanns K, et al. A hydrogen-dependent geochemical analogue of primordial carbon and energy metabolism. *Nat Ecol Evol*. 2020;4:534–42.
- 33 Varma SJ, Muchowska KB, Chatelain P, Moran J. Native iron reduces CO₂ to intermediates and endproducts of the acetyl-CoA pathway. *Nat Ecol Evol*. 2018;2:1019–24.
- 34 Saba T, Burnett JWH, Li J, Kechagiopoulos PN, Wang X. A facile analytical method for reliable selectivity examination in cofactor NADH regeneration. *Chem Commun*. 2020;56:1231–4.
- 35 Wang X, Yiu HHP. Heterogeneous catalysis mediated cofactor NADH regeneration for enzymatic reduction. *ACS Catal*. 2016;6:1880–6.
- 36 Kelley DS, Baross JA, Delaney JR. Volcanoes, fluids, and life at mid-ocean ridge spreading centers. *Annu Rev Earth Planet Sci*. 2002;30:385–491.
- 37 Schrenk MO, Brazelton WJ, Lang SQ. Serpentinization, carbon, and deep life. *Rev Mineral Geochem*. 2013;75:575–606.
- 38 Charlou JL, Donval JP, Fouquet Y, Jean-Baptiste P, Holm N. Geochemistry of high H₂ and CH₄ vent fluids issuing from ultramafic rocks at the Rainbow hydrothermal field (36°14'N, MAR). *Chem Geol*. 2002;191:345–59.
- 39 Suzuki S, Nealson KH, Ishii S. Genomic and in-situ transcriptomic characterization of the candidate phylum NPL-UPL2 from highly alkaline highly reducing serpentinized groundwater. *Front Microbiol*. 2018;9:1–13.
- 40 Klein F, Bach W. Fe-Ni-Co-O-S phase relations in peridotite-seawater interactions. *J Petrol*. 2009;50:37–59.
- 41 Sousa FL, Preiner M, Martin WF. Native metals, electron bifurcation, and CO₂ reduction in early biochemical evolution. *Curr Opin Microbiol*. 2018;43:77–83.
- 42 Hawco NJ, Mcilvin MM, Bundy RM, Tagliabue A. Minimal cobalt metabolism in the marine cyanobacterium *Prochlorococcus*. *Proc Natl Acad Sci USA*. 2020;117:15740.
- 43 Eckenhoff WT, Mcnamara WR, Du P, Eisenberg R. Cobalt complexes as artificial hydrogenases for the reductive side of water splitting. *Biochim Biophys Acta*. 2013;1827:958–73.
- 44 Ilic S, Pandey Kadel U, Basdogan Y, Keith JA, Glusac KD. Thermodynamic hydricities of biomimetic organic hydride donors. *J Am Chem Soc*. 2018;140:4569–79.
- 45 McCollom TM, Seewald JS. Serpentinities, hydrogen, and life. *Elements*. 2013;9:129–34.
- 46 Ragsdale SW. Nickel-based enzyme systems. *J Biol Chem*. 2009;284:18571–5.
- 47 Fuchs G. CO₂ fixation in acetogenic bacteria: variations on a theme. *FEMS Microbiol Lett*. 1986;39:181–213.
- 48 Xavier JC, Preiner M, Martin WF. Something special about CO-dependent CO₂ fixation. *FEBS Lett*. 2018;285:4181–95.
- 49 Degraaf RA, Behar KL. Detection of cerebral NAD⁺ by *in vivo* ¹H NMR spectroscopy. *NMR Biomed*. 2014;27:802–9.
- 50 Shabalin K, Nerinovski K, Yakimov A, Kulikova V, Svetlova M, Solovjeva L, et al. NAD metabolome analysis in human cells using ¹H NMR spectroscopy. *Int J Mol Sci*. 2018;19:3906.
- 51 Christmann K. Adsorption of hydrogen on a Nickel (100) surface. *Zeitschrift Für Naturforsch*. 1979;34:22–9.
- 52 Christmann K. Hydrogen transfer on metal surfaces. In: Hynes JT, Klinman JP, Limbach HH, Schowen RL, editors. Hydrogen-transfer reactions. Weinheim, Germany: Wiley-VCH Verlag GmbH & Co. KGaA; 2007. p. 751–86.
- 53 Christmann K. Interaction of hydrogen with solid surfaces. *Surf Sci Rep*. 1988;9:1–163.
- 54 Oppenheimer NJ. NAD hydrolysis: Chemical and enzymatic mechanisms. *Mol Cell Biochem*. 1994;138:245–51.
- 55 Rover LJ, Fernandes JCB, de Oliveira G, Kubota LT, Katekawa E, Serrano SHP. Study of NADH stability using ultraviolet-visible spectrophotometric analysis and factorial design. *Anal Biochem*. 1998;55:50–5.
- 56 Gayer KH, Woontner L. The solubility of ferrous hydroxide and ferric hydroxide in acidic and basic media at 25°. *J Phys Chem*. 1956;60:1569–71.
- 57 Fábos V, Yuen AKL, Masters AF, Maschmeyer T. Exploring the myth of nascent hydrogen and its implications for biomass conversions. *Chem - an Asian J*. 2012;7:2629–37.
- 58 Michiels K, Spooren J, Meynen V. Production of hydrogen gas from water by the oxidation of metallic iron under mild hydrothermal conditions, assisted by *in situ* formed carbonate ions. *Fuel*. 2015;160:205–16.
- 59 Morawski B, Casy G, Illaszewicz C, Griengl H, Ribbons DW. Stereochemical course of two arene-cis-diol dehydrogenases specifically induced in *Pseudomonas putida*. *J Bacteriol*. 1997;179:4023–9.
- 60 Rowbotham JS, Reeve HA, Vincent KA. Hybrid chemo-, bio-, and electrocatalysis for atom-efficient deuteration of cofactors in heavy water. *ACS Catal*. 2021;11:2596–604.

- 61 Kasza RV, Griffiths K, Shapter JG, Norton PR, Harrington DA. Interaction of water with stepped Ni (760): Associative versus dissociative adsorption and autocatalytic decomposition. *Surf Sci.* 1996;356:195–208.
- 62 Zhou X, Wang L, Fan X, Wilfong B, Liou SC, Wang Y, et al. Isotope effect between H₂O and D₂O in hydrothermal synthesis. *Chem Mater.* 2020;32:769–75.
- 63 Farjamnia A, Jackson B. The dissociative chemisorption of water on Ni(111): Mode- and bond-selective chemistry on metal surfaces. *J Chem Phys.* 2015;142:234705.
- 64 Wang T, Ren D, Huo Z, Song Z, Jin F, Chen M, et al. A nanoporous nickel catalyst for selective hydrogenation of carbonates into formic acid in water. *Green Chem.* 2017;19:716–21.
- 65 Bhatia B, Sholl DS. Chemisorption and diffusion of hydrogen on surface and subsurface sites of flat and stepped nickel surfaces. *J Chem Phys.* 2005;122:204707.
- 66 Weng MH, Chen H, Wang Y, Ju S, Chang J. Kinetics and mechanisms for the adsorption, dissociation, and diffusion of hydrogen in Ni and Ni/YSZ Slabs: a DFT study. *Langmuir.* 2012;28:5596–605.
- 67 Christmann K. Hydrogen transfer on metal surfaces. In Hynes JT, Klinman JP, Limbach H-H, Schowen RL, editors. Hydrogen-transfer reactions. WILEY-VCH Verlag; 2007. p. 751–86.
- 68 Pourbaix M. Establishment and interpretation of potential-pH equilibrium diagrams of Fe Co, Ni. In Atlas of electrochemical equilibria in aqueous solutions. National Association of Corrosion Engineers; 1974. p. 307–343.
- 69 Haynes JW, Lide DR, Bruno TJ, editors. CRC Handbook of chemistry and physics, 93rd edn. Taylor and Francis Group: CRC Press; 2012.
- 70 Duo J, Jin F, Wang Y, Zhong H, Lyu L, Yao G, et al. NaHCO₃-enhanced hydrogen production from water with Fe and in-situ highly efficient and autocatalytic NaHCO₃ reduction into formic acid. *Chem Commun.* 2016;52:3316–9.
- 71 Pereira DPH, do Nascimento Vieira A, Kleinermanns K, Martin WF, Preiner M. Serpentinizing systems and hydrogen activation in early metabolism. *Life.* 2021;8:41.
- 72 Weber JM, Henderson BL, LaRowe DE, Goldman AD, Perl SM, Billings K, et al. Testing abiotic reduction of NAD⁺ directly mediated by iron/sulfur minerals. *Astrobiology.* 2021;22:1–10.
- 73 Lang SQ, Brazelton WJ. Habitability of the marine serpentinite subsurface: a case study of the Lost City hydrothermal field. *Philos Trans R Soc A.* 2020;378:20180429.
- 74 Lamadrid HM, Rimstidt JD, Schwarzenbach EM, Klein F, Ulrich S, Dolocan A, et al. Effect of water activity on rates of serpentinization of olivine. *Nat Commun.* 2017;8:16107.
- 75 do Nascimento Vieira A, Kleinermanns K, Martin WF, Preiner M. The ambivalent role of water at the origins of life. *FEBS Lett.* 2020;594:2727–33.
- 76 Huang H, Wang S, Moll J, Thauer RK. Electron bifurcation involved in the energy metabolism of the acetogenic bacterium *Moorella thermoacetica* growing on glucose or H₂ plus CO₂. *J Bacteriol.* 2012;194:3689–99.
- 77 Lewis EA, Le D, Murphy CJ, Jewell AD, Mattera MFG, Liriano ML, et al. Dissociative hydrogen adsorption on close-packed cobalt nanoparticle surfaces. *J Phys Chem C.* 2012;116:25868–73.
- 78 Huynh MHV, Meyer TJ, Cn CH, Nh DOM, Kno PF, The C. Colossal kinetic isotope effects in proton-coupled electron transfer. *Proc Natl Acad Sci.* 2004;101:13138–41.
- 79 McCollom TM, Klein F, Solheid P, Moskowitz B, Mccollom TM. The effect of pH on rates of reaction and hydrogen generation during serpentinization. *Philos Trans A.* 2020;378:20180428.
- 80 Weiss MC, Preiner M, Xavier JC, Zimorski V, Martin F. The last universal common ancestor between ancient Earth chemistry and the onset of genetics. *PloS Genet.* 2018;14:e1007518.
- 81 Muchowska KB, Varma SJ, Moran J. Nonenzymatic metabolic reactions and life's origins. *Chem Rev.* 2020;120:7708–44.
- 82 Plümper O, King HE, Geisler T, Liu Y, Pabst S, Savov IP, et al. Subduction zone forearc serpentinites as incubators for deep microbial life. *Proc Natl Acad Sci.* 2017;114:4324–29.
- 83 McCollom TM. Abiotic methane formation during experimental serpentinization of olivine. *Proc Natl Acad Sci USA.* 2016;113:13965–70.
- 84 Saba T, Li J, Burnett JWH, Howe RF, Kechagiopoulos PN, Wang X. NADH regeneration: a case study of Pt-catalyzed NAD⁺ reduction with H₂. *ACS Catal.* 2021;11:283–9.

Supporting information

Additional supporting information may be found online in the Supporting Information section at the end of the article.

Table S1. Single values of performed experiments.

Table S2. Relative quantity of ¹H atoms in the fourth position of the nicotinamide ring of NADH.

Fig. S1. Overview of experimental setup for timecourse NAD⁺ reduction experiments.

Fig. S2. Overview of ¹H-NMR spectra of all conducted experiments.

Fig. S3. Experiments with pretreated metals after 4 h at 40 °C under H₂ with a far lower concentration of metal powder.

Fig. S4. pH shift during experiments.

Fig. S5. Change of sample colouration during reaction.

Fig. S6. The effect of a higher concentrated buffer on pH stability and consequent NAD stability monitored via ¹H-NMR.

Fig. S7. Stability of NAD⁺ and NADH under different pH.

Fig. S8. FTIR measurements of Ni, Co and Fe before and after reaction.

Fig. S9. ¹H-NMR spectra of ²H₂O experiment with H₂-pretreated Fe under Ar.

Fig. S10. Schematic of hot filtration experiments.

Fig. S11. NADH synthesis before (Reaction 1) and after (Reaction 2) hot filtration.

Fig. S12. ¹H-NMR spectra of NAD⁺ with iron, cobalt and nickel oxides after reaction.

Equation S1. Calculation of H₂ concentration – Henry's law.

Equation S2. Calculation of electrochemical potential of H₂ at a given partial pressure and pH – Nernst equation.

Publication II – A possible pre-enzymatic role of the “non-functional” tail of NAD: specific reduction on mineral surfaces

Year: 2024

Authors: Delfina P. Henriques Pereira*, Xiulan Xie, Tuğçe Beyazay, Nicole Paczia, Zainab Subrati, Jürgen Belz, Kerstin Volz, Harun Tüysüz, Martina Preiner*

In revision for: Proceedings of the National Academy of Sciences (PNAS)

Contribution: First and corresponding author.

Involved in planning all experiments. Supervised preliminary work related to the publication, and performed all published experiments with NMN, NAD and metals. The obtained samples were prepared by me for analysis. The measurement was often performed by experts, except cyclic voltammetry (CV), which I did personally. Helped developing the protocol for ¹H-NMR quantification and LC-MS measurements. Analysed and discussed the data obtained from CV, LC-MS, and qNMR. Responsible for organizing the Supplementary Information and assisting with writing and making figures for the main text.

Summary: This publication is insightful of the effects that minerals with different Ni/Fe ratios can have on the 1,4-regioselectivity of nicotinamide cofactors. While NAD is reduced in a stable manner despite of the catalysts, nicotinamide mononucleotide (NMN) is over-reduced and hydrolysed easily by Ni catalysts. The ADP moiety seems to stabilize 1,4-NADH under prebiotic conditions, preventing further reactions, an interesting observation considering that many ancient cofactors have this “handle”.

Main Manuscript for

A possible pre-enzymatic role of the “non-functional” tail of NAD: specific reduction on mineral surfaces

Delfina P. Henriques Pereira^{*a,b}, Xiulan Xie^c, Zainab Subrati^{a,b}, Tuğçe Beyazay^d, Nicole Paczia^e, Jürgen Belz^f, Kerstin Volz^f, Harun Tüysüz^{d,g}, Martina Preiner^{*a,b}

^a Microcosm Earth Center

Max-Planck-Institute for Terrestrial Microbiology and Philipps-University Marburg
Hans-Meerwein-Str. 4; 35032 Marburg (Germany)

^b Geochemical Protoenzymes Research Group

Max-Planck-Institute for Terrestrial Microbiology
Karl-von-Frisch-Str. 10; 35043 Marburg (Germany)

^c Department of Chemistry

Philipps University Marburg
Hans-Meerwein-Str. 4; 35032 Marburg (Germany)

^d Heterogeneous Catalysis

Max-Planck-Institut für Kohlenforschung
Kaiser-Wilhelm-Platz 1; 45470 Mülheim an der Ruhr (Germany)

^e Metabolomics and small molecule mass spectrometry

Max-Planck-Institute for Terrestrial Microbiology
Karl-von-Frisch-Str. 10; 35043 Marburg (Germany)

^f Department of Physics

Philipps University Marburg
Hans-Meerwein-Straße 6; 35032 Marburg (Germany)

^g IMDEA Materials Institute

C/ Eric Kandel 2, 28906 – Getafe, Madrid (Spain)

*Corresponding authors: Martina Preiner, Delfina P. Henriques Pereira

Email: martina.preiner@mpi-marburg.mpg.de; delfina.pereira@mpi-marburg.mpg.de

Author Contributions: Conceptualization: M.P. & D.P.H.P. Methodology: M.P. & D.P.H.P. Investigation: D.P.H.P., M.P., Z.S., T.B. Validation: D.P.H.P., Z.S. & X.X. Formal analysis: X.X., J.B., N.P., D.P.H.P. & M.P. Resources: H.T., K.V. Writing Original Draft: M.P. & D.P.H.P. Writing Review & Editing: all authors. Visualization: M.P., D.P.H.P. & X.X. Supervision: M.P.

Competing Interest Statement: Disclose any competing interests here.

Classification: Biological Sciences, Biochemistry – Chemistry.

Paste the major and minor classification here. Dual classifications are permitted, but cannot be within the same major classification.

Keywords: nucleotide cofactors; hydrogen; emergence of life; mineral catalysis; protometabolism

This PDF file includes:

Main Text
Figures 1 to 6
Table 1

Abstract

Nucleotide-derived cofactors could function as a missing link between the informational and the metabolic part at life's emergence. One well-known example is nicotinamide dinucleotide (NAD), one of the evolutionarily most conserved redox cofactors found in metabolism. Here, we propose that the role of these cofactors could even extend to missing links between geo- and biochemistry. We first show how NAD⁺ can be reduced specifically to the biologically relevant form of NADH under close-to nature conditions with nickel-iron-alloys found in water-rock-interaction settings rich in hydrogen (serpentinizing systems). Our study then revealed that the adenosine monophosphate (AMP) "tail" of the dinucleotide, a shared trait between many organic cofactors, seems to play a crucial mechanistic role in preventing overreduction of the nicotinamide-bearing nucleotide in our mineral-based setup. Experiments with nicotinamide mononucleotide (NMN), a precursor molecule to NAD lacking the AMP part, show that NMN gets reduced far less specifically than NAD, leading to a variety of reduction side products. When reduced in direct competition, the concentration of 1,4-NADH always surpasses that of NMNH. Furthermore testing the reducing abilities of both NADH and NMNH under abiotic conditions showed that both molecules act as equally effective, soluble hydride donors, while overreduction products were shown to have less reducing strength. This and the observation that reduction specificity also depends on type of present transition metal, leads to the conclusion that the environment could have had an important influence on a prebiotic, pre-enzymatic selection of cofactors.

Significance Statement

Many central organic cofactors share a molecular structure: the adenosine-derived "tail". So far, it is mostly seen as a recognition handle for enzymes with no specific prebiotic role. Using the example of the most central redox cofactor nicotinamide dinucleotide (NAD), we demonstrate how this attachment enables a specific hydride transfer from mineral surfaces. These findings lay the foundation for potentially explaining how this "tail" became a universal structure in metabolism and a promising approach towards investigating the emergence of metabolism.

Main Text

Introduction

To form connections between undirected geochemical reactions and the first, directed, potentially even autocatalytic chemical reactions ultimately leading to metabolism, organic cofactors have dropped in and out of focus of research for decades (1–10). These cofactors are a common denominator between “information first” and “metabolism first” emergence of life hypotheses and thus might help to actively bridge this dated temporal separation of life’s most central components (1, 11). The prebiotic synthesis of several organic cofactors was described or hypothesized via numerous synthetic ways (3, 9, 11). Based on theoretical work cofactors could have preceded enzymatic reactions playing central parts of self-sustaining non-enzymatic reaction networks (2, 12). Many central cofactors are structurally related, mostly via an adenosine-derived “tail” added to a chemically active group (s. Fig.1). In biology, this tail mainly seems to have a recognition function for enzymes (13, 14). The chemical properties and impact of this tail to the molecular dynamics of the molecule, however, remain largely underexplored, with only a few exceptions (5). Even when cofactors do not exhibit an obvious molecular connection such as adenosine, many (e.g. pterins or folates) derive from nucleotides in their biosynthesis (8, 15–17).

An important aspect of evaluating the role of common nucleotide structures in organic cofactors as the adenosine-derived “tail” is to investigate its function in a non-biochemical setting (5). So to take one of the most central organic cofactors, NAD, as an example: how much are the hydride transfers onto and from the nicotinamide influenced by the non-redox active adenosine

part? Getting insight into the mechanisms in question is one of the main goals of this study, focussing on extant biomolecules rather than unknown prebiotic precursors.

NAD is a central redox cofactor in metabolism and is presumed to trace back to the Last Universal Common Ancestor (LUCA) of Archaea and Bacteria – and

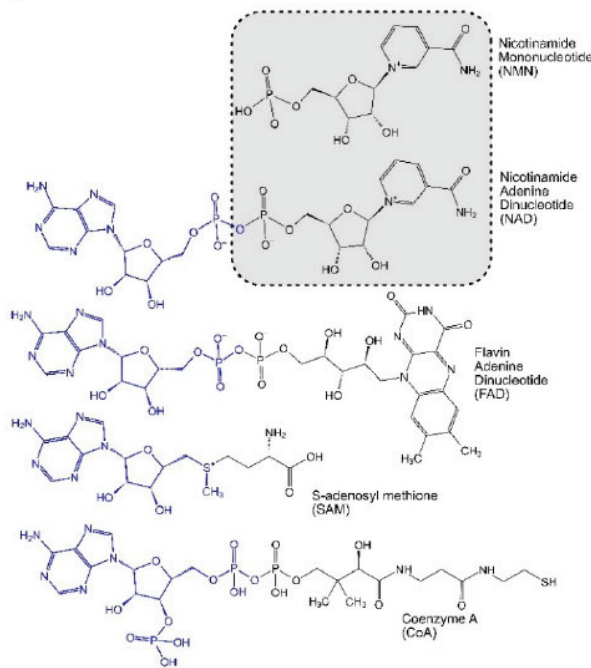


Figure 1. A selection of central organic cofactors with an adenosine-based tail (blue) connected to a functional part that determines the role of these cofactors in metabolism (black): Electron/hydride transfer, methyl transfer or acetyl-transfer. In grey, the function-associated half of nicotinamide dinucleotide (NAD) is highlighted: nicotinamide mononucleotide (NMN).

possibly beyond (2, 18, 19). In a previous study we demonstrated that NAD^+ can react with H_2 and metal powder (Ni, Co, Fe) to specifically form the biologically relevant form of reduced NAD (1,4-NADH) under hydrothermal conditions, however using the metal powders in great excess (333:1) (20). Another study achieved NAD^+ reduction without H_2 – but also rather low yields – with iron sulfides (21). These publications introduced

organic cofactors as possible transition points between geo- and biochemistry. Prior to these studies, only application-oriented heterogeneous catalysis pathways for the hydrogenation of NAD⁺ had been described (22).

When it comes to NAD's prebiotic synthesis pathways, several have been proposed e.g. via mineral-assisted synthesis under hydrothermal conditions (9, 23) or achieved in parts via nitrile- and amino acid derived pathways (11, 24, 25). This study starts from the assumption that nicotinamides were synthesized under prebiotic conditions and aims to evaluate whether the described adenine-derived tail could have played a role in a non-enzymatic context as well.

Approaching prebiotic redox reactions, one has to think about a possible primary electron source in the geochemical setting. Here, we are mainly investigating the options of water-rock-interaction systems, where protons of water are being reduced to hydrogen (H₂) gas by electrons of Fe(II) containing minerals (serpentinizing systems) (26, 27). Minerals found in such systems are known to promote hydrogen activation and electron transfer for CO₂ fixation (28–30). Apart from water-rock interactions constituting a rather simple, likely wide-spread geological scenario on a mostly unknown early Earth, H₂ as an ancient electron source makes a lot of sense from a biological perspective as well. Looking at the reconstructed physiology of LUCA, it is likely that these first cells lived as anaerobic autotrophs, so were fixing carbon dioxide (CO₂) with the electrons provided by H₂ (19, 31–33) – a metabolic pathway still employed by many autotrophic prokaryotes today (34). In order to access the electrons of H₂, these organisms possess enzymes called hydrogenases, which, depending on the exact organism, employ either Fe or Fe and Ni in their active centers (35).

Incidentally, serpentinizing systems are rich in Fe and, depending on the system, can also be abundant in Ni as well. Hotter systems tend to feature Ni-Fe-alloys with higher nickel composition, while cooler ones are richer in iron (36). Nickel-containing intermetallic compounds such as awaruite (Ni₃Fe) or taenite (NiFe₃ to Ni₂Fe) are products of the reaction of H₂ with Ni(II) compounds in serpentinizing systems (36–38) and are also found in meteorites (39). Native metals are also not impossible to find, if the conditions on site are reducing enough (40, 41). In this study, we first tested various naturally occurring Ni- and Fe-containing compounds as “proto-hydrogenases” for NAD⁺ reduction and then compared NAD to NMN under hydrothermal conditions, to assess the relevancy of the adenosine-derived tail in pre-enzymatic reduction. We investigated the stability, reducibility and specificity of these organic cofactors and reduction products.

Results

Screening naturally occurring iron and nickel containing minerals. Ni-Fe containing minerals found in hydrothermal settings were tested for the reduction of NAD⁺ under conditions comparable to those found in mild serpentinizing hydrothermal systems (40 °C, 0.133 M phosphate buffer pH 8.5, 5 bar H₂, **SI Appendix Scheme S1**). These nanoparticulate mineral powders were synthesized from scratch via the nano-casting method by using tea leaves as a template and were previously

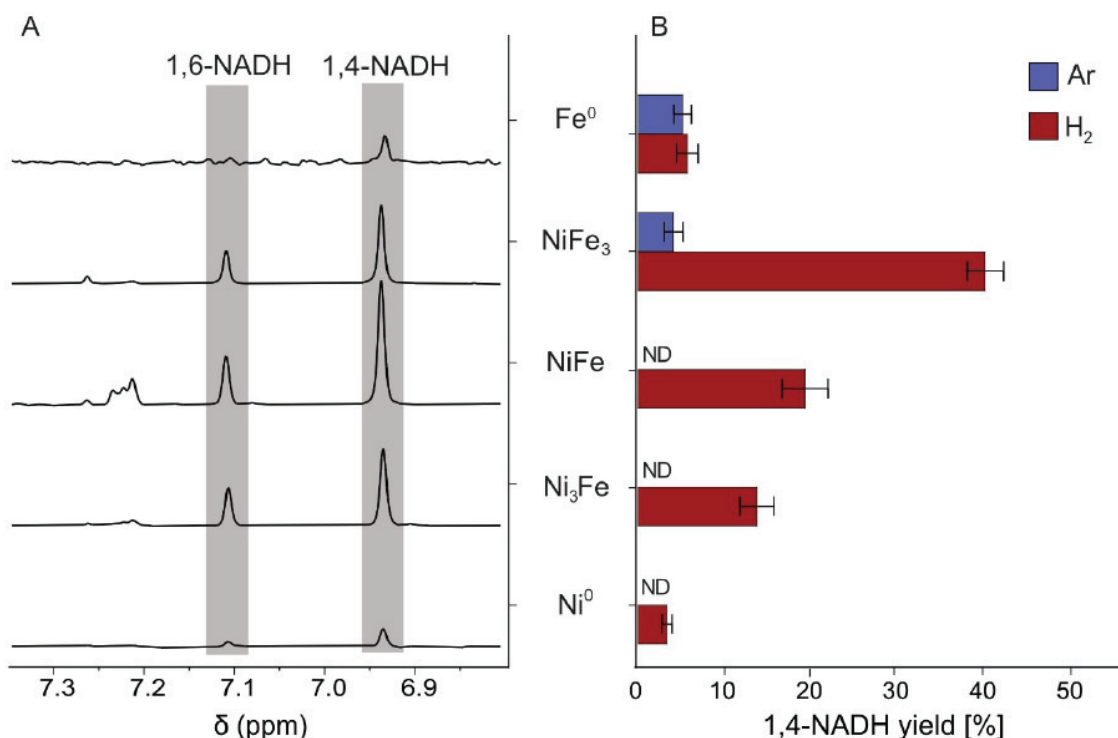


Figure 2. NAD⁺ reduction at 40 °C over 4 h with equimolar amounts (normalized to 1 metal atom per NAD molecule) of several Ni-Fe-alloys and 5 bar of H₂ (or Ar). A) Segment of the ¹H-NMR spectra where the chemical shift of the hydrogen on the 2nd nicotinamide carbon is visible upon reduction. 1,4-NADH features a characteristic peak at δ = 6.9 ppm and 1,6-NADH at δ = 7.1 ppm (*SI Appendix Table 1*). B) Yield of 1,4-NADH obtained for several metals after 4 h under H₂ and Ar. Reduction under Ar is detected only with minerals whose metal content is ≥ 75% Fe. With 5 bar of H₂, all metals can facilitate 1,4-NADH synthesis. Mixed alloys are more efficient than the pure metals. All spectra and yields can be found in *SI Appendix Tabs. S2–S3, SI Figs. S1 and S2*.

characterized (29, 42). The metal content in these reactions is equivalent to that of the cofactor (1 metal atom per cofactor). The resulting H₂ concentration at our conditions is 3.6 mM (using Henry's law, s. *SI Appendix Equations S1–S3* and references (18, 26)), which is comparable to the H₂ concentrations found in the effluent of serpentinizing systems (43, 44). The buffer was bubbled with N₂ for 1 h and handled inside a glove box to approximate the anoxic conditions on early Earth. Several controls were implemented, including controls without metal and H₂, respectively. The liquid phase was analysed by ¹H-NMR.

After 4 h under H₂, 1,4- and 1,6-NADH formed in all samples at different yields, the reaction with nanoparticulate NiFe₃ (nNiFe₃) yielding the most NADH (Fig. 2). Control experiments starting from 1,4-NADH showed that 1,6-NADH is very likely a product of rearrangement from 1,4-NADH – with only a marginal influence of the used metals (*SI Appendix Scheme S2, SI Tabs. S4 and S5, SI Figs. S3*). Samples under Ar also produced NADH with a Fe-rich minerals (nNiFe₃, nFe). In addition to transferring hydrides from H₂ to NAD⁺, iron can oxidize, donating its own electrons either by producing nascent H₂ gas, ultimately reducing NAD⁺ or by direct electron transfer to NAD⁺. This

process can also be used as a proxy for the constant H₂-production in serpentinizing systems (20). Ni by itself is H₂-dependent in the promotion of NAD⁺ reduction.

STEM imaging before and after the reactions (the latter including a washing and dilution step to assure true surface alteration) confirms that Fe, both under Ar and H₂, gets associated with phosphate ions in ratio that suggests the formation of iron phosphate. Ni does not associate with phosphate, suggesting it stays in its native form (*SI Appendix methods and SI Figs. S4–S7*).

In Ni-rich minerals, the Fe is expected to slowly reduce NAD under Ar conditions. However, it is likely that the resulting products do not reach the detection threshold within 4 h. Overall, bimetallic minerals are significantly more efficient than the individual transition metals when hydrogen is available. Introducing one Ni atom to a Fe atom increases the yield by 300% (nNiFe vs. nFe). Their properties, already observed in a previous study (20), seem to complement each other for the reduction of NAD⁺ with H₂: Fe being mostly an electron donor, while Ni promotes hydride transfer from H₂. These complementary roles have also been described in other publications, suggesting charge transfers from Fe (more electropositive) to Ni could increase the electron density in Ni (29, 45).

The “universal” adenine nucleotide in organic cofactors. Many central cofactors share an adenosine-derived tail (Fig. 1) attached to a “functional” part. In the case of NAD, we define NMN as the functional part (containing the hydride-transferring nicotinamide) and adenosine monophosphate (AMP) as the adenosine-derived tail. NAD is stable in water, with its pH range depending on the reduction state of the nicotinamide: NADH is more stable at pH>7, while NAD⁺ is more stable under acidic conditions (20). To investigate the role of the AMP-tail in a prebiotic context, several experiments were designed to compare NAD and NMN. We initially focussed on nNiFe₃, the most efficient of the Ni-Fe minerals in the above described NAD experiment (s. Fig. 2). All other reaction conditions (buffer, pH, temperature, metal to cofactor ratio) were maintained (*SI Appendix Schemes S3*). Products were quantified via ¹H-NMR spectroscopy.

Without metals, NMN does not react and remained stable (*SI Appendix Figs. S8 and S9*). Under Ar, NMN still got reduced due to the abundant iron in the mineral compound, but more slowly than under H₂ (*SI Appendix Tabs. S6 and S7*).

Additionally to the 2 h experiment with NAD⁺ under H₂ showed the increase of 1,4- and 1,6-NADH to be steady and inversely proportional to the decrease of NAD⁺ in solution (**Fig. 3C**). After 4 h with nNiFe₃, on average 57% of NAD⁺ was reduced with 26% remaining oxidized. The remaining 17% can in part be attributed to nicotinamide formation but also unassigned degradation reactions and loss via surface absorption (46).

NMN, however, shows a completely different reaction profile (Fig. 3D). After only 1 h, 69% of the starting NMN had been consumed, and a variety of products was observed in 1D ¹H-NMR (Fig. 3A). 2D-NMR spectroscopy facilitated the identification of the overreduction of NMN's nicotinamide ring with two and three hydrogenation sites, so 1,4,6-NMNH₃ (**2c**), and 1,2,4,6-NMNH₅ (**2d**) respectively (Figs. 3A, B and D). While the fully reduced species **2d** formed quickly and its concentration remained constant over time, the concentration of twice reduced **2c** increased with once reduced 1,4-NMNH decreasing. This indicates that not all reductions are a step-wise process (s. Fig. 3B), especially in the case of **2d**.

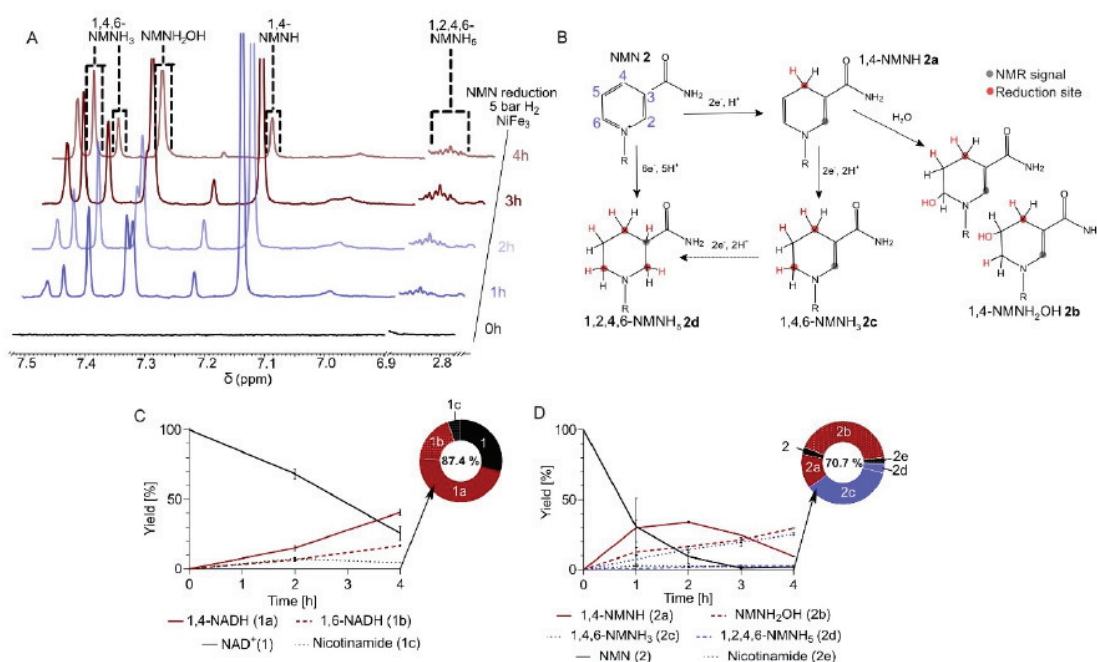


Figure 3. The reduction of NMN and NAD⁺ promoted with equimolar quantities of NiFe₃ nanopowder (normalized to the number of metal atoms) and 5 bar of H₂ (40 °C) was monitored for 4 h (*SI Appendix Schemes S2 and S3*). Both reactions were carried out in oxygen-free, aqueous solutions at a pH of 8.5 (0.133 M phosphate buffer). A) ¹H-NMR (600MHz) spectra monitoring NMN reduction over time. Dashed lines mark the peaks used for identifying and quantifying reduced NMN species previously identified via 2D NMR (*SI Appendix Table S8*). Due to the complexity of the mixture not all peaks could be assigned (*SI Appendix Scheme S4 and S5, Figs. S11–22*) B) Proposed mechanism for NMN reduction with H₂ and Ni-Fe minerals. The reduction site and additional protons are highlighted in red. Full arrows represent proposed reaction mechanisms supported by the data obtained, while the dashed arrow is an additional reaction that could not be entirely excluded. Grey circles indicate the proton providing the NMR signal for quantification. In bold font numeral assignments for NMN reduction products are made. C) Time course of NAD⁺ reduction (*SI Appendix Schemes S6*). Reduced NAD species are plotted as relative percentage to a metal-free control sample (*SI Methods*) – all time points represent the mean and SD of at least triplicates of the same reaction. The ring chart represents the distribution of products after 4 h, percentage in the center indicates the entirety of assigned products. D) Time course of NMN reduction (*SI Appendix Schemes S7*). Reduced NMN species are plotted as relative percentage to a metal-free control sample – all time points represent the mean and SD of at least triplicates of the same reaction. The ring chart represents the distribution of products after 4 h, percentage in the center indicates the entirety of assigned products. Yields shown in C) and D) are also listed in detail in *SI Appendix Tab. S9 and S10 and SI Appendix Fig. S23 and S24*

Under Ar, 2d did not form at all, demonstrating that H₂ is necessary for the full hydrogenation of the nicotinamide ring (*SI Appendix Tab. S7, Fig. S9*). 2c, however, was also forming under Ar, albeit in far lower yields (3%) than under H₂ (25%) after 4h. The yield of 1,4-NMNH was relatively similar in both atmospheres (7% under Ar; 10% under H₂). Transferring these observations to environmental conditions suggests that less reducing conditions could be favourable for specific NMN reduction.

The above mentioned products accumulated in different amounts, 1,4-NMNH being the main product after 1 h under H₂ (Fig. 3A and D). Other side products formed at a comparable rate, rapidly depleting the reagent NMN. Consequently, the production of 1,4-NMNH seems to have stopped after 2 h and subsequently began to decrease in concentration. The concentration of **2c** continuously increased over time. Even though the concentration of 1,4-NMNH decreased from 35% to 9% in 2 h, the total amount of reduced NMN remained relatively stable, exceeding 60%. This suggests that 1,4-NMNH is the first and main product of NMN reduction, which can subsequently undergo further reduction to other species, mainly **2c**.

We were able to exclude two products commonly found in NAD⁺ reduction, where the 2nd or 6th carbon of the nicotinamide ring is reduced (22, 47, 48). Subsequently, reduction products presumably starting with these two one-time reduced products could be excluded (*SI Appendix Scheme S4 and S8, Figs. S12, S13, S25–28*). In the case of NADH, its 1,2-reduced form is known to be unstable, so it is likely this is the case with 1,2-NMNH as well, leading to its absence in our reaction (49).

In the case of 1,4-NMNH loss over time, we saw several routes: i) mainly the further reduction to **2c**, ii) 1,4-NMNH getting hydrolysed at its 5th or 6th position, and iii) 1,4-NMNH engaging in various dimerization reactions with 1,6-NMNH (Diels-Alder type reactions; *SI Appendix Scheme S5*). Via Liquid Chromatography Mass Spectroscopy (LC-MS) we were able to exclude such

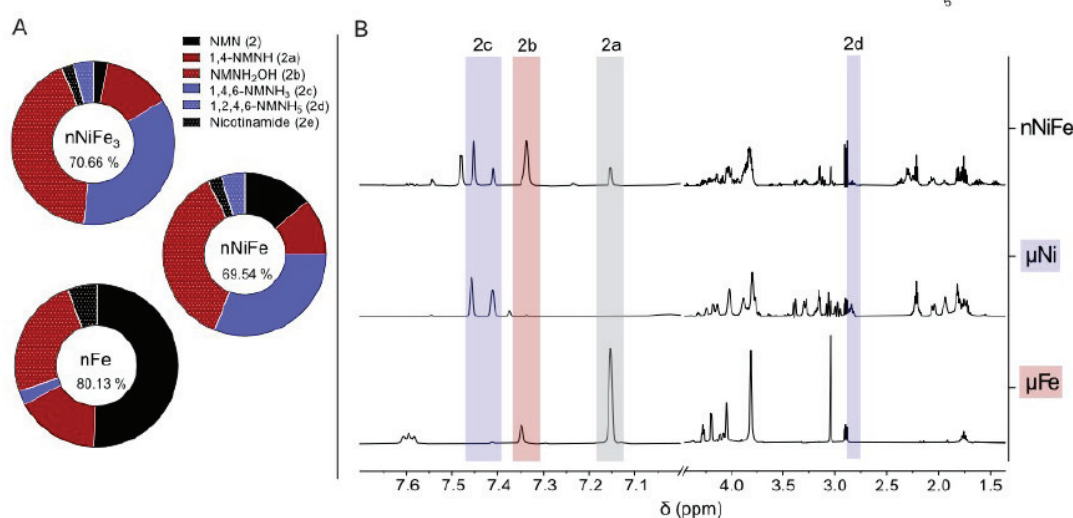


Figure 4. Selectivity and efficiency of NMN reduction with H₂ gas is influenced by the type of metal prevalent. (A) Product spectra of NMN reduction with decreasing Ni ratio. The proportion of overreduction products decreases abruptly when no Ni is used (nFe), but so does the overall NMN conversion (s. also *SI Appendix Tab. S6 and Fig. S8*). (B) The reduction of NMN assisted by nNiFe alloys (cofactor ratio 1:1) yields products that directly correlate with the products obtained when utilizing the metals separately in micropowder form (metal-cofactor ratio 200:1). μNi⁰ promotes the accumulation of **2c** and **2d** (purple) and other side products. 1,4-NMNH (grey) seems to not react further when using μFe⁰, accumulating over time, but hydrolyse in parts further to **2b**. Note that this comparison is a qualitative one as it would not be appropriate to compare the yields between nano- and micropowder. Yields for micropowder reactions shown in Fig. 4 are listed in *SI Appendix Tab. S11*.

products and confirmed the presence of a hydration product, so an OH⁻ being added to 1,4-NMNH (Fig. 4B, *SI Appendix Figs. S20–22*). We were able to assign the hydration product NMNH₂OH (**2b**) to a peak in the ¹H-NMR (*SI Appendix Figs. S18 and S19*). Both **2b** and **2c** have several conformational isomers, which result in several peaks within the ¹H-NMR spectrum as indicated in Fig. 4A.

An often reported side-product of NAD reduction (e.g. via cyclic voltammetry) is a 4,4'-linked NAD dimer (50), which also qualifies as a possible side reaction of NMN reduction. Here, after careful interpretation of our 2D NMRs of the 1 h and 4 h reaction with NMN and the 4h reaction with NAD, we can exclude the presence of such dimers (s. *SI Appendix Fig. S14*; no peak at 40 to 50 ppm in ¹³C of a bridging methine corresponding to the linkage). This was also confirmed via LC-MS (no double charged molecules were detected). As these dimers are a direct result of radical-forming 1e⁻ transfers onto NAD (51), we can draw the conclusion that direct hydride or 2e⁻ transfer is the present mechanism in our reactions.

After quantification of all identified species, we can account for at least 70.7% of transformed NMN for all reactions, often more. Unidentified species encountered in lower yields can also stem from the differently reduced versions of the degradation product nicotinamide (52). It is furthermore possible, as mentioned above, that some NMN was lost due to interaction with the mineral surface. Overall, there is notable and surprising difference between the reduction profile of the dinucleotide and the mononucleotide, the origin of which will be addressed in the discussion.

To each its own metal and mechanism? Starting from the observation that during NMN reduction, 1,4-NMNH is a main product decreasing with the length of the reaction, we hypothesized that less efficient catalysts might help to avoid overreduction and thus reduce NMN more specifically than the previously used rather efficient nanoparticulate NiFe-alloys. As both nNi and nFe visibly worked less efficiently for NAD⁺ reduction, but Fe promoted reduction in higher yields, we decided to work with the same nanoparticulate NiFe and Fe powder (nNiFe, nFe; 1:1 ratio to the cofactor) powder used for NAD⁺ reduction (Fig. 4A). Reducing the ratio of Fe (nNiFe) also reduces the amount of converted NMN, while keeping the ratio of 1,4-NMNH to side products quite similar. The nFe powder by itself converted far less NMN but also did not promote the formation of three times reduced **2d**, while twice reduced **2c** is only produced in almost untraceable amounts. The hydration product **2b** visible as a peak at 7.35 ppm still accumulated over the 4 h reaction time.

In order to explore whether this observation is a mere metal-dependent effect, we repeated experiments with NMN and H₂ over commercially available Fe and Ni micropowder (μFe, particle size: <150 μm; μNi, particle size: 3–7 μm). This separates the metal dependency from the general reduction efficiency of nanoparticulate powders due to a large surface area. The metal-cofactor ratio was 200:1 to guarantee the detection of even low concentration side products. The results (Fig. 4B) show a remarkable trend to overreduction with μNi, while μFe mostly displays two main products: 1,4-NMNH and **2b**, the latter being the hydrolysis product of the former. Comparing the spectra of NMN reduction with μNi only and μFe only with those of nNiFe, the distinct product patterns of each metal becomes apparent.

Nickel has long been recognized as a hydrogenation catalyst (53), – but why does it, when not combined with Fe, only reluctantly reduce NAD (Fig. 2 and (20)) and yet overreduce NMN, not leaving any traceable amount of single-reduced species? The answer probably lies again in the

structural differences between NAD and NMN. NMN can be more easily absorbed to a hydrogenated Ni surface, possibly over the entirety of its nicotinamide ring (s. *SI Appendix Scheme S9*). This could also explain the fast formation of its fully reduced product **2d** shown in Fig. 4C. NAD in a staggered formation could only absorb partly on the surface, avoiding overreduction (54).

If this is true, why does Fe not overreduce NMN as readily as Ni? Here, we can reflect on the mechanisms postulated by us in Pereira et al. (20), that Fe both serves as a (less effective) hydrogenation catalyst and a strong electron donor, either via direct electron transfer to the nicotinamide cofactor or the formation of nascent hydride groups on its surface.

Assuming that Fe predominantly reduces NMN through direct electron transfer, the reduction process prioritizes the species with the most favourable redox potential first—namely, 1,4-NMNH (and 1,4-NADH, in the case of NAD). This hypothesis was substantiated by cyclic voltammetry (CV) measurements, which revealed that 1,4-NMNH exhibits the highest oxidation potential among all the reduction products obtained from NMN (*SI Appendix Tab. S12, Figs. S30–33*).

Another possible explanation could be that the Ni catalyst does not alter as much as the Fe surface, meaning there would be a constant supply of hydrides available. For Fe, the previously described association with phosphate from the buffer could block active centres, which further prevent over reduction.

While the combination of nickel's hydrogenation strengths and iron's electron donation increases the yield of 1,4-NADH immensely compared to Fe or Ni separately (Fig. 2), the addition Ni does not increase the directed reduction of NMN to 1,4-NMNH.

Table 1. Overview of yields of mixtures of NAD⁺ and NMN in comparison to separate reduction. Row 1 shows the quantification of NAD⁺ (n=3) and NMN (n=3) in individual reactions with μ Ni and μ Fe, row 2 shows reactions of mixtures of NAD⁺ and NMN (for all n=3). In all experiments, the metal powder concentration lies at 600 mM, so for row 1, the metal to cofactor ratio is 50:1, for row 2 it is 25:1. All yields are calculated per to 12 mM of starting cofactor. Unpaired t-tests were used to evaluate whether the differences in concentration between 1,4-NADH and 1,4-NMNH in the competition experiments are significant: *two-tailed P value = 0.0166, significant difference; ***two-tailed P value = 0.0008, very significant difference. All additional data for these experiments can be found in *SI Appendix Tabs. S13–16, Figs. S34–37 and Schemes S10–12*.

Cofactors	metal	1,4-NADH	1,6-NADH	NAD ⁺	1,4-NMNH (2a)	NMNH ₂ OH (2b)	1,4,6-NMNH ₃ (2c)	1,2,4,6-NMNH (2d)	NMN
NAD ⁺ NMN 12mM	Fe	8.12% ± 1.25	1.60% ± 0.24	57.52% ± 2.85	47.95 % ± 11.89	11.43% ± 2.03	0.00% ± 0.00	0.00% ± 0.00	23.48% ± 15.84
	Ni	19.89% ± 0.15	5.26% ± 0.15	53.12% ± 1.82	4.85% ± 3.47	13.79% ± 4.53	44.13% ± 7.07	9.83% ± 3.11	0.92% ± 0.40
NAD ⁺ + NMN 12 mM	Fe	11.33%* ± 1.20	2.17% ± 0.28	45.10 ± 10.60	7.06%* ± 0.93	2.26% ± 0.71	0.00% ± 0.00	0.00% ± 0.00	75.15% ± 11.26
	Ni	13.63%*** ± 0.83	3.51% ± 0.35	63.82% ± 17.08	5.70%*** ± 0.92	7.33% ± 0.31	3.74% ± 0.95	0.00% ± 0.00	79.55% ± 1.75

Competing interests. At this point, we have formulated the hypothesis, how the addition of an adenosine-derived tail to the functional nicotinamide group could harbour an advantage for specific reduction in a mineral-based environment. To test this hypothesis, we conducted experiments with both NMN and NAD⁺ in the same reaction mixture using μNi and μFe as metal promoters at pH 8.5 to explore the reduction of both cofactors in direct competition (Tab.1). As controls, we used reduction experiments of NAD⁺ and NMN separately. For the mixed experiments, both cofactors (à 12 mM) were combined with 600 mM of metal powder, leading to a 25:1 metal to cofactor ratio. In all cases, the 1,4-NADH concentration surpassed that of 1,4-NMNH considerably (Tab. 1). This shows how a dinucleotidic structure could potentially have been an advantage on a non-enzymatic level. Furthermore, the results indicate that NAD, while obtaining rather comparable reduction yields for itself in all experiments, seems to have a dampening effect on NMN (over)reduction when both cofactors are in the mixture.

Ultimately, reducing NAD and NMN with the help of H₂ and metal catalysts is just one part of these cofactors' role in the prebiotic path towards the first functioning cells – being able to act as a reductant is equally important.

The reduction capability of NMNH and NADH. Looking at all side products of both NAD⁺ and NMN reduction, one has to ask the question: which ones can be a reductant for further reactions and which ones cannot? As already mentioned above, investigating the redox potential of both 1,4-NADH and 1,4-NMNH standards via cyclic voltammetry helped comparing their oxidation potential with that of the reaction mixtures of NiFe-assisted reduction of NAD⁺ and NMN with H₂ (*SI Appendix Tab. S12, Figs. S30–33*). In the case of NiFe-assisted NAD⁺ reduction, the resulting mixture shows only the oxidation potential of 1,4-NADH, while in the case of NMN reduction, the oxidation potential of both 1,4-NMNH and that of a second reduced species (most likely the species with the 2nd highest concentration, **2c**) is measured. As the second signal has a lower oxidation potential (meaning is harder to oxidize), we postulate that in the case of NMN, as for NAD, the 1,4-species is the most relevant reductant, not only in a biological but also in a prebiotic context (55–57). One could argue that it is possible that the 1,4 position of an overreduced species would show a similar oxidation potential as a single reduced 1,4-species. However, as the oxidation of the latter leads to the aromatization of the nicotinamide ring, this reaction would be energetically favourable. This theoretically also applies to the

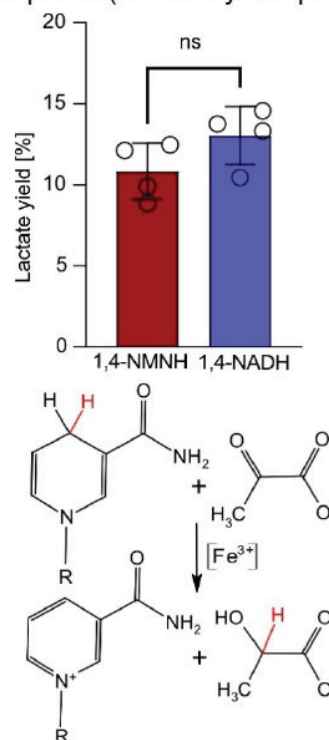


Figure 5. Reduction of pyruvate to lactate with 1,4-NMNH (n=4) and 1,4-NADH (n=4). The method of the reaction was performed according to (10) with the help of Fe(III) chloride as a catalyst in 17 h. Both nicotinamides perform equally well in this reaction. In both cases, lactate forms in comparable amounts – 2 repetitions per reaction (for original NMR spectra and quantification s. *SI Appendix Table S17 and Figs. S38 and S39*). Unpaired t-test (two-tailed P value = 0.1303) shows the difference between NADH and NMNH-dependent pyruvate reduction to be not significant (ns).

single-reduced 1,6-NADH, but we could not isolate this side product to test it as we did for 1,4-NADH and 1,4-NMNH in the following. Recently, it was shown, that Fe^{3+} ions (among other metal ions and also minerals) can promote the reaction of 1,4-NADH with pyruvate to lactate abiotically (*SI Appendix Scheme S13*) (10). Here, we used this reaction as a proxy to compare the reducing capabilities of 1,4-NMNH and 1,4-NADH, showing that both molecules can reduce pyruvate to equal amounts under aqueous conditions with Fe^{3+} in 17 h at 40°C (pH<5), based on recently published experiments by Mayer and Moran (10). These results underline that both 1,4-NMNH and 1,4-NADH are equally good hydride donors and thus that the adenosine nucleotide tail does not – or at least not strongly – influence the efficiency of the catalysed hydride transfer (Fig. 5).

The conditions used for reduction and for oxidation in this paper diverge – while for reduction slightly alkaline conditions are used, oxidation is conducted under acidic conditions. 1,4-NADH is known to hydrolyse under acidic conditions (58). We performed qualitative experiments at pH 5.5 over μFe and μNi with both NAD^+ and NMN (*SI Appendix Scheme S14 and S15, Figs. S40 and S41*) to confirm this applies to both nicotinamides in a similar manner. These experiments show the formation of hydrolysis products of the 1,4-species of both cofactors in the case of Ni, while, over Fe, also 1,4-NMNH and 1,4-NADH can be detected probably due to the increase in pH (up to pH 8) during the latter experiments. So although NAD^+ and NMN will be reduced under acidic conditions, they are hydrolysed quickly.

The oxidation of 1,4-NADH and 1,4-NMNH, however, seems to work preferably under acidic conditions (10). So fluctuations in pH might be necessary to combine both reduction and oxidation in the most effective way.

Discussion

In this study, we have shown that both nicotinamide mono- and dinucleotide can be reduced under conditions found in serpentinizing systems, i.e. with H_2 gas promoted by Fe and Ni containing minerals. We demonstrated that NMN is much more reactive than NAD^+ in a time course experiment with NiFe_3 nanopowder. Within 1 h, more NMN is consumed than NAD^+ in 4 h, under the same experimental conditions. The first and main product of both reactions seems to be 1,4-NADH/NMNH. However, while 1,4-NADH remains stable in solution, 1,4-NMNH quickly undergoes further reduction to form increasingly reduced products. From previous studies we know that 1,4-NADH does not get overreduced and remains stable even when the experimental conditions are more reducing or a higher metal to cofactor ratio is employed (20).

Where does this specificity for 1,4-NADH come from? It is known and well-described that NAD(H) in aqueous solution alternates between a folded (Fig. 6) and open conformation (59–63). This could shield the nicotinamide ring from excessive overreduction – and possibly also from side reactions such as hydrolysis. We deduce from these results that – in a mineral-dependent prebiotic context – the adenosine-derived tail can be essential for the targeted reduction of the 1,4-position, as well as for the stability of this specific reduction product.

We also evaluated the role of both Fe and Ni individually in NMN reduction – separated from the general efficiency of nanopowders. We found, that Ni tends to be responsible for most of the overreduction products in NMN reduction while Fe promotes the formation of 1,4-NMNH, the main other side-product being the hydrolysis product **2b**. However, looking at experiments with less Ni to cofactor ratio (e.g. Tab. 1, row 1), Ni also promotes the formation of **2b**, indicating that the hydrolysis product forms whenever 1,4-NMNH is not overreduced very quickly. Based on these results, one can discuss how environmental conditions such as metal availability could have

influenced the prebiotic selection process of redox cofactors. This study has shown that the adenosine-derived tail of NAD stabilizes the functional nicotinamide part of the molecule. Like that, the reduction (and thus also oxidation) properties of NAD could have been maintained within a broader variety of environmental conditions than without the tail. We validated this hypothesis further by performing experiments with both NMN and NAD⁺ in the same reaction mixture using μNi and μFe as metal promoters. These results show that NAD⁺ always produces more of the 1,4-species than NMN, the latter forming more sideproducts. An additional observation was that NAD seems to be actively decreasing NMN (over)reduction, most likely lowering the interaction of NMN with the metal surfaces – clearly also those metal-cofactor interactions leading to full hydrogenation of the nicotinamide ring (Tab. 1). NAD potentially assisting NMN in increasing its reduction specificity is an effect in need of further investigation.

Cyclic voltammetry experiments showed that the oxidation potential of single-reduced species, while all further side products fall behind. Concerning the single-reduced side product 1,6-NADH, we assume it to have a comparable redox potential as 1,4-NADH, although we cannot account for possible steric hindrances during actual reduction reactions. In a biological context, only oxidation at the 1,4-position of the nicotinamide ring is observed. Prebiotically, a 1,6-species could also be relevant for reduction, but this, to our knowledge, has not yet been observed in an experimental setup.

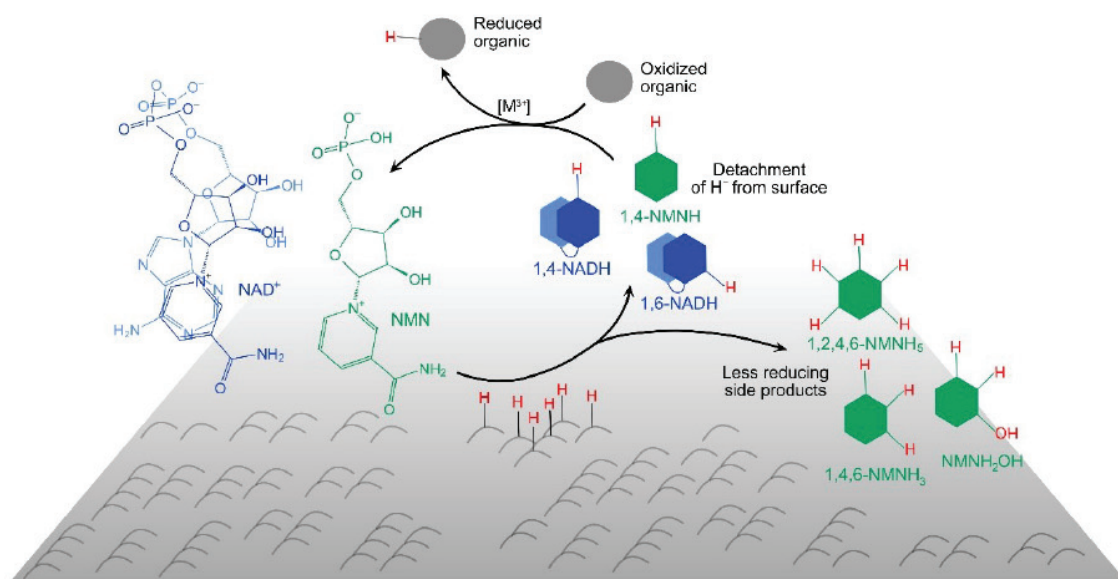


Figure 6. Summarizing figure showing all educts and products detected during simultaneous reduction of NAD⁺ and NMN. NMN produces more side products than NAD, possibly creating a mechanistic bottleneck for the back reaction, for which only one-time reduced nicotinamides have a comparable reducing strength – both overreduction products such as NMNH₃ and hydrolysis products such as NMNH₂OH could likely not compete as reducing agents in a prebiotic scenario. Consequently, only single-reduced species such 1,4-NADH and 1,4-NMNH could be coupled for reduction reactions, thus detaching the reduction from a mineral surface. Based on assessments of the redox potential, we assume 1,6-NADH being able to reduce equally well as 1,4-NADH – not accounting for possible steric hindrances.

The higher reducing strength of single-reduced nicotinamide species creates a mechanistic bottleneck for the back reaction – both overreduction and hydrolysis products could likely not compete as reducing agents in a prebiotic scenario. Additionally, we have shown here that both 1,4-NMNH and 1,4-NADH act equally well as a hydride source in a non-enzymatic context, using a protocol established by colleagues (10). So considering that the synthesis of both 1,4-species from their according oxidized forms is highly influenced by effectiveness and mechanism of the hydrogenation catalysts, it is possible that the environment had an important influence on the prebiotic selection of nicotinamides.

In our experimental setup, reduction and oxidation do not occur under the same conditions: slight alkaline conditions for reduction as the reduced forms of NMN and NAD are prone to hydrolyse under acidic conditions; acidic conditions for oxidation as 1,4-NADH is known to hydrolyse more efficiently than (58). It is a challenge to triangulate conditions under which both oxidation and reduction can occur at the same time, it is however likely, that slightly fluctuating conditions are necessary to direct oxidation and reduction.

Considering that redox cofactors could have presented a means to detach hydrides from mineral surfaces to transport them to other geochemical conditions, a separation of conditions for reduction and oxidation would actually make sense. Fluctuations in pH would be not only a bear necessity to combine both reduction and oxidation, but a natural mechanism to boost the role of organic hydride carriers to begin with (Fig. 6).

The geochemical settings this work is focussing on (serpentinizing systems), exist in both acidic and alkaline conditions, though geologically separated from each other (26, 43). Alternating physicochemical conditions on a micro-compartment level within serpentinizing systems have been observed and further hypothesized as driving force for prebiotic reactions (64–67). However, the real effect of such alternations still needs to be investigated in both laboratory and natural settings – including a variety of different geochemical settings.

Conclusion and Implications

Here, we observed that the distinct structure of nicotinamide mono- and dinucleotide molecules influences the reduction product spectrum associated with the nicotinamide ring. There is a significant difference in how both molecules react to the addition of nickel to iron-containing catalysts – while most of the overreduction of NMN seems to be due to the contribution of nickel, the specific reduction of NAD⁺ to 1,4-NADH and smaller amounts of 1,6-NADH with Ni-Fe-alloys is much faster than with iron or nickel alone. The overreduction of NMN, only consisting of nicotinamide and a phosphorylated ribose part, inevitably would lead to the molecule being a less effective hydride donor. The rather quick overreduction could be due to NMN being able to interact more directly with the mineral/metal surface than NAD. The additional AMP part attributes NAD its well-described staggered position in solution (59–62) which could prevent it from associating to the mineral surface the same way NMN does (Fig. 6; *SI Appendix Scheme S9*). Further, possibly theoretical, investigation will be necessary to get a definite answer.

Looking at the reverse reaction, based on previous work by colleagues with 1,4-NADH (10), we were able to confirm that both 1,4-NMNH and 1,4-NADH act equally well as a hydride source in a non-enzymatic context.

When it comes to the concrete question of prebiotic selection of organic cofactors, our study suggests that the ability to provide hydrides might not be the bottleneck, but rather the setup of the environment in which these reactions would have taken place. Overall, in the case of NAD and NMN, the dinucleotide would be more adapt to a variety of environments, ensuring specific, one-time reduction of the nicotinamide. In direct competition experiments we performed over the course

of 4 h, the concentration of the 1,4-species of NAD always surpasses that of NMN. However, the mononucleotide might be advantageous in an environment with less efficient catalysts as it reduces faster, this ultimately also depends on how exactly reduction and oxidation reaction can be coupled under prebiotic conditions. Assuming that redox cofactors could have presented a way to detach hydrides from a mineral surface under certain conditions (33) to expose them to different environmental conditions, a molecular structure stabilizing the optimal reducing form (NAD) would be preferable over one that does not (NMN, Fig. 6). A next step would aim for the self-sustaining combination of both reduction and oxidation of these redox cofactors. Furthermore, more research will be necessary to understand the depths of molecular structure in prebiotic selection, including molecules we do not see in biochemistry today.

Lastly, our observations of a stabilizing function of adenosine-derived tails could be applied other cofactors such as FAD, CoA or SAM. It seems feasible that also there, the extended structure could have been of merit in a prebiotic setting prior to a biological function (14, 68).

Materials and Methods

Metal preparation. The synthesis of Ni^0 , Fe^0 and Ni-Fe Nanoparticles was carried out as described by Beyazay et al. (29). Commercially bought Fe^0 (reduced, <149 μm , Carl Roth, referred to as μFe^0) and Ni^0 micropowders (3-7 micron, Thermo Scientific, referred to as μNi^0) were treated under 5 bar of H_2 , at 50 °C for 16 h before being used. A detailed characterization of these metals can be found in the same publication.

Experimental setup with Ni-Fe alloys. Under anaerobic conditions, using a glovebox (JACOMEX), 3 mL of anoxic 0.133 M phosphate buffer solution (PBS; pH 8.5; potassium phosphate monobasic and sodium phosphate dibasic, Sigma-Aldrich, in HPLC-grade water); bubbled with N_2 for 1 h containing 36 or 18 μmol of the organic nicotinamide (Nam) compound NAD^+ (>95.0%, TCI) or NMN (100% Uthever, MoleQlar; >98.0%, TCI; *SI Appendix Fig. S42*) were placed in 5 mL glass vials (beaded rim) with a polytetrafluoroethylene (PTFE)-coated stirring bar. Equimolar amounts (relative to the cofactor) of metal atoms of Fe, NiFe_3 , NiFe , Ni_3Fe , or Ni nanopowders were added to the bottom of each vial, with the exception of a metal-free control (*SI Appendix Tab. S18*). Alternatively, experiments with Fe and Ni micropowders had 1.8 or 7.2 mmols of metal and 36 μmol of cofactor (metal-cofactor ratio 50 or 200:1) in 0.5 M PBS (pH 8.5 or pH 5.5). The vials were sealed with a crimp cap with a PTFE-coated membrane. To allow gas exchange between the interior and the exterior of the glass vial, a syringe needle was inserted through the crimp cap membrane before the vials were placed in the high-pressure reactor.

Standard high-pressure reaction. After pressurizing the reactor (Berghof Reactor 300) with either 5 bar of Ar gas (99.999%, Air Liquid) or 5 bar of H_2 gas (99.9% Nippon Gases), the reactions were started and regulated by a controlled reactor heating system (Berghof Products + Instruments). Reactions were performed from 1 h to 4 h at 40 °C and 400 rpm, in a Berghof Reactor Heating System (BR-HS). Afterward, reactors were depressurized under anaerobic conditions and the samples (metal powders and solution) were transferred to 2 mL Eppendorf tubes and centrifuged for 20 min, at 4 °C, and 13,000 rpm (Fresco 17 Microcentrifuge). The supernatants were subjected to different analyses, which are described below.

Reduction of pyruvate with Fe^{3+} and 1,4-NMNH or 1,4-NADH. These experiments followed the protocol described in Tables S15 and S16 of the paper Mayer et al. 2024 (10). An aqueous mixture of 0.1 mL with 0.1 M pyruvate (Pyruvic acid, Carl Roth), 0.2 M 1,4-NADH (95%, Thermo Scientific), and 0.06 M FeCl_3 (98% anhydrous, Grüssing GmbH) reacted overnight at 40 °C and 400 rpm (pH<5). For the removal of metal ions, it was added 0.2 mL of a thiolate/phosphate solution (100 mg NaSH, 100 mg NaOH in 10 mL saturated aqueous Na_3PO_4), and left to settle in the fridge (4 °C) for 3 h. Instead of a DMSO standard as used in the referenced protocol, 0.1 mL of a 7mM DSS stock solution was added at the end of the experiment. To reach a certain volume, 0.2 mL of D_2O were also added before the sample was measured. ^1H -NMR spectra were obtained by an AV III HD 250 MHz Spectrometer with a Double Resonance Broad Band (BBOF) probe head. The same experiment was repeated with 1,4-NMNH (97%, AmBeed) instead of 1,4-NADH.

Quantitative proton nuclear magnetic resonance (qNMR) analysis. To monitor reactions, as well as detect and quantify the formation of reduced NADH and side products we established a protocol for quantitative proton nuclear magnetic resonance (^1H -NMR).^(28, 69) The internal standard was a 7 mM solution of sodium 3-(trimethylsilyl)-1-propanesulfonate (DSS, CH_3 peak at 0 ppm; >98.0%, TCI) in deuterium oxide (D_2O 99.8 atom%D, AcroSeal, Thermo Scientific), mixed 1:6 with the supernatant of our samples. qNMR spectra were obtained on a Bruker AVANCE-NEO 600 MHz spectrometer equipped with a 5 mm iprobe TBO with z-gradient. Thirty-two scans were made for each sample with a relaxation delay of 40 s (600 MHz) and a spectral width from -3 to 13. Analysis and integration were performed using MestReNova (v.15.0.1). Metal-free controls (ran under the same conditions as the quantified, metal-containing samples) were used as references to the initial amount of NAD/NMN in the sample to account for evaporation and possible degradation under the given pH, temperature and time. The average initial amount of cofactor in the controls was used as $t = 0$ h and to normalize the reaction yields.

Standards. ^1H -NMR standards were prepared with 24 mM of the compound and 1 mM of DSS dissolved in D_2O (*SI Appendix Figs. S43*). The spectra were obtained by a AV III HD 250 MHz Spectrometer with a BBOF probe head.

Product Characterization through 2D-NMR. 2D ^1H -NMR enabled the assignment of peaks for 1,4-NMNH and NMN in accordance with literature and in comparison to the pair NAD/NADH (*SI Appendix Tabs. S19 and S20; Figs. S44–58*) (70). Reduction products were also characterized through different 2D-NMR correlation spectra (*SI Appendix Scheme S4; Figs. S11–19*). 3 mL of sample from a 1h and 4 h reduction of NMN with equimolar amounts of NiFe_3 (5 bar H_2 , 40 °C, 400 rpm) were dried using a vacuum concentrator (SpeedVac DNA 130, Savant). The remaining solution and pellet were suspended in 500 μL of D_2O to increase the concentration of the products and resolution of the NMR spectra. The same procedure was performed for a NAD^+ sample after a 4 h reaction with equimolar amounts of NiFe_3 (5 bar H_2 , 40 °C, 400 rpm). Two-dimensional correlation spectra of ^1H , ^1H DQF-COSY (Double-Quantum Filtered CORrelated SpectroscopY), ^1H , ^1H TOCSY (Total CORrelated SpectroscopY), ^1H , ^{13}C HMBC (Heteronuclear Multiple Bond Correlation spectroscopy) were recorded with standard pulse programs.⁽⁷¹⁾ Edited HSQC (Heteronuclear Single Quantum Coherence spectroscopy) spectra were recorded using sensitivity improvement with echo/anti-echo gradient selection and multiplicity editing during selection step^{6,7}

NOESY (Nuclear Overhauser Effect Spectroscopy) spectrum was recorded with mixing time of 1.5 s. Chemical shifts are referenced with sodium salt of trimethylsilylpropanesulfonic acid (DSS). Spectra were obtained with the same instrument as qNMR and compared to a list of possible products.

Supporting Information

All Supporting Information (methods, figures showing analytic data, tables, schemes) is comprehensively presented in a single pdf file.

Data Availability Statement

The data that support the findings of this study are available in the SI Appendix of this article. Original analysis files (LC-MS, NMR) will be provided by the corresponding authors upon reasonable request.

Acknowledgements

D.P.H.P and M.P. thank Bill Martin for discussions and support. D.P.H.P and M.P thank Alicia Casitas and team for providing access and help to cyclic voltammetry measurements. X.X. thanks Armin Geyer for discussions and the DFG funding for NMR spectrometer NEO600 (Forschungsgroßgeräte project number 508097909). M.P. thanks the Max Planck Society and the International Max Planck Research School 'Principles of microbial life' for funding. H.T. thanks MPG, the Volkswagen Foundation (96_742) and Deutsche Forschungsgemeinschaft (TU 315/8-1 / TU 315/8-3). This project was supported by the European Regional Development Fund (ERDF) and the Recovery Assistance for Cohesion and the Territories of Europe (REACT-EU).

References

1. A. D. Goldman, B. Kacar, Cofactors are Remnants of Life's Origin and Early Evolution. *Journal of Molecular Evolution* **89**, 127–133 (2021).
2. J. C. Xavier, W. Hordijk, S. Kauffman, M. Steel, W. F. Martin, Autocatalytic chemical networks at the origin of metabolism. *Proceedings of the Royal Society B: Biological Sciences* **287**, 20192377 (2020).
3. A. Kirschning, The coenzyme/protein pair and the molecular evolution of life. *Natural Product Reports* **38**, 993–1010 (2021).
4. S. Basak, S. Nader, S. S. Mansy, Protometabolic reduction of NAD⁺ with α -keto acids. *JACS Au* **1**, 371–374 (2021).
5. L. Sebastianelli, H. Kaur, Z. Chen, R. Krishnamurthy, S. S. Mansy, A Magnesium Binding Site And The Anomeric Effect Regulate The Abiotic Redox Chemistry Of Nicotinamide Nucleotides. *Chemistry A European J* e202400411 (2024). <https://doi.org/10.1002/chem.202400411>.
6. H. B. White, Coenzymes as fossils of an earlier metabolic state. *Journal of Molecular Evolution* **7**, 101–104 (1976).
7. E. Werner, S. Pinna, R. J. Mayer, J. Moran, Metal/ADP Complexes Promote Phosphorylation of Ribonucleotides. *Journal of American Chemical Society* **145**, 21630–21637 (2023).
8. F. L. Sousa, W. F. Martin, Biochemical fossils of the ancient transition from geoenergetics to bioenergetics in prokaryotic one carbon compound metabolism. *Biochimica et Biophysica Acta - Bioenergetics* **1837**, 964–981 (2014).
9. J. C. Fontecilla-Camps, Geochemical continuity and catalyst/cofactor replacement in the emergence and evolution of life. *Angewandte Chemie - International Edition* **58**, 42–48 (2019).

10. R. J. Mayer, J. Moran, Metal ions turn on a stereoselective nonenzymatic reduction of keto acids by the coenzyme NADH. *Chem* **10**, 2564–2576 (2024).
11. H. J. Kim, S. A. Benner, A Direct Prebiotic Synthesis of Nicotinamide Nucleotide. *Chemistry - A European Journal* **24**, 581–584 (2018).
12. J. C. Xavier, S. Kauffman, Small-molecule autocatalytic networks are universal metabolic fossils. *Philosophical Transactions of the Royal Society A: Mathematical, Physical and Engineering Sciences* **380**, 20210244 (2022).
13. K. A. Denessiouk, V.-V. Rantanen, M. S. Johnson, Adenine recognition A motif present in ATP- CoA- NAD- NADP- and FAD-dependent proteins. *Proteins: Structure, Function and Bioinformatics* **44**, 282–29 (2001).
14. L. M. Longo, *et al.*, On the emergence of P-Loop NTPase and Rossmann enzymes from a Beta-AlphaBeta ancestral fragment. **9**, e64415 (2020).
15. D. E. Graham, R. H. White, Elucidation of methanogenic coenzyme biosyntheses: from spectroscopy to genomics. *Nat. Prod. Rep.* **19**, 133–147 (2002).
16. V. D. Cr  cy-Lagard, *et al.*, Comparative Genomics Guided Discovery of Two Missing Archaeal Enzyme Families Involved in the Biosynthesis of the Pterin Moiety of Tetrahydromethanopterin and Tetrahydrofolate. *ACS Chem. Biol.* **7**, 1807–1816 (2012).
17. G. Schwarz, R. R. Mendel, Molybdenum cofactor biosynthesis and molybdenum enzymes. *Annu. Rev. Plant Biol.* **57**, 623–647 (2006).
18. J. L. E. Wimmer, *et al.*, The autotrophic core: an ancient network of 404 reactions converts H₂, CO₂, and NH₃ into amino acids, bases, and cofactors. *Microorganisms* **9**, 458 (2021).
19. J. L. E. Wimmer, *et al.*, Energy at origins: favorable thermodynamics of biosynthetic reactions in the Last Universal Common Ancestor (LUCA). *Frontiers in Microbiology* **12**, 793664 (2021).
20. D. P. Henriques Pereira, *et al.*, Role of geochemical protoenzymes (geozymes) in primordial metabolism: Specific abiotic hydride transfer by metals to the biological redox cofactor NAD⁺. *The FEBS Journal* 16329 (2022). <https://doi.org/10.1111/febs.16329>.
21. J. M. Weber, *et al.*, Testing abiotic reduction of NAD⁺ directly mediated by iron/sulfur minerals. *Astrobiology* **22**, 1–10 (2021).
22. T. Saba, *et al.*, NADH Regeneration: a case study of Pt-catalyzed NAD⁺ reduction with H₂. *ACS Catalysis* **11**, 283–289 (2021).
23. S. D. Copley, E. Smith, H. J. Morowitz, The origin of the RNA world: Co-evolution of genes and metabolism. *Bioorganic Chemistry* **35**, 430–443 (2007).
24. J. Yi, *et al.*, A Nonenzymatic Analog of Pyrimidine Nucleobase Biosynthesis. *Angewandte Chemie* **134**, e202117211 (2022).
25. M. Bechtel, N. Kurre, O. Trapp, A Prebiotic Pathway to Nicotinamide Adenine Dinucleotide. *Chemistry A European J* e202402055 (2024). <https://doi.org/10.1002/chem.202402055>.
26. L. Schwander, *et al.*, Serpentinization as the source of energy, electrons, organics, catalysts, nutrients and pH gradients for the origin of LUCA and life. *Front. Microbiol.* **14**, 1257597 (2023).
27. D. E. Allen, W. E. Seyfried, Serpentinization and heat generation: Constraints from Lost City and Rainbow hydrothermal systems. *Geochimica et Cosmochimica Acta* **68**, 1347–1354 (2004).
28. M. Preiner, *et al.*, A hydrogen-dependent geochemical analogue of primordial carbon and energy metabolism. *Nature Ecology & Evolution* **4**, 534–542 (2020).
29. T. Beyazay, *et al.*, Influence of composition of nickel-iron nanoparticles for abiotic CO₂ conversion to early prebiotic organics. *Angewandte Chemie - International Edition* **62**, e202218189 (2023).

30. T. Beyazay, *et al.*, Ambient temperature CO₂ fixation to pyruvate and subsequently to citramalate over iron and nickel nanoparticles. *Nature Communications* **14**, 570 (2023).
31. M. C. Weiss, *et al.*, The physiology and habitat of the last universal common ancestor. *Nature Microbiology* **1**, 16116 (2016).
32. E. R. R. Moody, *et al.*, The nature of the last universal common ancestor and its impact on the early Earth system. *Nat Ecol Evol* **8**, 1654–1666 (2024).
33. M. Brabender, *et al.*, Ferredoxin reduction by hydrogen with iron functions as an evolutionary precursor of flavin-based electron bifurcation. *Proc. Natl. Acad. Sci. U.S.A.* **121**, e2318969121 (2024).
34. G. Fuchs, Alternative pathways of carbon dioxide fixation: Insights into the early evolution of life? *Annual Review of Microbiology* **65**, 631–658 (2011).
35. R. K. Thauer, Hydrogenases and the global H₂ cycle. *European Journal of Inorganic Chemistry* **7**, 919–921 (2011).
36. R. Frost, On the stability of sulfides, oxides, and native metals in serpentinite. *Journal of Petrology* **26**, 31–63 (1985).
37. F. Klein, W. Bach, Fe-Ni-Co-O-S Phase Relations in Peridotite-Seawater Interactions. *Journal of Petrology* **50**, 37–59 (2009).
38. D. I. Foustoukos, M. Bizimis, C. Frisby, S. B. Shirey, Redox controls on Ni-Fe-PGE mineralization and Re/Os fractionation during serpentinization of abyssal peridotite. *Geochimica et Cosmochimica Acta* **150**, 11–25 (2015).
39. J. A. P. M. Devienne, T. A. Berndt, W. Williams, L. Nagy, Magnetic Recording Stability of Taenite-Containing Meteorites. *Geophysical Research Letters* **50**, e2022GL102602 (2023).
40. V. Dekov, Native nickel in the TAG hydrothermal field sediments (Mid-Atlantic Ridge, 26°N): Space trotter, guest from mantle, or a widespread mineral, connected with serpentinization? *J. Geophys. Res.* **111**, 2005JB003955 (2006).
41. C. Kanellopoulos, *et al.*, A New Occurrence of Terrestrial Native Iron in the Earth's Surface: The Ilia Thermogenic Travertine Case, Northwestern Euboea, Greece. *Geosciences* **8**, 287 (2018).
42. M. Yu, G. Moon, E. Bill, H. Tüysüz, Optimizing Ni-Fe oxide electrocatalysts for oxygen evolution reaction by using hard templating as a toolbox. *Applied Energy Materials* **2**, 1199–1209 (2019).
43. J. L. Charlou, J. P. Donval, Y. Fouquet, P. Jean-Baptiste, N. Holm, Geochemistry of high H₂ and CH₄ vent fluids issuing from ultramafic rocks at the Rainbow hydrothermal field (36°14'N, MAR). *Chemical Geology* **191**, 345–359 (2002).
44. C. Konn, *et al.*, Extending the dataset of fluid geochemistry of the Menez Gwen, Lucky Strike, Rainbow, TAG and Snake Pit hydrothermal vent fields: Investigation of temporal stability and organic contribution. *Deep-Sea Research Part I: Oceanographic Research Papers* **179**, 103630 (2022).
45. G. D. Yadav, M. R. Kharkara, Liquid-phase hydrogenation of saturated and unsaturated nitriles: Activities and selectivities of bimetallic nickel-copper and nickel-iron catalysts supported on silica. *Applied Catalysis A: General* **126**, 115–123 (1995).
46. L. Jr. Rover, *et al.*, Study of NADH stability using ultraviolet±visible spectrophotometric analysis and factorial design. *Analytical Biochemistry* **55**, 50–55 (1998).
47. T. Saba, J. W. H. Burnett, J. Li, P. N. Kechagiopoulos, X. Wang, A facile analytical method for reliable selectivity examination in cofactor NADH regeneration. *Chemical Communications* **56**, 1231–1234 (2020).
48. S. E. Godtfredsen, M. Ottesen, N. R. Andersen, On the mode of formation of 1,6-dihydro-NAD in NADH preparations. *Carlsberg Research Communications* **44**, 65–75 (1979).
49. S. Chaykin, L. Meissner, The borohydride reduction products of DPN. *Biochemical and Biophysical Research Communications* **14**, 233–240 (1964).

50. I. Ali, T. Khan, S. Omanovic, Direct electrochemical regeneration of the cofactor NADH on bare Ti, Ni, Co and Cd electrodes: The influence of electrode potential and electrode material. *Journal of Molecular Catalysis A: Chemical* **387**, 86–91 (2014).
51. N. H. A. Besisa, K.-S. Yoon, M. Yamauchi, *In situ* electrochemical regeneration of active 1,4-NADH for enzymatic lactic acid formation via concerted functions on Pt-modified TiO₂/Ti. *Chem. Sci.* **15**, 3240–3248 (2024).
52. A. Zarei, *et al.*, Dihydronicotinamide riboside: synthesis from nicotinamide riboside chloride, purification and stability studies. *RSC Adv.* **11**, 21036–21047 (2021).
53. H. Adkins, H. I. Cramer, The use of nickel as a catalyst for hydrogenation. *J. Am. Chem. Soc.* **52**, 4349–4358 (1930).
54. A. Damian, S. Omanovic, Electrochemical reduction of NAD⁺ on a polycrystalline gold electrode. *Journal of Molecular Catalysis A: Chemical* **253**, 222–233 (2006).
55. R. A. Weusthuis, P. L. Folch, A. Pozo-Rodríguez, C. E. Paul, Applying Non-canonical Redox Cofactors in Fermentation Processes. *iScience* **23**, 101471 (2020).
56. R. D. Braun, K. S. V. Santhanam, P. J. Elving, Electrochemical oxidation in aqueous and nonaqueous media of dihydropyridine nucleotides NMNH, NADH, and NADPH. *J. Am. Chem. Soc.* **97**, 2591–2598 (1975).
57. P. J. Elving, C. O. Schmakel, K. S. V. Santhanam, P. Zuman, Nicotinamide-Nad Sequence: Redox Processes and Related Behavior: Behavior and Properties of Intermediate and Final Products. *C R C Critical Reviews in Analytical Chemistry* **6**, 1–67 (1976).
58. S. L. Johnson, P. T. Tuazon, Acid-catalyzed hydration of reduced nicotinamide adenine dinucleotide and its analogs. *Biochemistry* **16**, 1175–1183 (1977).
59. R. V. Hull, P. S. Conger, R. J. Hoobler, Conformation of NADH studied by fluorescence excitation transfer spectroscopy. *Biophysical Chemistry* **90**, 9–16 (2001).
60. P. E. Smith, J. J. Tanner, Conformations of nicotinamide adenine dinucleotide (NAD⁺) in various environments. *Journal of Molecular Recognition* **13**, 27–34 (2000).
61. S. K. Hoffmann, J. Goslar, S. Lijewski, Electron Paramagnetic Resonance and Electron Spin Echo Studies of Co²⁺ Coordination by Nicotinamide Adenine Dinucleotide (NAD⁺) in Water Solution. *Appl Magn Reson* **44**, 817–826 (2013).
62. R. Parthasarathy, S. M. Fridley, Conformational Variability of NAD⁺ in the Free and Bound States: a Nicotinamide Sandwich in NAD⁺ Crystals. *Science* **226**, 969–971 (1984).
63. D. A. Volkov, I. A. Gorbunova, O. S. Vasyutinskii, Conformational states of NADH in water–alcohol solutions studied by molecular dynamics simulations. *Journal of Photochemistry and Photobiology A: Chemistry* **449**, 115422 (2024).
64. H. M. Lamadrid, *et al.*, Effect of water activity on rates of serpentinization of olivine. *Nature Communications* **8**, 16107 (2017).
65. M. Andreani, *et al.*, The rocky road to organics needs drying. *Nature Communications* **14**, 347 (2023).
66. A. do Nascimento Vieira, K. Kleinermanns, W. F. Martin, M. Preiner, The ambivalent role of water at the origins of life. *FEBS Letters* **594**, 2727–2733 (2020).
67. H. Lee, M. Russell, R. Nakamura, Water Chemistry at the Nanoscale: Clues for Resolving the “Water Paradox” Underlying the Emergence of Life. *ChemistryEurope* e202400038 (2024). <https://doi.org/10.1002/ceur.202400038>.
68. A. C. Sanchez-Rocha, M. Makarov, L. Pravda, M. Novotný, K. Hloučková, Coenzyme-Protein Interactions since Early Life. *eLife* **13** (2024).
69. S. J. Varma, K. B. Muchowska, P. Chatelain, J. Moran, Native iron reduces CO₂ to intermediates and endproducts of the acetyl-CoA pathway. *Nature Ecology and Evolution* **2**, 1019–1024 (2018).

70. R. Zapata-Pérez, *et al.*, Reduced nicotinamide mononucleotide is a new and potent NAD⁺ precursor in mammalian cells and mice. *The FASEB Journal* **35**, e21456 (2021).
71. S. Berger, S. Braun, *200 and more NMR experiments: a practical course*, 2. expand. ed., 1. repr (WILEY-VCH, 2011).

Supporting Information for

A possible pre-enzymatic role of the “non-functional” tail of NAD: specific reduction on mineral surfaces

Delfina P. Henriques Pereira^{*a,b}, Xiulan Xie^c, Zainab Subrati^c, Tuğçe Beyazay^d, Nicole Paczia^e, Jürgen Belz^f, Kerstin Volz^f, Harun Tüysüz^{d,g}, Martina Preiner^{*a,b}

^a Microcosm Earth Center

Max-Planck-Institute for Terrestrial Microbiology and Philipps-University Marburg
Hans-Meerwein-Str. 4; 35032 Marburg (Germany)

^b Geochemical Protoenzymes Research Group

Max-Planck-Institute for Terrestrial Microbiology
Karl-von-Frisch-Str. 10; 35043 Marburg (Germany)

^c Department of Chemistry

Philipps University Marburg
Hans-Meerwein-Str. 4; 35032 Marburg (Germany)

^d Heterogeneous Catalysis

Max-Planck-Institut für Kohlenforschung
Kaiser-Wilhelm-Platz 1; 45470 Mülheim an der Ruhr (Germany)

^e Metabolomics and small molecule mass spectrometry

Max-Planck-Institute for Terrestrial Microbiology
Karl-von-Frisch-Str. 10; 35043 Marburg (Germany)

^f Department of Physics

Philipps University Marburg
Hans-Meerwein-Straße 6; 35032 Marburg (Germany)

^g IMDEA Materials Institute

C/ Eric Kandel 2, 28906 – Getafe, Madrid (Spain)

^{*}Corresponding authors:

Martina Preiner, martina.preiner@mpi-marburg.mpg.de; Delfina P. Henriques Pereira, delfina.pereira@mpi-marburg.mpg.de

This PDF file includes:

Supporting text
Equations S1–3
Figures S1–58
Tables S1–20
Scheme S1–15
References

Supporting Methods

Liquid Chromatography Mass Spectroscopy (LC-MS). Samples were prepared from the supernatant of a reaction with 36 μmol NMN, 36 μmol Fe^0 (nanopowder) in 3 mL of 0.133 M PBS (pH 8.5). The reaction ran for 4 h at 40 °C in a high pressure reactor with 5 bar of H_2 . Afterwards the supernatant was diluted 1:200 with HPLC grade H_2O . 2 replicas were measured and compared to the supernatant of the control (without metal powder) and a standard with equivalent amounts of 1,4-NMN to NMN in the samples. The chromatographic separation was performed on a Thermo Scientific Vanquish high performance liquid chromatography (HPLC) System using a SeQuant ZIC-pHILIC column (150 \times 2.1 mm, 5 μm particle size, peek coated, Merck) connected to a guard column of similar specificity (20 \times 2.1 mm, 5 μm particle size, Phenomenex) a constant flow rate of 0.1 mL/min with mobile phase A with mobile phase comprised of 10 mM ammonium acetate in water, pH 9, supplemented with medronic acid to a final concentration of 5 μM (A) and 10 mM ammonium acetate in 90:10 acetonitrile to water, pH 9, supplemented with medronic acid to a final concentration of 5 μM (B) at 40 °C. The injection volume was, dependent on the expected analyte concentration, between 1 μL and 5 μL . The mobile phase profile consisted of the following steps and linear gradients: 0 – 1 min constant at 75% B; 1 – 6 min from 75 to 40% B; 6 to 9 min constant at 40% B; 9 – 9.1 min from 40 to 75% B; 9.1 to 20 min constant at 75% B. A Thermo Scientific ID-X Orbitrap mass spectrometer was used in negative ionization mode with an electrospray ionization source and the following conditions: HESI spray voltage at 5500 V, sheath gas at 25 arbitrary units, auxiliary gas at 5 arbitrary units, no sweep gas, ion transfer tube temperature at 275 °C, and Vaporizer temperature at 75 °C. Detection was performed in full scan mode using the orbitrap mass analyzer at a mass resolution of 120 000 in the mass range 330–360 (m/z). The extracted ion chromatograms of the $[\text{M}-\text{H}]^-$ were generated using Freestyle software (Thermo Scientific) applying a mass accuracy of 5 ppm. Comparative predicted natural isotope distribution was calculated using ChemCalc z. Peak spectra were extracted from the apex of the peak. A Background subtraction was performed from an injection of water using the spectrum extracted at the same retention time.

Cyclic Voltammetry. The redox potential of NAD and NMN were compared through cyclic voltammetry performed at 1 mM of each compound in H_2O at 25°C using as electrolyte disodium hydrogen phosphate and potassium phosphate (0.133 M PBS), at a scan rate of 50 mV/s. A three-electrode electrochemical cell has been used: glassy carbon as the working electrode, platinum wire as an auxiliary electrode, and Ag/AgNO_3 (0.01 M) as a reference electrode.

Scanning Transmission Electron Microscope (STEM). In preparation for the STEM measurement, 1 mg of Ni-Fe-particles were dispersed in 400 μL methanol (HPLC grade; Fisher Scientific) using an ultrasonic bath (Bandelin) for 5 s. Subsequently, 20 μL the dispersion were diluted with additional 90 μL of methanol, dispersed in the ultrasonic bath again. A drop of the dispersion was placed on the Cu 300 Mesh lacey carbon grid (EMS) and left to dry. In the case of particles recovered after a reaction, the particles were washed with water (HPLC grade, Fisher Scientific), dried and handled accordingly to pristine particles above. Measurements of drop-cast NiFe particles were carried out using an aberration-corrected JEOL JEM-2200FS STEM equipped with a Bruker XFlash 5060 Energy Dispersive X-ray Spectrometer (EDX) operated in analytical mode with a spatial resolution of approximately 1-2 Ångströms.

Henry's Law

Equation S1 H₂ concentration

$$H^{cp} = \frac{c_a}{p}$$

H^{cp} : Henry's constant

c_a : concentration

p: pressure

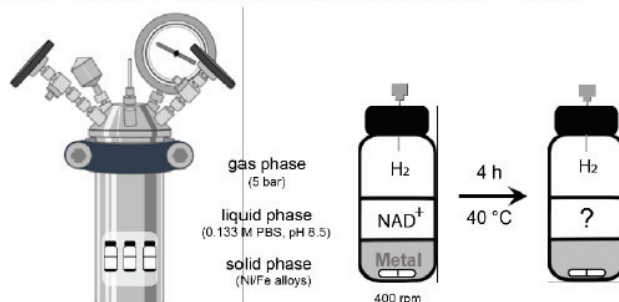
Equation S2 Henry's constant for H₂:

$$H^{cp}(H_2, 298\text{ K}) = 7.8 \times 10^{-4} \frac{\text{mol}}{\text{L} \times \text{atm}}$$

Equation S3 Temperature dependency of Henry's constant:

$$H^{cp}(H_2, T_2) = H^{cp}(H_2, 298\text{ K}) \times e^{(500 \left(\frac{1}{T_2} - \frac{1}{298\text{ K}} \right))}$$

Heterogeneous catalysis of NAD⁺ reduction with H₂ and Ni/Fe alloys



Scheme S1 The reduction of NAD⁺ with Ni/Fe alloys was tested with the protocol described in detail in Methods, and according to the scheme above. The amount of metal and NAD⁺ was 36 μ mol, which reacted together for 4 h, at 40 °C, under alkaline conditions and 5 bars of H₂. The same reaction was made under Ar as a control.

Table S1 For quantification of each compound, a peak was selected in their spectra. The values listed below indicate the ppm value where the peak can be found at approximately pH 8.5 (0.133M PBS).

Molecule	NAD ⁺	Nam	1,6-NADH	1,4-NADH
δ (ppm) for quantification	9.12	8.93	7.11	6.94

Table S2 After 4 h under 5 bar of H₂, samples with different nanoparticular Ni/Fe alloys yielded different amounts of 1,4-NADH, 1,6-NADH and nicotinamide (Nam), from the starting material NAD⁺, as listed below. The starting metal and cofactor were 36 μ mol mixed in 3 mL of 0.133 M PBS (pH 8.5), as shown in **Scheme S1**. The yields were calculated relative to the metal-free sample (100% NAD⁺). Reactions with nNi, nNi₃Fe, and nNiFe were performed with six replicas; Fe⁰ and w/o metal were done with five replicas; nNiFe₃ amounted to four. To determine the turn over frequency (TOF) of each reaction, 1,4-NADH and 1,6-NADH were considered as products and the total amount of metal atoms were considered as the amount of catalyst, instead of the number of molecules.

	H ₂	NAD ⁺	SD	1,4-NADH	SD	1,6-NADH	SD	Nam	SD	TOF [mol/s]
4h	nNi ⁰	72.63%	3.5%	3.68%	0.5%	1.19%	0.2%	6.37%	0.3%	3.57E-06
	nNi ₃ Fe	61.20%	2.7%	14.09%	1.8%	6.84%	1.1%	7.47%	0.2%	1.54E-05
	nNiFe	31.10%	2.1%	19.66%	2.4%	7.90%	1.2%	7.88%	0.7%	2.02E-05
	nNiFe ₃	25.59%	4.4%	40.60%	1.8%	16.70%	0.6%	4.48%	0.1%	3.02E-05
	nFe ⁰	52.23%	7.6%	6.01%	1.1%	0.00%	0.0%	7.04%	0.6%	4.41E-06

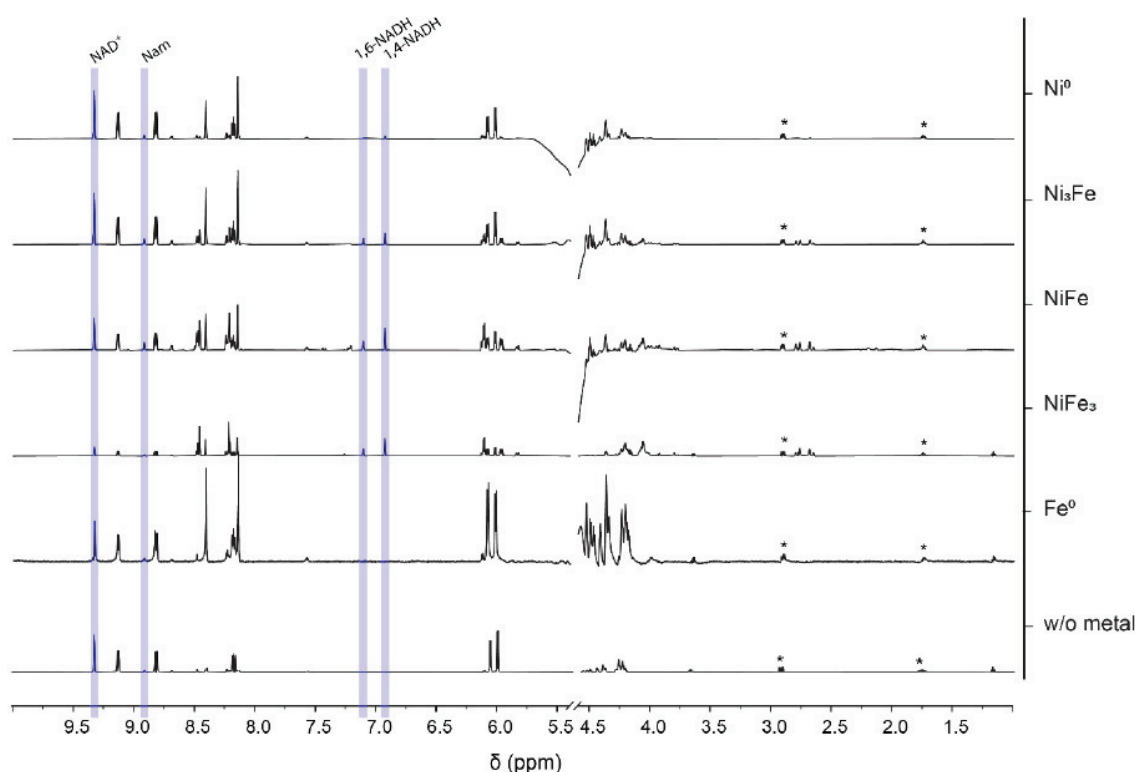


Fig. S1 The NMR spectra of replica samples of NAD⁺ in PBS (0.133 M, pH 8.5) after 4 h with 5 bar of H₂ and a metal 1:1 cofactor ratio, as shown in **Scheme S1**, are stacked together in this figure. The metal used in each sample is indicated on the right side of each spectra. After 4h reacting, the supernatant was collected and DSS added as an internal standard. The spectra were edited to only include relevant peaks, having been removed a DSS peak at 0 ppm and water peak at 4.8 ppm. No other peaks were found in the areas removed. Some DSS peaks are still visible (*). The peaks used for qualitative analysis and subsequent qNMR are highlighted in blue, according to **Table S1**.

Table S3 After 4 h under 5 bar of Ar, samples with different nanoparticular Ni/Fe alloys yielded different amounts of 1,4-NADH, 1,6-NADH and Nam, from the starting material NAD⁺, as listed below. The starting metal and cofactor were 36 μmol mixed in 3 mL of 0.133 M PBS (pH 8.5), as shown in **Scheme S1** with Ar. The yields were calculated relative to the metal-free sample (100% NAD⁺). Reactions with nNi, nNi₃Fe, and nNiFe were performed with six replicas; nFe⁰ and w/o metal were done with five replicas; nNiFe₃ amounted to four. To determine the TOF of each reaction, 1,4-NADH and 1,6-NADH were considered as products and the total amount of metal atoms were considered as the amount of catalyst, instead of the number of molecules.

	Ar	NAD ⁺	SD	1,4-NADH	SD	1,6-NADH	SD	Nam	SD	TOF [mol/s]
4h	nNi ⁰	80.94%	1.7%	0.00%	0.0%	0.00%	0.0%	7.48%	0.2%	0.00E+00
	nNi ₃ Fe	62.68%	8.0%	0.00%	0.0%	0.00%	0.0%	6.61%	1.5%	0.00E+00
	nNiFe	85.24%	2.5%	0.00%	0.0%	0.00%	0.0%	8.48%	0.3%	0.00E+00
	nNiFe ₃	88.84%	1.2%	4.43%	0.9%	1.64%	0.3%	4.55%	0.0%	3.20E-06
	nFe ⁰	77.00%	6.0%	5.44%	0.9%	0.00%	0.0%	20.33%	2.3%	3.99E-06

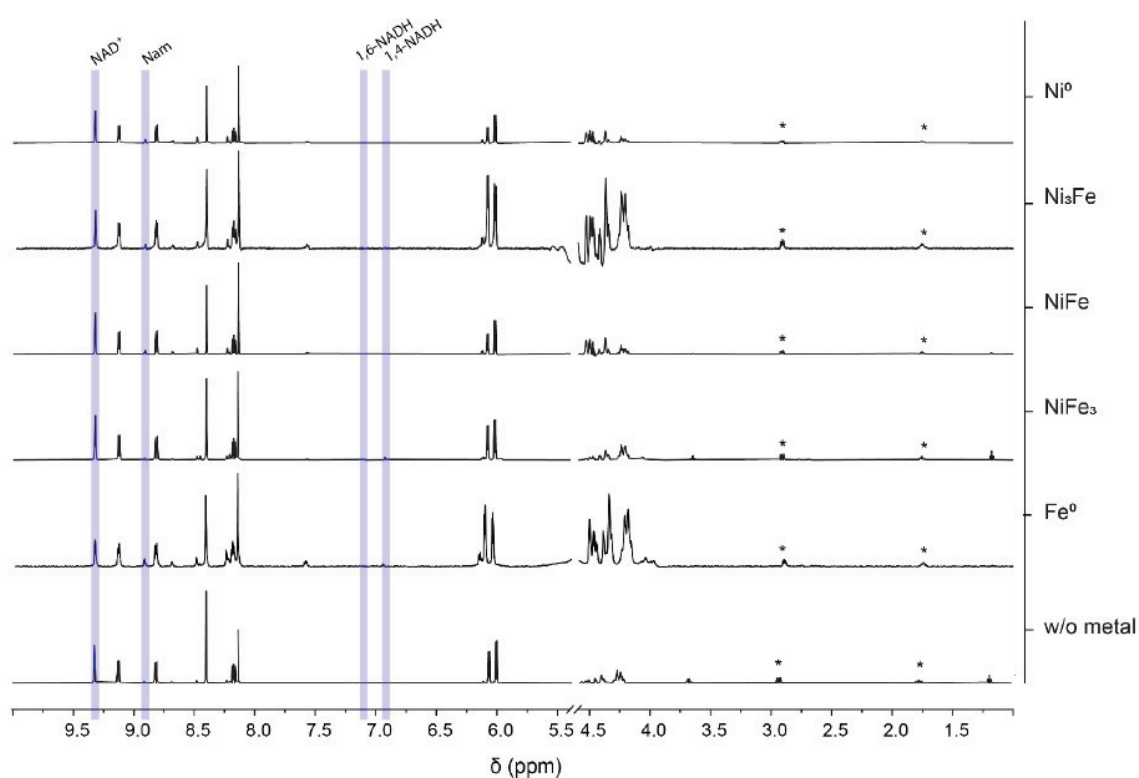


Fig. S2 The NMR spectra of replica samples of NAD⁺ in PBS (0.133 M, pH 8.5) after 4 h with 5 bar of Ar and a metal 1:1 cofactor ratio, as shown in **Scheme S1** with Ar, are stacked together in this figure. The nanoparticulate metalpowder used in each sample is indicated on the right. After 4h reacting, the supernatant was collected and DSS added as an internal standard. The spectra were edited to only include relevant peaks, having been removed a DSS peak at 0 ppm and water peak at 4.8 ppm. No other peaks were found in the areas removed. Some DSS peaks are still visible (*). The peaks used for qualitative analysis and subsequent qNMR are highlighted in blue, according to **Table S1**.

Specificity of each metal to 1,4-NADH production

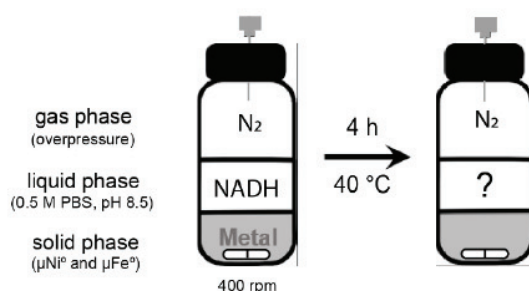
In the experiments described with NAD, the only other reduction product made other than 1,4-NADH, in significant amounts and identified through 2D-NMR, was 1,6-NADH. The amount of 1,6-NADH relative to the total amount of NADH detected in each sample was calculated and presented in the table below.

Table S4 After 4 h under 5 bar of H₂, as shown in **Scheme S1**, samples with different Ni/Fe alloys yielded different amounts of 1,4-NADH and 1,6-NADH, from the starting material NAD⁺. The starting amount of cofactor was 36 μ mol mixed in 3 mL of PBS (pH 8.5), with equimolar amounts of metal nanopowder (0.133 M PBS buffer) or 50 times more if using micropowder (0.5 M PBS buffer). The 1,6-NADH and 1,4-NADH yields were collected from **Table S2** and **Table S13**. To determine the specificity of each reaction to reduce NAD in the 4th or 6th carbon of the nicotinamide moiety, the amount of 1,6-NADH was normalized to the total amount of 1,x-NADH in the sample (1,4-NADH + 1,6-NADH). Calculating mere surface area differences between nNi and μ Ni powder results in a ratio of roughly 50:1, for nFe and μ Fe the ratio is 1:1400.

H ₂	1,6-NADH/NADH	SD
μ Ni ⁰	20,91%	0,34%
nNi ⁰	24,34%	1,36%
nNi ₃ Fe	32,63%	0,82%
nNiFe	28,58%	1,19%
nNiFe ₃	29,15%	0,20%
nFe ⁰	0,00%	0,00%
μ Fe ⁰	16,50%	0,80%

According to **Table S4**, micropowder metals tend to lead to the accumulation of less 1,6-NADH compared to nanopowders. 1,6-NADH was not detected in samples with nFe⁰, most likely due to the low NADH yield and high amounts of dissolved paramagnetic metal ions leading to line broadening. Contrastingly, nNiFe₃ is the only metal to produce 1,6-NADH under Ar, due to its comparably high TOF (s. **Table S3**). The ratio of 1,6-NADH to NADH seems to be maintained independently of the gas phase and yield between 20 and 30%.

To further understand the accumulation of 1,6-NADH, the reaction above was reproduced under an inert N₂ atmosphere, and starting with a solution of 1,4-NADH instead of NAD⁺ and with duplicates.



Scheme S2 The conversion of 1,4-NADH to 1,6-NADH was tested according to the scheme above. The amount of 1,4-NADH was 36 μmol , and 50 times more metal was added to each vial (μFe^0 and μNi^0) which reacted together for 4 h, at 40 °C, under alkaline conditions and a N_2 overpressure.

Table S5 After 4 h under an overpressure of N_2 , as shown in **Scheme S2**, samples with μNi and μFe yielded different amounts of 1,4-NADH and 1,6-NADH, from the starting material 1,4-NADH. The starting cofactor was 36 μmol mixed in 3 mL of 0.5 M PBS (pH 8.5) and with 1.8 mmol of μFe or μNi . To determine the specificity of each reaction to reduce NAD in the 4th of 6th carbon of the nicotinamide moiety, the amount of 1,6-NADH was normalized to the total amount of NADH in the sample (1,4-NADH + 1,6-NADH). All conditions had duplicates.

N_2	1,6-NADH/NADH	SD
control	15.3%	0,00%
μFe^0	10,11%	0,78%
μNi^0	12,91%	0,33%

Starting from a solution of only 1,4-NADH, all samples yielded more 1,6-NADH than when starting from NAD^+ (**Table S5**). Additionally, the metal-containing experiments did not accumulate more 1,6-NADH than the control. Given the differences observed between metals in **Table S4**, it is clear that metals can influence the production of 1,6-NADH, but it also seems that in the case of micropowders, it mostly results from an equilibrium reaction of NADH in solution.

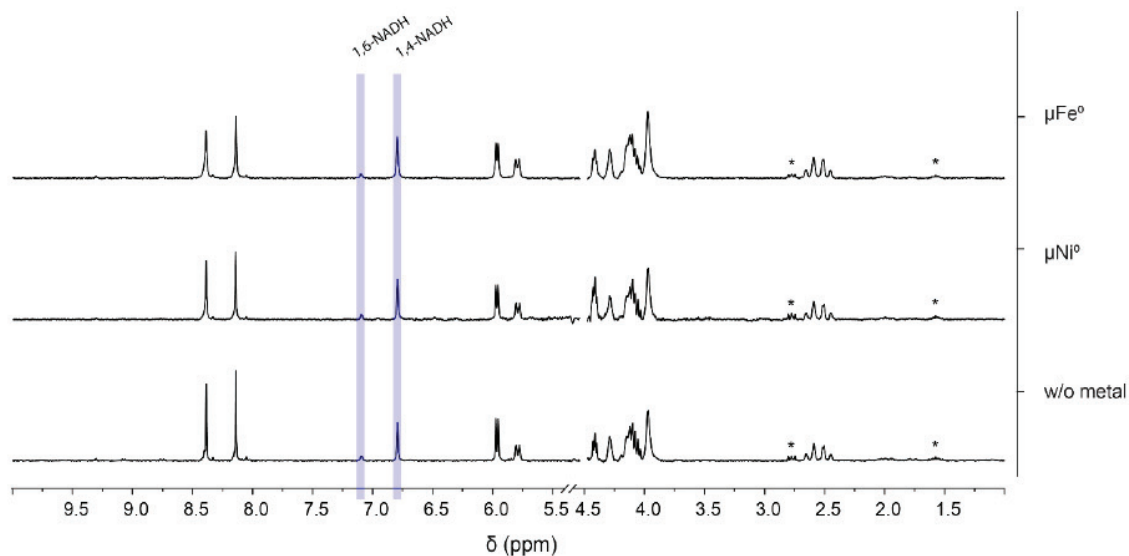


Fig. S3 The NMR spectra of replica samples of 1,4-NADH in PBS (0.5 M, pH 8.5), as shown in **Scheme S2**, are stacked together in this figure. The metal used in each sample is the micropowder indicated on the right. After 4h reacting, the supernatant was collected and DSS added as an internal standard. The spectra were edited to only include relevant peaks, having been removed a DSS peak at 0 ppm and water peak at 4.8 ppm. No other peaks were found in the areas removed. Some DSS peaks are still visible (*). The peaks used for qualitative analysis and subsequent qNMR are highlighted in blue, according to **Table S1**.

Scanning Transmission Electron Microscope of Ni-Fe-nanopowders

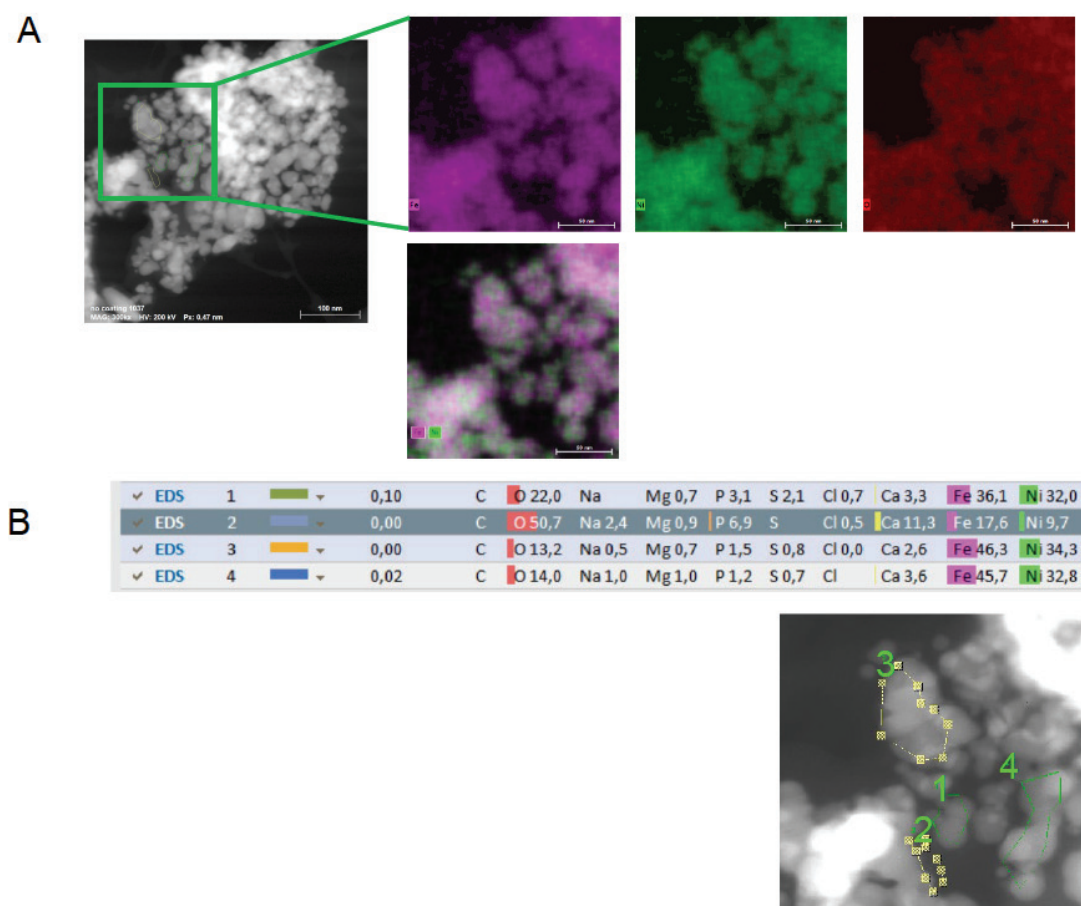


Fig. S4 NiFe (1:1) nanopowder pre-reaction STEM observation. (A) STEM-EDS analyses show that NiFe nanopowder shows a mostly even distribution of nickel and iron throughout the nanoparticles. (B) On average, there is slightly more Fe than Ni. A thin oxide layer covers the particles, probably shielding the particles from further oxidation. In comparison with NiFe₃ particles (**Fig. S5**), NiFe shows less Fe-rich regions.

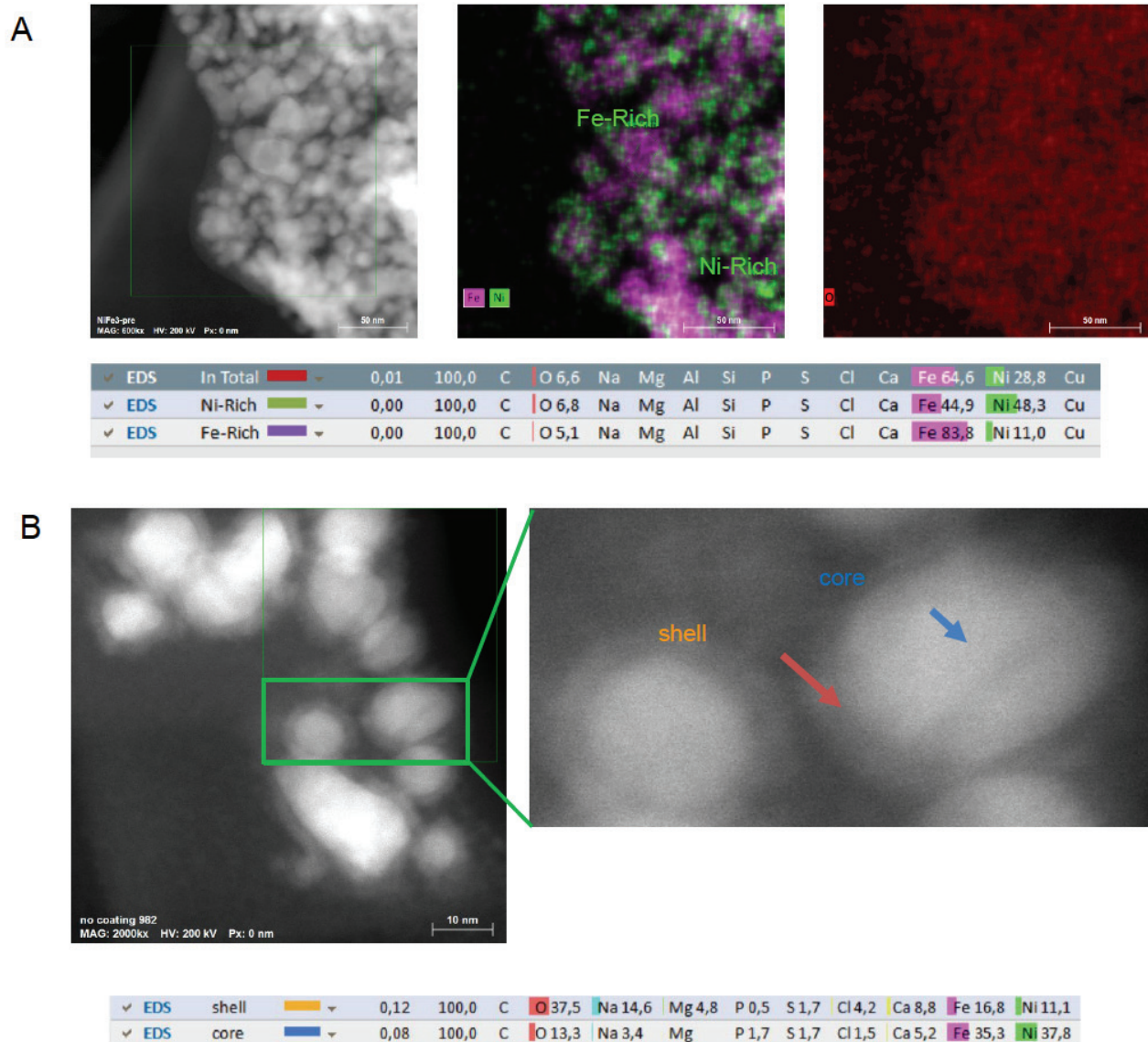


Fig. S5 NiFe₃ (1:3) nanopowder pre-reaction STEM observation. (A) STEM-EDS analyses show that NiFe₃ nanopowder shows the overall distribution of Ni and Fe is 1:3, but we find both metals are not distributed completely evenly, probably leading to the well hydrogenation yields in the reactions. There are iron rich areas that can predominantly be oxidized, delivering nascent H₂ to the NiFe regions of the same powder. (B) A thin oxide layer covers the particles, probably shielding them from further oxidation before the reaction.

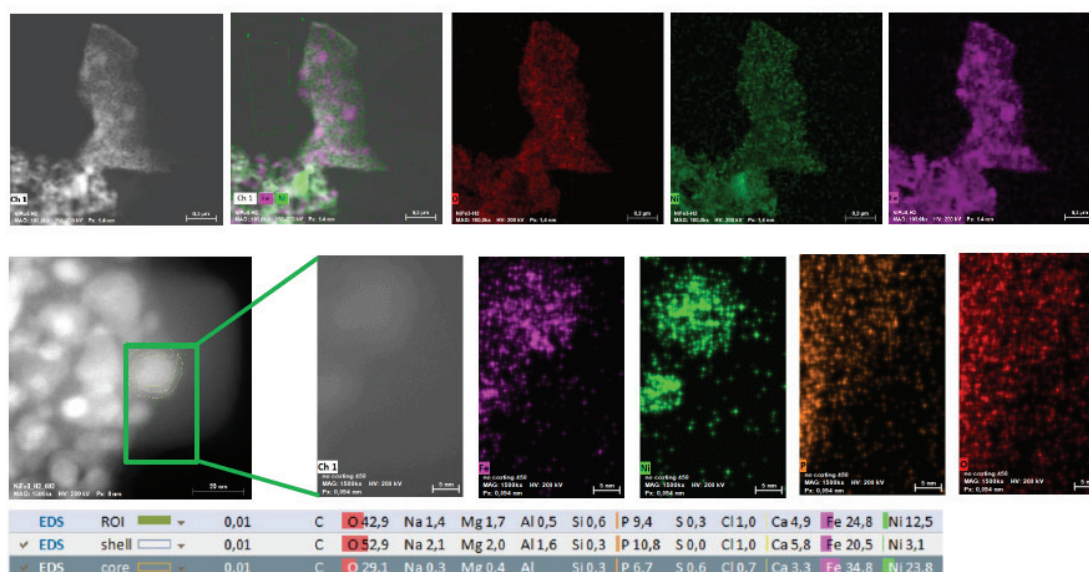


Fig. S6 NiFe_3 (1:3) nanopowder after reaction in H_2 atmosphere – STEM observation. STEM-EDS analyses show that the Fe of NiFe_3 nanopowder gets associated with the phosphate used in the buffer. This is being determined via the ratios between Fe, P and O (1.5:1:4) in the elemental analysis of the shells forming around the nanoparticles. From previous work (1) we know, that Fe is capable of producing nascent hydrogen while being oxidized, these findings are a more direct proof of this happening. The growing phosphate layer could also ultimately lead to the $\text{Fe}(0)$ containing minerals to decrease their reaction-promoting ability – we posit that the H_2 in the atmosphere can re-cycle the oxidized Fe back to Fe^0 and thus keep the reaction going for a longer period of time.

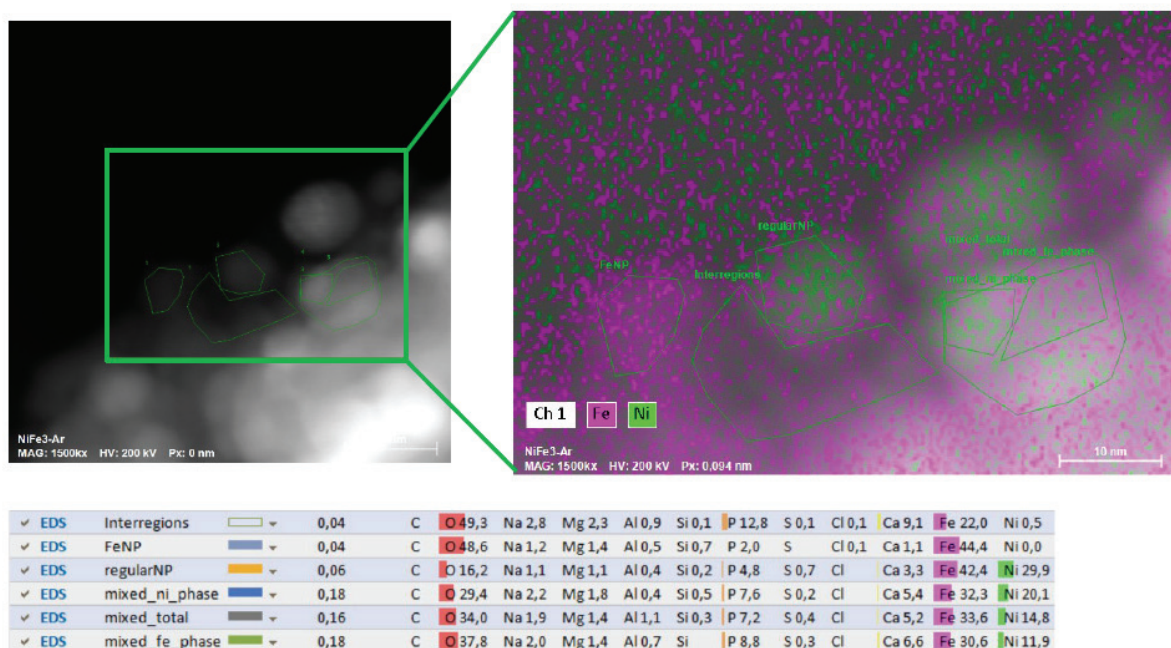
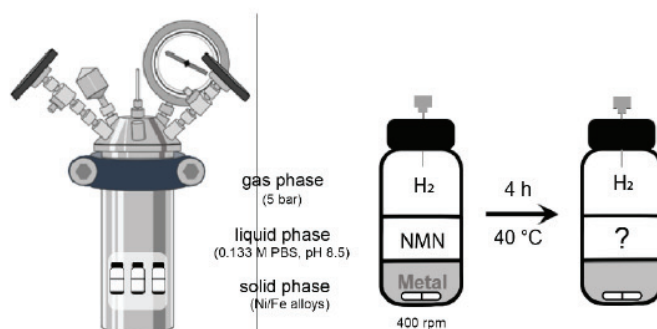


Fig. S7 NiFe₃ (1:3) nanopowder after reaction in Ar atmosphere – STEM observation. STEM-EDS analyses indicate that the Fe of NiFe₃ nanopowder likely gets oxidized, forming Fe₃(PO₄)₂ with the phosphate buffer. The cleaning process of the nanoparticles after the reaction (s. Methods) strengthens the assumption that Fe and phosphate are more than just loosely associated. This is being determined via the ratios between Fe, P and O. This mapping shows that the regions between the nanoparticles almost consist exclusively of iron-phosphates precipitating from the reactions.

Heterogeneous catalysis of NMN reduction with H₂ and Ni/Fe alloys



Scheme S3 The reduction of NMN with nanoparticular Ni/Fe alloys was tested with the protocol described in detail in Methods, and according to the scheme above. The amount of metal and NMN was 36 or 18 μmol , which reacted together for 4 h, at 40 °C, under alkaline conditions and 5 bars of H₂. The same reaction was made under Ar as a control.

Table S6 After 4 h under 5 bar of H₂, as shown in **Scheme S3**, samples with different nanoparticular Ni/Fe alloys yielded different amounts of 1,4-NMNH, 1,4,6-NMNH, NMNH₂OH, 1,2,4,6-NMNH₅ and nicotinamide (Nam), from the starting material NMN, as listed below. The starting metal and cofactor were 36 or 18 μmol mixed in 3 mL of 0.133 M PBS (pH 8.5). The yields were calculated relative to the metal-free sample (100% NMN). To determine the TOF of each reaction, the sum of 1,4-NMNH, 1,4,6-NMNH₃ and 1,2,4,6-NMNH₅ was considered as the amount of product, and the total amount of metal atoms were considered as the mount of catalyst, instead of the number of molecules. Each condition was tested in duplicates and a metal-free control.

	H ₂	NMN	SD	1,4-NMNH	SD	1,4,6-NMNH ₃	SD	NMNH ₂ OH	SD	1,2,4,6-NMNH ₅	SD	Nam	SD	TOF [mol/s]
4h	nNiFe	9.61%	6.4%	7.74%	0.5%	21.63%	3.2%	25.39%	0.6%	3.24%	0.6%	1.93%	0.3%	2.12E-05
	nNiFe ₃	2.01%	0.1%	9.46%	0.4%	25.22%	0.7%	29.49%	0.0%	2.73%	0.4%	1.75%	0.1%	1.12E-05
	nFe ⁰	40.51%	5.1%	13.23%	1.0%	2.29%	0.3%	19.47%	2.1%	0.00%	0.0%	4.63%	0.2%	2.63E-05

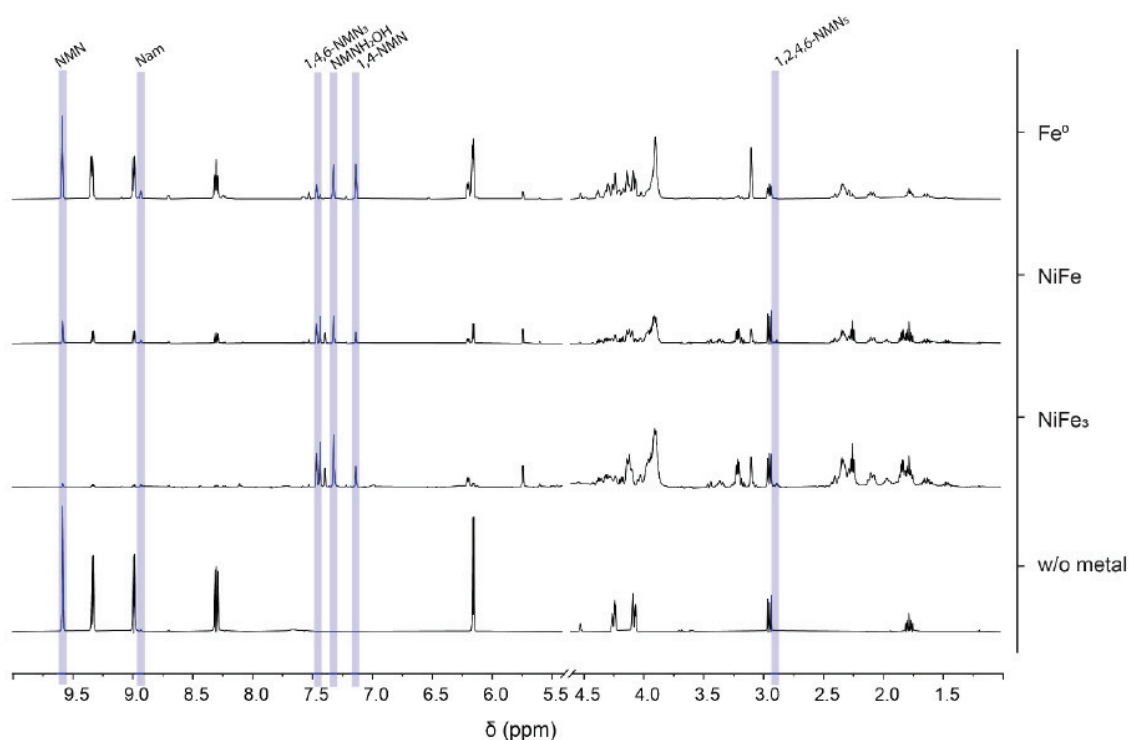


Fig. S8 The NMR spectra of replica samples of NMN in PBS (0.133 M, pH 8.5) reacted for 4h with 5 bar of H₂ and a metal 1:1 cofactor ratio, as shown in **Scheme S3**, are stacked together in this figure. The metal used in each reaction is specified on the right of each spectra. After the 4h reaction, the supernatant was collected and DSS added as an internal standard. The spectra were edited to only include relevant peaks, having been removed a DSS peak at 0 ppm and water peak at 4.8 ppm. No other peaks were found in the areas removed. Some DSS peaks are still visible (*). The peaks used for qualitative analysis and subsequent qNMR are highlighted in blue, according to **Table S8**.

Table S7 After 4 h under 5 bar of Ar, as shown in **Scheme S3** with Ar, samples with different nanoparticular Ni/Fe alloys yielded different amounts of 1,4-NMNH, 1,4,6-NMNH, NMNH₂OH, 1,2,4,6-NMNH₅ and nicotinamide (Nam), from the starting material NMN, as listed below. The starting metal and cofactor were 36 or 18 μmol mixed in 3 mL of 0.133 M PBS (pH 8.5). The amount of metal atoms was the same as the cofactor. The yields were calculated relative to the metal-free sample (100% NMN). To determine the TOF of each reaction, the sum of 1,4-NMNH, 1,4,6-NMNH₃ and 1,2,4,6-NMNH₅ was considered as the amount of product, and the total amount of metal atoms were considered as the mount of catalyst, instead of the number of molecules.

	Ar	NMN	SD	1,4-NMNH	SD	1,4,6-NMNH ₃	SD	NMNH ₂ OH	SD	1,2,4,6-NMNH ₅	SD	Nam	SD	TOF [mol/s]
4h	nNiFe	65.07%	1.0%	4.40%	0.4%	2.92%	0.0%	7.52%	0.3%	0.00%	0.0%	1.90%	0.1%	4.75E-06
	nNiFe ₃	54.40%	0.2%	6.72%	0.4%	3.39%	0.4%	13.31%	0.4%	0.00%	0.0%	2.38%	0.2%	6.56E-06
	nFe ⁰	87.37%	1.2%	0.97%	0.0%	0.00%	0.0%	0.80%	0.2%	0.00%	0.0%	5.36%	0.2%	1.33E-06

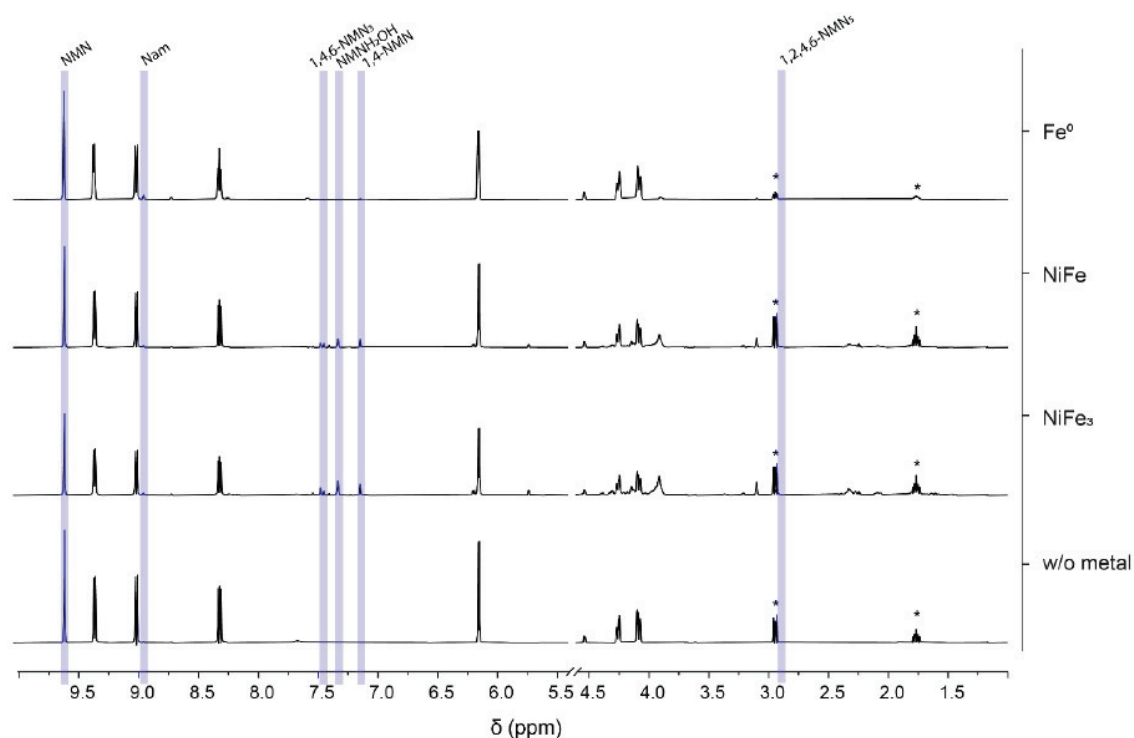


Fig. S9 The NMR spectra of replica samples of NMN in PBS (0.133 M, pH 8.5) reacted for 4h with 5 bar of Ar and a metal 1:1 cofactor ratio, as shown in **Scheme S3** with Ar, as indicated on the left side, are stacked together in this figure. The metal used in each reaction is specified on the right of each spectra. After the 4h reaction, the supernatant was collected and DSS added as an internal standard. The spectra were edited to only include relevant peaks, having been removed a DSS peak at 0 ppm and water peak at 4.8 ppm. No other peaks were found in the areas removed. Some DSS peaks are still visible (*). The peaks used for qualitative analysis and subsequent qNMR are highlighted in blue, according to **Table S8**.

Table S8 For quantification of each compound, a peak was selected in their spectra. The values listed a bellow indicate the ppm value where the peak can be found at approximately pH 8.5 (0.133M PBS).

Molecule	NMN	Nam	1,4,6-NMN	NMNH ₂ OH	1,4-NMNH	1,2,4,6-NMN
δ (ppm) for quantification	9.58	8.93	7.41/7.45	7.34	7.15	2.85

Reduction products of NMN and NAD characterized through NMR spectroscopy

Fig. S10 shows the ^1H spectrum of substrate **1** in 0.133 M PBS at 298 K. Characteristic signals at 9.581, 9.337, 8.990, 8.308, 6.187, 4.472 ppm were observed for H-2, H-6, H-4, H-5, H-1' and H-4' respectively. Furthermore, two double doublets at 4.197 and 4.025 ppm were detected for the diastereotopic methylene $\text{CH}_2\text{-5'}$.

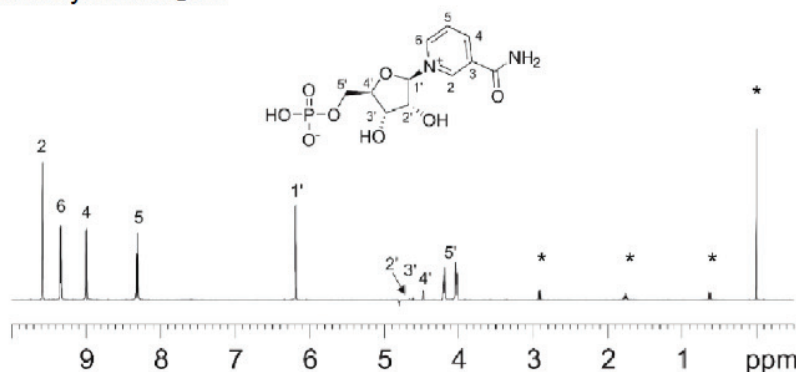


Fig. S10 ^1H spectrum of substrate NMN^+ (**1**) in 0.133 M PBS with the internal reference DSS (*) at 298 K.

Identification of products of substrate **1**

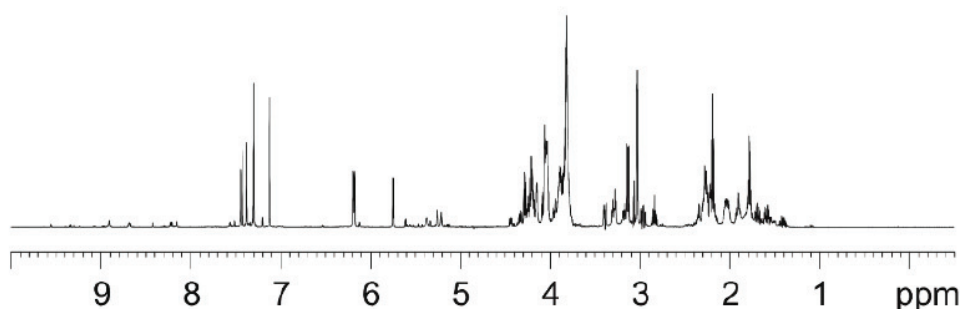


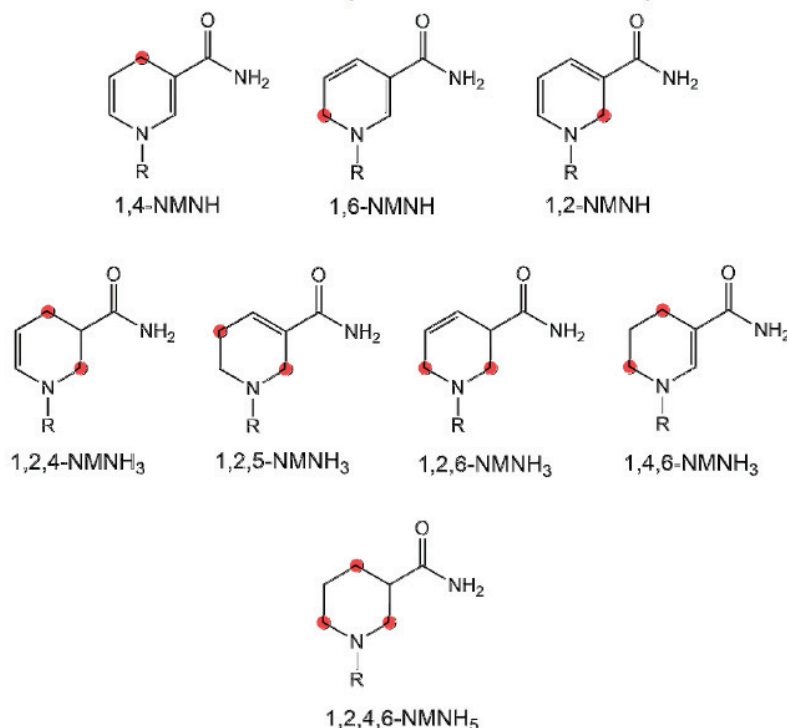
Fig. S11 ^1H spectrum of the products NMNH in 0.133 M PBS at 298 K.

The figure above presents ^1H spectrum of products solution of substrate **1** after 4 h of incubation. This spectrum shows a strong reduction in the intensity of signals from 8.3 to 9.6 ppm, which means a large degradation of the substrate. A large number of signals from 1.3 to 7.5 ppm were observed, which reveals the formation of a group of more than three different species of products. As shown in **Scheme S4**, three single reduction products, the 1,2-NMNH, 1,4-NMNH and 1,6-NMNH may form. Further reduction of the nicotineamide may follow, thus 1,2,4-, 1,2,5-, 1,2,6-, 1,4,6-, and 1,2,4,6-NMNH_x may form, too.

Due to the large number of species in the reaction solution, efforts to separate the products through LC-MS turned out to be in vain. The different NMN reduced species share the same retention time with the implemented protocol. Nevertheless, with enough amount of substance in hands we managed to use NMR spectroscopy to characterize the obtained products. It is well-known that multidimensional NMR spectroscopy plays an important role in the structure determination in

synthetic chemistry, molecular biology and biochemistry and catalysis. By using two-dimensional NMR spectra, not only the functional groups but also the connectivity among them within a molecule can be characterised. Thus, the structure of peptides and biomacromolecules can be determined.^(2–4)

The great challenge we were facing was to deal with a huge signal overlap caused by the mixture of various species. Fortunately, by using TOCSY signals belong to the same molecule (within one spin network) can be identified. The edited $^1\text{H} - ^{13}\text{C}$ HSQC spectra extend the scope of information, where characteristic ^{13}C chemical shifts can be made used for the structure identification. Furthermore, the sign of crosspeaks in the edited HSQC spectra provides unambiguous identification of methylene and methine groups. By careful analysis of the TOCSY and edited HSQC spectra we were able to determine the main species of those reduction products.



Scheme S4 Tentative reduction products of NMN reduction. Red marks the reduced carbon.

The single reduction product 1.1

Starting from the well-resolved signal at 3.057 ppm, TOCSY crosspeaks (**Fig. S12**) show connectivities with signals at 7.147, 6.214, 5.774, and 5.022 ppm. The edited HSQC spectrum (**Fig. S13**) shows crosspeaks between 3.057 – 22.0 ppm for a CH_2 group, 7.147 – 138.2 ppm, 6.214 – 124.8 ppm and 5.022 – 105.3 ppm for three aromatic CH groups, and 5.774 – 91.7 ppm for a CH group at the anomeric position of a sugar. Those defined fragments correspond well to the three species of single reduction as shown in **Scheme S4**. Upon a close inspection into the ^{13}C chemical shift at 22.0 ppm, we concluded product **1.1** to be 1,4-NMNH. The ^{13}C signal of the CH_2 group in both 1,2- and 1,6-NMNH (at the α -position of a tertiary amine) would appear at a much lower field (in the range 45 – 50 ppm).⁽⁵⁾ Since no such crosspeaks were detected, we excluded the formation of 1,2- and 1,6-NMNH from our products. Two well resolved major peaks at 7.15 ppm (d, 1.5 Hz)

and 6.24 ppm (ddt, 8.1, 1.9, 1.7 Hz) were observed. In addition, a pair of very close doublets were observed at 3.056 ppm (1.6 Hz) and 3.062 ppm (1.7 Hz). Those peaks correspond well to ^1H signals at positions 2, 6 and 4 in the **Table S18**, respectively.

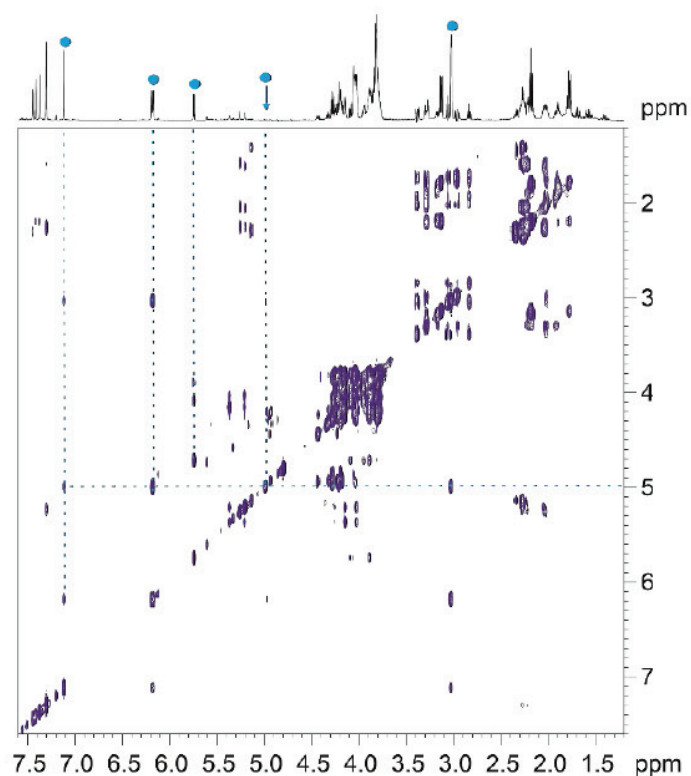


Fig. S12 ^1H - ^1H TOCSY spectrum of NMN products in 0.133 M PBS at 298 K.

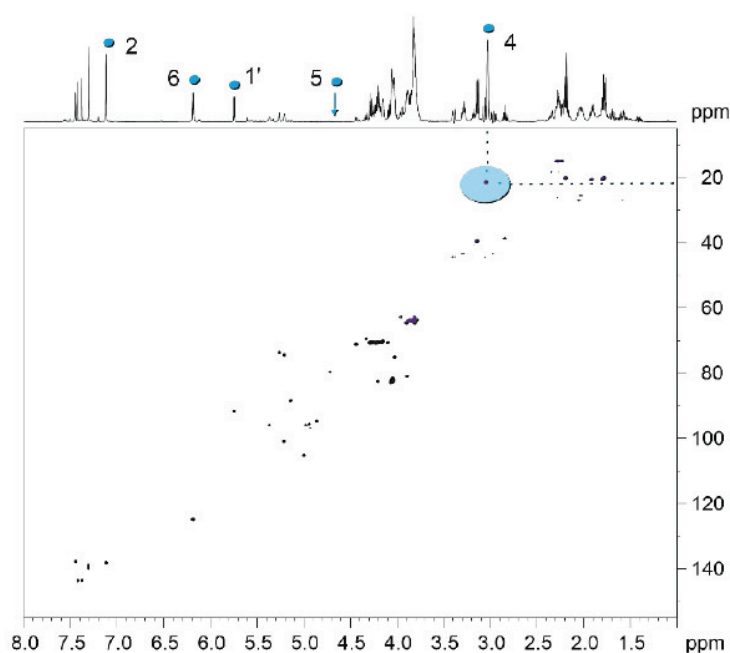


Fig. S13 The edited ^1H - ^{13}C HSQC spectrum of products of **1** at 298 K.

Products of follow up reactions

As shown in **Scheme S4**, two of the tetrahydro-products, 1,2,4- and 1,2,6-NMNH₃ contain a CH group within the hetero cyclic ring. This CH group should show a characteristic crosspeak in the edited HSQC spectrum of ¹³C chemical shift in the region 40 – 50 ppm (38), with a sign opposite to a CH₂ group. A close inspection of the spectrum shows none of such signals detected. We thus excluded these two species from our products.

Nevertheless, one crosspeak at 2.868 – 38.8 ppm was detected. Close inspection of the crosspeaks in the corresponding region of the TOCSY spectrum (**Fig. S15**) revealed a connectivity pattern for a meta-substituted piperidine. Therefore, a hexahydro product **1.2** was identified, which is 1,2,4,6-NMNH₅. The highlighted peak is for the methine CH and the ¹H signal at 2.87 ppm stands for proton at carbon 3.

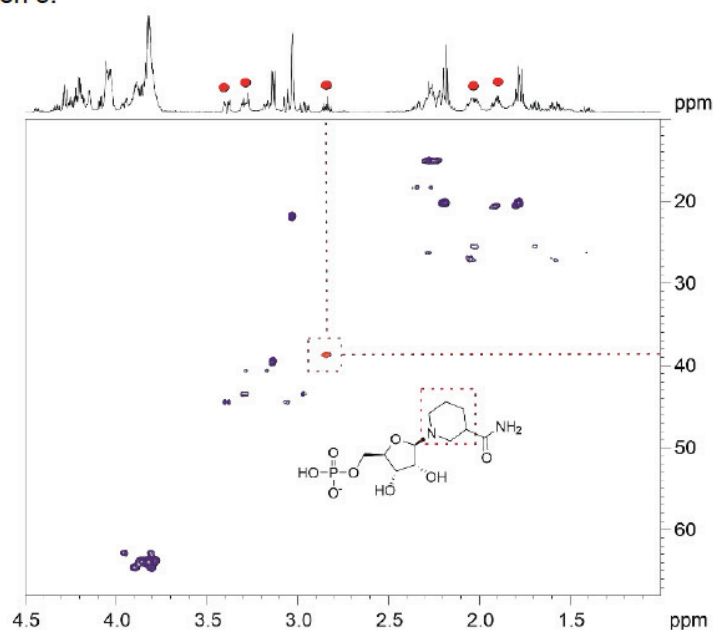


Fig. S14. Section of edited ¹H-¹³C HSQC spectrum of products of **1** at 298 K.

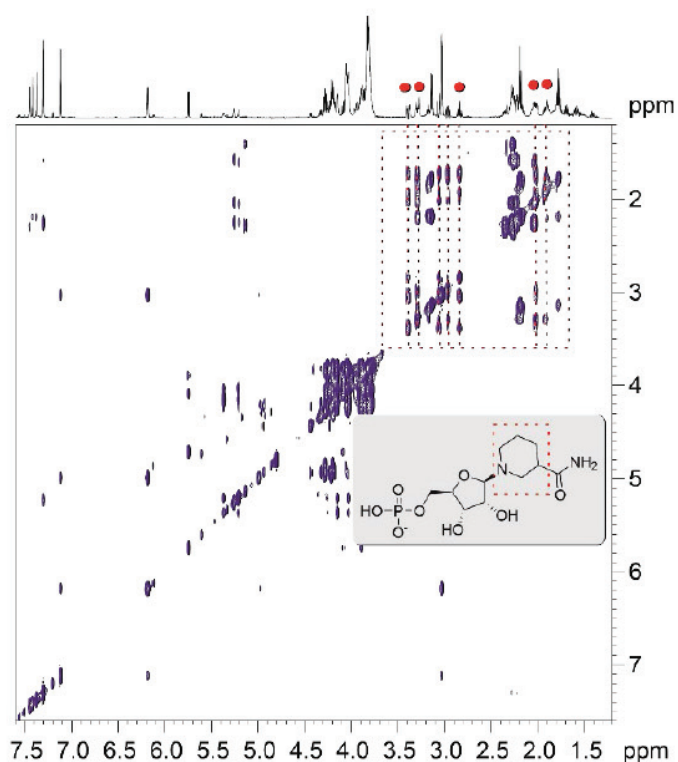


Fig. S15 Section of ^1H - ^1H TOCSY spectrum of products of **1** at 298 K.

Similarly, crosspeaks at 7.448/7.405 – 143.7 (not shown **Fig. S16**), 3.165 – 39.7, 2.215 – 20.3, and 1.808 – 20.3 ppm were detected in the edited HSQC spectrum (**Fig. S16**), together with connectivities observed with TOCSY. The tetrahydro-product **1.3** was identified to be 1,4,6-NMNH₃.

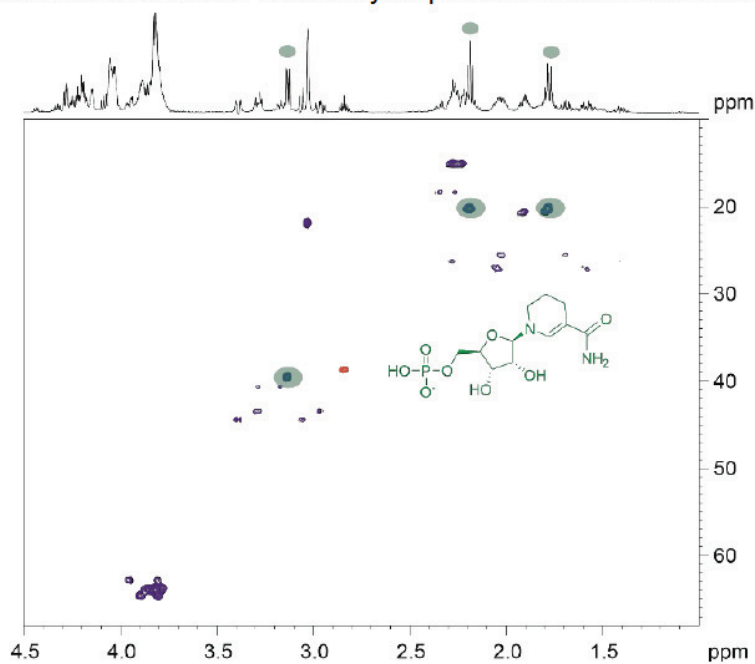


Fig. S16 Section of edited ^1H - ^{13}C HSQC spectrum of products of **1** at 298 K.

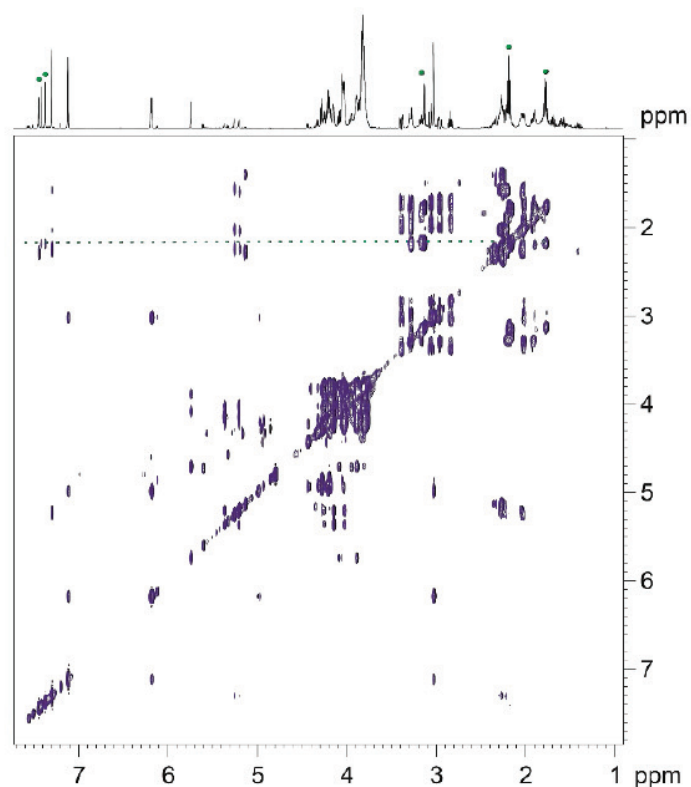


Fig. S17 Section of ^1H - ^1H TOCSY spectrum of products of **1** at 298 K.

In summary, in the reaction mixture of substrate **1**, we were able to identify product **1.1** (1,4-NMNH), product **1.2** (1,2,4,6-NMNH₅), and product **1.3** (1,4,6-NMNH₃).

Identification of hydration product NMNH₂OH.

In order to identify the peak at 7.35 ppm in the ^1H spectrum we put further efforts. Via LC-MS a hydration product with molecular formula $\text{C}_{11}\text{H}_{18}\text{N}_2\text{O}_9\text{P}^-$ and 353.07323 m/z (mass accuracy of 5 ppm) was revealed (**Fig. S22**). Following the first reduction step, hydration upon 1,4-NMNH took place and products 1,4-NMNH₂OH formed. Thus, crosspeaks at 7.35 – 138.9, 7.35 – 139.9, 5.29 – 73.9, 5.24 – 74.6, 2.25/2.31 – 15.3 and 2.07/1.06 – 27.1 ppm were detected in the edited HSQC spectrum (**Fig. S19**). Together with connectivity in TOCSY spectrum (**Fig. S18**) hydration products as revealed by LC-MS were verified.

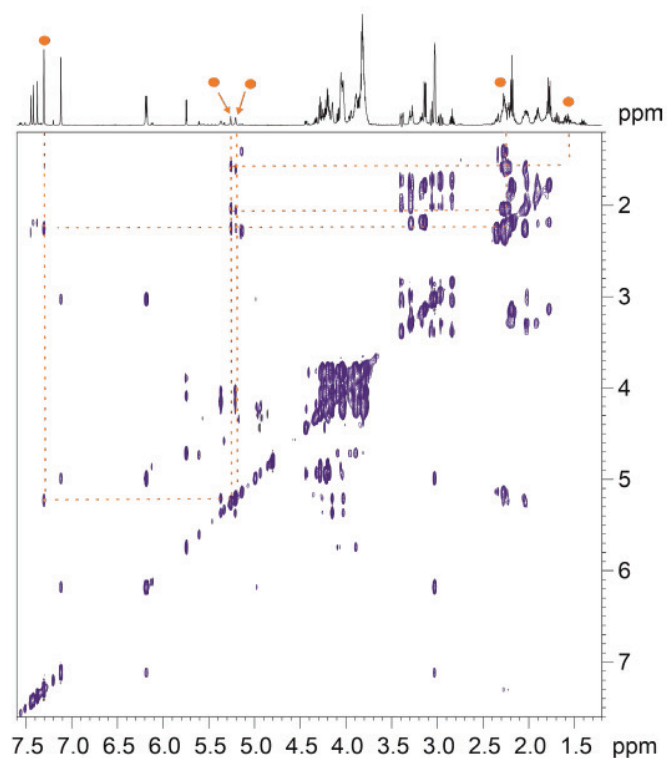


Fig. S18 Section of ^1H - ^1H TOCSY spectrum of products of **1** at 298 K. with highlight for the hydration products.

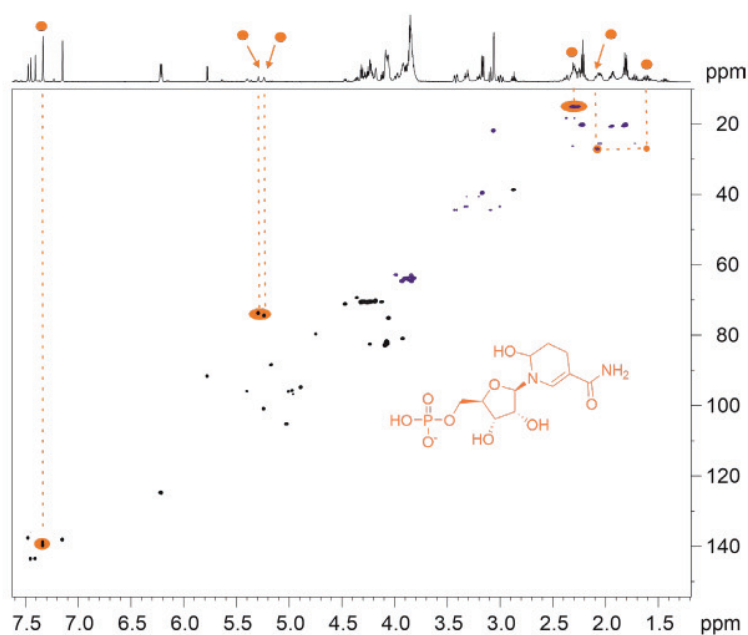


Fig. S19 Section of edited ^1H - ^{13}C HSQC spectrum of products of **1** at 298 K. with highlight for the hydration products.

In summary, in the reaction mixture of substrate **1** we were able to identify product **1.1** (1,4-NMNH), product **1.2** (1,2,4,6-NMNH₅), product **1.3** (1,4,6-NMNH₃) and verify the hydration product 1,4 (NMNH₂OH).

Characterization of the 2nd reaction product with Fe⁰ and LC-MS (7.35 ppm in ¹H-NMR)

In order to identify the second product of NMN reduction with H₂ and Fe⁰, sample from such reaction (NMN 18 μmol, nanopowder Fe⁰ 18 μmol, 4 h. 40 °C. 5 bar H₂) was subjected to 2D-NMR and LC-MS qualitative analysis.

LC-MS analysis is in agreement that the main product is 1,4-NMNH. Three different molecules seem to be detected through chromatography, and one matches the retention time of the 1,4-NMN standard. It is possible that we have different conformations of this product in our samples. Its absence in the control confirms it to be a product obtained during the described reaction.

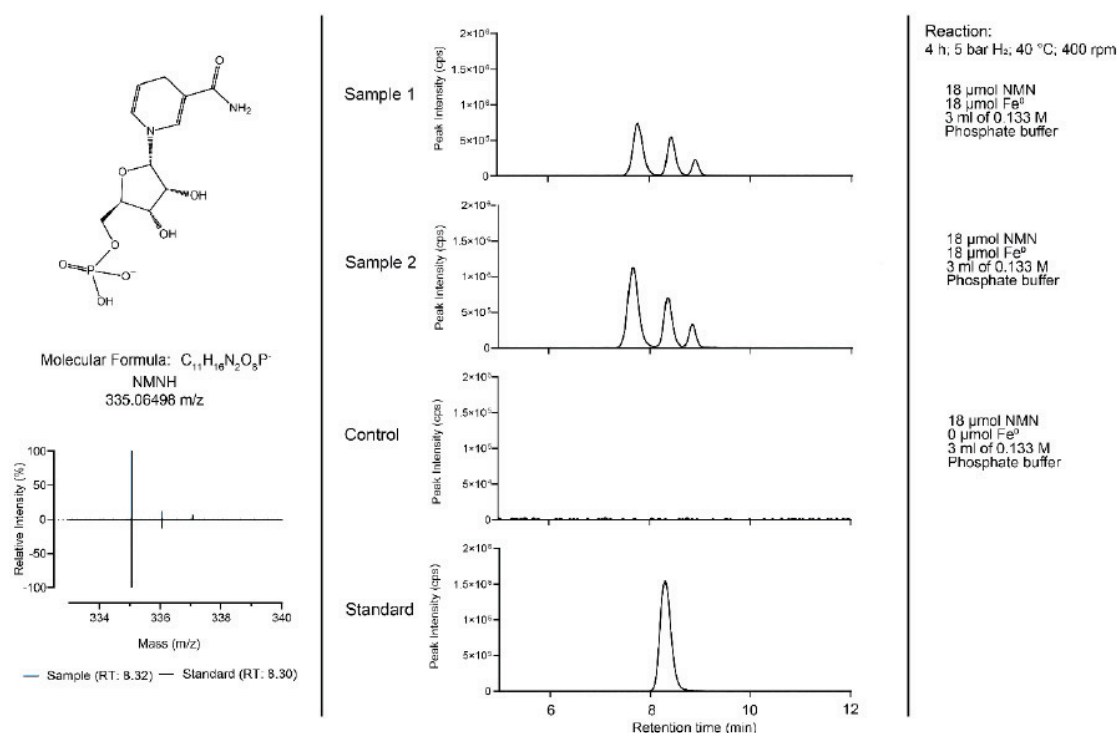
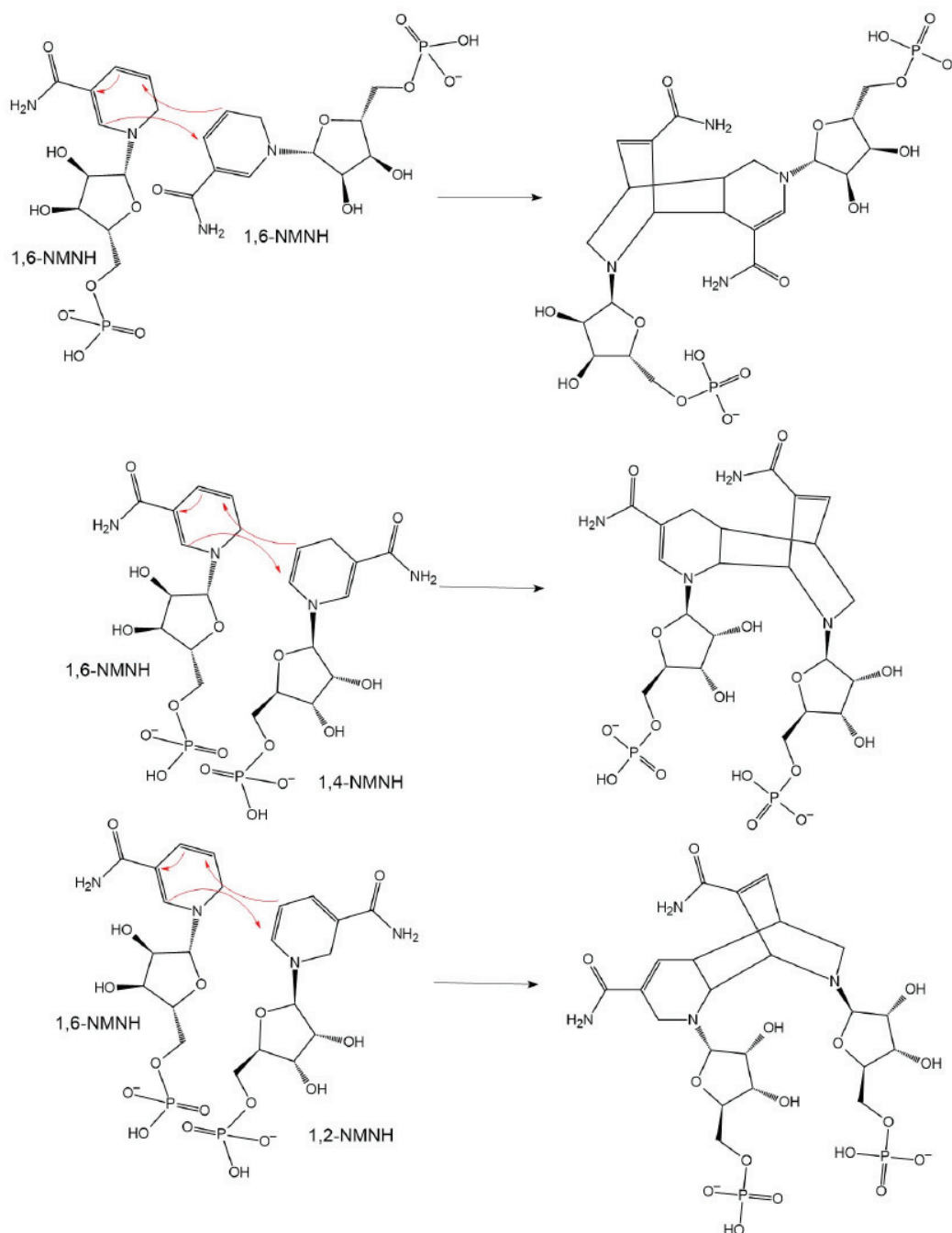


Fig. S20 The Extracted Ion Chromatogram (EIC) of mass 335.06368 (mass accuracy of 5 ppm) against the Retention Time (RT) reveals molecules of the mass 335.0649 m/z in the samples from the reaction described on the right. Samples were diluted 1:20 with waster after the reaction for measurement. The natural isotope distribution of the 1,4-NMNH standard (335.06498 m/z) matches that of the samples.

All Diels Alder products suggested in **Scheme S5** share the same mass and charge, which is also the same mass-to-charge of NMNH. Even though molecules of mass 335.06498, were revealed in the chromatogram, analysis of the isotope distribution revealed no doubled charged molecules, thus excluding Diels Alder reactions as products of the reaction with Fe^0 .



Scheme S5 Possible Diels-Alder reactions to consume 1,4-NMNH

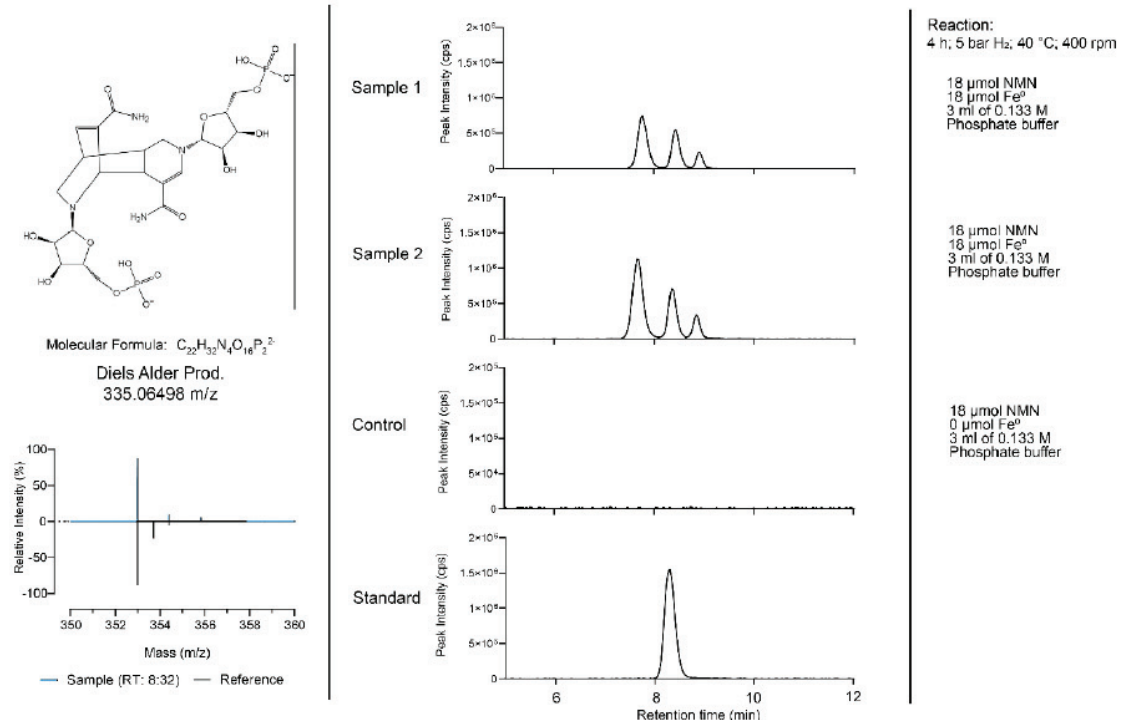


Fig. S21 The Extracted Ion Chromatogram (EIC) of mass 335.06368 (mass accuracy of 5 ppm) against the Retention Time (RT) reveals molecules of the mass 335.0649 m/z in the samples from the reaction described on the right. Samples were diluted 1:20 with waster after the reaction for measurement. The standard was prepared in water at similar final concentrations. The theoretical natural isotope distribution of the proposed Diels Alder products (335.06498 m/z), extracted from the website ChemCalc, is compared to that of the samples.

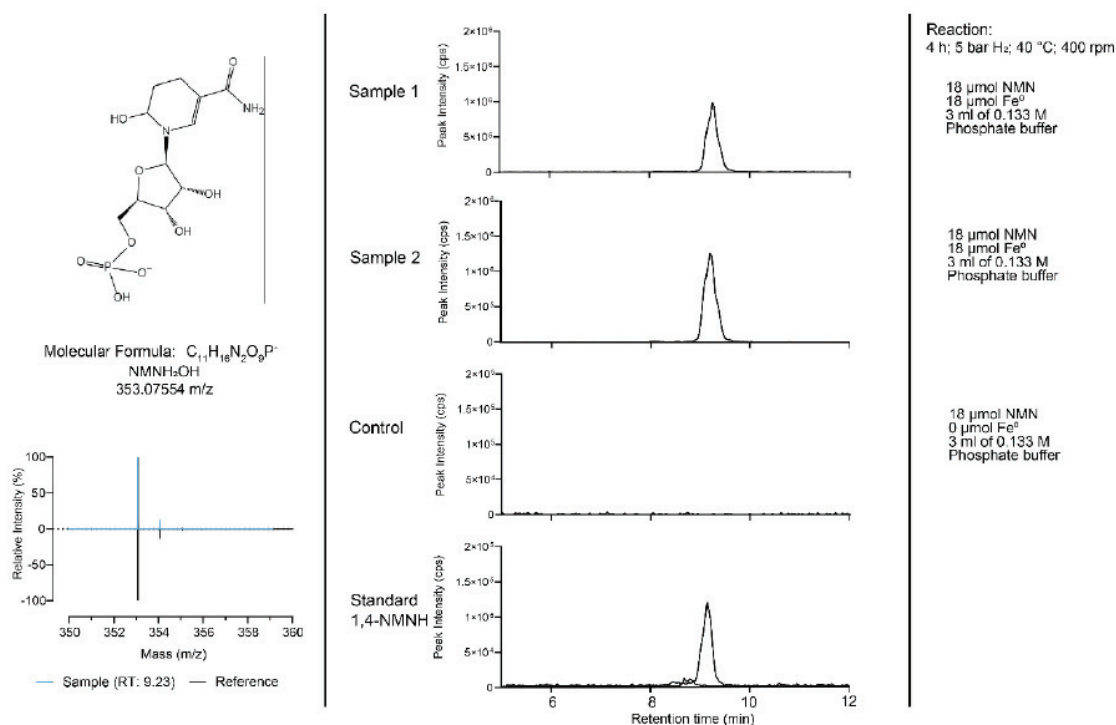
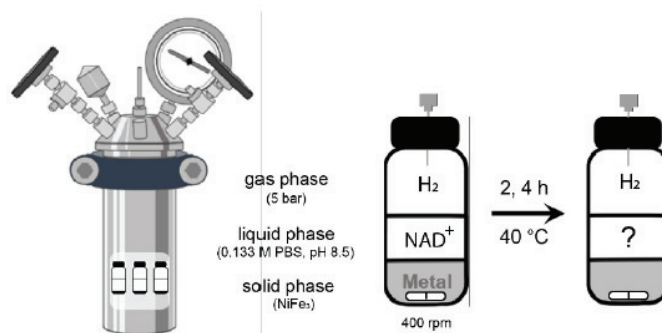


Fig. S22 The Extracted Ion Chromatogram (EIC) of mass 353.07323 (mass accuracy of 5 ppm) against the Retention Time (RT) reveals molecules of the mass 353.07323 m/z in the samples from the reaction described on the right. Samples were diluted 1:20 with waster after the reaction for measurement. The standard was prepared in water at similar final concentrations. The theoretical natural isotope distribution of NMNH₂OH (353.07554 m/z), extracted from the website ChemCalc, is compared to that of the samples.

Further analysis of the samples revealed high amounts of a molecule of mass 353.07554 in the samples, which were not in the control. The mass and the isotope distribution of the sample matches that of NMNH₂OH. The same signal was detected in the 1,4-NMNH standard, however, the relative abundance to the standard itself, shows it is likely a small contamination from the synthesis of the standard or a consequence of sample preparation and injection into the LC-MS column. The relative abundance of this molecule to 1,4-NMNH, in the samples, is much more significant, being likely a product of the Fe^0 reaction. Its abundance suggests it could be the molecule detected at 7.35 ppm (¹H-NMR). 2D-NMR analysis confirmed the proposed structure to be of NMNH₂OH (Fig. S18 and Fig. S19).

Overtime reduction of NAD/NMN with H₂ and NiFe₃

For quantification of each product, the ppm values of **Table S1**, and **Table S6** should be considered.



Scheme S6 The reduction of NAD⁺ with nNiFe₃ alloys was tested with the protocol described in detail in Methods, and according to the scheme above. The amount of metal and NAD⁺ was 36 μmol, which reacted together for 2 and 4 h, at 40 °C, under alkaline conditions and 5 bars of H₂. The same reaction was made under Ar as a control.

Table S9 After 2 and 4 h under 5 bar of H₂, as shown in **Scheme S6**, samples with NiFe₃ yielded different amounts of 1,4-NADH, 1,6-NADH, and Nam, from the starting material NAD⁺. The starting metal and cofactor were 36 μmol mixed in 3 mL of 0.133 M PBS (pH 8.5). The amount of metal atoms was the same as the cofactor. The yields were calculated relative to the metal-free sample (100% NAD⁺). To determine the TOF of each reaction, the sum of 1,4-NADH, and 1,6-NADH was considered as the amount of product, and the total amount of metal atoms was considered as the mount of catalyst, instead of the number of molecules. Experiments of 2h had duplicates while 4h long experiments had four replicas.

	H ₂	NAD ⁺	SD	1,4-NADH	SD	1,6-NADH	SD	Nam	SD	TOF [mol/s]
4h	nNiFe ₃	25.59%	4.4%	40.60%	1.8%	16.70%	0.6%	4.48%	0.1%	3.02E-05
2h		68.38%	2.5%	15.05%	1.3%	6.61%	0.6%	7.41%	0.4%	3.18E-05

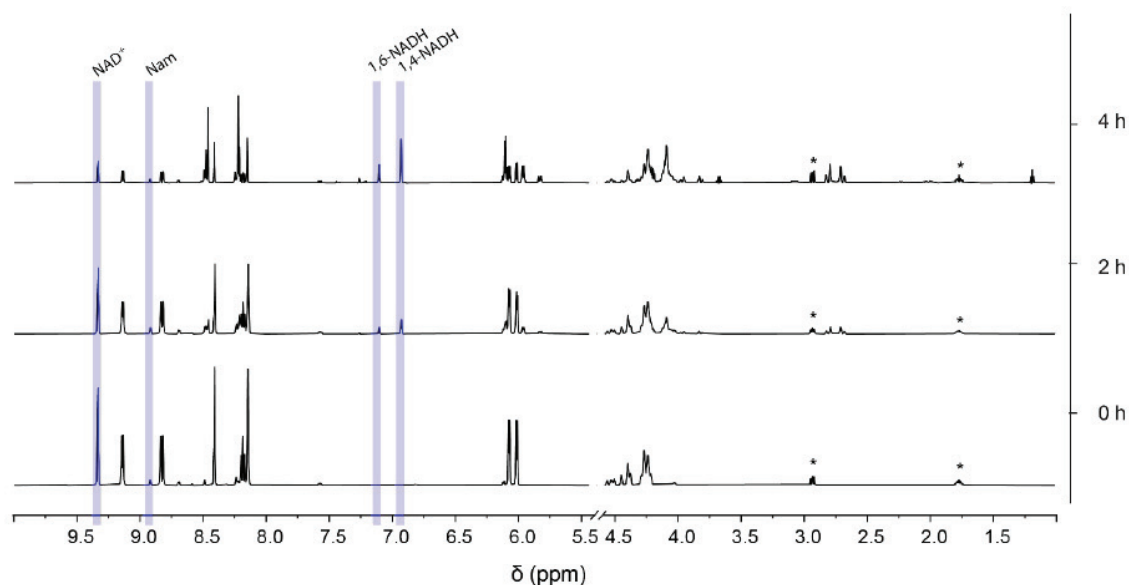
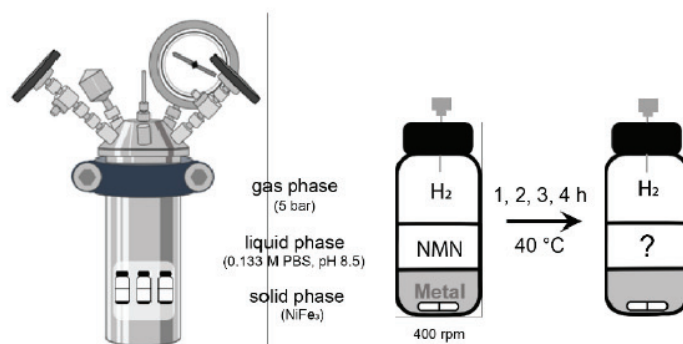


Fig. S23 The NMR spectra of replica samples of 36 μmol NAD^+ in PBS (0.133 M, pH 8.5) with 5 bar of H_2 and 36 μmol NiFe_3 (1:1 cofactor ratio), as shown in **Scheme S6**, are stacked together in this figure. After 0, 2 and 4 h, the supernatant was collected and DSS added as an internal standard. The spectra were edited to only include relevant peaks, having been removed a DSS peak at 0 ppm and water peak at 4.8 ppm. No other peaks were found in the areas removed. Some DSS peaks are still visible (*). The peaks used for qualitative analysis and subsequent qNMR are highlighted in blue, according to **Table S1**.



Scheme S7 The reduction of NMN with NiFe_3 was tested with the protocol described in detail in **Methods**, and according to the scheme above. The amount of metal and NMN was 36 or 18 μmol , which reacted together for 1, 2, 3, and 4 h, at 40 °C, under alkaline conditions and 5 bars of H_2 . The same reaction was made under Ar as a control.

Table S10 After 1, 2, 3, and 4 h under 5 bar of H₂, as shown in **Scheme S7**, samples with NiFe₃ yielded different amounts of 1,4-NMNH, NMNH₂OH, 1,4,6-NMNH₃, 1,2,4,6-NMNH₅, and nicotinamide (Nam), from the starting material NMN. The starting metal and cofactor were 36 μ mol mixed in 3 mL of 0.133 M PBS (pH 8.5). The amount of metal atoms was the same as the cofactor. The yields were calculated relative to the metal-free sample (100% NMN). To determine the TOF of each reaction, the sum of 1,4-NMNH, 1,4,6-NMNH₃, 1,2,4,6-NMNH₅ was considered as the amount of product, and the total amount of metal atoms was considered as the amount of catalyst, instead of the number of molecules. 2h and 4h were tested with duplicates while 1h and 3h with triplicates.

	H ₂	NMN	SD	1,4-NMNH	SD	1,4,6-NMNH ₃	SD	NMNH ₂ OH	SD	1,2,4,6-NMNH ₅	SD	Nam	SD	TOF [mol/s]
4h	nNiFe ₃	2.01%	0.1%	9.46%	0.4%	25.22%	0.7%	29.49%	0.0%	2.73%	0.4%	1.75%	0.1%	1.12E-05
3h		1.21%	0.6%	24.74%	0.0%	19.72%	2.6%	21.32%	1.4%	2.82%	0.6%	2.05%	0.2%	7.10E-05
2h		9.38%	3.5%	34.03%	0.7%	14.48%	1.4%	16.64%	0.3%	1.78%	0.4%	2.54%	0.2%	7.55E-05
1h		30.80%	16.7%	29.84%	7.1%	7.40%	2.7%	12.67%	2.7%	0.73%	0.5%	2.87%	0.3%	1.14E-04

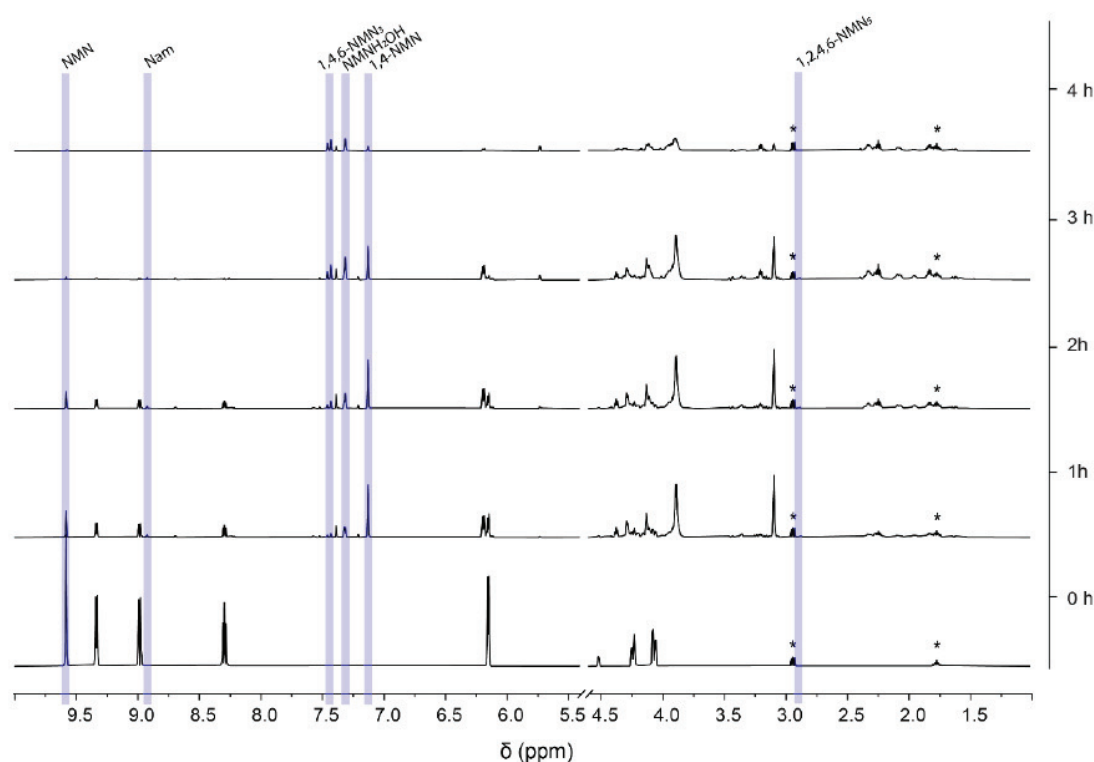


Fig. S24 The NMR spectra of replica samples of 36 or 18 μ mol NMN in PBS (0.133 M, pH 8.5) with 5 bar of H₂ and equimolar amounts of nNiFe₃ (1:1 ratio), as shown in **Scheme S7**, are stacked together in this figure. After 0, 1, 2, 3 and 4 h, the supernatant was collected and DSS added as an internal standard. The spectra were edited to only include relevant peaks, having been removed a DSS peak at 0 ppm and water peak at 4.8 ppm. No other peaks were found in the areas removed. Some DSS peaks are still visible (*). The peaks used for qualitative analysis and subsequent qNMR are highlighted in blue, according to **Table S6**.

Identification of products of substrate 2

Fig. S25 shows the ^1H spectrum of substrate **2** in 0.133 M PBS at 298 K. Characteristic signals at 9.339, 9.156, 8.825, 8.198 ppm were observed for H-2, H-6, H-4 and H-5 of the nicotinamide unit, signals at 8.379 and 8.019 ppm were detected for H-8 and H-2 of the adenine unit, while two signals at 6.097 and 5.993 ppm for H-1' of nicotinamide and adenine. Respectively, negligible impurities may exist.

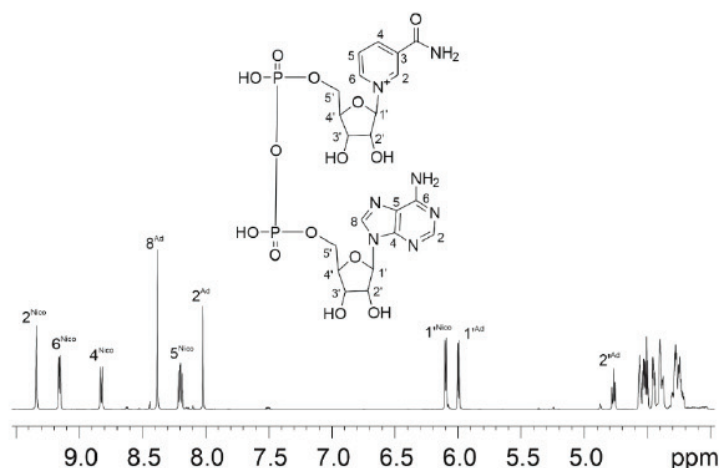


Fig. S25 ^1H spectrum of substrate NAD^+ (**2**) in 0.133 M PBS at 298 K.

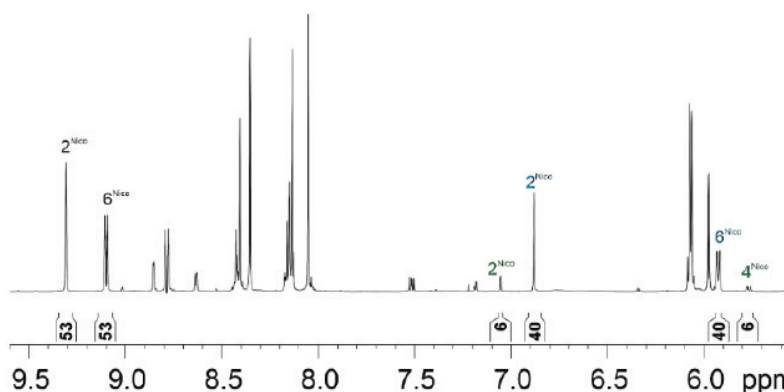
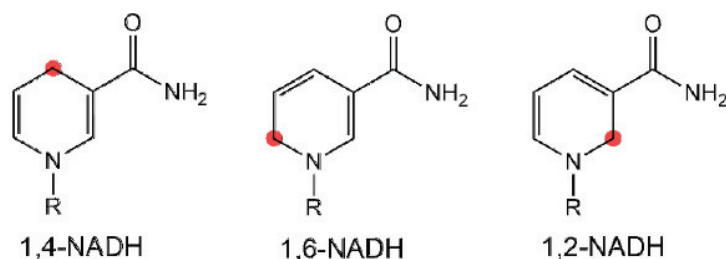


Fig. S26 ^1H spectrum in the region 5.6 – 9.6 ppm of products of substrate **2** at 298 K. The labels show signal assignment (cyan for the major and green for the minor product) and the integral values show the conversion rates.

The ^1H spectrum in the region 5.6 – 9.6 ppm of the reaction solution of substrate **2** after 4 hours of incubation in 0.133 M PBS is shown in **Fig. S26**. Different to the situation of substrate **1**, remaining of the substrate **2** was observed. One major and one minor product could be detected. Signal integral revealed a conversion rate of 40% and 6% for the major and the minor product, respectively. Further products of a scale comparable to impurities may form too.



Scheme S8 Tentative reduction products of substrate **2**.

Scheme S8 shows the possible products of a single reduction of substrate **2**. Section of the TOCSY spectrum is shown in **Fig. S27**. To start, the double doublet characteristic of a methylene at 2.647 and 2.616 ppm. crosspeaks with signals at 6.903, 5.946, and 4.725 ppm were detected. As shown in **Fig. S27**, these signals correspond to the main product. In the edited HSQC spectrum (**Fig. S28**) crosspeaks 2.647 – 21.8 and 2.616 – 21.8 ppm were observed. This ^{13}C chemical shift corresponds to the $\text{C}_{\text{N-4}}$ (22.3 ppm) of 1,4-NADH.(1) Similarly, a minor double doublet at 3.913 and 3.776 ppm was observed, whose crosspeaks with signals at 7.075, 5.785 and 5.000 ppm were detected. These signals were assigned to the second product. A close inspection of the edited HSQC spectrum revealed crosspeaks at 3.913 – 41.6 and 3.776 – 41.6 ppm. This ^{13}C chemical shift corresponds to the $\text{C}_{\text{N-6}}$ (42.1 ppm) published for 1,6-NADH.(6) We thus concluded 1,4-NADH and 1,6-NADH to be major and minor products of substrate **2**.

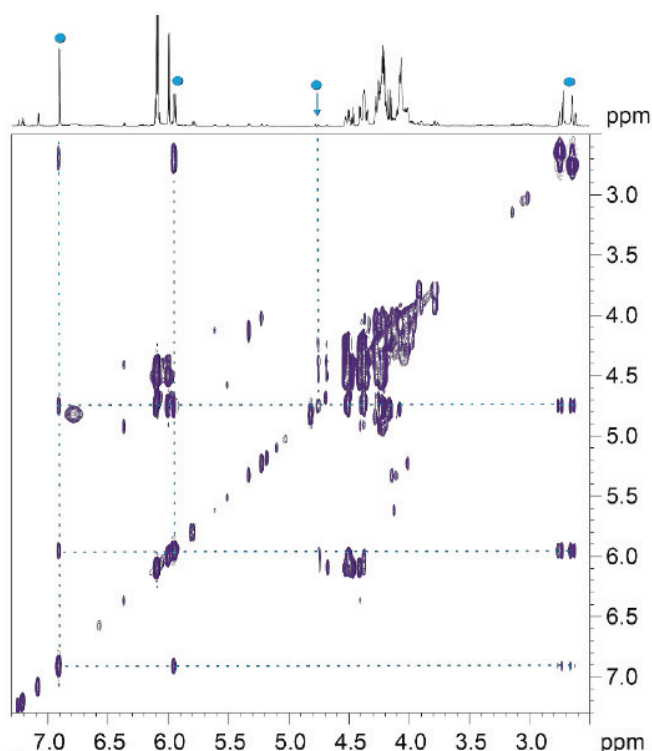


Fig. S27 Section of ^1H - ^1H TOCSY spectrum of products of **2** at 298 K. Connectivity among the signals of the major product is highlighted.

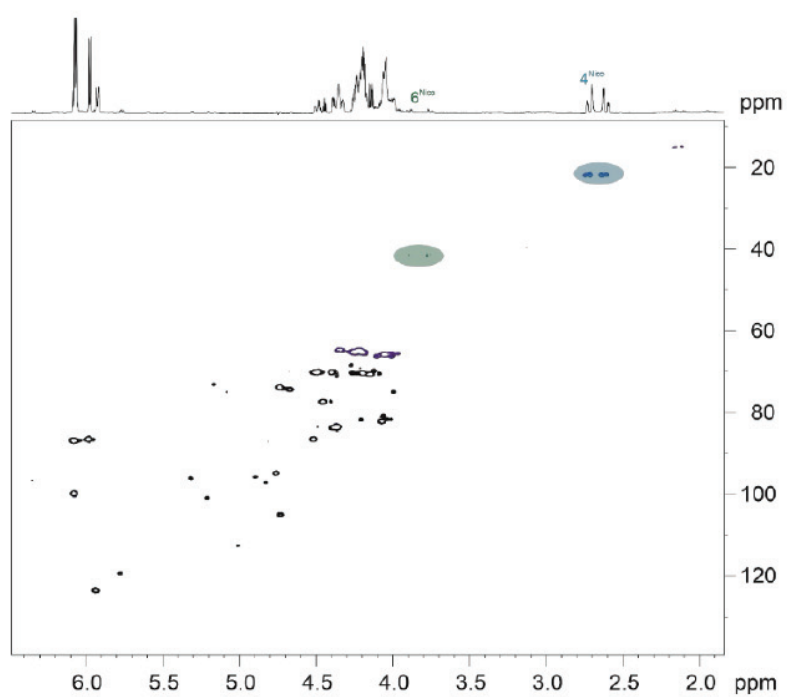


Fig. S28 Section of edited ^1H - ^{13}C HSQC spectrum of products of **2** at 298 K.

Reduction of NMN with μNi^0 and μFe^0 (1:200)

Table S11 After 4 h under 5 bar of H_2 , as shown in **Scheme S11**, samples with μNi^0 or μFe^0 yielded different amounts of 1,4-NMNH, 1,4,6-NMNH₃, 1,2,4,6-NMNH₅, NMNH₂OH, and nicotinamide (Nam), from the starting material NMN. The starting metal and cofactor were 3.2 mmol and 18 μmol , respectively, mixed in 3 mL of 0.5 M PBS (pH 8.5). The amount of metal atoms was two hundred times of the cofactor. The yields were calculated relative to the metal-free sample (100% NMN). To determine the TOF of each reaction, the sum of 1,4-NMNH, 1,4,6-NMNH₃, and 1,2,4,6-NMNH₅ was considered as the amount of product. Fe-containing experiments were performed in duplicate and Ni-containing in triplicate.

	H_2	NMN	SD	1,4-NMNH	SD	1,4,6-NMNH ₃	SD	NMNH ₂ OH	SD	1,2,4,6-NMNH ₅	SD	Nam	SD	TOF [mol/s]
4h	μNi^0	0.70%	0.5%	1.04%	1.2%	37.05%	3.0%	4.02%	3.1%	11.49%	3.1%	0.21%	0.3%	1.5082E-07
	μFe^0	20.07%	17.8%	44.73%	20.3%	0.23%	0.0%	9.53%	4.2%	0.81%	0.3%	25.43%	5.5%	1.3925E-07

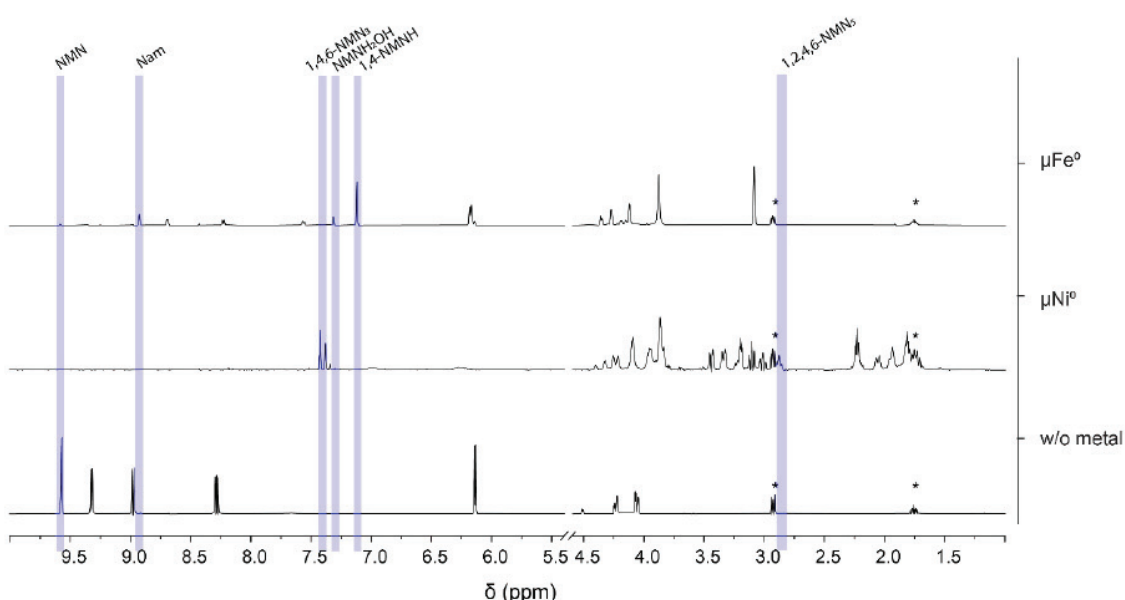
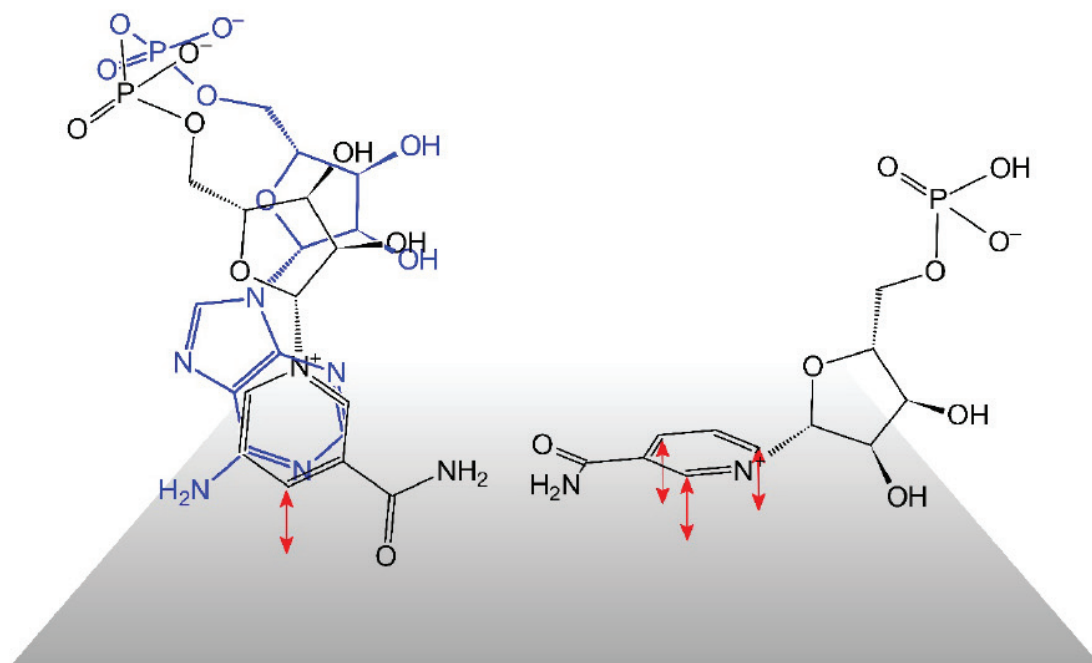


Fig. S29 The NMR spectra of replica samples of 18 μmol NMN in PBS (0.5 M, pH 8.5) with 5 bar of H_2 and 3.2 mmol μFe^0 , μNi^0 (200:1 cofactor ratio), or no metal, as shown in **Scheme S11**, are stacked together in this figure. After the 4h reaction, the supernatant was collected and DSS added as an internal standard. The spectra were edited to only include relevant peaks, having been removed a DSS peak at 0 ppm and water peak at 4.8 ppm. No other peaks were found in the areas removed. Some DSS peaks are still visible (*). The peaks used for qualitative analysis and subsequent qNMR are highlighted in blue, according to **Table S6**.

Proposed surface interaction between NAD/NMN and Ni/Fe minerals



Scheme S9 Proposed surface interaction with NAD⁺ and NMN. Due to its dinucleotide structure, NAD alternates between the folded and open conformation. This could prevent surface hydrides from reaching all carbons of the nicotinamide ring. NMN does not have such conformation and would be able to interact more directly with the surface.

Cyclic Voltammetry of standards and reaction products

Standards were prepared at 1 mM of each compound in PBS (0.133 M, pH 8.5) at 25°C, a three-electrode electrochemical cell was prepared for cyclic voltammetry with glassy carbon as working electrode, platinum wire as auxiliary electrode and Ag/AgNO₃ (0.01 M) as reference electrode.

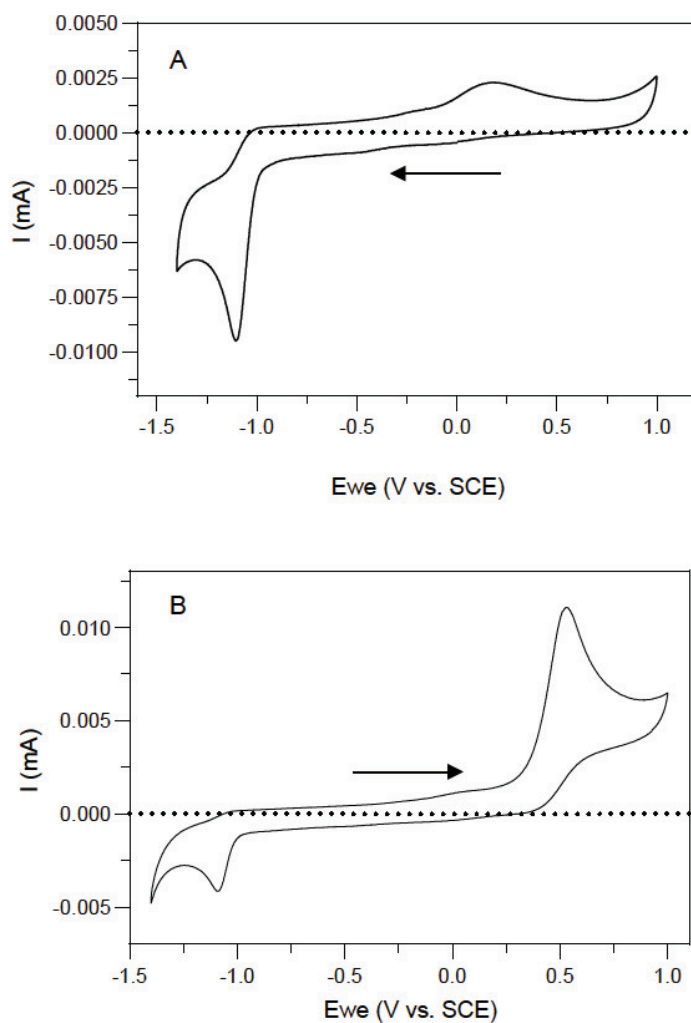


Fig. S30 Cyclic voltammogram of 1 mM of NAD⁺ (A) and 1,4-NADH (B) in PBS (pH 8.5) at 25 °C.

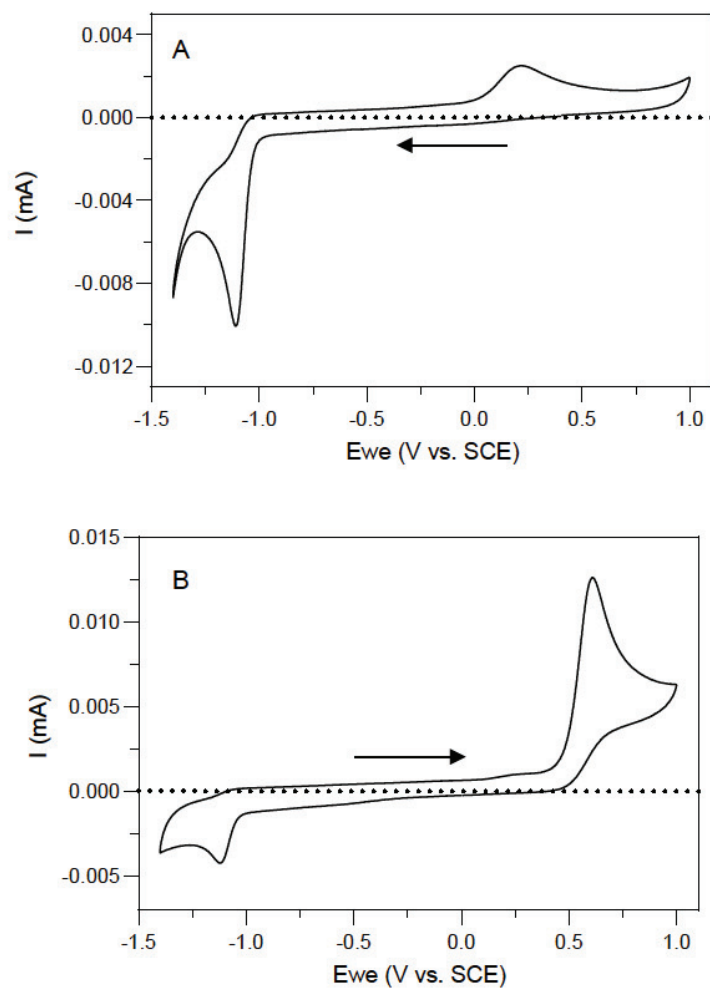


Fig. S31 Cyclic voltammogram of 1mM of NMN (A) and 1,4-NMNH (B) in PBS (pH 8.5) at 25 °C.

After a 4 h long reaction as described in **Scheme S6** and **Scheme S7** the supernatant was diluted with PBS (0.133 M at pH 8.5) to obtain 15 mL of sample.

Maintaining the same experimental setup (oxygen-free 0.133 M PBS at pH 8.5), a three-electrode electrochemical cell was prepared for cyclic voltammetry with glassy carbon as working electrode, platinum wire as auxiliary electrode and Ag/AgNO₃ (0.01 M) as reference electrode. Samples were collected after 4h under the conditions described above, and diluted with buffer to reach a similar concentration to that of the standards (1 mM).

Table S12 Table of oxidation potential

Reagent	E _a (V vs. SCE) ^a
1,4-NADH	0.531
1,4-NMNH	0.609
Reduced NAD ⁺	0.573
Reduced NMN	0.616; 1.000

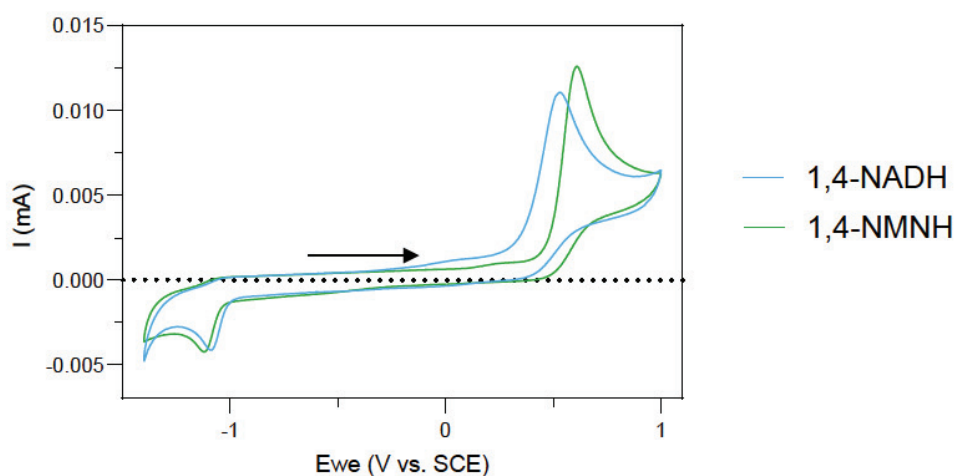


Fig. S32 Cyclic voltammogram of 1,4-NADH (1 mM; blue) and 1,4-NMNH (1 mM; green) in PBS (pH 8.5) at 25 °C.

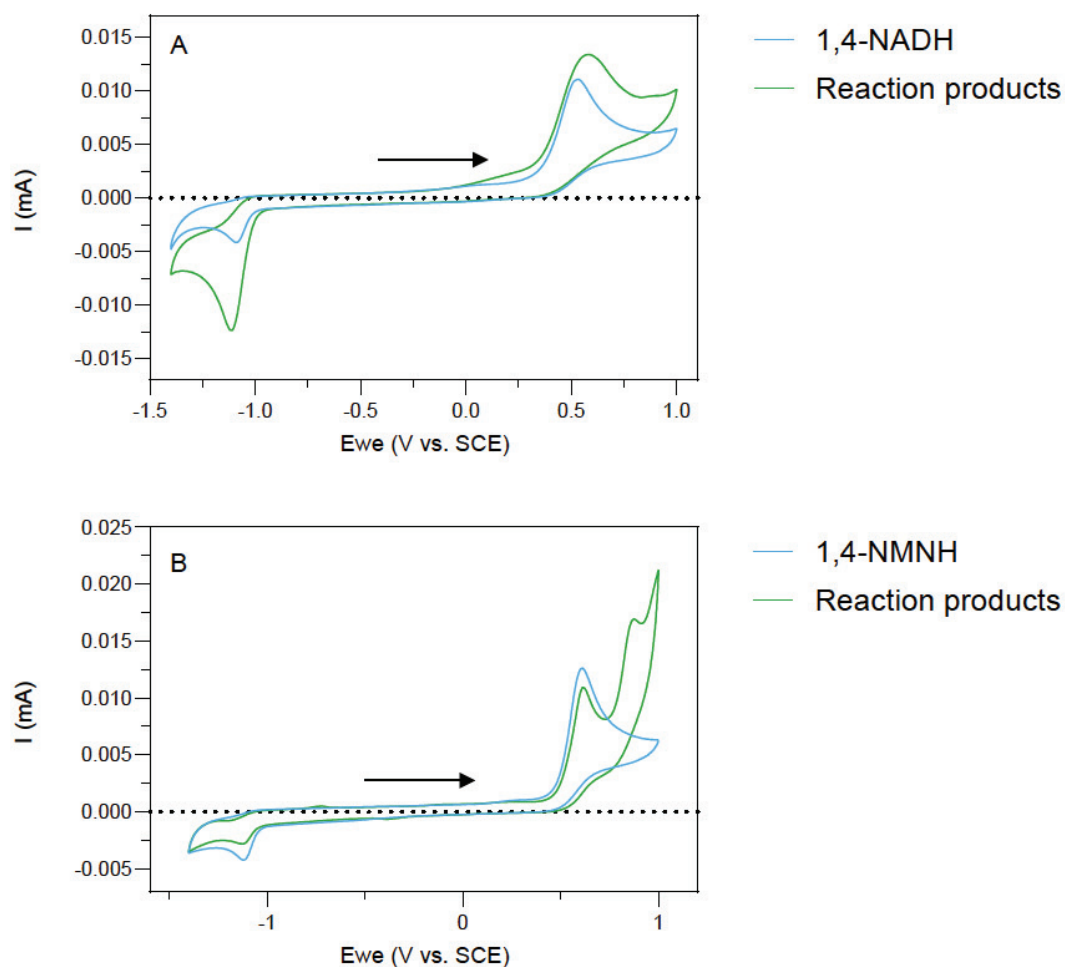
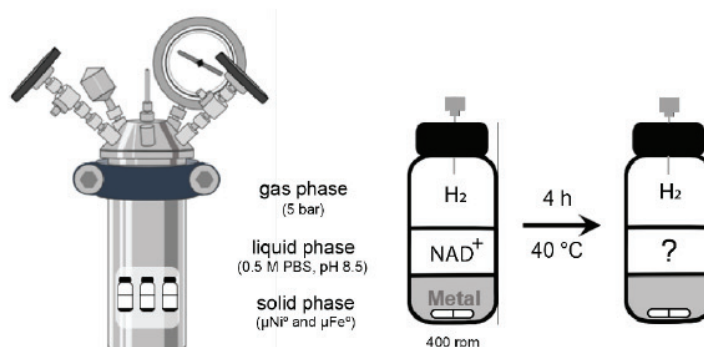


Fig. S33 A) Cyclic voltammogram of 1,4-NADH (1 mM in 0.133 M PBS pH 8.5; blue) and 12 mM of reduced NAD^+ with equimolar amounts of nNiFe (0.133 M PBS, 40 °C, 5 bar H_2 , diluted 1:5 after reaction; green), measured at 25 °C. B) Cyclic voltammogram of 1,4-NMNH (1 mM in 0.133 M PBS pH 8.5; blue) and 12 mM of reduced NMN with equimolar amounts of nNiFe (0.133 M PBS, 40 °C, 5 bar H_2 , diluted with PBS 1:5 after reaction; green), measured at 25 °C.

Reduction of NAD/NMN with μNi^0 and μFe^0

In an attempt to further understand the differences observed in reactions with NMN and Ni/Fe alloys as catalysts, compared to NAD, experiments with the individual metals in micropowder form were performed.

For quantification of each product, the ppm values of **Table S1**, and **Table S2** should be considered.



Scheme S10 The reduction of NAD^+ with μFe^0 (particle size: $<150\ \mu\text{m}$) and μNi^0 (particle size: $3\text{--}7\ \mu\text{m}$) was tested with the protocol described in detail in Methods, and according to the scheme above. The amount of NAD^+ was $36\ \mu\text{mol}$ and metal was $1.8\ \text{mmol}$, which reacted together for $4\ \text{h}$, at $40\ ^\circ\text{C}$, under alkaline conditions and $5\ \text{bars}$ of H_2 .

Table S13 After $4\ \text{h}$ under $5\ \text{bar}$ of H_2 , as shown in **Scheme S10**, samples with μNi^0 or μFe^0 yielded different amounts of 1,4-NADH, 1,6-NADH, and Nam, from the starting material NAD^+ . The starting metal and cofactor were $36\ \mu\text{mol}$ mixed in $3\ \text{mL}$ of $0.5\ \text{M}$ PBS ($\text{pH}\ 8.5$). The amount of metal atoms was 50 times the moles of cofactor. The yields were calculated relative to the metal-free sample ($100\%\ \text{NAD}^+$). To determine the TOF of each reaction, the sum of 1,4-NADH, and 1,6-NADH was considered as the amount of product. All conditions had duplicates and a metal-free control.

	H_2	NAD^+	SD	1,4-NADH	SD	1,6-NADH	SD	Nam	SD	TOF [mol/s]
4h	μNi^0	53.12%	1.8%	19.89%	0.2%	5.26%	0.1%	11.21%	0.0%	$3.69\text{E-}07$
	μFe^0	57.52%	2.9%	8.12%	1.2%	1.60%	0.2%	27.57%	2.2%	$1.43\text{E-}07$

In comparison to a former study with $\mu\text{Ni}(1)$ ($333:1$), where no 1,4-NADH was formed unless the powder was pretreated with H_2 before the reaction, the same powder produces a 13.6% yield of 1,4-NADH in the experiment described here ($50:1$). We attribute this different outcome to the degassing of this experiments' buffer opposed to no degassing in Pereira et al. 2022.(1) Degassing does not seem to have the same consequences to μFe , most likely due to the different reduction mechanism at place (Fe donating electrons while Ni depending on H_2 activation on its surface).

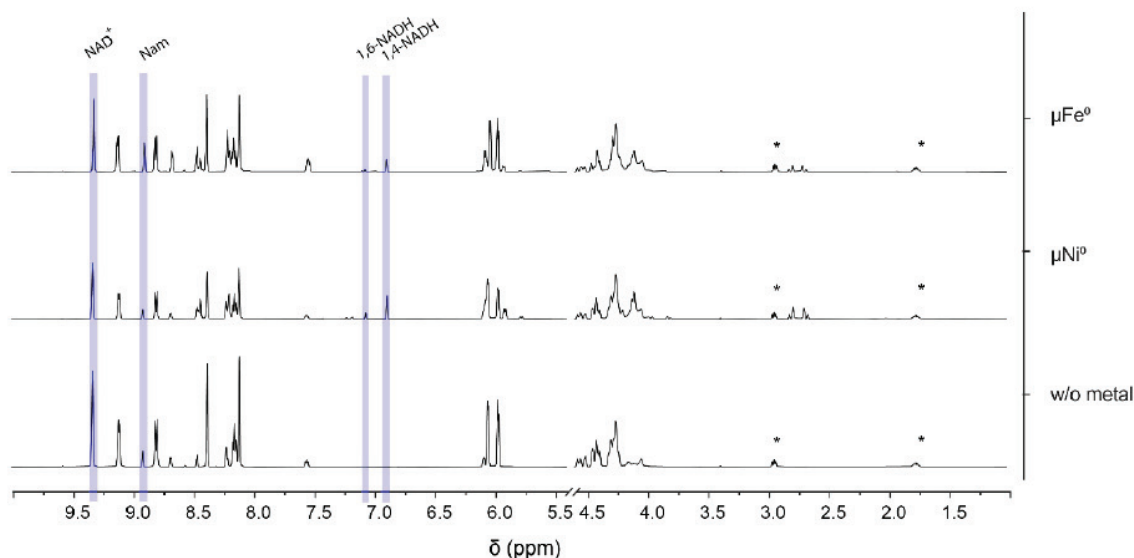
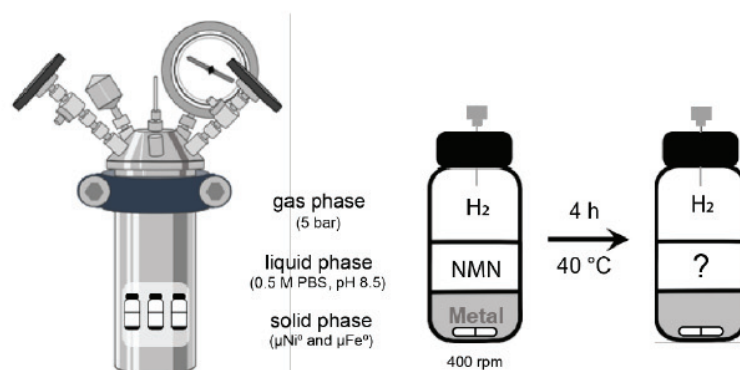


Fig. S34 The NMR spectra of replica samples of 36 μmol NAD^+ in PBS (0.5 M, pH 8.5) with 5 bar of H_2 and 1.8 mmol μFe^0 , μNi^0 (50:1 cofactor ratio), or no metal, as shown in **Scheme S10**, are stacked together in this figure. After the 4h reaction, the supernatant was collected and DSS added as an internal standard. The spectra were edited to only include relevant peaks, having been removed a DSS peak at 0 ppm and water peak at 4.8 ppm. No other peaks were found in the areas removed. Some DSS peaks are still visible (*). The peaks used for qualitative analysis and subsequent qNMR are highlighted in blue, according to **Table S1**.



Scheme S11 The reduction of NMN with μFe^0 and μNi was tested with the protocol described in detail in **Methods**, and according to the scheme above. The amount of NMN was 36 μmol and metal was 1.8 mmol (50:1) or 18 μmol and 3.6 mmol respectfully (200:1), which reacted together for 4 h, at 40 °C, under alkaline conditions and 5 bars of H_2 . The same reaction was made under Ar as a control.

Table S14 After 4 h under 5 bar of H₂, as shown in **Scheme S11**, samples with μNi^0 or μFe^0 yielded different amounts of 1,4-NMNH, 1,4,6-NMNH₃, NMNH₂OH, and nicotinamide (Nam), from the starting material NMN. The starting metal and cofactor were 1.8 mmol and 36 μmol , respectively, mixed in 3 mL of 0.5 M PBS (pH 8.5). The amount of metal atoms was fifty times of the cofactor. The yields were calculated relative to the metal-free sample (100% NMN). To determine the TOF of each reaction, the sum of 1,4-NMNH, 1,2,4,6-NMNH₅, and 1,4,6-NMNH₃ was considered as the amount of product. All conditions were tested in triplicate.

	H ₂	NMN	SD	1,4-NMNH	SD	1,4,6-NMNH ₃	SD	NMNH ₂ OH	SD	1,2,4,6-NMNH ₅	SD	Nam	SD	TOF [mol/s]
4h	μNi^0	0.92%	0.4%	4.85%	3.47%	44.13%	7.07%	13.79%	4.5%	9.83%	3.1%	0.50%	0.3%	3.55E-07
	μFe^0	23.48%	15.8%	47.95%	11.9%	0.00%	0.0%	11.43%	2.0%	0.00%	0.0%	14.88%	12.8%	1.72E-07

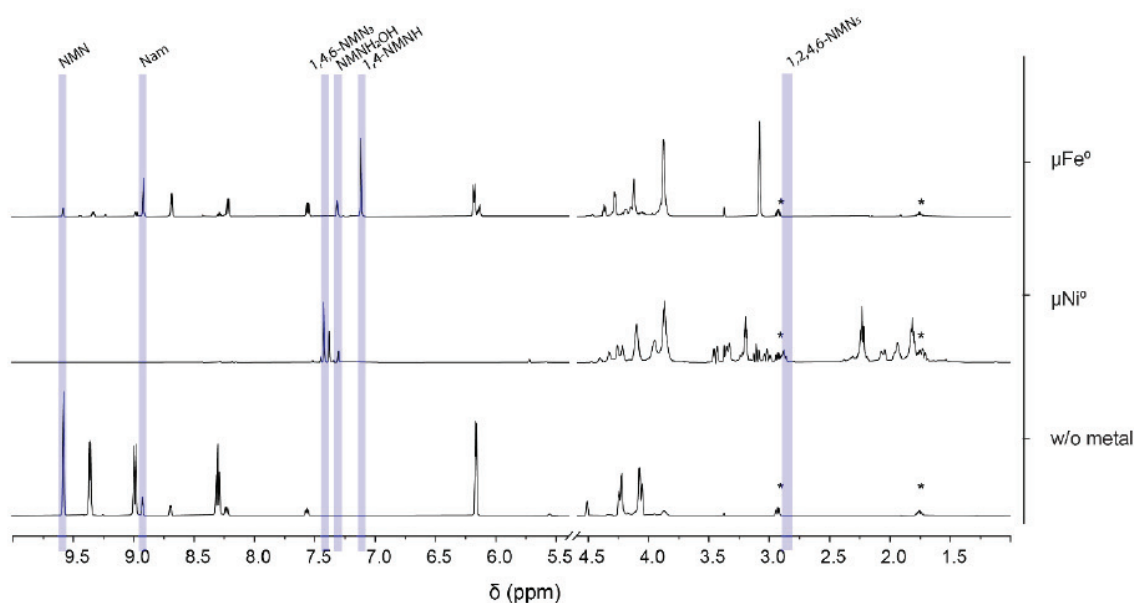


Fig. S35 The NMR spectra of replica samples of 36 μmol NMN in PBS (0.5 M, pH 8.5) with 5 bar of H₂ and 1.8 mmol μFe^0 , μNi^0 (50:1 cofactor ratio), or no metal, as shown in **Scheme S11**, are stacked together in this figure. After the 4h reaction, the supernatant was collected and DSS added as an internal standard. The spectra were edited to only include relevant peaks, having been removed a DSS peak at 0 ppm and water peak at 4.8 ppm. No other peaks were found in the areas removed. Some DSS peaks are still visible (*). The peaks used for qualitative analysis and subsequent qNMR are highlighted in blue, according to **Table S6**.

Table S15 After 4 h under 5 bar of Ar, as shown in **Scheme S11**, samples with μNi^0 or μFe^0 yielded different amounts of 1,4-NMNH, NMNH₂OH, and nicotinamide (Nam), from the starting material NMN. The starting metal and cofactor were 1.8 mmol and 36 μmol , respectively, mixed in 3 mL of 0.5 M PBS (pH 8.5). The amount of metal atoms was fifty times of the cofactor. The yields were calculated relative to the metal-free sample (100% NMN). To determine the TOF of each reaction, the sum of 1,4-NMNH, 1,4,6-NMNH₃, and 1,2,4,6-NMNH₅ was considered as the amount of product. All experiments were performed in duplicate.

	Ar	NMN	SD	1,4-NMNH	SD	1,4,6-NMNH ₃	SD	NMNH ₂ OH	SD	1,2,4,6-NMNH ₅	SD	Nam	SD	TOF [mol/s]
4h	μNi^0	86.34%	3.1%	0.00%	0.0%	0.00%	0.0%	0.00%	0.0%	0.00%	0.0%	9.48%	1.8%	0.00E+00
	μFe^0	45.66%	2.4%	22.21%	1.2%	0.00%	0.0%	5.44%	0.2%	0.00%	0.0%	22.25%	0.2%	3.34E-07

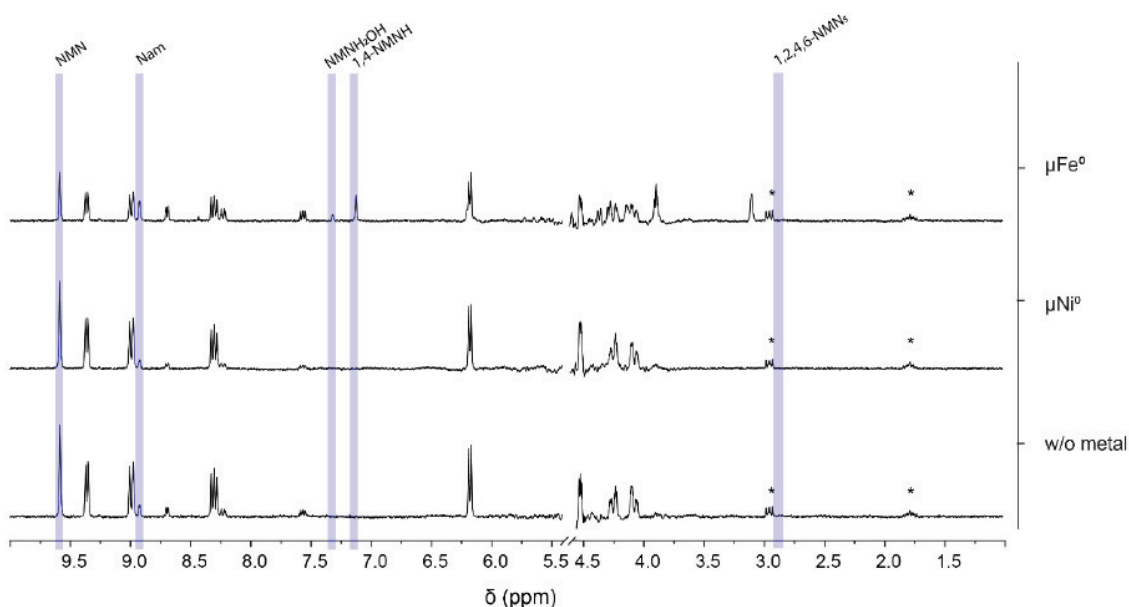
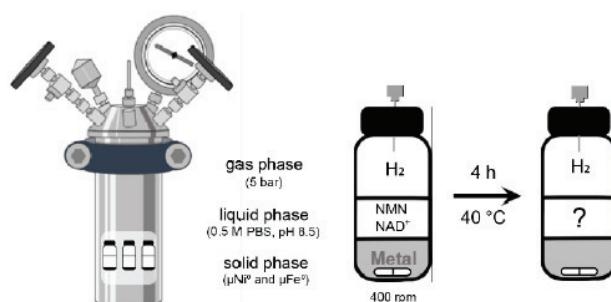


Fig. S36 The NMR spectra of replica samples of 36 μmol NMN in PBS (0.5 M, pH 8.5) with 5 bar of Ar and 1.8 mmol μFe^0 , μNi^0 (50:1 cofactor ratio), or no metal, as shown in **Scheme S11**, are stacked together in this figure. After the 4h reaction, the supernatant was collected and DSS added as an internal standard. The spectra were edited to only include relevant peaks, having been removed a DSS peak at 0 ppm and water peak at 4.8 ppm. No other peaks were found in the areas removed. Some DSS peaks are still visible (*). The peaks used for qualitative analysis and subsequent qNMR are highlighted in blue, according to **Table S6**.

“Competition” experiments

To further test the reactivity of NMN and NAD under prebiotic conditions, experiments with both cofactors in the same reaction mixture were designed.



Scheme S12 The reduction of a mixture of NMN and NAD⁺ with μFe^0 or μNi^0 was tested with the general protocol described in detail in **Methods**, and according to the scheme above. The amount of cofactor was 36 or 72 μmol (18 or 36 each, respectively) in 3 mL of pH 8.5 0.5 M PBS buffer, the metal amount was constantly 1.8 mmol (leading to a metal-cofactor ratio of 50:1 and 25:1, respectively). The reaction took place for 4 h at 40 °C under slightly alkaline conditions and 5 bars of H₂.

Table S16 After 4 h under 5 bar of H₂, as shown in **Scheme S12**, samples with μFe^0 or μNi^0 yielded different amounts of 1,4-NADH, 1,4-NMNH, NMNH₂OH, and nicotinamide (Nam), from the starting material NMN and NAD⁺. The starting cofactor mixture was 72 μmol (36 μmol each nucleotide) mixed in 3 mL of 0.5 M PBS (pH 8.5), with a metal-cofactor ratio of 25:1. The yields were calculated separately and relative to the metal-free sample (100% NMN and 100% NAD⁺; 12 mM each). To determine the TOF of each reaction, the sum of 1,4-NMNH, 1,4,6-NMNH₃, 1,2,4,6-NMNH₅, 1,4-NADH, and 1,6-NADH was considered as part of the reduction products. The NMN and NAD products are presented separately in order for the table to fit the page, but belong to the same set of triplicates.

	H ₂	1,4-NMNH	SD	1,4,6-NMNH ₃	SD	NMNH ₂ OH	SD	1,2,4,6-NMNH ₅	SD	NMN	SD
4h	μNi^0	5,70%	0,92%	3,74%	0,9%	7,33%	0,3%	0,00%	0,0%	79,55%	1,8%
		1,4-NADH	SD	1,6-NADH	SD	NAD ⁺	SD	TOF [mol/s]			
		13,63%	0,8%	3,51%	0,4%	63,8%	17,1%	3,90E-07			
	μFe^0	7,06%	0,9%	0,00%	0,0%	2,26%	0,7%	0,00%	0,0%	75,15%	11,3%
		1,4-NADH	SD	1,6-NADH	SD	NAD ⁺	SD	TOF [mol/s]			
		11,33%	1,2%	2,17%	0,3%	45,1%	10,6%	3,02E-07			

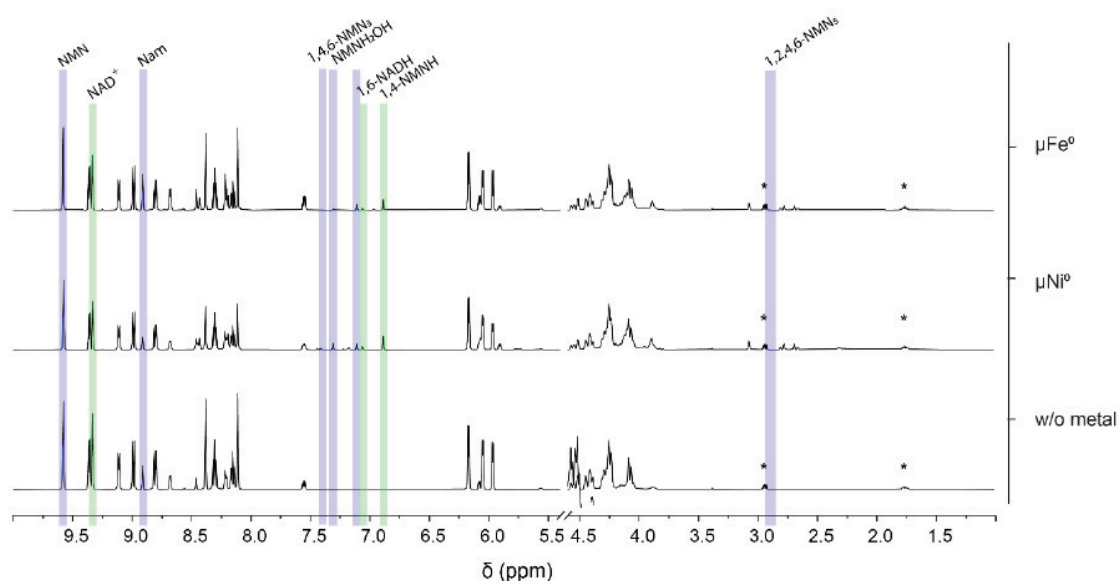
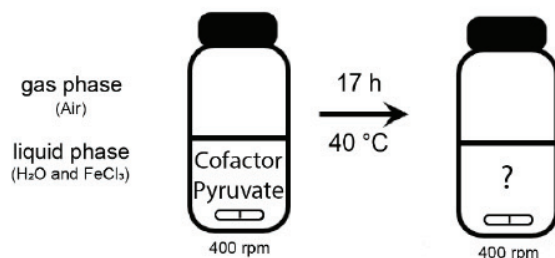


Fig. S37 The NMR spectra of replica samples with a mixture of 36 μmol NMN and 36 μmol NAD^+ in PBS (0.5 M, pH 8.5) with 5 bar of H_2 and 1.8 mmol μFe^0 , μNi^0 (25:1 metal-cofactor ratio), or no metal, as shown in **Scheme S12**, are stacked together in this figure. After the 4h reaction, the supernatant was collected and DSS added as an internal standard. The spectra were edited to only include relevant peaks, a DSS peak at 0 ppm and the water peak at 4.8 ppm have been removed. No other peaks were found in the areas removed. Other DSS peaks are still visible (*). The peaks used for qualitative analysis and subsequent qNMR are highlighted in blue (NMN products) and green (NAD products), according to **Table S1** and **Table S6**.

Abiotic oxidation of organic cofactors and reduction of pyruvate



Scheme S13 An aqueous mixture of 0.1 mL with 100 mM pyruvate, twice as much 1,4-NADH or 1,4-NMNH, and 60 mM FeCl₃ reacted overnight at 40 °C and 400 rpm to produce lactate, according to the scheme. The pH before and after the reaction is <5.

Table S17 After 17 h with FeCl₃, as shown in **Scheme S13**, samples with NMNH and NADH yielded similar amounts of lactate from pyruvate. The starting cofactor was 20 µmol mixed in 0.1 mL of water, with 6 µmol of FeCl₃ reacting overnight at 40 °C and 400 rpm (pH<5). The conditions were done in duplicates and yields were calculated relative to the initial amount of pyruvate.

	Air	lactate	SD
NMNH	FeCl ₃	10,84%	1,5%
NADH		13,03%	1,6%

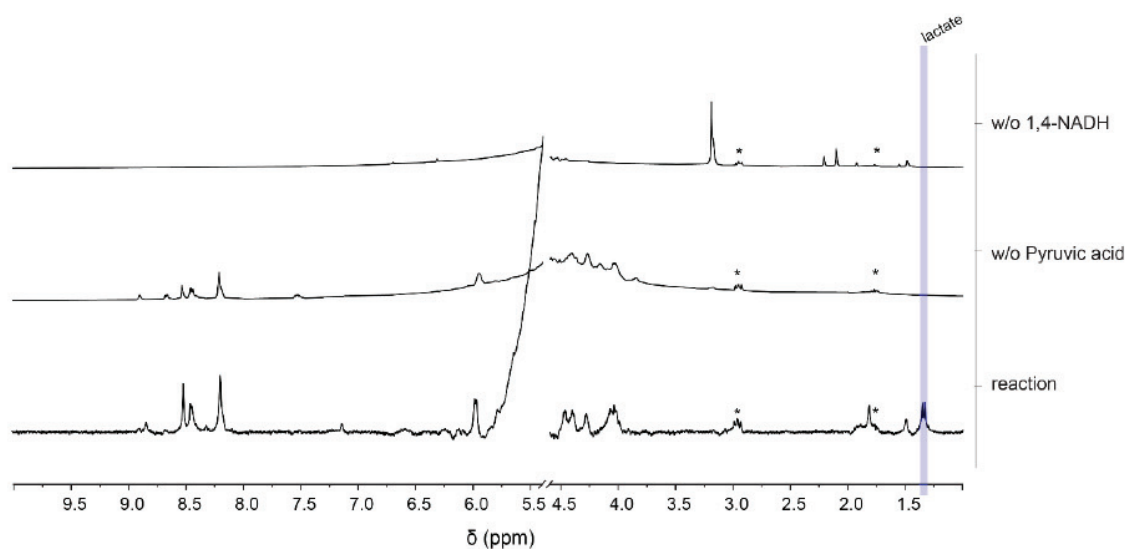


Fig. S38 A NMR spectrum of a replica sample of aqueous 1,4-NADH (20 mmol) were mixed in an Eppendorf tube with 10 mmol of pyruvic acid, and 60 mmol of FeCl₃, as indicated by **Scheme S13**, is stacked together in this figure with the respective controls. The latter were without NADH and without pyruvic acid as described on the right side of each spectra. The metals were precipitated with 0.2 mL of a thiolate/phosphate solution. The supernatant was collected and DSS added as an internal standard. The spectra were edited to only include relevant peaks, having been removed a DSS peak at 0 ppm and water peak at 4.8 ppm. No other peaks were found in the areas removed. Some DSS peaks are still visible (*). The peaks used for qualitative analysis and subsequent qNMR are highlighted in blue (1.33 ppm).

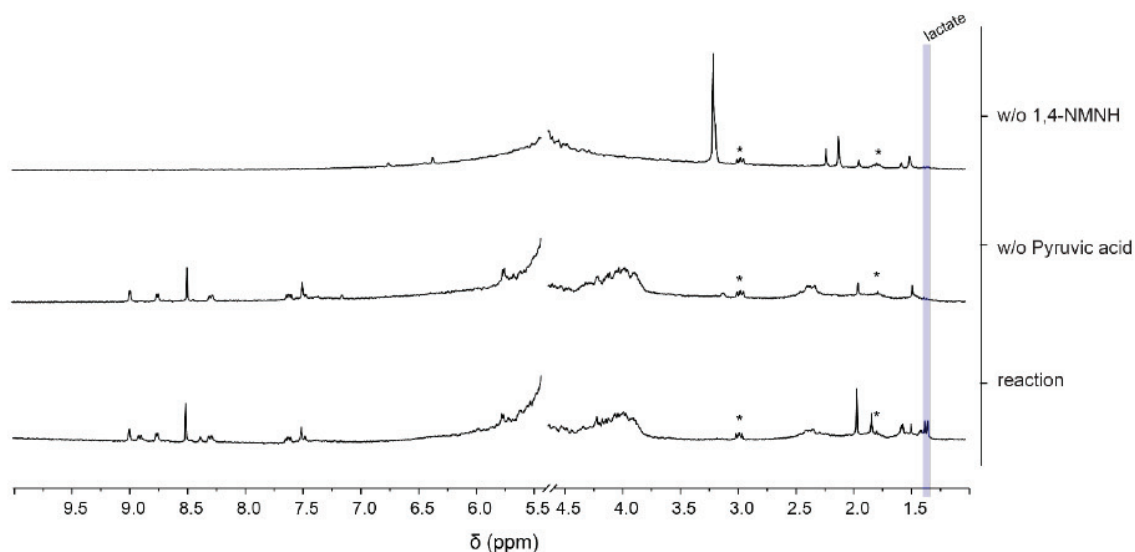
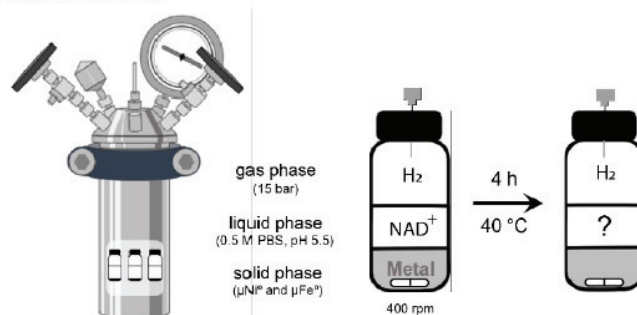


Fig. S39 A NMR spectrum of a replica sample of aqueous NMNH (20 mmol) were mixed in an Eppendorf tube with 10 mmol of pyruvic acid, and 6 mmol of FeCl₃, as indicated by **Scheme S13**, is stacked together in this figure with the respective controls. The latter were without NADH and without pyruvic acid as described on the right side of each spectra. The metals were precipitated with 0.2 mL of a thiolate/phosphate solution. The supernatant was collected and DSS added as an internal standard. The spectra were edited to only include relevant peaks, having been removed a DSS peak at 0 ppm and water peak at 4.8 ppm. No other peaks were found in the areas removed. Some DSS peaks are still visible (*). The peaks used for qNMR are highlighted in blue (1.33 ppm).

Reduction of NAD/NMN at pH 5.5



Scheme S14 The reduction of NAD^+ with μNi and μFe was tested with the protocol described in detail in **Methods**, and according to the scheme above. The amount of NAD^+ was 36 μmol , which reacted together for 4 h, at 40 °C, under alkaline conditions and 15 bars of H_2 . The metal in excess was 7.2 mmol. The same reaction was made with NADH as control to the stability of the reduced cofactor under acidic conditions (pH 5.5).

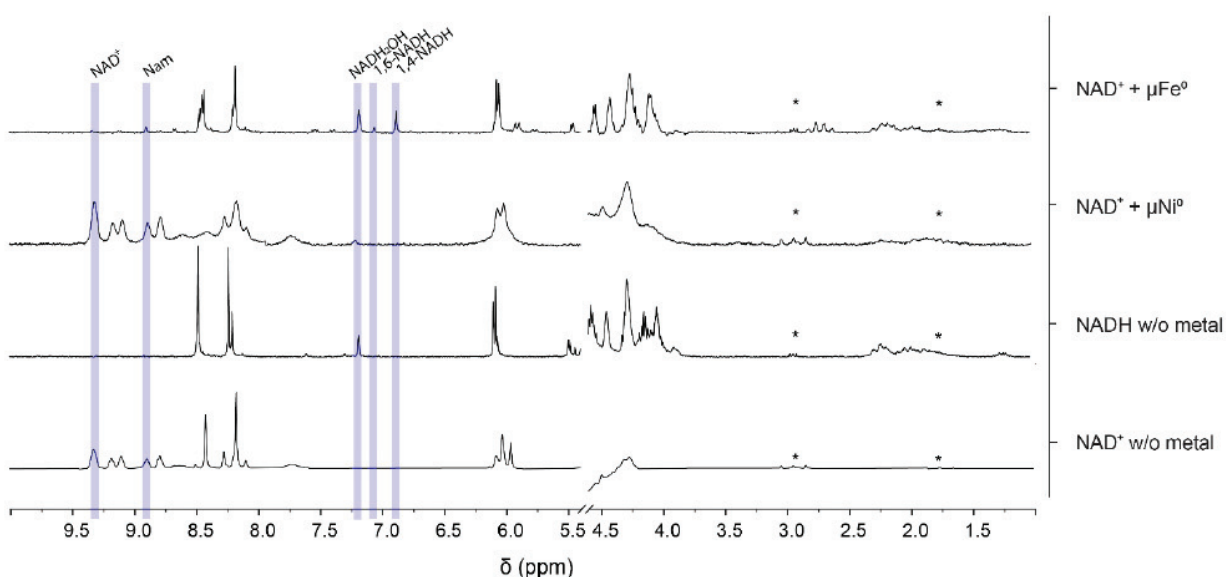
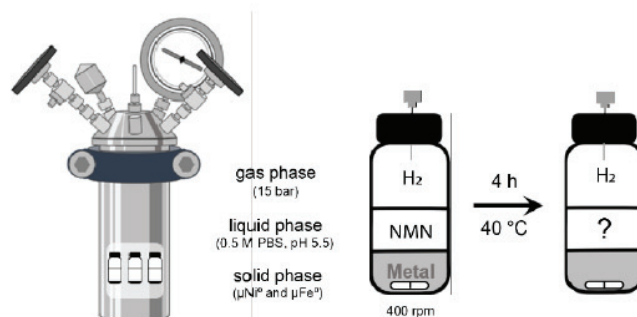


Fig. S40 The NMR spectra of replica samples with 36 μmol NAD^+ in PBS (0.5 M, pH 5.5) with 15 bar of H_2 and 7.2 mmol μFe^0 , μNi^0 (200:1 metal-cofactor ratio), or no metal, as shown in **Scheme S14**, are stacked together in this figure, together with an NADH control under the same conditions. After the 4h reaction, the supernatant was collected and DSS added as an internal standard. The spectra were edited to only include relevant peaks, a DSS peak at 0 ppm and the water peak at 4.8 ppm have been removed. Other DSS peaks are still visible (*). The peaks used for qualitative analysis are highlighted in blue (NAD products), according to **Table S1**.



Scheme S15 The reduction of NMN with μNi^0 and μFe^0 was tested with the protocol described in detail in **Methods**, and according to the scheme above. The amount of NMN was 36 μmol , which reacted together for 4 h, at 40 °C, under alkaline conditions and 15 bars of H_2 . The metal in excess was 7.2 mmol. The same reaction was made with NMNH as control to the stability of the reduced cofactor under acidic conditions (pH 5.5).

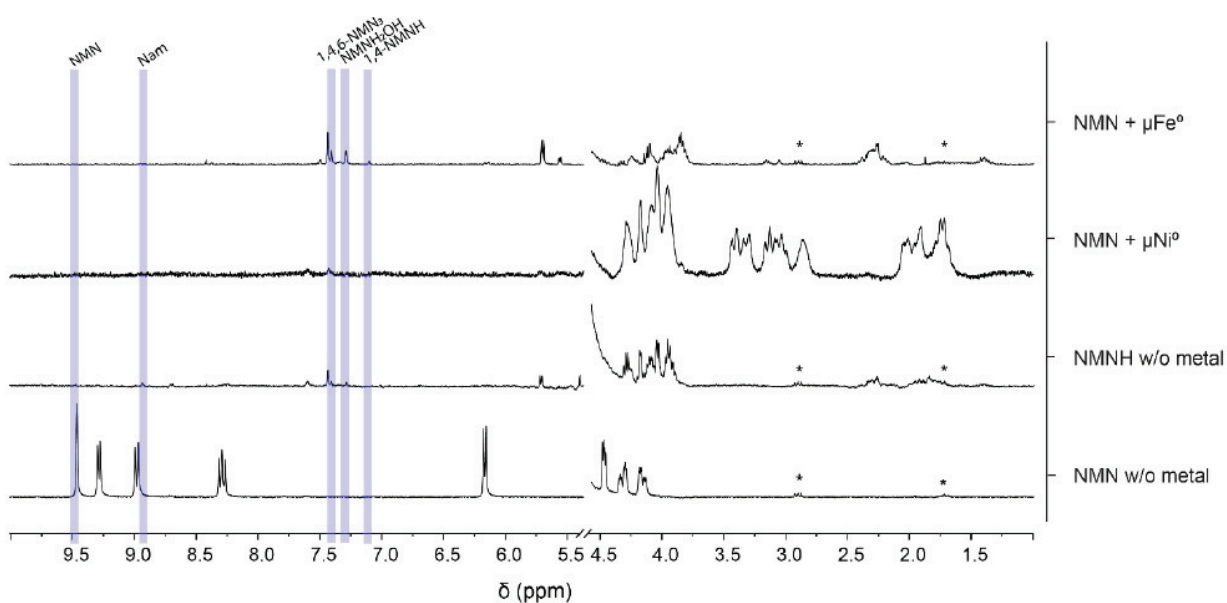


Fig. S41 The NMR spectra of replica samples with 36 μmol NMN in PBS (0.5 M, pH 5.5) with 15 bar of H_2 and 7.2 mmol μFe^0 , μNi^0 (200:1 metal-cofactor ratio), or no metal, as shown in **Scheme S15**, are stacked together in this figure, together with an NMNH control under the same conditions. After the 4h reaction, the supernatant was collected and DSS added as an internal standard. The spectra were edited to only include relevant peaks, a DSS peak at 0 ppm and the water peak at 4.8 ppm have been removed. Other DSS peaks are still visible (*). The peaks used for qualitative analysis are highlighted in blue (NMN products), according to **Table S6**.

Standards

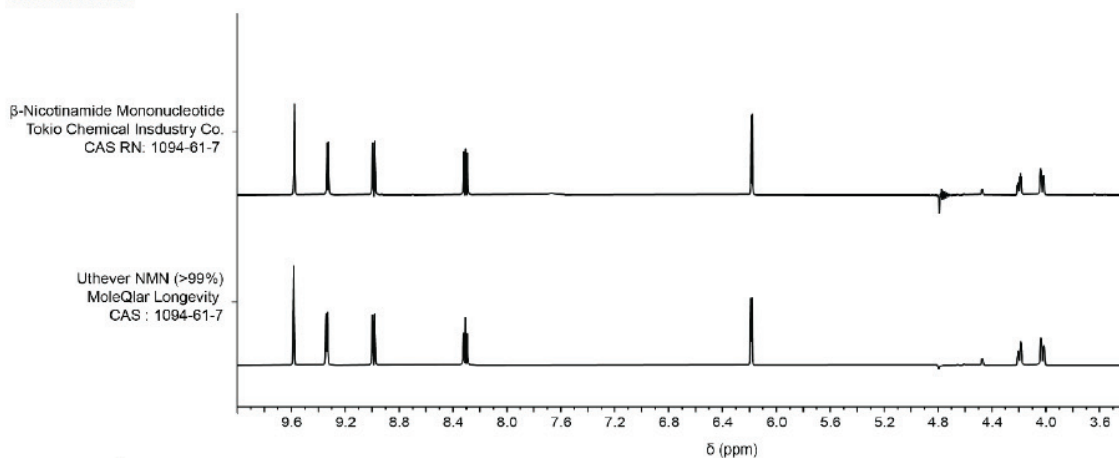


Fig. S42 ¹H-NMR comparison of the two different NMN supplies used in all experiments (12 mM of NMN in 0.133 M PBS pH 8.5). Empty spectra was cut out on both extremities, and water suppression hides the peak around 4.8.

Table S18 Standard metal preparation. The molecular weight (MW) was normalized to the amount of metal atoms of each metal powder. The mg of metal used in experiments with 18, 36, and 1800 μmol are listed for each metal used.

Metals	MW / metal atom	18 μmol (mg)	36 μmol (mg)	1.8 mmol (mg)
Fe	55.85	1.01	2.01	100.5
NiFe ₃	56.56	1.02	2.04	
NiFe	57.27	1.03	2.06	
Ni ₃ Fe	57.98	1.04	2.09	
Ni	58.69	1.06	2.11	105.7

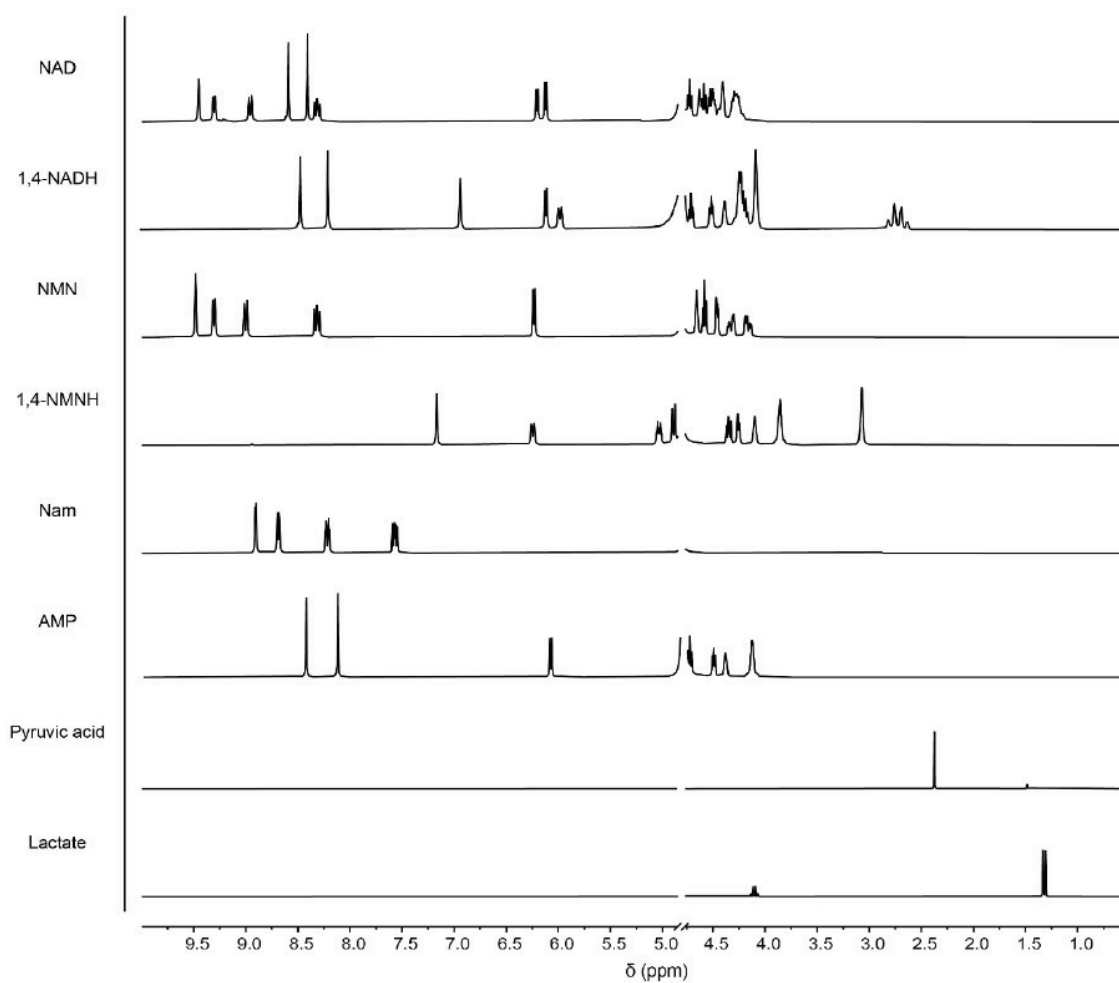


Fig. S43 ¹H-NMR standards of several molecules in D₂O. Empty spectra was cut out on both sides, as well as the water peak between 4.5 and 5 ppm.

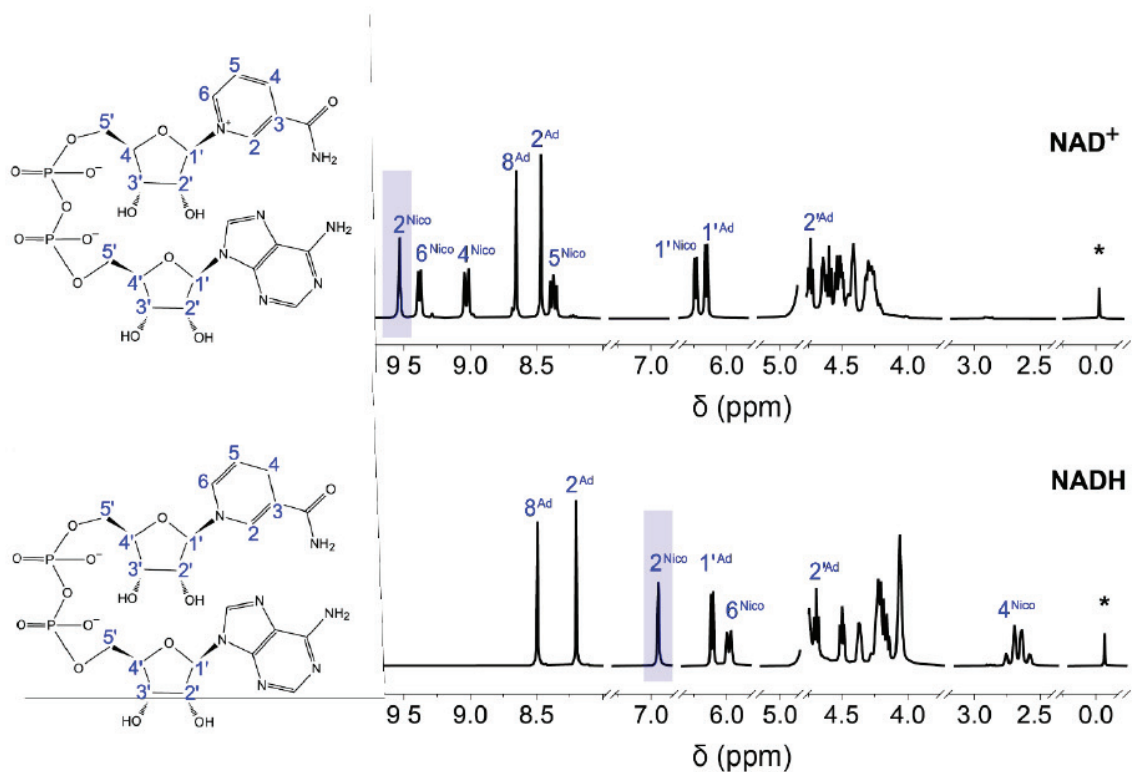
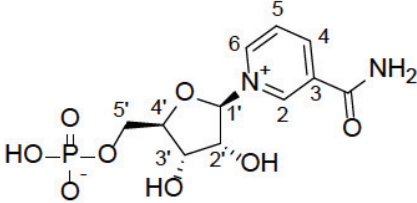


Fig. S44 According to 2D-NMR measurements and literature, the ^1H -NMR peaks obtained from NAD^+ (above) and NADH (below) can be assigned to hydrogens bound to the carbons indicated in the figure. Only spectra without any significant peaks were removed from the figure at several ppm values. Highlighted in blue is the peak used for qNMR. The standard DSS peak at 0 ppm is included and marked (*).

Characterization of NMN

A full assignment of the ^1H and ^{13}C resonance signals of NMN was fulfilled and the chemical shifts are listed in **Table S19**.

Table S19 NMR data of NMN in D_2O at 298 K

		
Position	δ_{H} (multi., J)	δ_{C}
2	9.47 (s)	142.6
3		136.7
C=O		168.6
4	8.99 (dt, 8.2, 1.1)	148.7
5	8.30 (dd, 8.0, 6.4)	131.3
6	9.29 (d, 6.2)	145.2
1'	6.22 (d, 5.6)	102.7
2'	4.34 (dd, 7.6, 5.3)	80.5
3'	4.45 (dd, 5.1, 2.5)	73.8
4'	4.65 (q, 2.5)	90.2 (d, 8.8)
5'	4.31 (ddd, 12.0, 4.3, 2.5) 4.15 (ddd, 12.0, 5.0, 2.1)	66.9 (d, 4.9)

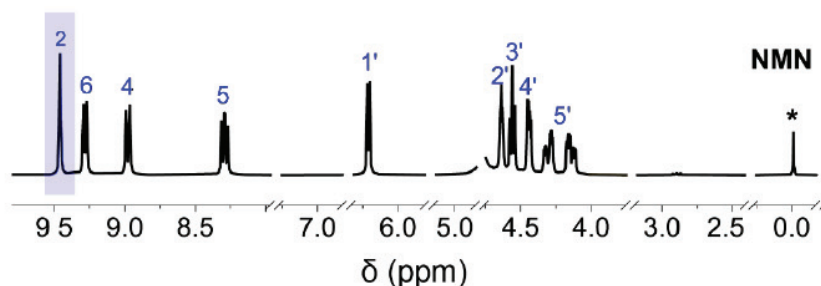


Fig. S45 ^1H spectrum of NMN standard in D_2O with internal reference DSS at 298 K. Empty spectra was removed, highlighting the substrate peaks, labelled according to **Table S19**. Highlighted in blue is the peak used for qNMR. The standard DSS peak at 0 ppm is included and marked (*).

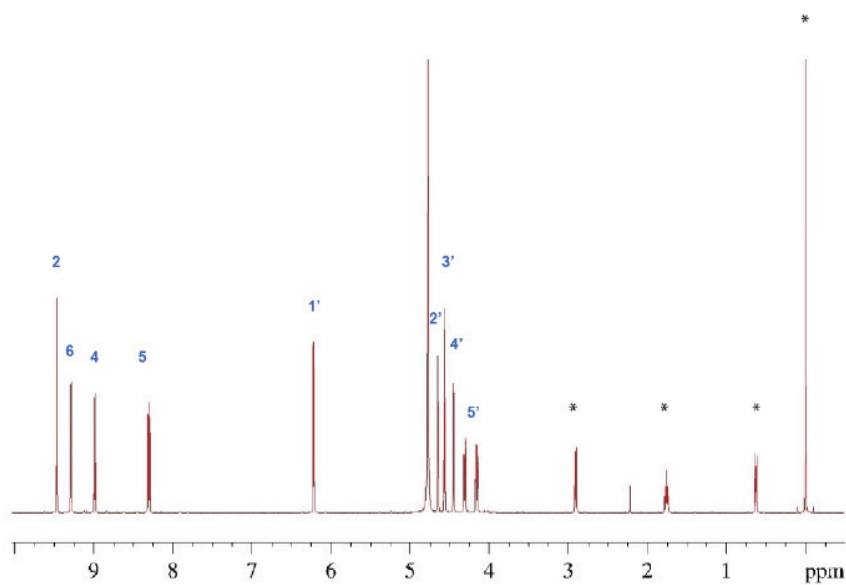


Fig. S46 Complete view of the ^1H spectrum of NMN standard in D_2O with internal reference DSS (*) at 298 K, labelled according to Table S1. Some H_2O is visible at about 4.8 ppm.

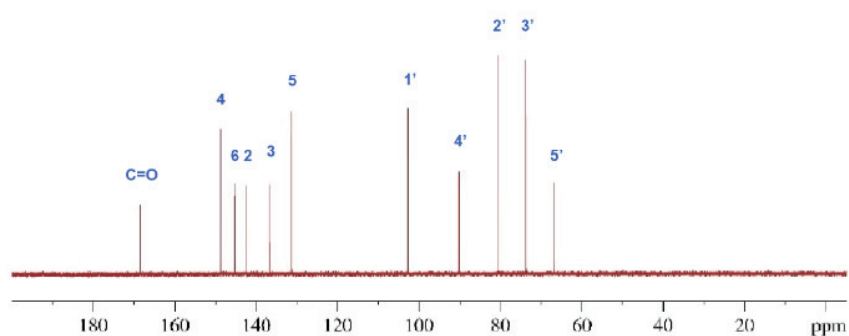


Fig. S47 ^{13}C spectrum of NMN standard in D_2O at 298 K, labelled according to Table S19.

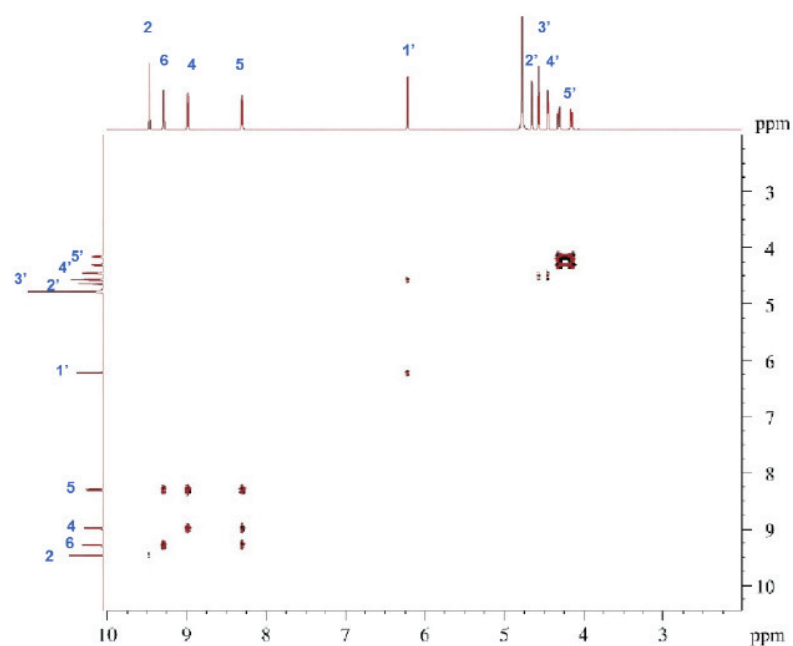


Fig. S48 ^1H - ^1H DQF-COSY spectrum of NMN standard in D_2O at 298 K, labelled according to **Table S19**.

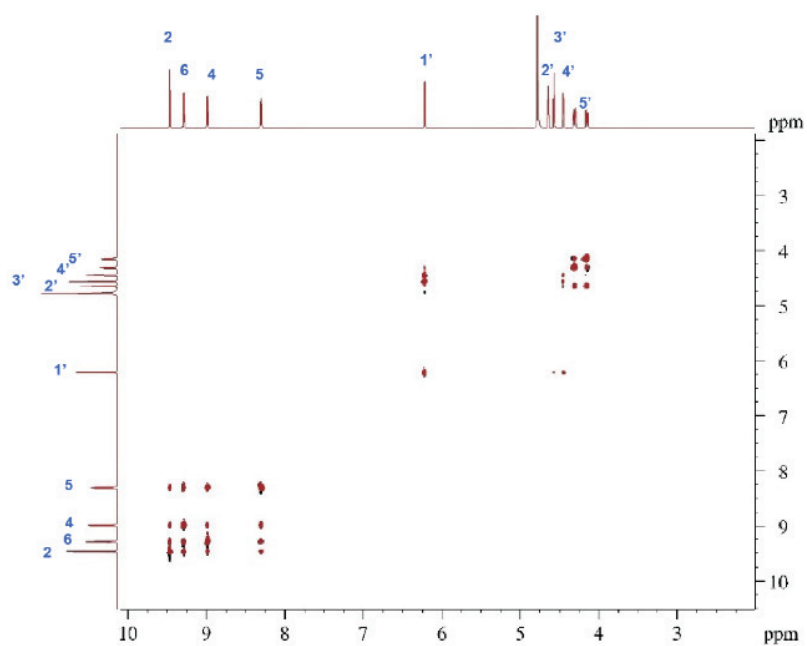


Fig. S49 ^1H - ^1H TOCSY spectrum of NMN standard in D_2O at 298 K, labelled according to **Table S19**.

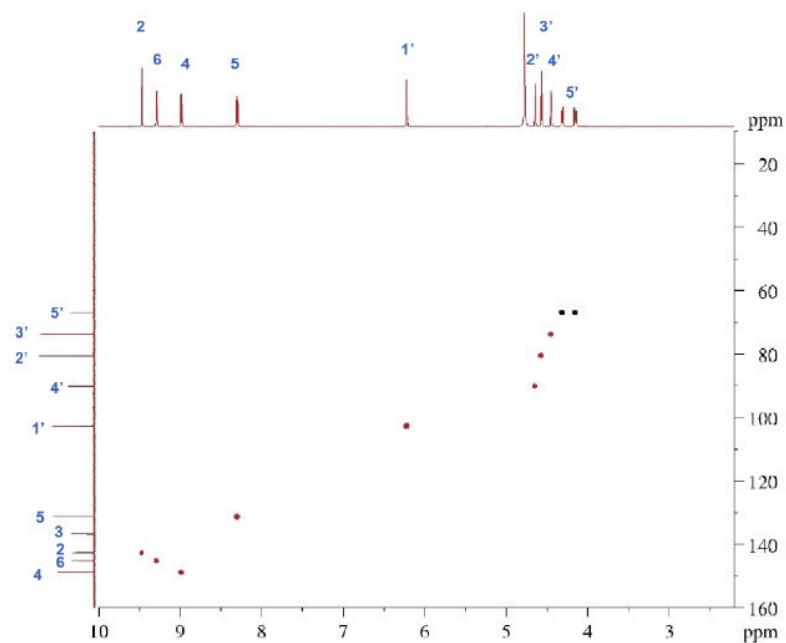


Fig. S50 Edited ^1H - ^{13}C HSQC spectrum of standard NMN standard in D_2O at 298 K, labelled according to **Table S19**.

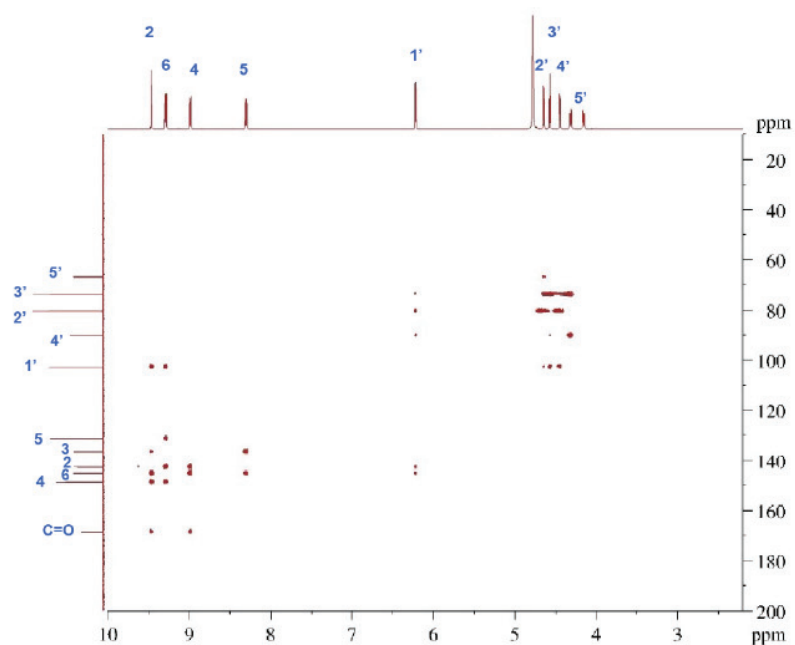
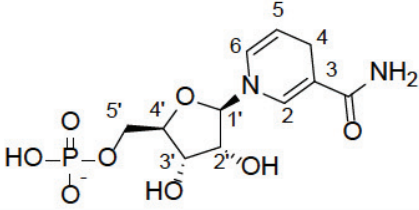


Fig. S51 The ^1H - ^{13}C HMBC spectrum of NMN standard in D_2O at 298 K, labelled according to **Table S19**.

Characterization of 1,4-NMNH

A full assignment of the ^1H and ^{13}C resonance signals of 1,4-NMNH was fulfilled and the chemical shifts are listed in.

Table S20 NMR data 1,4-NMNH in D_2O at 298 K

		
Position	δ_{H} (multi., J)	δ_{C}
2	7.15 (d, 1,6)	141.1
3		103.4
C=O		175.9
4	3.056 (d, 1.7); 3.062 (d, 1.7)	24.7
5	5.02 (m)	108.2
6	6.24 (ddt, 8.3, 1.4, 1.5)	127.7
1'	4.88 (m)	97.7
2'	4.34 (dd, 7.6, 5.3)	73.3
3'	4.25 (dd, 5.3, 2.0)	73.6
4'	4.09 (m)	86.0 (d, 8.8)
5'	3.87 – 3.81 (m)	66.6 (d, 4.1)

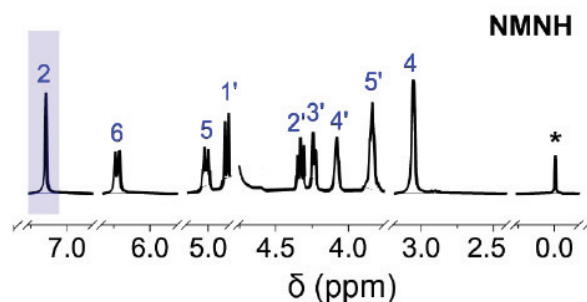


Fig. S52 ^1H spectrum of NMNH standard in D_2O with internal reference DSS at 298 K. Empty spectra was removed, highlighting the substrate peaks, labelled according to **Table S20** highlighted in blue is the peak used for qNMR.

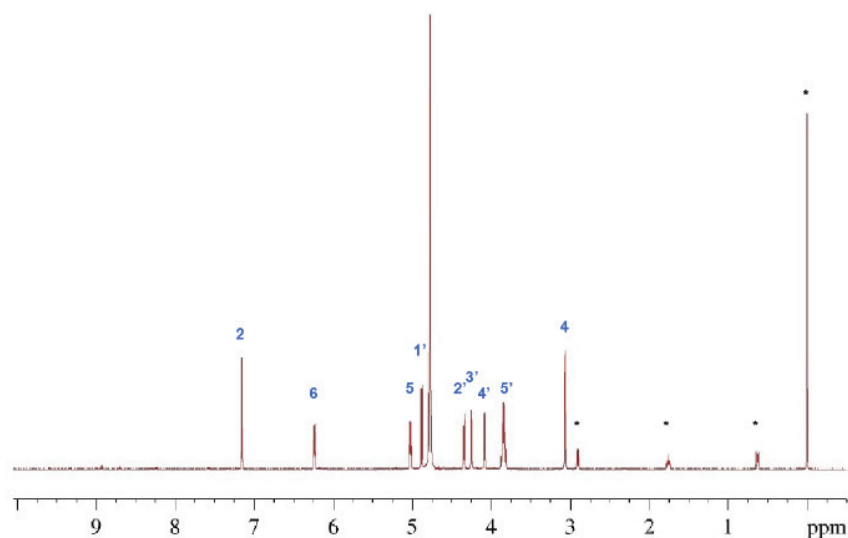


Fig. S53 Complete view of the ^1H spectrum of NMN standard in D_2O with internal reference DSS (*) at 298 K, labelled according to **Table S20**. Some H_2O is visible at about 4.8 ppm.

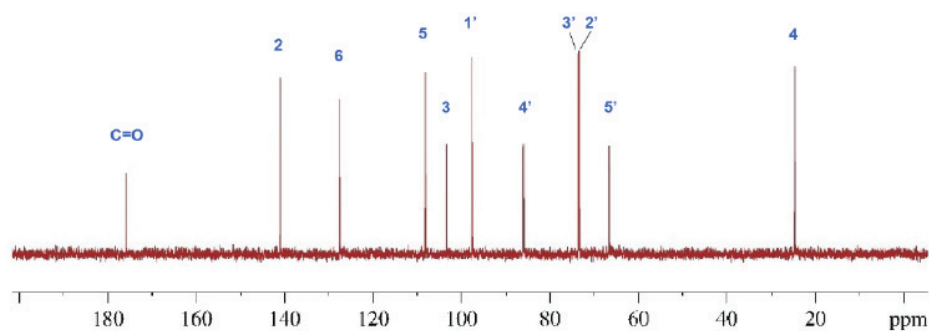


Fig. S54 ^{13}C spectrum of 1,4-NMNH in D_2O at 298 K, labelled according to **Table S20**.

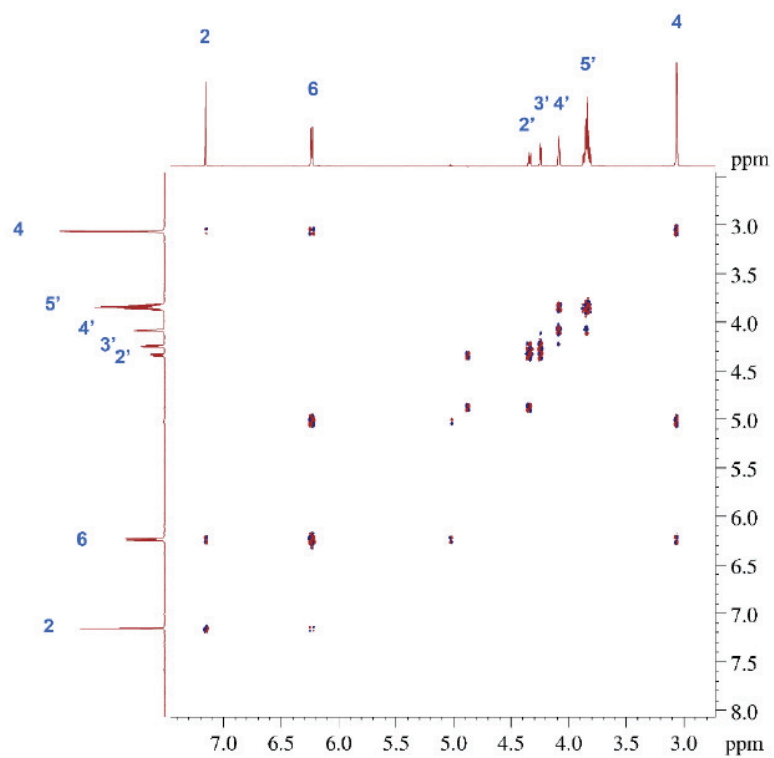


Fig. S55 ^1H - ^1H DQF-COSY spectrum of 1,4-NMNH in D_2O at 298 K, labelled according to **Table S20**.

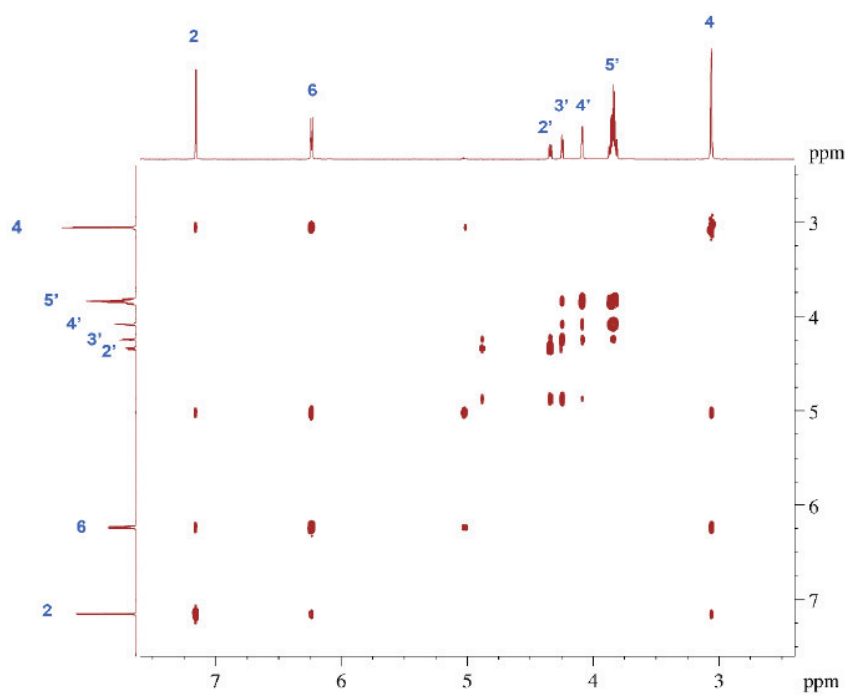


Fig. S56 ^1H - ^1H TOCSY spectrum of 1,4-NMNH in D_2O at 298 K, labelled according to **Table S20**.

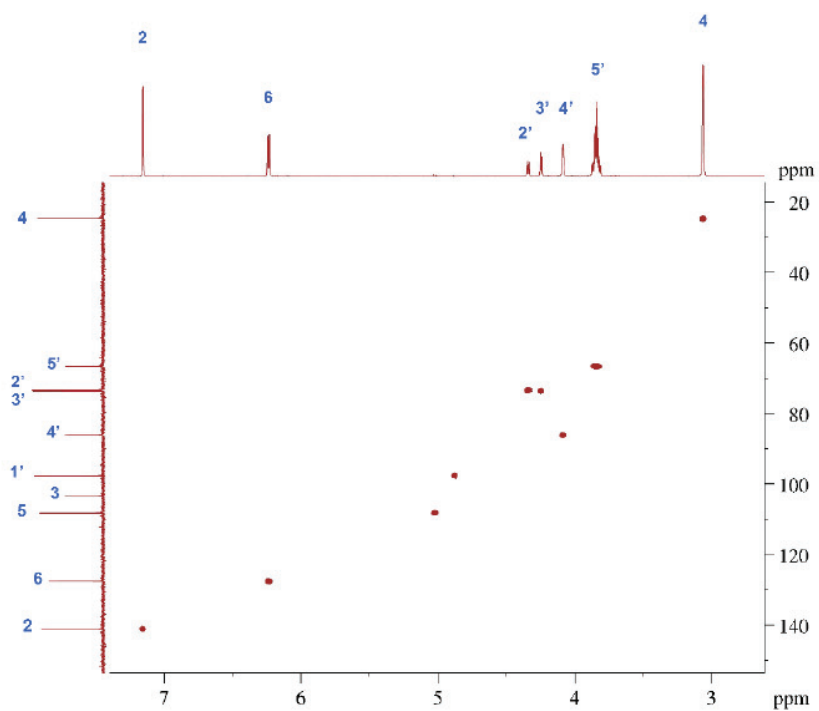


Fig. S57 Edited ^1H - ^{13}C HSQC spectrum of 1,4-NMNH in D_2O at 298 K, labelled according to **Table S20**.

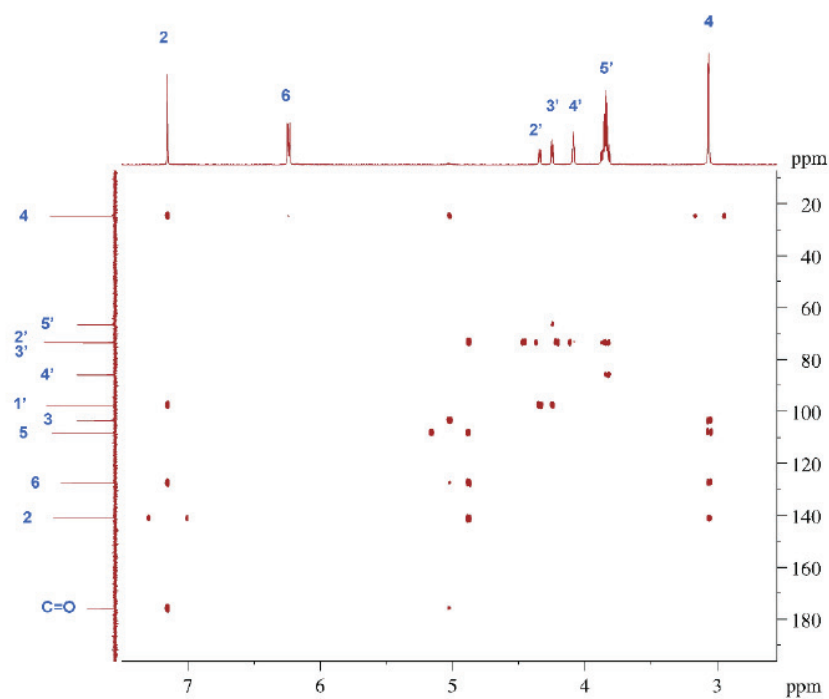


Fig. S58 The ^1H - ^{13}C HMBC spectrum of 1,4-NMNH in D_2O at 298 K, labelled according to **Table S20**.

References

1. D. P. Henriques Pereira, *et al.*, Role of geochemical protoenzymes (geozymes) in primordial metabolism: Specific abiotic hydride transfer by metals to the biological redox cofactor NAD⁺. *The FEBS Journal* 16329 (2022). <https://doi.org/10.1111/febs.16329>.
2. R. R. Ernst, G. Bodenhausen, A. Wokaun, *Principles of nuclear magnetic resonance in one and two dimensions*, Repr (Clarendon Press, 2004).
3. K. Wüthrich, *NMR of proteins and nucleic acids* (Wiley, 1986).
4. J. N. S. Evans, *Biomolecular NMR Spectroscopy* (Oxford University Press, 1996).
5. H.-O. Kalinowski, S. Berger, S. Braun, *¹³C-NMR-Spektroskopie* (Georg Thieme Verlag, 1988).
6. S. E. Godtfredsen, M. Ottesen, N. R. Andersen, On the mode of formation of 1,6-dihydro-NAD in NADH preparations. *Carlsberg Res. Commun.* **44**, 65–75 (1979).

Publication III – Ferredoxin reduction by hydrogen with iron functions as an evolutionary precursor of flavin-based electron bifurcation

Year: 2024

Authors: Max Brabender, Delfina P. Henriques Pereira, Natalia Mrnjavac, Manon Laura Schlikker, Zen-Ichiro Kimura, Jeerus Sucharitakul, Karl Kleinermanns, Harun Tüysüz, Wolfgang Buckel, Martina Preiner, and William F. Martin

Contribution: First author.

Developed the protocol used for the abiotic reduction of Fd and quantification. I was directly involved in planning all experiments as well as performing the initial tests with all Fe, Co, Ni alloys, oxides and native metals at pH 8.5. Analysed the data I collected and discussed all the data obtained. Helped reviewing and adapting the main text.

Published in: Proceedings of the National Academy of Sciences (PNAS)

DOI: 10.1073/pnas.2318969121

Summary: This research paper shows that the reduction of *Clostridium pasteurianum* ferredoxin is possible with H₂ and native iron (Fe⁰), and not with the other metals tested (Ni⁰, Co⁰, Mo⁰, NiFe, Ni₂Fe, Ni₃Fe, or Fe₃O₄). Results also show that it maintains its folded conformation in a metal-rich environment, under pH 10 at 40 °C. This demonstrates that electron bifurcation is not needed to reduce low potential cofactors under prebiotic conditions and supports the preconceived idea that the acetyl-CoA pathway is ancient.



Ferredoxin reduction by hydrogen with iron functions as an evolutionary precursor of flavin-based electron bifurcation

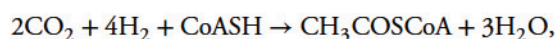
Max Brabender^{a,1,2} , Delfina P. Henriques Pereira^{b,1} , Natalia Mrnjavac^{a,1} , Manon Laura Schlikker^a , Zen-Ichiro Kimura^{a,c} , Jeerus Sucharitakul^d , Karl Kleiner^e, Harun Tüysüz^f , Wolfgang Buckel^{g,h,i} , Martina Preiner^b , and William F. Martin^a

Edited by Caroline Harwood, University of Washington, Seattle, WA; received October 31, 2023; accepted February 14, 2024

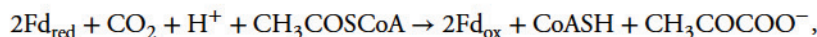
Autotrophic theories for the origin of metabolism posit that the first cells satisfied their carbon needs from CO₂ and were chemolithoautotrophs that obtained their energy and electrons from H₂. The acetyl-CoA pathway of CO₂ fixation is central to that view because of its antiquity: Among known CO₂ fixing pathways it is the only one that is i) exergonic, ii) occurs in both bacteria and archaea, and iii) can be functionally replaced in full by single transition metal catalysts in vitro. In order to operate in cells at a pH close to 7, however, the acetyl-CoA pathway requires complex multi-enzyme systems capable of flavin-based electron bifurcation that reduce low potential ferredoxin—the physiological donor of electrons in the acetyl-CoA pathway—with electrons from H₂. How can the acetyl-CoA pathway be primordial if it requires flavin-based electron bifurcation? Here, we show that native iron (Fe⁰), but not Ni⁰, Co⁰, Mo⁰, NiFe, Ni₂Fe, Ni₃Fe, or Fe₃O₄, promotes the H₂-dependent reduction of aqueous *Clostridium pasteurianum* ferredoxin at pH 8.5 or higher within a few hours at 40 °C, providing the physiological function of flavin-based electron bifurcation, but without the help of enzymes or organic redox cofactors. H₂-dependent ferredoxin reduction by iron ties primordial ferredoxin reduction and early metabolic evolution to a chemical process in the Earth's crust promoted by solid-state iron, a metal that is still deposited in serpentinizing hydrothermal vents today.

acetyl CoA pathway | transition metals | serpentinization | origin of metabolism | origin of life

Autotrophic theories for life's origins posit that the first organisms on Earth were CO₂-fixing microbes. In that view, relicts from primordial CO₂ fixation might have been preserved in modern metabolism, bringing CO₂ fixation pathways to bear the origin of metabolism and life (1). Among known routes of CO₂ fixation, the acetyl-CoA pathway is the most ancient (2). It is the only CO₂ fixation pathway known to operate in both archaea (methanogens) and bacteria (acetogens) (3) and the only one that is exergonic, releasing energy in the synthesis of acetyl-CoA (CH₃COSCoA) from H₂, CO₂, and coenzyme A (CoASH) via formate as an intermediate (4) according to



with $\Delta G_o' = -59$ kJ/mol (2). Roughly 70% of the resulting acetyl-CoA pool is further converted to pyruvate (CH₃COCOO⁻) by ferredoxin-dependent CO₂ fixation at the pyruvate synthase reaction



for the synthesis of amino acids, bases, cofactors, and cell mass (2). The enzymes of the acetyl-CoA pathway are replete with transition metals as electron carriers and catalysts (4–8), inorganic cofactors that are reasonably interpreted as relicts (9–12) from a geochemical setting (13) within which metabolism and life arose. In acetogens and methanogens growing on H₂ and CO₂, the acetyl-CoA pathway converts H₂ and CO₂ into formate (4), acetate, and pyruvate (2) via ~10 enzymatic reactions that require 14 cofactors and 127 proteins, including the cofactor biosynthesis pathways (14).

Newer findings reveal that under the conditions of H₂-producing (serpentinizing) hydrothermal vents (15, 16), the function of those 127 proteins can be replaced in toto by individual transition metal minerals such as Ni₃Fe or Fe₃O₄ in vitro. These catalysts not only convert CO₂ and H₂ with high specificity to formate, acetate, and pyruvate in the laboratory (17–20), they are deposited in serpentinizing hydrothermal vents in nature (21–23). They can even convert H₂ and CO₂ to pyruvate at concentrations of 200 μM (19), the physiological pyruvate concentration in the cytosol of acetogens growing on H₂ and CO₂ (24). Whether catalyzed by enzymes or metals, these ancient metabolic reactions

Significance

In the most ancient biochemical pathway known—the reductive acetyl-CoA pathway—the energy to fix CO₂ comes from geochemically produced H₂ gas, not from the sun. Cells that fix CO₂ with H₂ require an energetic trick: They split the electron pair in H₂, boosting the energy of one electron at the expense of the other to charge an ancient protein called ferredoxin with electrons. That requires enzymes and cofactors. How was ferredoxin charged before enzymes and cofactors arose? In alkaline, H₂-producing hydrothermal systems, the electron-donating potential of H₂ can reduce ferredoxins but requires the presence of a transition metal. We show that in water, raw iron will transfer electrons from H₂ to ferredoxin, uncovering a missing link in early metabolic evolution.

Author contributions: M.B., D.P.H.P., N.M., M.P., and W.F.M. designed research; M.B., D.P.H.P., and M.L.S. performed research; J.S. and H.T. contributed new reagents/analytic tools; M.B., D.P.H.P., N.M., Z.-I.K., K.K., W.B., M.P., and W.F.M. analyzed data; M.B., D.P.H.P., N.M., M.L.S., Z.-I.K., J.S., K.K., H.T., W.B., M.P., and W.F.M. edited the paper; and M.B., D.P.H.P., N.M., and W.F.M. wrote the paper.

The authors declare no competing interest.

This article is a PNAS Direct Submission.

Copyright © 2024 the Author(s). Published by PNAS. This open access article is distributed under Creative Commons Attribution-NonCommercial-NoDerivatives License 4.0 (CC BY-NC-ND).

¹M.B., D.P.H.P., and N.M. contributed equally to this work.

²To whom correspondence may be addressed. Email: max.brabender@hhu.de.

This article contains supporting information online at <https://www.pnas.org/lookup/suppl/doi:10.1073/pnas.2318969121/-DCSupplemental>.

Published March 21, 2024.

go forward because in the reaction of H_2 with CO_2 , the equilibrium lies on the side of reduced carbon compounds (25). Transition metal catalysts forge a functional link between ancient metabolism and modern serpentinizing hydrothermal systems, which synthesize formate via abiotic geochemical reactions in amounts sufficient to support microbial growth (26–30).

Though the reactions of the acetyl-CoA pathway naturally unfold from H_2 and CO_2 in the presence of transition metal catalysts in the laboratory, this does not, by itself, solve the problem of metabolic origins, because the biochemically catalyzed acetyl-CoA pathway as it occurs in cells presents a thermodynamic paradox. The CO_2 -reducing enzymes of the acetyl-CoA pathway require reduced ferredoxin, Fd, as their electron donor, whereby Fd is reduced with electrons from H_2 via hydrogenases (Fig. 1). However, the midpoint potential of H_2 under standard physiological conditions, $E'_0 = -414$ mV, is more positive than the midpoint potential of low potential ferredoxins, roughly -450 to -500 mV in cells (31) as required for CO_2 fixation ($E'_0 = -430$ mV), making Fd reduction with H_2 a steeply endergonic process (Fig. 1A), especially in environments with low H_2 partial pressures (31). How do cells push electrons energetically uphill to Fd for CO_2 fixation?

The discovery of flavin-based electron bifurcation (32, 33) revealed how the main groups of H_2 -dependent autotrophs, methanogens and acetogens, reduce ferredoxin with H_2 (34, 35). The two electrons from H_2 are transferred via a hydrogenase (36, 37) to an enzyme-bound flavin, where they diverge along exergonic and endergonic paths, respectively. One electron is transferred to a high potential acceptor such as NAD^+ or the heterodisulfide CoM-S-S-CoB, the other is transferred, in strict stoichiometry, to Fd as the low potential acceptor (Fig. 1A). Reduction of the high potential acceptor renders the overall Fd-reducing reaction exergonic (31–42). All flavin-based electron bifurcation redox couples known so far reduce Fd (39) or flavodoxins under Fe limitation (41). This indicates that the ancestral physiological function of flavin-based electron bifurcation was to supply reduced Fd as a low potential reductant for metabolism, in turn welding both flavin-based electron bifurcation and Fd into the foundation of autotrophic theories for the origin of metabolism because, in concert, they supply the electrons for FeS and FeNiS clusters in enzymes of the acetyl-CoA pathway (2–8, 31, 35, 43, 44).

While flavin-based electron bifurcation solves the bioenergetic problem of Fd reduction with H_2 in metabolism, it presents a paradox in prebiotic physiology (45, 46): Given the antiquity of the acetyl-CoA pathway, how was Fd reduced in early evolution i) before the origin of the more complicated Fe–Ni and Fe–Fe hydrogenases that oxidize H_2 (Fig. 1B) and ii) before the origin of the vastly more complicated multi-enzyme process of flavin-based electron bifurcation (31–42) (Fig. 1A) that is required for Fd reduction in H_2 -dependent chemolithoautotrophs? Because of its universality among anaerobes, and by functional, structural, and biogenetic simplicity (Fig. 1B), Fd is clearly more ancient than the hydrogenases (Fig. 1C) that supply reduced ferredoxin as the reductant for CO_2 fixation. The FeS clusters of Fd are not only simpler in structure than hydrogenase active sites, which extract electrons from H_2 for Fd reduction, they also lack the small molecule ligands that are added to iron during hydrogenase active site maturation (47–49) (Fig. 1C) by maturases that arose subsequent to the hydrogenase structural protein (50). In early biochemical evolution, simpler mechanisms must have therefore preceded hydrogenases and flavin-based electron bifurcation as a means of supplying reduced ferredoxin, though such mechanisms have not been experimentally identified so far. Here, we investigate the ability of native transition metals to reduce ferredoxin with H_2 in the absence of flavins or electron-bifurcating enzymes.

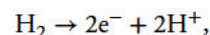
Results

We used H_2 as the source of electrons for Fd reduction because it is the reductant that drove primary production on Earth prior to the origin of photosynthesis starting with the first signs of life 3.8 billion years ago (51, 52). To activate H_2 we used native metals and metal alloys that are naturally deposited in serpentinizing systems (21–23). Serpentinization entails geochemical redox reactions between Fe(II) minerals and H_2O circulating through the Earth's crust (15, 16), generating H_2 as the source of energy and electrons for primary production by bifurcation-dependent anaerobic autotrophs that inhabit serpentinizing systems in the dark subsurface: acetogens (26, 53) and methanogens (27, 28). For assays, we used glass vials and 5 bar of H_2 , corresponding to 3.8 mM H_2 in the aqueous phase, well within the range of H_2 concentrations measured in the effluent of Lost City (29, 54) and other serpentinizing hydrothermal systems (46, 55). The reduction of ferredoxin from *Clostridium pasteurianum* purified from *Escherichia coli* can be followed by the standard photometric assay (56) by following the difference in absorption at 420 nm (Fig. 2).

Previous studies showed that Fe^0 , Ni^0 , and Co^0 can catalyze the reduction of NAD^+ to NADH under mild hydrothermal conditions: 5 bar H_2 , 40 °C (57). NAD^+ is a stronger oxidant ($E'_0 = -320$ mV) than *C. pasteurianum* Fd ($E'_0 = -412$ mV) (58) and NAD^+ reduction is a two-electron reaction involving hydride (H^-) transfer while ferredoxin reduction involves one-electron transfer to [4Fe4S] centers. A screen of transition metals revealed that Ni^0 , Co^0 , Mo^0 , $NiFe$, Ni_2Fe , Ni_3Fe , and Fe_3O_4 do not mediate H_2 -dependent Fd reduction, whereas Fe^0 reduces Fd in the presence of H_2 (Fig. 3). The concentration of Fd in reactions was 30 μ M, slightly lower than the physiological concentration in anaerobes, where Fd concentrations are in the range of 80 to 400 μ M (59).

Ferredoxin reduction by Fe^0 required roughly four hours at 40 °C (Fig. 4). Notably, *C. pasteurianum* Fd does not autoreduce under these conditions, as shown in Fig. 4 for reactions of Fd and H_2 without metal. This is also seen in reactions of Fig. 3 where no Fd reduction was detected. Ferredoxin reduction with Fe^0 at pH 8.5 required H_2 and solid-state iron (Fig. 3). The lack of autoreduction is noteworthy, because FeNiS and FeS enzymes of the acetyl-CoA pathway (acetyl-CoA synthase/carbon monoxide dehydrogenase and pyruvate synthase) are able to activate H_2 via latent hydrogenase activities (60). However, *C. pasteurianum* Fd does not oxidize H_2 , in agreement with the absence of hydrogenase activity for Fd from *Clostridium thermoaceticum* (60). The FeS clusters of *C. pasteurianum* Fd require an iron surface for reduction under the conditions tested here.

Early studies detected an effect of pH on the reduction of FeS proteins from *C. pasteurianum* and other sources, though the effects were generally small in the pH range of 6 to 9 (63). Subsequent studies did not detect pH-dependent effects (58). The conditions in our investigation are aligned with serpentinizing systems, where the midpoint potential of H_2 oxidation is directly influenced by pH through the reaction



which is pulled to the right at alkaline pH via proton removal, resulting in very negative midpoint potentials. In actively serpentinizing hydrothermal systems, pH can exceed 10 and the midpoint potentials can exceed -700 mV (26, 30, 46, 55). We observed a tendency for the pH to increase with reaction time in runs with Fe^0 despite the presence of 133 mM P_i buffer. To see whether the observed Fd reduction is due solely to a pH

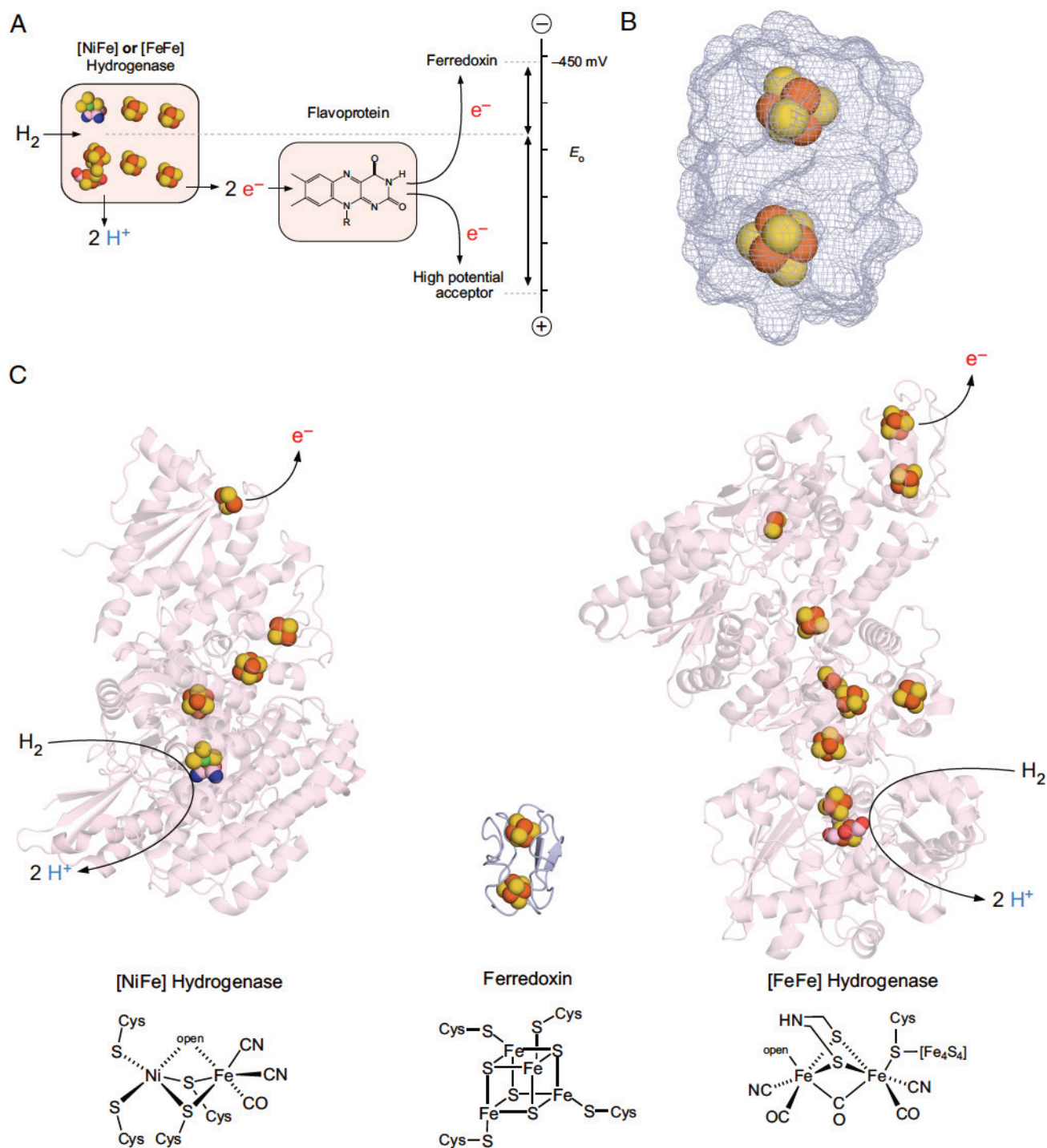


Fig. 1. Ferredoxin is the primordial one-electron carrier in metabolism. (A) Flavin-based electron bifurcation is required to reduce low potential ferredoxin for CO_2 fixation using electrons from H_2 (schematic). The flavoprotein and its high potential acceptor varies across organisms and pathways (31–42). (B) The structure of *C. pasteurianum* ferredoxin (PDB ID: 1CLF). Other renderings of ferredoxin are given in *SI Appendix, Fig. S1*. (C) The structure of the two forms of hydrogenase used to oxidize H_2 for Fd reduction and their catalytic metal clusters compared to Fd from *C. pasteurianum*. The structures are for MvhAGD, the [NiFe] hydrogenase from *Methanothermococcus thermolithotrophicus* (PDB ID: 5ODC) (36) and HydABC, the [FeFe] hydrogenase from *Acetobacterium woodii* (PDB ID: 8A5E) (37). The CN^- and aminodithiolate ligands are missing in the structure of the H-cluster of HydABC. One protomer of HydABC and one protomer of MvhAGD are shown, the biologically active complexes being a homodimer of heterotrimers and a homodimer of heterohexamers (including the heterodisulfide reductase), respectively. Under nickel limitation, some methanogens express a third form of hydrogenase with a unique iron-guanylylpyridinol cofactor that transfers electrons from H_2 directly to methenyl-tetrahydromethanopterin without FeS cluster intermediates (8).

effect (altered midpoint potential of H_2 oxidation) on metal-dependent water reduction, native metals were tested at pH 10. For Ni^0 and Co^0 , there was no observable Fd reduction with H_2 at pH 8.5 or pH 10 (Fig. 5B). At pH 8.5, Fd reduction required Fe^0

and H_2 , while at pH 10, there was also substantial Fd reduction without addition of exogenous H_2 (Fig. 5A). This was expected based on findings from NAD^+ reduction using ^2H labeling, where it was observed that at pH 10, Fe^0 generates endogenous $^2\text{H}^-$ from

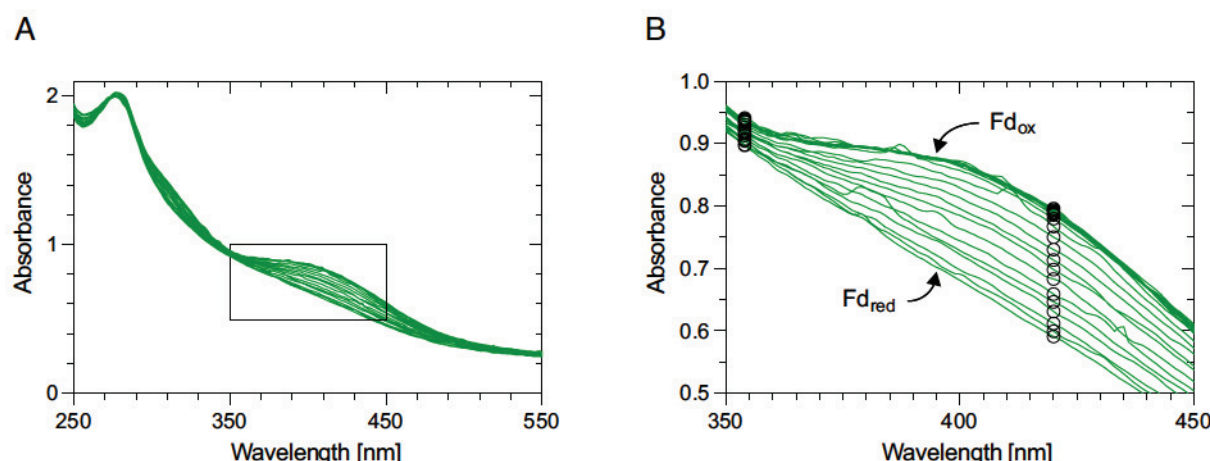


Fig. 2. Photometric assay of Fd reduction. (A) UV-Vis spectra following the oxidation of 30 μM of reduced Fd from *C. pasteurianum* in 0.133 M phosphate buffer at pH 8.5 through air exposure for 300 s. Fd was previously reduced through addition of two equivalents of sodium dithionite ($\text{Na}_2\text{S}_2\text{O}_4$). (B) Magnified boxed region in A showing the difference in absorption of the [4Fe4S] clusters at 420 nm and the isosbestic point at 354 nm (56), used for normalization. The time course of Fd reduction is shown in *SI Appendix, Fig. S2*.

$^2\text{H}_2\text{O}$ (57). The yield of reduced ferredoxin for Fe^0 without H_2 at pH 10 relative to the yield without H_2 at pH 8.5 (Fig. 5A) might result from the more negative H_2 midpoint potential at increased pH. Reduction of Fd cannot be tested with $^2\text{H}_2\text{O}$ in the same way as for NAD^+ (57) because Fd accepts single electrons rather than hydride. Surface oxidation of Fe^0 can generate soluble Fe^{2+} (64–66), which is not, however, a sufficiently strong reductant to reduce ferredoxin ($\text{Fe}^{2+} \rightarrow \text{Fe}^{3+} + \text{e}^-$, $E'_0 = -200$ mV) (67).

To further probe the effect of pH, we increased the buffer strength to 1.33 M P_i and incubated in the presence of H_2 at different pH values (Fig. 6). At pH 7, where the midpoint potential of the H_2 oxidation is $E_0 = -414$ mV, close to the midpoint potential of Fd, the reaction is incomplete. At pH 6, the reaction is blocked, as expected. Ferredoxin reduced by H_2 over Fe^0 is biologically active, it serves as a substrate to reduce NADP^+ in the reaction catalyzed by ferredoxin:NADP oxidoreductase from spinach chloroplasts (*SI Appendix, Fig. S4*).

Discussion

In water at 40 $^\circ\text{C}$, H_2 can reduce *C. pasteurianum* Fd at a concentration of 30 μM in the presence of Fe^0 within a few hours. The pH and partial pressure of H_2 used (5 bar, roughly 3.8 mM in solution according to Henry's law) correspond to conditions in actively serpentinizing hydrothermal vents (29, 46, 54, 55). The 30 μM Fd concentration used is close to that in cells. We found that iron was effective in reducing Fd with H_2 . Neither the Fe–Ni alloys tested nor magnetite were effective in Fd reduction. Though the mechanism of electron transfer from the heterogeneous Fe^0 surface to Fd is obscure, it requires Fe in the solid state in these experiments and likely entails chemisorption for H_2 activation (61, 62) with electron transfer mechanisms possibly similar to those that operate between FeS clusters in proteins (68, 69). Because Fe^0 conducts, H_2 oxidation and Fd reduction need not occur at the same site on iron particles. Several studies have used electrodes with externally applied potentials to promote

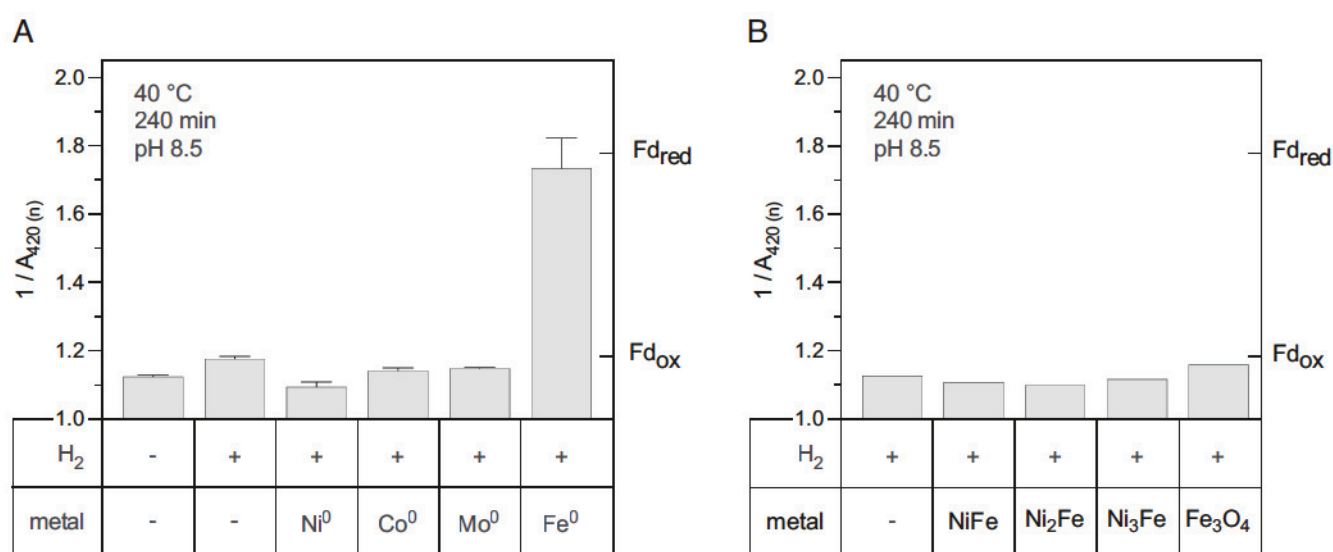


Fig. 3. Metals tested for H_2 -dependent Fd reduction. Reaction of 30 μM Fd from *C. pasteurianum* with 0.1 mmol (A) native metal and (B) metal alloys and magnetite under a hydrogen atmosphere [5 bar] in 0.133 M phosphate buffer at pH 8.5. Normalized absorption of [4Fe4S] clusters in Fd is shown (*Methods*). Raw data for iron shown in *SI Appendix, Fig. S3*.

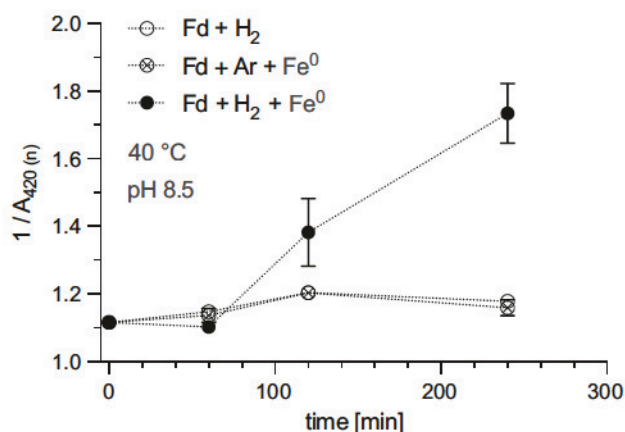


Fig. 4. Time course of Fe^0 -promoted H_2 -dependent Fd reduction. The lag time of about 1 h might reflect delayed formation of chemisorbed hydrogen on the iron surface (61, 62) or H_2 -dependent formation of active sites on the metal surface. A similar lag time was observed for H_2 -dependent NAD^+ reduction on Fe^0 (57).

prebiotic chemical reactions (70, 71). We applied no external potentials. At alkaline pH, serpentinization and Fe^0 produce the diffusible reductant H_2 by interactions with water. The reduction of Fd took place via redox reactions with exogenous H_2 and Fe^0 at pH 8.5 and without exogenous H_2 at pH 10. At pH 6, Fd reduction does not take place (Fig. 6). The reason why Fe^0 reduces Fd in our reactions while the other metals tested do not (Fig. 3) is likely due to the more negative midpoint potential of Fe^0 in reaction to the divalent ion relative to the other metals tested (57, 67) or to differences in H_2 chemisorption among metals tested (57), or both.

An Ancient Root to Modern Corrosion? Though motivated by the study of early evolution, our findings bear upon a modern problem: the corrosion of iron by microbes that use Fe^0 as an electron source. A number of H_2 -dependent anaerobic microbes that use the acetyl-CoA pathway, most notably methanogens and

acetogens, can use Fe^0 as an electron source for growth (64–66). Iron oxidation results in iron dissolution as Fe^{2+} and corrosion. The molecular mechanisms by which acetogens and methanogens extract electrons from Fe^0 are still unknown (66), but the transient formation of H_2 from oxide-generating reactions of iron and water—as suggested in a previous study of NAD^+ reduction (57) and as we suspect for Fd reduction without H_2 at pH 10 (Fig. 6)—are widely discussed (64–66).

While it is possible that use of Fe^0 as a source of electrons is a recent microbial adaptation to human metalworking technology, it is far more likely that this physiological capacity is ancient, a holdover from growth on ubiquitous Fe^0 and iron alloys (21–23) in serpentinizing systems, which are as old as water on Earth (15, 16). This would be highly compatible with phylogenetic and physiological evidence for the age of acetogens and methanogens (26, 53, 72–74), lineages that can grow on iron. Native metals are deposited in hydrothermal systems when serpentinization and H_2 production are active. When H_2 production through serpentinization stops, deposited Fe^0 is still available (21–23), which can serve as the sole electron source for several lineages of acetogens and methanogens (64–66). Our findings raise the possibility that FeS clusters localized in proteins at the cell surface mediate growth on iron as an electron source in organisms that do not use extracellular multi-heme cytochromes (66) or extracellular flavins to access electrons.

No Requirement for Membranes or Ion Gradients. The enzymatic process of flavin-based electron bifurcation requires neither membranes, ion gradients, nor membrane-integral proteins (31–42), hence it could have operated at a very early stage of biochemical evolution, before the origin of free-living cells and even before the origin of membranes. During the course of evolution, microbes evolved membrane-dependent protein complexes that generate reduced ferredoxin without flavin-based electron bifurcation. These include the energy-conserving hydrogenase Ech, which taps ion gradients at the plasma membrane to reduce Fd with H_2 (75, 76). It has been proposed that Ech-like functions might have been required for primordial ferredoxin reduction (77, 78), yet Ech is

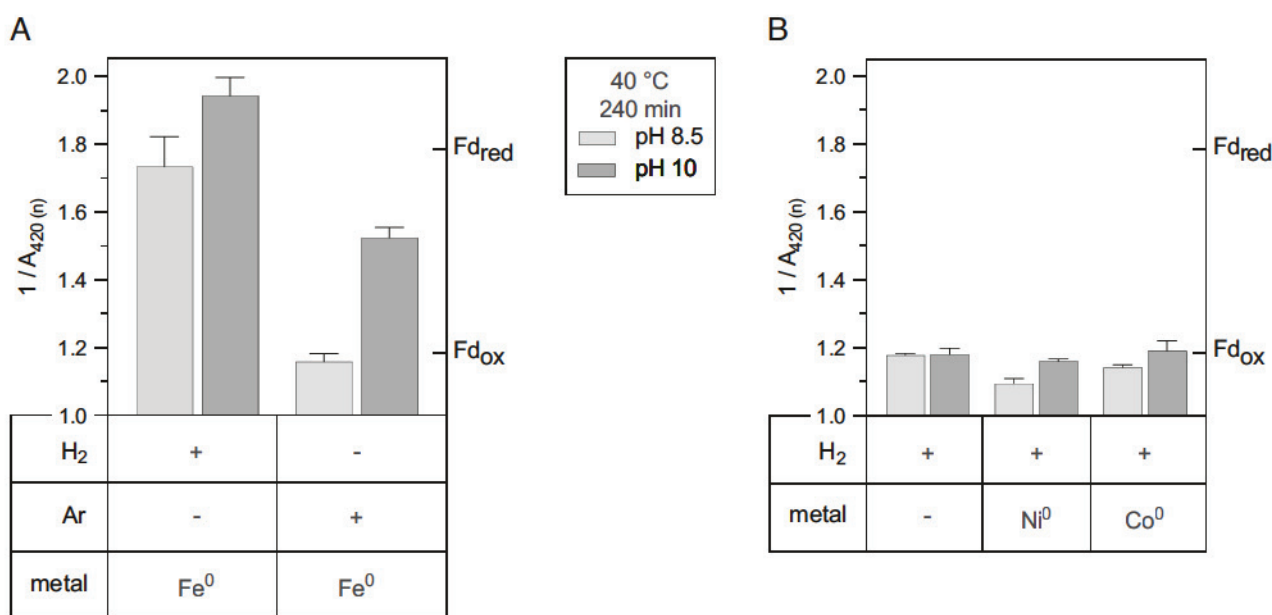


Fig. 5. H_2 -dependent Fd reduction at pH 10. Reaction of 30 μM Fd from *C. pasteurianum* with 0.1 mmol metal. (A) Native iron and (B) native cobalt and native nickel under a hydrogen atmosphere [5 bar] in 0.133 M phosphate buffer at pH 8.5 and pH 10. Normalized absorption of [4Fe4S] clusters in Fd is shown (Methods).

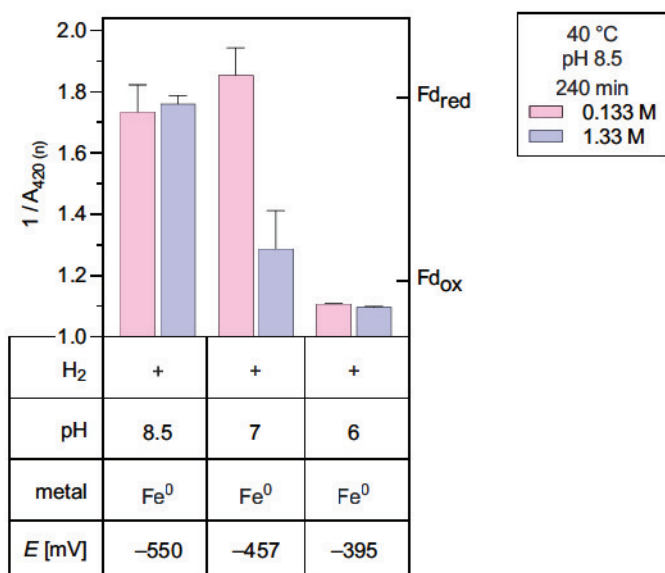


Fig. 6. pH dependence of Fd reduction with H₂. Reaction of 30 μ M Fd from *C. pasteurianum* with 0.1 mmol native iron under a hydrogen atmosphere [5 bar] in 0.133 M and 1.33 M phosphate buffer at pH 8.5. Normalized absorption of [4Fe4S] clusters in Fd is shown (Methods). The midpoint potential of H₂ was calculated using the Nernst equation.

evolutionarily derived from soluble Fe–Ni hydrogenases (79), which require electron bifurcation for autotrophic function, such that Ech can hardly be an ancestral Fd-reducing agent. Our findings show that neither ion gradients, membranes, nor Ech-like functions are required by the far simpler process of Fd reduction in the presence of H₂ and iron.

A Metal:Protein Hybrid Intermediate. In contrast to previous studies of inorganic-catalyzed prebiotic reactions (80), the substrate of our iron-dependent reaction is a protein with FeS clusters. Ferredoxin reduction with H₂ and Fe⁰ under serpentinizing conditions closes an important gap in early bioenergetic evolution, providing an example of a hybrid intermediate state in the evolution of metabolism subsequent to abiotic versions of the acetyl-CoA pathway (17–20, 81) yet prior to the origin of enzymes that perform flavin-based electron bifurcation (Fig. 7). The ancestral route of pyruvate synthesis from H₂ and CO₂ is readily catalyzed by a number of different transition metal catalysts, including Fe⁰, Ni⁰, Ni₃Fe, and Fe₃O₄ (17–20) that occur naturally in serpentinizing hydrothermal vents (Fig. 7A). With the advent of genes and proteins, primitive versions of the acetyl-CoA pathway (72, 82) comprising the Fd-dependent enzymes carbon monoxide dehydrogenase/acetyl-CoA synthase and pyruvate synthase (5–8) could replace inorganically catalyzed pyruvate synthesis, but the activity of the soluble enzymes remained tied to transition metals in the crust for the supply of reduced ferredoxin as a kind of electrochemical umbilical cord connecting H₂ activation (solid phase) to one-electron supply at enzymes (aqueous phase) (Fig. 7B).

Given geochemical availability of H₂ from serpentinization and CO₂ from seawater, this hybrid intermediate state would be indefinitely sustainable, but metabolic evolution would remain bound to the Earth's crust by the requirement for solid-state metals. Escape from the crust required a number of inventions, among them cellularization and the ability to fix CO₂ without the requirement for physical contact between cytosolic enzymes and metals in the crust. The origin of hydrogenases (36, 37, 50) and flavin-based electron bifurcation freed H₂-dependent ferredoxin

reduction from solid-state contact, but coupled Fd reduction to the simultaneous reduction of stronger oxidants (Fig. 7C). These eventually included NAD⁺ via the electron-bifurcating Fe–Fe hydrogenase reaction of acetogens (35) or CoM-S-S-CoB via the MvhADG/HdrABC complex (Fe–Ni hydrogenase/heterodisulfide reductase) of methanogens (34), coupling Fd-dependent CO₂ reduction to stoichiometrically balanced energy metabolism in these H₂-dependent chemolithoautotrophs (39). The evolutionary innovation of flavin-based electron bifurcation enabled the use of H₂ as an electron donor for Fd reduction at cytosolic pH values near 7. Despite their divergent mechanisms of pumping for ATP synthesis (43, 44), the acetyl-CoA pathway links methanogens and acetogens (84), primordial members of the archaeal and bacterial lineages (72–74), with serpentinizing environments (15, 16, 85), which they still inhabit today (26–30, 53, 74). Our findings provide a crucial missing link in early metabolic evolution, closing a gap in autotrophic theories by demonstrating a functional intermediate state in the transition from geochemical to enzymatic catalysis in H₂-dependent CO₂ fixation (Fig. 7), as required if life

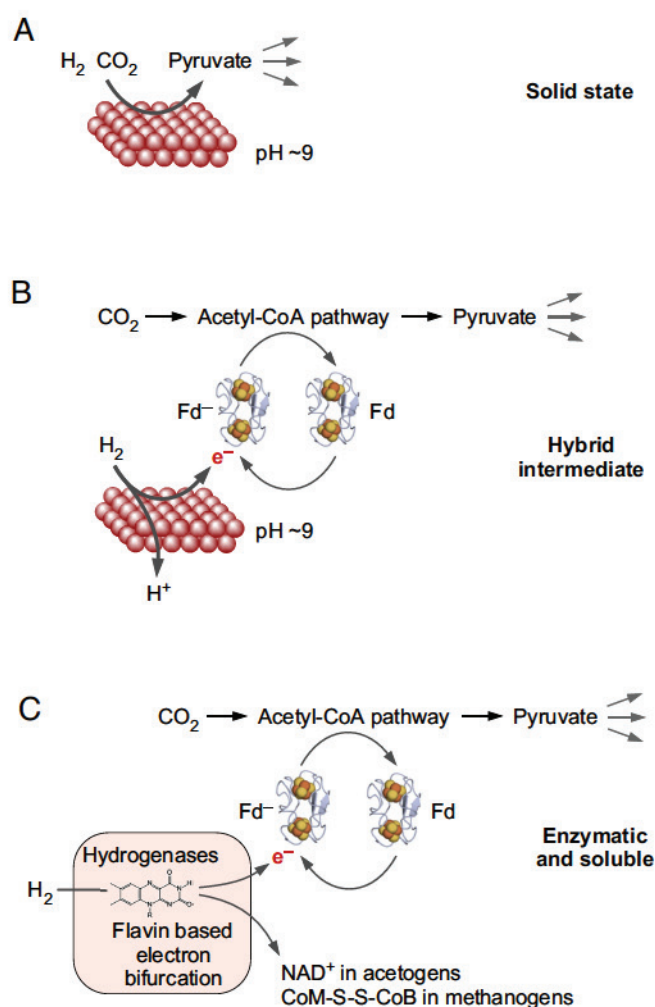


Fig. 7. Three phases in the evolution of autotrophy via the acetyl-CoA pathway. (A) Metal-catalyzed pyruvate synthesis from H₂ and CO₂ (17–20, 80) as the ancestral state of the acetyl-CoA pathway. (B) Iron-dependent ferredoxin reduction with H₂ as a source of the physiological reductant (reduced ferredoxin) for CODH/ACS (5, 7, 60) and PFOR (6, 34, 60) in an intermediate stage of physiological evolution before the origin of flavin-based electron bifurcation. (C) H₂ oxidation via Fe–Fe and Ni–Fe hydrogenases and flavin-based electron bifurcation for the synthesis of reduced ferredoxin in a fully soluble enzymatic system encoded by genes. The source of methyl groups for the ACS reaction in (B) can either be geochemical (72, 83) as in (A) or biochemical from CO₂ as in the extant acetyl-CoA pathway (2).

arose at hydrothermal vents (13) involving the acetyl-CoA pathway (83).

In the Light of Origin Theories. Do the present findings discriminate among theories for the origin of life? The main competing theories for origins encompass genetics first and metabolism first proposals. Genetics first theories posit, in current mainstream formulations, that RNA-based replicating systems preceded the origin of life-like metabolic pathways and that the RNA bases were synthesized with the help of atmospheric reactions giving rise to cyanide, $C\equiv N^-$, or $C\equiv N$ -containing compounds that fueled RNA synthesis until metabolism arose (86–88). In genetics first theories, reactions between H_2 and CO_2 play no role, as the reduced carbon species that initiate primordial amino acid and nucleobase synthesis contain reduced carbon with highly reactive $C\equiv N$ bonds (89–91). Because $C\equiv N$ -containing compounds are absent in modern biosynthesis, genetics first models do not intersect microbial metabolism, such that flavin-based electron bifurcation, H_2 -dependent CO_2 fixation, and the acetyl-CoA pathway do not address genetics first, and vice versa.

Metabolism first theories posit that organized and catalyzed chemical reaction networks having evident similarity to modern metabolic pathways are the starting point of life chemistry, from which genetic systems later emerged (92). In autotrophic theories, metabolism started from CO_2 , just like it does in the primary production of modern ecosystems (1). Autotrophic theories that draw upon hydrothermal vents (13) and H_2 from serpentinization to reduce CO_2 via the acetyl-CoA pathway to pyruvate strictly require evolutionary precursors of electron bifurcation (45, 46), readily accommodating the present findings. From pyruvate, the central intermediate of biosynthesis (2, 93), the paths to the incomplete reductive reductive citric acid cycle (94), amino acids, nucleotide, and cofactor synthesis are short, entailing only about 400 reactions (95). Amino acid and nucleobase syntheses from biochemical starting compounds can take place without enzymes (80, 96, 97), as suggested in these pages in 1963: “primitive organic cofactors (along with inorganic ions) acting on surfaces were the original ‘bio’ catalysts, active long before specific polypeptides evolved” (92). As Fe^0 presents a surface, our findings (Fig. 7) are in full accord with that depiction.

Origins theories that start with methane oxidation (98, 99) belong to the metabolism first category but not to autotrophic theories, because they start from CH_4 as the first carbon source (methanotrophy) as opposed to CO_2 (autotrophy). Methane requires strong oxidants such as nitrogen oxides, O_2 , or H_2O_2 to enter primordial metabolism (99), precluding a requirement for H_2 (98) hence electron bifurcation. Wächtershäuser explicitly excluded H_2 as the primordial source of electrons for metabolism, because of the uphill nature of CO_2 reduction with H_2 (100) under standard conditions. Smith and Morowitz (101) concluded that the site of life’s origin must have performed electron bifurcation; our findings identify a simpler and functional environmental precursor. Other proposals involve electrogenesis, using externally applied voltages on transition metal electrodes to generate potentials required to reduce CO_2 without H_2 (71). These theories miss the impact of pH on H_2 oxidation.

Conclusion

Iron-mediated, H_2 -dependent Fd reduction provides the function of electron bifurcation in water at H_2 partial pressures, temperatures, and pH that occur naturally at serpentinizing hydrothermal vents. It requires solid-state transition metal surfaces, with no need

for sulfide minerals, membranes, ion gradients, redox cofactors, externally applied voltage, or oxidants other than Fd, presenting a simple (one gas, one solid) and energetically smooth transition in physiological evolution from abiotic to enzymatic use of H_2 from serpentinization to reduce Fd (Fig. 7). These findings point to an early phase of biochemical evolution in which proteins (ferredoxin), hence ribosomes and the code existed in the last universal common ancestor (72), but metabolic electron acquisition from H_2 during autotrophic origins was still tied to transition metals in serpentinizing systems in the Earth’s crust. Acetogens, methanogens, other organisms that inhibit modern serpentinizing systems (26–30, 53, 74), and chemolithoautotrophs that fuel their acetyl-CoA pathway with electrons from H_2 , native iron (64–66) or phosphite (102) might harbor additional biochemical relicts from the earliest phases of physiological evolution.

Methods

Reactions were prepared under anaerobic conditions in a glovebox (GS 79821, GS Glovebox-System), using N_2 -washed 0.133 M or 1.33 M phosphate buffer in HPLC-grade water (pH 6, 7, 8.5 or 10; potassium phosphate monobasic and sodium phosphate dibasic (Honeywell Fluka)) containing Fd, pipetted into 5 mL glass vials (beaded rim) with metal powders (no powder in controls) and a polytetrafluoroethylene (PTFE)-coated stirring bar. Vials were sealed by a crimp cap with PTFE-coated membrane. To allow gas exchange, a syringe needle was placed through the crimp cap membrane before the vials were placed in the high-pressure reactor.

Ferredoxin. Aliquots of lyophilized ferredoxin from *C. pasteurianum* prepared in *E. coli* as described (55) were suspended in 3.5 mL of N_2 -washed phosphate buffer per reaction with 100 nmol Fd distributed throughout the experimental run (one replica for Ni_2Fe and Fe_3O_4 and three replicas for all other reactions) and the control. 0.8 mL of the solution was placed on top of 0.1 mmol iron powder (Fe^0 , 99.9+ % metals basis, particle size <10 μm , Alfa Aesar), cobalt powder (Co^0 , metal basis, particle size 1.6 μm , Alfa Aesar), nickel powder (Ni^0 , metal basis, particle size 3 to 7 μm , Alfa Aesar), molybdenum powder (Mo^0 , 100 Mesh, 99.95% metal basis, Alfa Aesar), magnetite (Fe_3O_4 , 97% trace metal basis, particle size 50 to 100 nm, Sigma-Aldrich), or Ni_2Fe (synthesis based on (30), kindly provided by Tuğçe Beyazay, Max Planck Institute for Coal Research, Mülheim, Germany). The remaining volume of the Fd stock was used as a pre-reaction control for UV-Vis spectroscopy. The ferredoxin and hydrogenase structures in Fig. 1 were rendered with Pymol (103).

Reaction. After pressurizing the reactor with either 5 bar of Ar gas (99.998%, Air Liquide) or 5 bar of H_2 gas (99.999%, Air Liquide), reactions were started and regulated by a temperature controller (BTC-3000, Berghof Products + Instruments GmbH). Reactions were performed at 40 °C. The reaction time spanned from 1 h to 4 h. Afterward, reactors were depressurized under anaerobic conditions and the samples (metal powders and solution) were transferred to 2-mL Eppendorf tubes and centrifuged for 15 min at 13,000 rpm (Biofuge Fresco, Hereaus). Supernatants were analyzed.

Reduction with Sodium Dithionite. To obtain standards of Fd, the protein was reduced using sodium dithionite (ACROS Organics, Geel). Ferredoxin was diluted in a N_2 -washed 133 mM phosphate buffer solution (pH 8.5). Sodium dithionite was prepared in a similar solution at pH 8.6. The reduction was carried out with two moles of sodium dithionite per one mole of ferredoxin. In a 3-mL UV quartz cuvette with a small PTFE-coated stirring bar at 400 rpm, reduced Fd was re-oxidized by air, measuring a full scan of the UV-Vis spectrum every 30 s until the protein was re-oxidized.

UV-Vis Spectrophotometry. Spectra were recorded in an Agilent Technologies Cary 300 UV-Vis Compact Peltier spectrophotometer using UV-quartz cuvettes covered with a rubber stopper. A 200 to 800 nm scan was taken for each sample. Absorption of the $[4Fe4S]$ clusters in Fd was normalized to the absorbance of the isosbestic point of the spectrum at 354 nm (56). Data were analyzed with

the Cary UV Workstation and Cary WinUV software. Midpoint potentials of H₂ were calculated with the Nernst equation for the standard hydrogen electrode.

Data, Materials, and Software Availability. PDF data have been deposited in HHU ResearchData (<https://doi.org/10.25838/d5p-51>) (104).

ACKNOWLEDGMENTS. We thank Dr. Tuğçe Beyazay of the Max Planck Institute for Coal Research, Mülheim, Germany for preparing the Ni_xFe alloys. This project has received funding from the European Research Council (ERC) under the European Union's Horizon 2020 research and innovation programme (grant agreement no. 101018894). For funding, W.F.M. thanks the ERC (101018894), the Deutsche Forschungsgemeinschaft (MA 1426/21-1), and the Volkswagen Foundation (Grant 96_742), H.T. thanks the Max-Planck Gesellschaft, the Deutsche Forschungsgemeinschaft (TU 315/8-1) and the Volkswagen Foundation (96_742), J.S. thanks the Thailand Research Fund (RSA5980062), Z.-I.K. thanks

the Japan Society for the Promotion of Science (20KK0343) and National Institute of Technology (KOSEN) for a sabbatical stipend to Düsseldorf, and W.B. and M.P. thank the Max-Planck Gesellschaft.

Author affiliations: ^aInstitute of Molecular Evolution, Faculty of Mathematics and Natural Sciences, Heinrich Heine University Düsseldorf, Düsseldorf 40225, Germany; ^bMicrocosm Earth Center, Research Group for Geochemical Protozymes, Max Planck Institute for Terrestrial Microbiology and Philipps University, Marburg 35032, Germany; ^cDepartment of Civil and Environmental Engineering, National Institute of Technology, Kure College, Kure, Hiroshima 737-8506, Japan; ^dDepartment of Biochemistry, Chulalongkorn University, Patumwan, Bangkok 10330, Thailand; ^eInstitute for Physical Chemistry, Faculty of Mathematics and Natural Sciences, Heinrich Heine University Düsseldorf, Düsseldorf 40225, Germany; ^fMax Planck Institute for Coal Research, Department of Heterogeneous Catalysis, Mülheim an der Ruhr 45470, Germany; ^gMax Planck Institute for Terrestrial Microbiology, Marburg 35043, Germany; ^hLaboratory for Microbiology, Department of Biology, Philipps University, Marburg 35043, Germany; and ⁱCenter for Synthetic Microbiology SYNMIKRO, Philipps University, Marburg 35043, Germany

- G. Fuchs, E. Stupperich, "Evolution of autotrophic CO₂ fixation" in *Evolution of Prokaryotes*, K. Schleifer, E. Stackenbrandt, Eds. (Academic Press, London, 1985), pp. 235–251.
- G. Fuchs, Alternative pathways of carbon dioxide fixation: Insights into the early evolution of life? *Annu. Rev. Microbiol.* **65**, 631–658 (2011).
- I. A. Berg, Ecological aspects of the distribution of different autotrophic CO₂ fixation pathways. *Appl. Environ. Microbiol.* **77**, 1925–1936 (2011).
- T. Wagner, U. Ermler, S. Shima, The methanogenic CO₂ reducing-and-fixing enzyme is bifunctional and contains 46 [4Fe–4S] clusters. *Science* **354**, 114–117 (2016).
- M. Can, F. A. Armstrong, S. W. Ragsdale, Structure, function, and mechanism of the nickel metalloenzymes, CO dehydrogenase, and acetyl-CoA synthase. *Chem. Rev.* **114**, 4149–4174 (2014).
- M. H. Charon, A. Volbeda, E. Chabriere, L. Pieulle, J. C. Fontecilla-Camps, Structure and electron transfer mechanism of pyruvate:ferredoxin oxidoreductase. *Curr. Opin. Struct. Biol.* **9**, 663–669 (1999).
- H. Dobbek, V. Svetlitchnyi, L. Gremer, R. Huber, O. Meyer, Crystal structure of a carbon monoxide dehydrogenase reveals a [Ni–4Fe–5S] cluster. *Science* **293**, 1281–1285 (2001).
- S. Shima, G. Huang, T. Wagner, U. Ermler, Structural basis of hydrogenotrophic methanogenesis. *Annu. Rev. Microbiol.* **74**, 713–733 (2020).
- F. Lipmann, "Projecting backward from the present stage of evolution of biosynthesis" in *The Origin of Prebiological Systems and of their Molecular Matrices*, S. W. Fox, Ed. (Academic Press, New York, NY, 1965), pp. 259–280.
- R. V. Eck, M. O. Dayhoff, Evolution of the structure of ferredoxin based on living relics of primitive amino acid sequences. *Science* **152**, 363–366 (1966).
- D. O. Hall, R. Cammack, K. K. Rao, Role for ferredoxins in the origin of life and biological evolution. *Nature* **233**, 136–138 (1971).
- G. Caserta et al., Unusual structures and unknown roles of FeS clusters in metalloenzymes seen from a resonance Raman spectroscopic perspective. *Coord. Chem. Rev.* **452**, 214287 (2022).
- J. A. Baross, S. E. Hoffman, Submarine hydrothermal vents and associated gradient environments as sites for the origin and evolution of life. *Orig. Life Evol. Biosph.* **15**, 327–345 (1985).
- N. Mnjavac, J. L. E. Wimmer, M. Brabender, L. Schwander, W. F. Martin, The Moon-forming impact and the autotrophic origin of life. *ChemPlusChem*. **88**, e202300270 (2023).
- N. H. Sleep, D. K. Bird, E. C. Pope, Serpentinite and the dawn of life. *Philos. Trans. R. Soc. Lond. B Biol. Sci.* **366**, 2857–2869 (2011).
- R. Tamblyn, J. Hermann, Geological evidence for high H₂ production from komatiites in the Archaean. *Nat. Geosci.* **16**, 1194–1199 (2023).
- M. Preiner et al., A hydrogen-dependent geochemical analogue of primordial carbon and energy metabolism. *Nat. Ecol. Evol.* **4**, 534–542 (2020).
- K. S. Belthle et al., Effects of silica modification (Mg, Al, Ca, Ti, and Zr) on supported cobalt catalysts for H₂ dependent CO₂ reduction to metabolic intermediates. *J. Am. Chem. Soc.* **144**, 21232–21243 (2022).
- T. Beyazay et al., Influence of composition of nickel-iron nanoparticles for abiotic CO₂ conversion to early prebiotic organics. *Angew. Chem. Int. Ed. Engl.* **62**, e202218189 (2023).
- T. Beyazay et al., Ambient temperature CO₂ fixation to pyruvate and subsequently to citramalate over iron and nickel nanoparticles. *Nat. Commun.* **14**, 570 (2023).
- J. A. Chamberlain, C. R. McLeod, R. J. Trull, G. R. Lachance, Native metals in the Muskox intrusion. *Can. J. Earth Sci.* **2**, 188–215 (1965).
- C. Kanellopoulos et al., A new occurrence of terrestrial native iron in the Earth's surface: The Iliia thermogenic travertine case, northwestern Euboea, Greece. *Geosciences* **8**, 287 (2018).
- P. K. Kepezhinskas, N. P. Kepezhinskas, N. V. Berdnikov, V. O. Krutikova, Native metals and intermetallic compounds in subduction-related ultramafic rocks from the Stanovoy mobile belt (Russian Far East): Implications for redox heterogeneity in subduction zones. *Ore Geol. Rev.* **127**, 103800 (2020).
- C. Furdul, S. W. Ragsdale, The role of pyruvate ferredoxin oxidoreductase in pyruvate synthesis during autotrophic growth by the Wood-Ljungdahl pathway. *J. Biol. Chem.* **275**, 28494–28499 (2000).
- R. K. Thauer, K. Jungermann, K. Decker, Energy conservation in chemotrophic anaerobic bacteria. *Bacteriol. Rev.* **41**, 100–180 (1977).
- D. R. Colman et al., Deep-branching acetogens in serpentinized subsurface fluids of Oman. *Proc. Natl. Acad. Sci. U.S.A.* **119**, e2206845119 (2022).
- M. O. Schrenk, D. S. Kelley, S. A. Bolton, J. A. Baross, Low archaeal diversity linked to subsurface geochemical processes at the Lost City hydrothermal field, mid-Atlantic ridge. *Environ. Microbiol.* **6**, 1086–1095 (2004).
- E. M. Fones et al., Diversification of methanogens into hyperalkaline serpentinizing environments through adaptations to minimize oxidant limitation. *ISME J.* **15**, 1121–1135 (2021).
- S. O. Lang, W. J. Brazelton, Habitability of the marine serpentinite subsurface: A case study of the Lost City hydrothermal field. *Philos. Trans. A Math. Phys. Eng. Sci.* **378**, 20180429 (2020).
- S. Suzuki, K. H. Nealson, S. Ishii, Genomic and *in-situ* transcriptomic characterization of the candidate phylum NPL-UPL2 From highly alkaline highly reducing serpentinized groundwater. *Front. Microbiol.* **9**, 3141 (2018).
- W. Buckel, R. K. Thauer, Energy conservation via electron bifurcating ferredoxin reduction and proton/Na⁺ translocating ferredoxin oxidation. *Biochim. Biophys. Acta* **1827**, 94–113 (2013).
- G. Herrmann, E. Jayamani, G. Mai, W. Buckel, Energy conservation via electron-transferring flavoprotein in anaerobic bacteria. *J. Bacteriol.* **190**, 784–791 (2008).
- F. Li et al., Coupled ferredoxin and crotonyl coenzyme A (CoA) reduction with NADH catalyzed by the butyryl-CoA dehydrogenase/Etf complex from *Clostridium kluyveri*. *J. Bacteriol.* **190**, 843–850 (2008).
- A. K. Kaster, J. Moll, K. Parey, R. K. Thauer, Coupling of ferredoxin and heterodisulfide reduction via electron bifurcation in hydrogenotrophic methanogenic archaea. *Proc. Natl. Acad. Sci. U.S.A.* **108**, 2981–2986 (2011).
- V. Müller, N. P. Chowdhury, M. Basen, Electron bifurcation: A long-hidden energy-coupling mechanism. *Annu. Rev. Microbiol.* **72**, 331–353 (2018).
- T. Wagner, J. Koch, U. Ermler, S. Shima, Methanogenic heterodisulfide reductase (HdrABC-MvhAGD) uses two noncubane [4Fe–4S] clusters for reduction. *Science* **357**, 699–703 (2017).
- A. Katsy et al., Molecular basis of the electron bifurcation mechanism in the [FeFe]-hydrogenase complex HydABC. *J. Am. Chem. Soc.* **145**, 5696–5709 (2023).
- C. E. Lubner et al., Mechanistic insights into energy conservation by flavin-based electron bifurcation. *Nat. Chem. Biol.* **13**, 655–659 (2017).
- W. Buckel, R. K. Thauer, Flavin-based electron bifurcation, a new mechanism of biological energy coupling. *Chem. Rev.* **118**, 3862–3886 (2018).
- G. J. Schut et al., An abundant and diverse new family of electron bifurcating enzymes with a non-canonical catalytic mechanism. *Front. Microbiol.* **13**, 946711 (2022).
- K. Kayastha, S. Vitt, W. Buckel, U. Ermler, Flavins in the electron bifurcation process. *Arch. Biochem. Biophys.* **701**, 108796 (2021).
- J. W. Peters, A. F. Miller, A. K. Jones, P. W. King, M. W. Adams, Electron bifurcation. *Curr. Opin. Chem. Biol.* **31**, 146–152 (2016).
- R. K. Thauer, A.-K. Kaster, H. Seedorf, W. Buckel, R. Hedderich, Methanogenic archaea: Ecologically relevant differences in energy conservation. *Nat. Rev. Microbiol.* **6**, 579–591 (2008).
- K. Schuchmann, V. Müller, Autotrophy at the thermodynamic limit of life: A model for energy conservation in acetogenic bacteria. *Nat. Rev. Microbiol.* **12**, 809–821 (2014).
- W. F. Martin, Hydrogen, metals, bifurcating electrons, and proton gradients: The early evolution of biological energy conservation. *FEBS Lett.* **586**, 485–493 (2012).
- E. S. Boyd, M. J. Amenabar, S. Poudel, A. S. Templeton, Bioenergetic constraints on the origin of autotrophic metabolism. *Philos. Trans. A Math. Phys. Eng. Sci.* **378**, 20190151 (2020).
- E. M. Shepard et al., [FeFe]-Hydrogenase maturation. *Biochemistry* **53**, 4090–4104 (2014).
- J. W. Peters et al., [FeFe]- and [NiFe]-hydrogenase diversity, mechanism, and maturation. *Biochim. Biophys. Acta Mol. Cell Res.* **1853**, 1350–1369 (2015).
- R. D. Britt, G. Rao, L. Tao, Bioassembly of complex iron-sulfur enzymes: Hydrogenases and nitrogenases. *Nat. Rev. Chem.* **4**, 542–549 (2020).
- D. W. Mulder et al., Stepwise [FeFe]-hydrogenase H-cluster assembly revealed in the structure of HydA^{DEF}. *Nature* **465**, 248–252 (2010).
- S. J. Mojzsis et al., Evidence for life on Earth before 3, 800 million years ago. *Nature* **384**, 55–59 (1996).
- Y. Ueno, K. Yamada, N. Yoshida, S. Maruyama, Y. Isozaki, Evidence from fluid inclusions for microbial methanogenesis in the early archaean era. *Nature* **440**, 516–519 (2006).
- H. Takami et al., A deeply branching thermophilic bacterium with an ancient acetyl-CoA pathway dominates a subsurface ecosystem. *PLoS One* **7**, e30559 (2012).
- D. S. Kelley et al., A serpentinite-hosted ecosystem: The Lost City hydrothermal field. *Science* **307**, 1428–1434 (2005).
- L. Schwander et al., Serpentinization as the source of energy, electrons, organics, catalysts, nutrients and pH gradients for the origin of LUCA and life. *Front. Microbiol.* **14**, 1257597 (2023).
- J. Sucharitakul et al., Modulations of the reduction potentials of flavin-based electron bifurcation complexes and semiquinone stabilities are key to control directional electron flow. *FEBS J.* **288**, 1008–1026 (2021).
- D. P. Henriques Pereira et al., Role of geochemical protoenzymes (geozymes) in primordial metabolism: Specific abiotic hydride transfer by metals to the biological redox cofactor NAD⁺. *FEBS J.* **289**, 3148–3162 (2022).
- R. C. Prince, M. W. Adams, Oxidation-reduction properties of the two Fe₄S₄ clusters in *Clostridium pasteurianum* ferredoxin. *J. Biol. Chem.* **262**, 5125–5128 (1987).

59. W. Thamer *et al.*, A two [4Fe-4S]-cluster-containing ferredoxin as an alternative electron donor for 2-hydroxyglutaryl-CoA dehydratase from *Acidaminococcus fermentans*. *Arch. Microbiol.* **179**, 197–204 (2003).
60. S. Menon, S. W. Ragsdale, Unleashing hydrogenase activity in carbon monoxide dehydrogenase/acetyl-CoA synthase and pyruvate:ferredoxin oxidoreductase. *Biochemistry* **35**, 15814–15821 (1996).
61. K. Christmann, Interaction of hydrogen with solid surfaces. *Surf. Sci. Rep.* **9**, 1–163 (1988).
62. D. R. Aireddy, K. Ding, Heterolytic dissociation of H₂ in heterogeneous catalysis. *ACS Catal.* **12**, 4707–4723 (2022).
63. R. S. Magliozzo, B. A. McIntosh, W. V. Sweeney, Origin of the pH dependence of the midpoint reduction potential in *Clostridium pasteurianum* ferredoxin: Oxidation state-dependent hydrogen ion association. *J. Biol. Chem.* **257**, 3506–3509 (1982).
64. S. Kato, I. Yumoto, Y. Kamagata, Isolation of acetogenic bacteria that induce biocorrosion by utilizing metallic iron as the sole electron donor. *Appl. Environ. Microbiol.* **81**, 67–73 (2015).
65. J. Philips, Extracellular electron uptake by acetogenic bacteria: Does H₂ consumption favor the H₂ evolution reaction on a cathode or metallic iron? *Front. Microbiol.* **10**, 2997 (2020).
66. D. Xu, T. Gu, D. R. Lovley, Microbially mediated metal corrosion. *Nat. Rev. Microbiol.* **21**, 705–718 (2023).
67. A. J. Bard, R. Parsons, J. Jordan, *Standard Potentials in Aqueous Solution* (CRC Press, Boca Raton, 1985).
68. C. C. Page, C. C. Moser, X. Chen, P. L. Dutton, Natural engineering principles of electron tunnelling in biological oxidation–reduction. *Nature* **402**, 47–52 (1999).
69. H. B. Gray, J. R. Winkler, Electron tunneling through proteins. *Q. Rev. Biophys.* **36**, 341–372 (2003).
70. A. Roldan *et al.*, Bio-inspired CO₂ conversion by iron sulfide catalysts under sustainable conditions. *Chem. Commun.* **51**, 7501–7504 (2015).
71. N. Kitada *et al.*, Thioester synthesis through geoelectrochemical CO₂ fixation on Ni sulfides. *Commun. Chem.* **4**, 37 (2021).
72. M. C. Weiss *et al.*, The physiology and habitat of the last universal common ancestor. *Nat. Microbiol.* **1**, 1–8 (2016).
73. T. A. Williams *et al.*, Integrative modeling of gene and genome evolution roots the archaeal tree of life. *Proc. Natl. Acad. Sci. U.S.A.* **114**, E4602–E4611 (2017).
74. R. Mei, M. Kaneko, H. Imachi, M. K. Nobu, The origin and evolution of methanogenesis and Archaea are intertwined. *PNAS Nexus* **31**, pgad023 (2023).
75. R. Hedderich, Energy-converting (NiFe) hydrogenases from archaea and extremophiles: Ancestors of complex I. *J. Bioenerg. Biomembr.* **36**, 65–75 (2004).
76. M. C. Schoelmerich, V. Müller, Energy conservation by a hydrogenase-dependent chemiosmotic mechanism in an ancient metabolic pathway. *Proc. Natl. Acad. Sci. U.S.A.* **116**, 6329–6334 (2019).
77. N. Lane, W. F. Martin, The origin of membrane bioenergetics. *Cell* **151**, 1406–1416 (2012).
78. S. A. Harrison *et al.*, Life as a guide to its own origins. *Annu. Rev. Ecol. Syst.* **54**, 327–350 (2023).
79. E. S. Boyd, G. J. Schut, M. W. W. Adams, J. W. Peters, Hydrogen metabolism and the evolution of biological respiration. *Microbe* **9**, 361–367 (2014).
80. K. B. Muchowska, S. J. Varma, J. Moran, Nonenzymatic metabolic reactions and life's origins. *Chem. Rev.* **120**, 7708–7744 (2020).
81. S. J. Varma, K. B. Muchowska, P. Chatelain, J. Moran, Native iron reduces CO₂ to intermediates and end-products of the acetyl-CoA pathway. *Nat. Ecol. Evol.* **2**, 1019–1024 (2018).
82. F. L. Sousa, M. Preiner, W. F. Martin, Native metals, electron bifurcation, and CO₂ reduction in early biochemical evolution. *Curr. Opin. Microbiol.* **43**, 77–83 (2018).
83. T. M. McCollom, J. S. Seewald, Serpentinites, hydrogen, and life. *Elements* **9**, 129–134 (2013).
84. W. Martin, M. J. Russell, On the origin of biochemistry at an alkaline hydrothermal vent. *Philos. Trans. R. Soc. Lond. B Biol. Sci.* **362**, 1887–1926 (2007).
85. C. Schöne *et al.*, Deconstructing *Methanosarcina acetivorans* into an acetogenic archaeon. *Proc. Natl. Acad. Sci. U.S.A.* **119**, e2113853119 (2022).
86. D. D. Sasselov, J. P. Grotzinger, J. D. Sutherland, The origin of life as a planetary phenomenon. *Sci. Adv.* **6**, eaax3419 (2020).
87. S. A. Benner *et al.*, When did life likely emerge on earth in an RNA-first process? *ChemSystemsChem* **2**, e1900035 (2020).
88. B. Damer, D. Deamer, The hot spring hypothesis for an origin of life. *Astrobiology* **20**, 429–452 (2020).
89. B. H. Patel, C. Percivalle, D. J. Ritson, C. D. Duffy, J. D. Sutherland, Common origins of RNA, protein and lipid precursors in a cyanosulfidic protometabolism. *Nat. Chem.* **7**, 301–307 (2015).
90. P. Canavelli, S. Islam, M. W. Powner, Peptide ligation by chemoselective aminonitrile coupling in water. *Nature* **571**, 546–549 (2019).
91. S. Becker *et al.*, Unified prebiotically plausible synthesis of pyrimidine and purine RNA ribonucleotides. *Science* **366**, 76–82 (2019).
92. R. E. Eakin, An approach to the evolution of metabolism. *Proc. Natl. Acad. Sci. U.S.A.* **49**, 360–366 (1963).
93. W. F. Martin, Older than genes: The acetyl CoA pathway and origins. *Front. Microbiol.* **11**, 817 (2020).
94. K. B. Muchowska, S. J. Varma, J. Moran, Synthesis and breakdown of universal metabolic precursors promoted by iron. *Nature* **569**, 104–107 (2019).
95. J. L. E. Wimmer *et al.*, Energy at origins: Favorable thermodynamics of biosynthetic reactions in the last universal common ancestor (LUCA). *Front. Microbiol.* **12**, 793664 (2021).
96. R. J. Mayer, J. Moran, Quantifying reductive amination in nonenzymatic amino acid synthesis. *Angew. Chem. Int. Ed. Engl.* **61**, e202212237 (2022).
97. J. Yi *et al.*, A nonenzymatic analog of pyrimidine nucleobase biosynthesis. *Angew. Chem. Int. Ed. Engl.* **61**, e202117211 (2022).
98. W. Nitschke, M. J. Russell, Beating the acetyl coenzyme A-pathway to the origin of life. *Philos. Trans. R. Soc. Lond. B Biol. Sci.* **368**, 20120258 (2013).
99. O. Farr *et al.*, Methanol on the rocks: Green rust transformation promotes the oxidation of methane. *J. Roy. Soc. Interface* **20**, 20230386 (2023).
100. G. Wächtershäuser, Before enzymes and templates: Theory of surface metabolism. *Microbiol. Rev.* **52**, 452–484 (1988).
101. E. Smith, H. J. Morowitz, *The Origin and Nature of Life on Earth* (Cambridge University Press, 2016).
102. Z. Mao *et al.*, AMP-dependent phosphite dehydrogenase, a phosphorylating enzyme in dissimilatory phosphite oxidation. *Proc. Natl. Acad. Sci. U.S.A.* **120**, e230974312 (2023).
103. L. L. C. Schrödinger, The PyMOL Molecular Graphics System (Version 2.5.4, 2022). <https://pymol.org/2/>. Accessed 23 October 2023.
104. M. Brabender *et al.*, Ferredoxin reduction by hydrogen with iron functions as an evolutionary precursor of flavin-based electron bifurcation. HHU ResearchData. <https://doi.org/10.25838/d5p-51>. Deposited 3 November 2023.

Conclusion and Outlook

The importance of metals in the origin of life has been discussed for 30 years (Eck and Dayhoff, 1966; Fried *et al.*, 2022; Lipmann, 1965; Martin and Kleinermanns, 2024; Russell and Martin, 2004; Wächtershäuser, 1992; Williams and Fraústo da Silva, 1997) especially when considering the inorganic cofactors at the centre of modern enzymes. From a bottom-up approach, there has been an increased interest in studying earth minerals as catalysts under similar conditions (Barge *et al.*, 2020; Beyazay *et al.*, 2023c; Preiner *et al.*, 2020; Song *et al.*, 2024). From a top-down approach, the importance of cofactors is undeniable and supports this interest: core enzymes have always relied on cofactors for their activity and are what can make prebiotic reaction networks autocatalytic (Xavier *et al.*, 2020). Considering that proteins were probably the first biopolymers to exist, but that nucleotide cofactors may have contributed to more efficient proto-metabolism early on (Fried *et al.*, 2022), this work focused on testing both organic cofactors and protein-bound inorganic cofactors in a prebiotic environment. To this end, it has been successfully demonstrated that both can interact with metals in hydrothermal systems in a stable and functional manner, contributing to the construction of a timeline of the origin of life. All publications address the stability of both inorganic and organic cofactors involved in the experiments, in addition to proposing mechanisms for the identified reactions. Publication 1 and 3 show that NAD is specifically reduced at the 4th position by many Ni, Fe and Co containing metals with H₂. The complete reduction of ferredoxin was shown in publication 2, but only with Fe⁰. Both NADH and Fd_{rd} were easy to produce, stable in alkaline solutions, and by-products were little to none below pH 9. To this effect, publication 3 concludes that the ADP moiety is most important (for NAD) in Ni-rich environments, otherwise it is over-reduced and hydrolysed. Finally, all 3 show that high levels of metal and water activity are not nearly as toxic to these cofactors as they can be in modern life. In turn, we have shown that hydrides can be formed from H₂O reduction by Fe⁰, similar to serpentinization, at much lower temperatures than those reported in serpentinizing systems. Taken together, these results are a first step toward understanding if and how a cofactor-dependent proto-metabolism might have existed above a serpentinizing system.

To further test this hypothesis, we are currently working with other organic cofactors of interest and testing their reduction with H_2 in the case of electron carriers and CO_2/H_2 for methyl carriers. During the preparation of this thesis, preliminary work with flavins showed that they can also be reduced under conditions similar to those described for NAD and Fd. Even though the midpoint potential of the $-1/-2$ pair in free flavins is not as negative as in prosthetic flavins, their properties still hold, and it would be very interesting to test if they could facilitate the reduction of Fd with more abundant minerals than Fe^0 .

Another intuitive next step is to investigate subsequent reactions: hydrides and electrons have been successfully transferred from the gas phase (H_2) through a metal surface to soluble cofactors, but can they be transferred from these cofactors to relevant metabolites in solution without enzymes? Mayer and Moran (2024) have already explored this idea using metal ions to reduce pyruvate with NADH. However, this has only been achieved under acidic conditions where NADH is naturally degraded over time and dissolved metals also degrade NAD. Thus, further experiments with NAD and other cofactors are needed. It is also important to continue to explore prebiotic synthesis in the Hadean Earth. For example, Sanchez-Rocha (Sanchez-Rocha *et al.*, 2024) has shown that ancient cofactors are more likely to bind to early amino acids in enzyme binding sites than late cofactors, and more likely to do so via metal ions. In this paper, they postulate that organic cofactors may have been key to resolving the tertiary structures and catalytic functions of prebiotic enzymes, which is worth investigating experimentally.

We are still a long way from knowing if these theoretical scenarios were real, in fact we can never know for sure, but the ever-growing body of data from both top-down (Fried *et al.*, 2022; Sanchez-Rocha *et al.*, 2024; Xavier *et al.*, 2020) and bottom-up approaches increasingly supports an early origin of organic cofactors (Brabender *et al.*, 2024; Henriques Pereira *et al.*, 2022; Weber *et al.*, 2022; Nogal *et al.*, 2024; Mayer and Moran, 2024; Sebastianelli *et al.*, 2024). While these findings do not rule out an alternative origin of life for hydrothermal systems, they support the idea that many key metabolic mechanisms (e.g. H_2 -dependent reduction of low potential cofactors) are prebiotically possible in these environments, transformed into life and perfected by evolution.

References

- Aireddy, D.R., Ding, K., 2022. Heterolytic dissociation of H₂ in heterogeneous catalysis. *ACS Catal.* 12, 4707–4723. <https://doi.org/10.1021/acscatal.2c00584>
- Anderson, B.M., Anderson, C.D., 1963. The effect of buffers on nicotinamide adenine dinucleotide hydrolysis. *J. Biol. Chem.* 238, 1475–1478. [https://doi.org/10.1016/S0021-9258\(18\)81208-X](https://doi.org/10.1016/S0021-9258(18)81208-X)
- Anderson, R.F., 1983. Energetics of the one-electron reduction steps of riboflavin, FMN and FAD to their fully reduced forms. *Biochim. Biophys. Acta BBA - Bioenerg.* 722, 158–162. [https://doi.org/10.1016/0005-2728\(83\)90169-X](https://doi.org/10.1016/0005-2728(83)90169-X)
- Argueta, E.A., Amoh, A.N., Kafle, P., Schneider, T.L., 2015. Unusual non-enzymatic flavin catalysis enhances understanding of flavoenzymes. *FEBS Lett.* 589, 880–884. <https://doi.org/10.1016/j.febslet.2015.02.034>
- Barge, L.M., Flores, Erika., VanderVelde, D.G., Weber, J.M., Baum, Marc.M., Castonguay, A., 2020. Effects of geochemical and environmental parameters on abiotic organic chemistry driven by iron hydroxide minerals. *J. Geophys. Res. Planets* 125, e2020JE006423. <https://doi.org/10.1029/2020JE006423>
- Baross, J.A., Hoffman, S.E., 1985. Submarine hydrothermal vents and associated gradient environments as sites for the origin and evolution of life. *Orig. Life Evol. Biosph.* 15, 327–345. <https://doi.org/10.1007/BF01808177>
- Barrows, L.R., Magee, P.N., 1982. Nonenzymatic methylation of DNA by S-adenosylmethionine *in vitro*. *Carcinogenesis* 3, 349–351. <https://doi.org/10.1093/carcin/3.3.349>
- Bazhenova, T.A., Bazhenova, M.A., Petrova, G.N., Mironova, S.A., Strelets, V.V., 2000. Catalytic behavior of the nitrogenase iron-molybdenum cofactor extracted from the enzyme in the reduction of C₂H₂ under nonenzymatic conditions. *Kinet. Catal.* 41, 499–510. <https://doi.org/10.1007/BF02756066>
- Bekker, A., Holland, H.D., Wang, P.-L., Rumble, D., Stein, H.J., Hannah, J.L., Coetzee, L.L., Beukes, N.J., 2004. Dating the rise of atmospheric oxygen. *Nature* 427, 117–120. <https://doi.org/10.1038/nature02260>
- Benkovic, S.J., 1978. On the mechanisms of folate cofactors. *Acc. Chem. Res.* 11, 314–320. <https://doi.org/10.1021/ar50128a005>
- Beyazay, T., Belthle, K.S., Farès, C., Preiner, M., Moran, J., Martin, W.F., Tüysüz, H., 2023a. Ambient temperature CO₂ fixation to pyruvate and subsequently to citramalate over iron and nickel nanoparticles. *Nat. Commun.* 14, 570. <https://doi.org/10.1038/s41467-023-36088-w>
- Beyazay, T., Martin, W.F., Tüysüz, H., 2023b. Direct synthesis of formamide from CO₂ and H₂O with nickel–iron nitride heterostructures under mild hydrothermal conditions. *J. Am. Chem. Soc.* 145, 19768–19779. <https://doi.org/10.1021/jacs.3c05412>
- Beyazay, T., Ochoa-Hernández, C., Song, Y., Belthle, K.S., Martin, W.F., Tüysüz, H., 2023c. Influence of composition of nickel-iron nanoparticles for abiotic CO₂ conversion to early prebiotic organics. *Angew. Chem. Int. Ed.* 62, e202218189. <https://doi.org/10.1002/anie.202218189>
- Bonfio, C., Valer, L., Scintilla, S., Shah, S., Evans, D.J., Jin, L., Szostak, J.W., Sasselov, D.D., Sutherland, J.D., Mansy, S.S., 2017. UV-light-driven prebiotic synthesis of iron–sulfur clusters. *Nat. Chem.* 9, 1229–1234. <https://doi.org/10.1038/nchem.2817>

- Bottke, W.F., Vokrouhlický, D., Marchi, Simone S., Swindle, T., Scott, E.R.D., Weirich, J.R., Levison, H.F., 2015. Dating the Moon-forming impact event with asteroidal meteorites. *Science* 348, 321–323. <https://doi.org/10.1126/science.aaa0602>
- Brabender, M., Henriques Pereira, D.P., Mrnjavac, N., Schlikker, M.L., Kimura, Z.-I., Sucharitakul, J., Kleineremanns, K., Tüysüz, H., Buckel, W., Preiner, M., Martin, W.F., 2024. Ferredoxin reduction by hydrogen with iron functions as an evolutionary precursor of flavin-based electron bifurcation. *Proc. Natl. Acad. Sci.* 121, e2318969121. <https://doi.org/10.1073/pnas.2318969121>
- Buckel, W., Thauer, R.K., 2018. Flavin-based electron bifurcation, ferredoxin, flavodoxin, and anaerobic respiration with protons (Ech) or NAD⁺ (Rnf) as electron acceptors: A historical review. *Front. Microbiol.* 9, 401. <https://doi.org/10.3389/fmicb.2018.00401>
- Buckel, W., Thauer, R.K., 2013. Energy conservation via electron bifurcating ferredoxin reduction and proton/Na⁺ translocating ferredoxin oxidation. *Biochim. Biophys. Acta BBA - Bioenerg.* 1827, 94–113. <https://doi.org/10.1016/j.bbabi.2012.07.002>
- Buyske, D.A., Handschumacher, R.E., Schilling, E.D., Strong, F.M., 1954. The stability of Coenzyme A¹. *J. Am. Chem. Soc.* 76, 3575–3577. <https://doi.org/10.1021/ja01642a065>
- Cafferty, B.J., Fialho, D.M., Hud, N.V., 2018. Searching for possible ancestors of RNA: The self-assembly hypothesis for the origin of proto-RNA, in: Menor-Salván, C. (Ed.), *Prebiotic Chemistry and Chemical Evolution of Nucleic Acids, Nucleic Acids and Molecular Biology*. Springer International Publishing, Cham, pp. 143–174. https://doi.org/10.1007/978-3-319-93584-3_5
- Canivet, J., Süß-Fink, G., Štěpnička, P., 2007. Water-soluble phenanthroline complexes of rhodium, iridium and ruthenium for the regeneration of NADH in the enzymatic reduction of ketones. *Eur. J. Inorg. Chem.* 2007, 4736–4742. <https://doi.org/10.1002/ejic.200700505>
- Charlou, J.L., Donval, J.P., Fouquet, Y., Jean-Baptiste, P., Holm, N., 2002. Geochemistry of high H₂ and CH₄ vent fluids issuing from ultramafic rocks at the Rainbow hydrothermal field (36°14'N, MAR). *Chem. Geol.*
- Chenault, H.K., Simon, E.S., Whitesides, G.M., 1988. Cofactor regeneration for enzyme-catalysed synthesis. *Biotechnol. Genet. Eng. Rev.* 6, 221–270. <https://doi.org/10.1080/02648725.1988.10647849>
- Cohen, S.E., Can, M., Wittenborn, E.C., Hendrickson, R.A., Ragsdale, S.W., Drennan, C.L., 2020. Crystallographic characterization of the carbonylated A-cluster in carbon monoxide dehydrogenase/acetyl-coA synthase. *ACS Catal.* 10, 9741–9746. <https://doi.org/10.1021/acscatal.0c03033>
- Copley, S.D., Smith, E., Morowitz, H.J., 2007. The origin of the RNA world: Co-evolution of genes and metabolism. *Bioorganic Chem.* 35, 430–443. <https://doi.org/10.1016/j.bioorg.2007.08.001>
- Corliss, J. b, Baross, J., Hoffman, S., 1981. An hypothesis concerning the relationships between submarine hot springs and the origin of life on Earth. *Oceanol. Acta Spec. Issue*.
- Crapitto, A.J., Campbell, A., Harris, A., Goldman, A.D., 2022. A consensus view of the proteome of the last universal common ancestor. *Ecol. Evol.* 12, e8930. <https://doi.org/10.1002/ece3.8930>
- Crick, F.H.C., 1968. The origin of the genetic code. *J. Mol. Biol.* 38, 367–379. [https://doi.org/10.1016/0022-2836\(68\)90392-6](https://doi.org/10.1016/0022-2836(68)90392-6)

- Damer, B., Deamer, D., 2020. The hot spring hypothesis for an origin of life. *Astrobiology* 20, 429–452. <https://doi.org/10.1089/ast.2019.2045>
- Dekov, V., 2006. Native nickel in the TAG hydrothermal field sediments (Mid-Atlantic Ridge, 26°N): Space trotter, guest from mantle, or a widespread mineral, connected with serpentinization? *J. Geophys. Res. Solid Earth* 111, 2005JB003955. <https://doi.org/10.1029/2005JB003955>
- Denessiouk, K.A., Rantanen, V., Johnson, M.S., 2001. Adenine recognition: A motif present in ATP-, CoA-, NAD-, NADP-, and FAD-dependent proteins. *Proteins Struct. Funct. Bioinforma.* 44, 282–291. <https://doi.org/10.1002/prot.1093>
- Dyson, F.J., 1999. *Origins of life*, 2nd revised ed. ed. Cambridge university press, Cambridge.
- Eck, R.V., Dayhoff, M.O., 1966. Evolution of the Structure of Ferredoxin Based on Living Relics of Primitive Amino Acid Sequences. *Science* 152, 363–366. <https://doi.org/10.1126/science.152.3720.363>
- Ertl, G., 1983. Primary steps in catalytic synthesis of ammonia. *J. Vac. Sci. Technol. Vac. Surf. Films* 1, 1247–1253. <https://doi.org/10.1116/1.572299>
- Etiopie, G., Sherwood Lollar, B., 2013. Abiotic methane on Earth. *Rev. Geophys.* 51, 276–299. <https://doi.org/10.1002/rog.20011>
- Fine, J.L., Pearlman, R.E., 2023. On the origin of life: an RNA-focused synthesis and narrative. *RNA* 29, 1085–1098. <https://doi.org/10.1261/rna.079598.123>
- Fischer, J.D., Holliday, G.L., Rahman, S.A., Thornton, J.M., 2010. The structures and physicochemical properties of organic cofactors in biocatalysis. *J. Mol. Biol.* 403, 803–824. <https://doi.org/10.1016/j.jmb.2010.09.018>
- Fitch, W.M., Bruschi, M., 1987. The evolution of prokaryotic ferredoxins--with a general method correcting for unobserved substitutions in less branched lineages. *Mol. Biol. Evol.* 4, 381–394. <https://doi.org/10.1093/oxfordjournals.molbev.a040452>
- Fontecilla-Camps, J.C., 2019. Geochemical continuity and catalyst/cofactor replacement in the emergence and evolution of life. *Angew. Chem. Int. Ed.* 58, 42–48. <https://doi.org/10.1002/anie.201808438>
- Förster, J., Famili, I., Fu, P., Palsson, B.Ø., Nielsen, J., 2003. Genome-scale reconstruction of the *Saccharomyces cerevisiae* metabolic network. *Genome Res.* 13, 244–253. <https://doi.org/10.1101/gr.234503>
- Foustoukos, D.I., Bizimis, M., Frisby, C., Shirey, S.B., 2015. Redox controls on Ni–Fe–PGE mineralization and Re/Os fractionation during serpentinization of abyssal peridotite. *Geochim. Cosmochim. Acta* 150, 11–25. <https://doi.org/10.1016/j.gca.2014.11.025>
- Fried, S.D., Fujishima, K., Makarov, M., Cherepashuk, I., Hlouchova, K., 2022. Peptides before and during the nucleotide world: an origins story emphasizing cooperation between proteins and nucleic acids. *J. R. Soc. Interface* 19, 20210641. <https://doi.org/10.1098/rsif.2021.0641>
- Fuchs, G., 2011. Alternative pathways of carbon dioxide fixation: Insights into the early evolution of life? *Annu. Rev. Microbiol.* 65, 631–658. <https://doi.org/10.1146/annurev-micro-090110-102801>
- Gayon, J., Malaterre, C., Morange, M., Raulin-Cerceau, F., Tirard, S., 2010. Defining life: conference proceedings. *Orig. Life Evol. Biospheres* 40, 119–120. <https://doi.org/10.1007/s11084-010-9189-y>
- Gilbert, W., 1986. Origin of life: The RNA world. *Nature* 319, 618–618. <https://doi.org/10.1038/319618a0>

- Goldford, J.E., Smith, H.B., Longo, L.M., Wing, B.A., McGlynn, S.E., 2024. Primitive purine biosynthesis connects ancient geochemistry to modern metabolism. *Nat. Ecol. Evol.* 8, 999–1009. <https://doi.org/10.1038/s41559-024-02361-4>
- Goldman, A.D., Kacar, B., 2021. Cofactors are remnants of life's origin and early evolution. *J. Mol. Evol.* 89, 127–133. <https://doi.org/10.1007/s00239-020-09988-4>
- Graham, D.E., White, R.H., 2002. Elucidation of methanogenic coenzyme biosyntheses: from spectroscopy to genomics. *Nat. Prod. Rep.* 19, 133–147. <https://doi.org/10.1039/B103714P>
- Greening, C., Biswas, A., Carere, C.R., Jackson, C.J., Taylor, M.C., Stott, M.B., Cook, G.M., Morales, S.E., 2016. Genomic and metagenomic surveys of hydrogenase distribution indicate H₂ is a widely utilised energy source for microbial growth and survival. *ISME J.* 10, 761–777. <https://doi.org/10.1038/ismej.2015.153>
- Grozeva, N.G., Klein, F., Seewald, J.S., Sylva, S.P., 2020. Chemical and isotopic analyses of hydrocarbon-bearing fluid inclusions in olivine-rich rocks. *Philos. Trans. R. Soc. Math. Phys. Eng. Sci.* 378, 20180431. <https://doi.org/10.1098/rsta.2018.0431>
- Guengerich, F.P., 2016. Metals in biology 2016: Molecular basis of selection of metals by enzymes. *J. Biol. Chem.* 291, 20838–20839. <https://doi.org/10.1074/jbc.R116.749259>
- Hachisuka, S., Sato, T., Atomí, H., 2017. Metabolism dealing with thermal degradation of NAD⁺ in the hyperthermophilic archaeon *Thermococcus kodakarensis*. *J. Bacteriol.* 199, 10.1128/jb.00162-17. <https://doi.org/10.1128/jb.00162-17>
- Harden, A., Young, W.J., 1906. The alcoholic ferment of yeast-juice. *Proc. R. Soc. Lond. Ser. B Contain. Pap. Biol. Character* 77, 405–420.
- Harrison, S.A., Lane, N., 2018. Life as a guide to prebiotic nucleotide synthesis. *Nat. Commun.* 9, 5176. <https://doi.org/10.1038/s41467-018-07220-y>
- Hartmann, W.K., Davis, D.R., 1975. Satellite-sized planetesimals and lunar origin. *Icarus* 24, 504–515. [https://doi.org/10.1016/0019-1035\(75\)90070-6](https://doi.org/10.1016/0019-1035(75)90070-6)
- Hawco, N.J., McIlvin, M.M., Bundy, R.M., Tagliabue, A., Goepfert, T.J., Moran, D.M., Valentin-Alvarado, L., DiTullio, G.R., Saito, M.A., 2020. Minimal cobalt metabolism in the marine *Cyanobacterium prochlorococcus*. *Proc. Natl. Acad. Sci.* 117, 15740–15747. <https://doi.org/10.1073/pnas.2001393117>
- Hemmerich, P., Veeger, C., Wood, H.C.S., 1965. Progress in the chemistry and molecular biology of flavins and flavocoenzymes. *Angew. Chem. Int. Ed. Engl.* 4, 671–687. <https://doi.org/10.1002/anie.196506711>
- Henriques Pereira, D.P., Leethaus, J., Beyazay, T., Do Nascimento Vieira, A., Kleinermanns, K., Tüysüz, H., Martin, W.F., Preiner, M., 2022. Role of geochemical protoenzymes (geozymes) in primordial metabolism: specific abiotic hydride transfer by metals to the biological redox cofactor NAD⁺. *FEBS J.* 289, 3148–3162. <https://doi.org/10.1111/febs.16329>
- Henriques Pereira, D.P., Xie, X., Beyazay, T., Paczia, N., Subrati, Z., Belz, J., Volz, K., Tüysüz, H., Preiner, M., 2025. A possible pre-enzymatic role of the “non-functional” tail of NAD: specific reduction on mineral surfaces. In revision for: *Proc. Natl. Acad. Sci.*
- Heveling, J., 2012. Heterogeneous catalytic chemistry by example of industrial applications. *J. Chem. Educ.* 89, 1530–1536. <https://doi.org/10.1021/ed200816g>
- Holland, H.D., 1999. When did the Earth's atmosphere become oxic? A Reply.

- Holland, H.D., 1984. The chemical evolution of the atmosphere and oceans. Princeton University Press. <https://doi.org/10.2307/j.ctv15r58kg>
- Holm, N. G., Oze, C., Mousis, O., Waite, J.H., Guilbert-Lepoutre, A., 2015. Serpentinization and the formation of H₂ and CH₄ on celestial bodies (planets, moons, comets). *Astrobiology* 15, 587–600. <https://doi.org/10.1089/ast.2014.1188>
- Holm, N.G., Charlou, J.L., 2001. Initial indications of abiotic formation of hydrocarbons in the Rainbow ultramafic hydrothermal system, Mid-Atlantic Ridge. *Earth Planet. Sci. Lett.* 191, 1–8. [https://doi.org/10.1016/S0012-821X\(01\)00397-1](https://doi.org/10.1016/S0012-821X(01)00397-1)
- Ji, H.-F., Kong, D.-X., Shen, L., Chen, L.-L., Ma, B.-G., Zhang, H.-Y., 2007. Distribution patterns of small-molecule ligands in the protein universe and implications for origin of life and drug discovery. *Genome Biol.* 8, R176. <https://doi.org/10.1186/gb-2007-8-8-r176>
- Jordan, S.F., Ioannou, I., Ramm, H., Halpern, A., Bogart, L.K., Ahn, M., Vasiliadou, R., Christodoulou, J., Maréchal, A., Lane, N., 2021. Spontaneous assembly of redox-active iron-sulfur clusters at low concentrations of cysteine. *Nat. Commun.* 12, 5925. <https://doi.org/10.1038/s41467-021-26158-2>
- Kandemir, T., Schuster, M.E., Senyshyn, A., Behrens, M., Schlögl, R., 2013. The Haber–Bosch process revisited: On the real structure and stability of “ammonia iron” under working conditions. *Angew. Chem. Int. Ed.* 52, 12723–12726. <https://doi.org/10.1002/anie.201305812>
- Kanellopoulos, C., Valsami-Jones, E., Voudouris, P., Stouraiti, C., Moritz, R., Mavrogenatos, C., Mitropoulos, P., 2018. A new occurrence of terrestrial native iron in the Earth’s surface: The Ilia thermogenic travertine case, northwestern Euboea, Greece. *Geosciences* 8, 287. <https://doi.org/10.3390/geosciences8080287>
- Kaplan, N.O., Colowick, S.P., Barnes, Catherine.Carr., 1951. Effect of alkali on diphosphopyridine nucleotide. *J. Biol. Chem.* 191, 461–472. [https://doi.org/10.1016/S0021-9258\(18\)55951-2](https://doi.org/10.1016/S0021-9258(18)55951-2)
- Kelley, D.S., Baross, J.A., Delaney, J.R., 2002. Volcanoes, fluids, and life at mid-ocean ridge spreading centers. *Annu. Rev. Earth Planet. Sci.* 30, 385–491. <https://doi.org/10.1146/annurev.earth.30.091201.141331>
- Kelley, D.S., Karson, J.A., Blackman, D.K., Früh-Green, G.L., Butterfield, D.A., Lilley, M.D., Olson, E.J., Schrenk, M.O., Roe, K.K., Lebon, G.T., Rivizzigno, P., the AT3-60 Shipboard Party, 2001. An off-axis hydrothermal vent field near the Mid-Atlantic Ridge at 30° N. *Nature* 412, 145–149. <https://doi.org/10.1038/35084000>
- Kelley, D.S., Karson, J.A., Früh-Green, G.L., Yoerger, D.R., Shank, T.M., Butterfield, D.A., Hayes, J.M., Schrenk, M.O., Olson, E.J., Proskurowski, G., Jakuba, M., Bradley, A., Larson, B., Ludwig, K., Glickson, D., Buckman, K., Bradley, A.S., Brazelton, W.J., Roe, K., Elend, M.J., Delacour, A., Bernasconi, S.M., Lilley, M.D., Baross, J.A., Summons, R.E., Sylva, S.P., 2005. A serpentinite-hosted ecosystem: The Lost City hydrothermal field. *Science* 307, 1428–1434. <https://doi.org/10.1126/science.1102556>
- Kepezhinskas, P.K., Kepezhinskas, N.P., Berdnikov, N.V., Krutikova, V.O., 2020. Native metals and intermetallic compounds in subduction-related ultramafic rocks from the Stanovoy mobile belt (Russian Far East): Implications for redox heterogeneity in subduction zones. *Ore Geol. Rev.* 127, 103800. <https://doi.org/10.1016/j.oregeorev.2020.103800>

- Kim, H., Benner, S.A., 2018. A direct prebiotic synthesis of nicotinamide nucleotide. *Chem. – Eur. J.* 24, 581–584. <https://doi.org/10.1002/chem.201705394>
- Kirschning, A., 2021a. The coenzyme/protein pair and the molecular evolution of life. *Nat. Prod. Rep.* 38, 993–1010. <https://doi.org/10.1039/D0NP00037J>
- Kirschning, A., 2021b. Coenzymes and their role in the evolution of life. *Angew. Chem. Int. Ed.* 60, 6242–6269. <https://doi.org/10.1002/anie.201914786>
- Klein, F., Bach, W., 2009. Fe-Ni-Co-O-S phase relations in peridotite-seawater interactions. *J. Petrol.* 50, 37–59. <https://doi.org/10.1093/petrology/egn071>
- Klein, F., Bach, W., McCollom, T.M., 2013. Compositional controls on hydrogen generation during serpentinization of ultramafic rocks. *Lithos* 178, 55–69. <https://doi.org/10.1016/j.lithos.2013.03.008>
- Kubas, G.J., 2007. Fundamentals of H₂ binding and reactivity on transition metals underlying hydrogenase function and H₂ production and storage. *Chem. Rev.* 107, 4152–4205. <https://doi.org/10.1021/cr050197j>
- Lang, S.Q., Butterfield, D.A., Schulte, M., Kelley, D.S., Lilley, M.D., 2010. Elevated concentrations of formate, acetate and dissolved organic carbon found at the Lost City hydrothermal field. *Geochim. Cosmochim. Acta* 74, 941–952. <https://doi.org/10.1016/j.gca.2009.10.045>
- Leigh, G.J., 2004. Haber-Bosch and other industrial processes, in: Smith, B.E., Richards, R.L., Newton, W.E. (Eds.), *Catalysts for Nitrogen Fixation*. Springer Netherlands, Dordrecht, pp. 33–54. https://doi.org/10.1007/978-1-4020-3611-8_2
- Lipmann, F., 1965. Projecting backward from the present stage of evolution of biosynthesis, in: *The Origins of Prebiological Systems and of Their Molecular Matrices*. Elsevier, pp. 259–280. <https://doi.org/10.1016/B978-1-4832-2861-7.50028-4>
- Liu, L., 2004. The inception of the oceans and CO₂-atmosphere in the early history of the Earth. *Earth Planet. Sci. Lett.* 227, 179–184. <https://doi.org/10.1016/j.epsl.2004.09.006>
- Ljungdhal, L.G., 1986. The autotrophic pathway of acetate synthesis in acetogenic bacteria. *Annu. Rev. Microbiol.* 40, 415–450. <https://doi.org/10.1146/annurev.mi.40.100186.002215>
- Loutet, S.A., Chan, A.C.K., Kobylarz, M.J., Verstraete, M.M., Pfaffen, S., Ye, B., Arrieta, A.L., Murphy, M.E.P., 2015. The fate of intracellular metal ions in microbes, in: Nriagu, J.O., Skaar, E.P. (Eds.), *Trace Metals and Infectious Diseases*. MIT Press, Cambridge (MA).
- Lubitz, W., Ogata, H., Rüdiger, O., Reijerse, E., 2014. Hydrogenases. *Chem. Rev.* 114, 4081–4148. <https://doi.org/10.1021/cr4005814>
- Lubner, C.E., Jennings, D.P., Mulder, D.W., Schut, G.J., Zadvornyy, O.A., Hoben, J.P., Tokmina-Lukaszewska, M., Berry, L., Nguyen, D.M., Lipscomb, G.L., Bothner, B., Jones, A.K., Miller, A.-F., King, P.W., Adams, M.W.W., Peters, J.W., 2017. Mechanistic insights into energy conservation by flavin-based electron bifurcation. *Nat. Chem. Biol.* 13, 655–659. <https://doi.org/10.1038/nchembio.2348>
- Maenaka, Y., Suenobu, T., Fukuzumi, S., 2012. Efficient catalytic interconversion between NADH and NAD⁺ accompanied by generation and consumption of hydrogen with a water-soluble iridium complex at ambient pressure and temperature. *J. Am. Chem. Soc.* 134, 367–374. <https://doi.org/10.1021/ja207785f>

- Martin, W., Baross, J., Kelley, D., Russell, M.J., 2008. Hydrothermal vents and the origin of life. *Nat. Rev. Microbiol.* 6, 805–814. <https://doi.org/10.1038/nrmicro1991>
- Martin, W., Russell, M.J., 2003. On the origins of cells: a hypothesis for the evolutionary transitions from abiotic geochemistry to chemoautotrophic prokaryotes, and from prokaryotes to nucleated cells. *Philos. Trans. R. Soc. Lond. B. Biol. Sci.* 358, 59–85. <https://doi.org/10.1098/rstb.2002.1183>
- Martin, W., Weiss, M., Neukirchen, S., Nelson-Sathi, S., Sousa, F., 2016. Physiology, phylogeny, and LUCA. *Microb. Cell* 3, 582–587. <https://doi.org/10.15698/mic2016.12.545>
- Martin, W.F., 2020. Older than genes: The acetyl CoA pathway and origins. *Front. Microbiol.* 11, 817. <https://doi.org/10.3389/fmicb.2020.00817>
- Martin, W.F., Kleinermanns, K., 2024. The geochemical origin of microbes, 1st ed. CRC Press, Boca Raton. <https://doi.org/10.1201/9781003378617>
- Martínez Giménez, J.A., Tabares Seisdedos, R., 2022. A cofactor-based mechanism for the origin of the genetic code. *Orig. Life Evol. Biospheres* 52, 149–163. <https://doi.org/10.1007/s11084-022-09628-5>
- Maruyama, S., Kurokawa, K., Ebisuzaki, T., Sawaki, Y., Suda, K., Santosh, M., 2019. Nine requirements for the origin of Earth's life: Not at the hydrothermal vent, but in a nuclear geyser system. *Geosci. Front.* 10, 1337–1357. <https://doi.org/10.1016/j.gsf.2018.09.011>
- Matos, J.R., Wong, C.-H., 1987. S-adenosylmethionine: stability and stabilization. *Bioorganic Chem.* 15, 71–80. [https://doi.org/10.1016/0045-2068\(87\)90008-3](https://doi.org/10.1016/0045-2068(87)90008-3)
- Mayer, R.J., Moran, J., 2024. Metal ions turn on a stereoselective nonenzymatic reduction of keto acids by the coenzyme NADH. *Chem* 10, 2564–2576. <https://doi.org/10.1016/j.chempr.2024.05.007>
- McCollom, T.M., Bach, W., 2009. Thermodynamic constraints on hydrogen generation during serpentinization of ultramafic rocks. *Geochim. Cosmochim. Acta* 73, 856–875. <https://doi.org/10.1016/j.gca.2008.10.032>
- McDermott, J.M., Seewald, J.S., German, C.R., Sylva, S.P., 2015. Pathways for abiotic organic synthesis at submarine hydrothermal fields. *Proc. Natl. Acad. Sci.* 112, 7668–7672. <https://doi.org/10.1073/pnas.1506295112>
- Metzler, D.E., Snell, E.E., 1952. Deamination of serine: I. Catalytic deamination of serine and cysteine by pyridoxal and metal salts. *J. Biol. Chem.* 198, 353–361. [https://doi.org/10.1016/S0021-9258\(18\)55589-7](https://doi.org/10.1016/S0021-9258(18)55589-7)
- Miller, S.L., Schlesinger, G., 1993. Prebiotic syntheses of vitamin coenzymes: I. Cysteamine and 2-mercaptoethanesulfonic acid (coenzyme M). *J. Mol. Evol.* 36. <https://doi.org/10.1007/BF00182177>
- Mizuhara, S., Handler, P., 1954. Mechanism of thiamine-catalyzed reactions¹. *J. Am. Chem. Soc.* 76, 571–573. <https://doi.org/10.1021/ja01631a071>
- Moody, E.R.R., Álvarez-Carretero, S., Mahendrarajah, T.A., Clark, J.W., Betts, H.C., Dombrowski, N., Szánthó, L.L., Boyle, R.A., Daines, S., Chen, X., Lane, N., Yang, Z., Shields, G.A., Szöllősi, G.J., Spang, A., Pisani, D., Williams, T.A., Lenton, T.M., Donoghue, P.C.J., 2024. The nature of the last universal common ancestor and its impact on the early Earth system. *Nat. Ecol. Evol.* <https://doi.org/10.1038/s41559-024-02461-1>
- Mrnjavac, N., Wimmer, J.L.E., Brabender, M., Schwander, L., Martin, W.F., 2023. The Moon-forming impact and the autotrophic origin of life. *ChemPlusChem* 88, e202300270. <https://doi.org/10.1002/cplu.202300270>

- Nghe, P., Hordijk, W., Kauffman, S.A., Walker, S.I., Schmidt, F.J., Kemble, H., Yeates, J.A.M., Lehman, N., 2015. Prebiotic network evolution: six key parameters. *Mol. Biosyst.* 11, 3206–3217. <https://doi.org/10.1039/C5MB00593K>
- Nitschke, W., Russell, M.J., 2012. Redox bifurcations: Mechanisms and importance to life now, and at its origin: A widespread means of energy conversion in biology unfolds.... *BioEssays* 34, 106–109. <https://doi.org/10.1002/bies.201100134>
- Noffke, A.L., Habtemariam, A., Pizarro, A.M., Sadler, P.J., 2012. Designing organometallic compounds for catalysis and therapy. *Chem. Commun.* 48, 5219. <https://doi.org/10.1039/c2cc30678f>
- Nogal, N., Luis-Barrera, J., Vela-Gallego, S., Aguilar-Galindo, F., De La Escosura, A., 2024. NADH-mediated primordial synthesis of amino acids. *Org. Chem. Front.* 11, 1924–1932. <https://doi.org/10.1039/D4QO00050A>
- Oey, I., Thuy, N., Hendrickx, M., 2003. Pressure and temperature stability of folates: a kinetic study. 12th World Food Congr.
- Oparin, A., 1938. The origin of life. N. Y. Dover Publ. Inc.
- Orgel, L. E., 1968. Evolution of the genetic apparatus. *J. Mol. Biol.* 38, 381–393. [https://doi.org/10.1016/0022-2836\(68\)90393-8](https://doi.org/10.1016/0022-2836(68)90393-8)
- Page, C.C., Moser, C.C., Chen, X., Dutton, P.L., 1999. Natural engineering principles of electron tunnelling in biological oxidation-reduction. *Nature* 402, 47–52. <https://doi.org/10.1038/46972>
- Pearce, B.K.D., Pudritz, R.E., Semenov, D.A., Henning, T.K., 2017. Origin of the RNA world: The fate of nucleobases in warm little ponds. *Proc. Natl. Acad. Sci.* 114, 11327–11332. <https://doi.org/10.1073/pnas.1710339114>
- Penny, D., Poole, A., 1999. The nature of the last universal common ancestor. *Curr. Opin. Genet. Dev.* 9, 672–677. [https://doi.org/10.1016/S0959-437X\(99\)00020-9](https://doi.org/10.1016/S0959-437X(99)00020-9)
- Preiner, M., Igarashi, K., Muchowska, K.B., Yu, M., Varma, S.J., Kleinermanns, K., Nobu, M.K., Kamagata, Y., Tüysüz, H., Moran, J., Martin, W.F., 2020. A hydrogen-dependent geochemical analogue of primordial carbon and energy metabolism. *Nat. Ecol. Evol.* 4, 534–542. <https://doi.org/10.1038/s41559-020-1125-6>
- Preiner, M., Xavier, J.C., Sousa, F.L., Zimorski, V., Neubeck, A., Lang, S.Q., Greenwell, H.C., Kleinermanns, K., Tüysüz, H., McCollom, T.M., Holm, N.G., Martin, W.F., 2018. Serpentinization: Connecting geochemistry, ancient metabolism and industrial hydrogenation. *Life* 8, 41. <https://doi.org/10.3390/life8040041>
- Proskurowski, G., Lilley, M.D., Seewald, J.S., Früh-Green, G.L., Olson, E.J., Lupton, J.E., Sylva, S.P., Kelley, D.S., 2008. Abiogenic hydrocarbon production at Lost City hydrothermal field. *Science* 319, 604–607. <https://doi.org/10.1126/science.1151194>
- Ragsdale, S.W., Kumar, M., 1996. Nickel-containing carbon monoxide dehydrogenase/acetyl-CoA synthase. *Chem. Rev.* 96, 2515–2540. <https://doi.org/10.1021/cr950058+>
- Ragsdale, S.W., Pierce, E., 2008. Acetogenesis and the Wood–Ljungdahl pathway of CO₂ fixation. *Biochim. Biophys. Acta BBA - Proteins Proteomics* 1784, 1873–1898. <https://doi.org/10.1016/j.bbapap.2008.08.012>
- Rona, P.A., Klinkhammer, G., Nelsen, T.A., Trefry, John.H., Elderfield, H., 1986. Black smokers, massive sulphides and vent biota at the Mid-Atlantic Ridge. *Nature* 321, 33–37. <https://doi.org/10.1038/321033a0>

- Russell, M.J., Martin, W., 2004. The rocky roots of the acetyl-CoA pathway. *Trends Biochem. Sci.* 29, 358–363. <https://doi.org/10.1016/j.tibs.2004.05.007>
- Saito, M.A., Sigman, D.M., Morel, F.M.M., 2003. The bioinorganic chemistry of the ancient ocean: the co-evolution of cyanobacterial metal requirements and biogeochemical cycles at the Archean–Proterozoic boundary? *Inorganica Chim. Acta* 356, 308–318. [https://doi.org/10.1016/S0020-1693\(03\)00442-0](https://doi.org/10.1016/S0020-1693(03)00442-0)
- Sanchez-Rocha, A.C., Makarov, M., Pravda, L., Novotný, M., Hlouchová, K., 2024. Coenzyme-protein interactions since early life. *eLife*. <https://doi.org/10.7554/elife.94174.1>
- Schwander, L., Brabender, M., Mrnjavac, N., Wimmer, J.L.E., Preiner, M., Martin, W.F., 2023. Serpentinization as the source of energy, electrons, organics, catalysts, nutrients and pH gradients for the origin of LUCA and life. *Front. Microbiol.* 14, 1257597. <https://doi.org/10.3389/fmicb.2023.1257597>
- Schwarz, G., Mendel, R.R., 2006. Molybdenum cofactor biosynthesis and molybdenum enzymes. *Annu. Rev. Plant Biol.* 57, 623–647. <https://doi.org/10.1146/annurev.arplant.57.032905.105437>
- Sebastianelli, L., Kaur, H., Chen, Z., Krishnamurthy, R., Mansy, S.S., 2024. A magnesium binding site and the anomeric effect regulate the abiotic redox chemistry of nicotinamide nucleotides. *Chem. – Eur. J.* 30, e202400411. <https://doi.org/10.1002/chem.202400411>
- Seyfried, W.E., Pester, N.J., Tutolo, B.M., Ding, K., 2015. The Lost City hydrothermal system: Constraints imposed by vent fluid chemistry and reaction path models on seafloor heat and mass transfer processes. *Geochim. Cosmochim. Acta* 163, 59–79. <https://doi.org/10.1016/j.gca.2015.04.040>
- Shima, S., Huang, G., Wagner, T., Ermler, U., 2020. Structural basis of hydrogenotrophic methanogenesis. *Annu. Rev. Microbiol.* 74, 713–733. <https://doi.org/10.1146/annurev-micro-011720-122807>
- Shima, S., Warkentin, E., Thauer, R.K., Ermler, U., 2002. Structure and function of enzymes involved in the methanogenic pathway utilizing carbon dioxide and molecular hydrogen. *J. Biosci. Bioeng.* 93, 519–530. [https://doi.org/10.1016/S1389-1723\(02\)80232-8](https://doi.org/10.1016/S1389-1723(02)80232-8)
- Shin, J., Song, Y., Jeong, Y., Cho, B.-K., 2016. Analysis of the core genome and pan-genome of autotrophic acetogenic bacteria. *Front. Microbiol.* 7. <https://doi.org/10.3389/fmicb.2016.01531>
- Sleep, N.H., Bird, D.K., Pope, E.C., 2011. Serpentinite and the dawn of life. *Philos. Trans. R. Soc. B Biol. Sci.* 366, 2857–2869. <https://doi.org/10.1098/rstb.2011.0129>
- Sleep, N.H., Meibom, A., Fridriksson, Th., Coleman, R.G., Bird, D.K., 2004. H₂-rich fluids from serpentinization: Geochemical and biotic implications. *Proc. Natl. Acad. Sci.* 101, 12818–12823. <https://doi.org/10.1073/pnas.0405289101>
- Song, Y., Beyazay, T., Tüysüz, H., 2024. Effect of alkali- and alkaline-earth-metal promoters on silica-supported Co–Fe alloy for autocatalytic CO₂ fixation. *Angew. Chem. Int. Ed.* 63, e202316110. <https://doi.org/10.1002/anie.202316110>
- Sousa, F.L., Martin, W.F., 2014. Biochemical fossils of the ancient transition from geoenergetics to bioenergetics in prokaryotic one carbon compound metabolism. *Biochim. Biophys. Acta BBA - Bioenerg.* 1837, 964–981. <https://doi.org/10.1016/j.bbabi.2014.02.001>

- Sousa, F.L., Preiner, M., Martin, W.F., 2018. Native metals, electron bifurcation, and CO₂ reduction in early biochemical evolution. *Curr. Opin. Microbiol.* 43, 77–83. <https://doi.org/10.1016/j.mib.2017.12.010>
- Steele, A., Benning, L.G., Wirth, R., Schreiber, A., Araki, T., McCubbin, F.M., Fries, M.D., Nittler, L.R., Wang, J., Hallis, L.J., Conrad, P.G., Conley, C., Vitale, S., O'Brien, A.C., Riggi, V., Rogers, K., 2022. Organic synthesis associated with serpentinization and carbonation on early Mars. *Science* 375, 172–177. <https://doi.org/10.1126/science.abg7905>
- Suda, K., Gilbert, A., Yamada, K., Yoshida, N., Ueno, Y., 2017. Compound- and position-specific carbon isotopic signatures of abiogenic hydrocarbons from on-land serpentinite-hosted Hakuba Happo hot spring in Japan. *Geochim. Cosmochim. Acta* 206, 201–215. <https://doi.org/10.1016/j.gca.2017.03.008>
- Tagawa, K., Arnon, D.I., 1962. Ferredoxins as electron carriers in photosynthesis and in the biological production and consumption of hydrogen gas. *Nature* 195, 537–543. <https://doi.org/10.1038/195537a0>
- Tashiro, T., Ishida, A., Hori, M., Igisu, M., Koike, M., Méjean, P., Takahata, N., Sano, Y., Komiya, T., 2017. Early trace of life from 3.95 Ga sedimentary rocks in Labrador, Canada. *Nature* 549, 516–518. <https://doi.org/10.1038/nature24019>
- Thauer, R.K., 2011. Hydrogenases and the global H₂ cycle. *Eur. J. Inorg. Chem.* 2011, 919–921. <https://doi.org/10.1002/ejic.201001255>
- Tremmel, P., Griesser, H., Steiner, U.E., Richert, C., 2019. How small heterocycles make a reaction network of amino acids and nucleotides efficient in water. *Angew. Chem. Int. Ed.* 58, 13087–13092. <https://doi.org/10.1002/anie.201905427>
- Tyagi, A., Penzkofer, A., Batschauer, A., Wolf, E., 2009. Thermal degradation of (6R,S)-5,10-methenyltetrahydrofolate in aqueous solution at pH 8. *Chem. Phys.* 358, 132–136. <https://doi.org/10.1016/j.chemphys.2009.01.005>
- Ueda, H., Shibuya, T., 2021. Composition of the primordial ocean just after its formation: constraints from the reactions between the primitive crust and a strongly acidic, CO₂-rich fluid at elevated temperatures and pressures. *Minerals* 11, 389. <https://doi.org/10.3390/min11040389>
- Valdez, C.E., Smith, Q.A., Nechay, M.R., Alexandrova, A.N., 2014. Mysteries of metals in metalloenzymes. *Acc. Chem. Res.* 47, 3110–3117. <https://doi.org/10.1021/ar500227u>
- Vance, S.D., Melwani Daswani, M., 2020. Serpentinite and the search for life beyond Earth. *Philos. Trans. R. Soc. Math. Phys. Eng. Sci.* 378, 20180421. <https://doi.org/10.1098/rsta.2018.0421>
- Wächtershäuser, G., 1992. Groundworks for an evolutionary biochemistry: The iron-sulphur world. *Prog. Biophys. Mol. Biol.* 58, 85–201. [https://doi.org/10.1016/0079-6107\(92\)90022-X](https://doi.org/10.1016/0079-6107(92)90022-X)
- Wagner, G.R., Payne, R.M., 2013. Widespread and enzyme-independent N ϵ -acetylation and N ϵ -succinylation of proteins in the chemical conditions of the mitochondrial matrix*. *J. Biol. Chem.* 288, 29036–29045. <https://doi.org/10.1074/jbc.M113.486753>
- Wang, Z., Wang, L., Cui, Y., Xing, Y., Su, W., 2022. Research on nickel-based catalysts for carbon dioxide methanation combined with literature measurement. *J. CO₂ Util.* 63, 102117. <https://doi.org/10.1016/j.jcou.2022.102117>
- Warburg, O.H., Christian, W., 1936. Pyridin, der wasserstoffübertragende Bestandteil von Gärungsfermenten. *Helv. Chim. Acta* 19, 79–88.

- Weber, J.M., Henderson, B.L., LaRowe, D.E., Goldman, A.D., Perl, S.M., Billings, K., Barge, L.M., 2022. Testing abiotic reduction of NAD⁺ directly mediated by iron/sulfur minerals. *Astrobiology* 22, 25–34. <https://doi.org/10.1089/ast.2021.0035>
- Weiss, M.C., Sousa, F.L., Mrnjavac, N., Neukirchen, S., Roettger, M., Nelson-Sathi, S., Martin, W.F., 2016. The physiology and habitat of the last universal common ancestor. *Nat. Microbiol.* 1, 16116. <https://doi.org/10.1038/nmicrobiol.2016.116>
- White, H.B., 1976. Coenzymes as fossils of an earlier metabolic state. *J. Mol. Evol.* 7, 101–104. <https://doi.org/10.1007/BF01732468>
- White, L.M., Bhartia, R., Stucky, G.D., Kanik, I., Russell, M.J., 2015. Mackinawite and greigite in ancient alkaline hydrothermal chimneys: Identifying potential key catalysts for emergent life. *Earth Planet. Sci. Lett.* 430, 105–114. <https://doi.org/10.1016/j.epsl.2015.08.013>
- Williams, R.J.P., Fraústo da Silva, J.J.R., 1997. The natural selection of the chemical elements: the environment and life's chemistry, 1. publ. in paperback. ed. Clarendon Press, Oxford.
- Wimmer, J.L.E., Xavier, J.C., Vieira, A.D.N., Pereira, D.P.H., Leidner, J., Sousa, F.L., Kleinermanns, K., Preiner, M., Martin, W.F., 2021. Energy at origins: favorable thermodynamics of biosynthetic reactions in the last universal common ancestor (LUCA). *Front. Microbiol.* 12, 793664. <https://doi.org/10.3389/fmicb.2021.793664>
- Woese, C.R., 1965. On the evolution of the genetic code. *Proc. Natl. Acad. Sci.* 54, 1546–1552. <https://doi.org/10.1073/pnas.54.6.1546>
- Woese, C.R., Fox, G.E., 1977. Phylogenetic structure of the prokaryotic domain: The primary kingdoms. *Proc. Natl. Acad. Sci.* 74, 5088–5090. <https://doi.org/10.1073/pnas.74.11.5088>
- Wood, H.G., Ragsdale, S.W., Pezacka, E., 1986. The acetyl-CoA pathway: a newly discovered pathway of autotrophic growth. *Trends Biochem. Sci.* 11, 14–18. [https://doi.org/10.1016/0968-0004\(86\)90223-9](https://doi.org/10.1016/0968-0004(86)90223-9)
- Wu, H., Tian, C., Song, X., Liu, C., Yang, D., Jiang, Z., 2013. Methods for the regeneration of nicotinamide coenzymes. *Green Chem.* 15, 1773. <https://doi.org/10.1039/c3gc37129h>
- Xavier, J.C., Hordijk, W., Kauffman, S., Steel, M., Martin, W.F., 2020. Autocatalytic chemical networks at the origin of metabolism. *Proc. R. Soc. B Biol. Sci.* 287, 20192377. <https://doi.org/10.1098/rspb.2019.2377>
- Zabinski, R.F., Toney, M.D., 2001. Metal ion inhibition of nonenzymatic pyridoxal phosphate catalyzed decarboxylation and transamination. *J. Am. Chem. Soc.* 123, 193–198. <https://doi.org/10.1021/ja0026354>
- Zeichner, S.S., Aponte, J.C., Bhattacharjee, S., Dong, G., Hofmann, A.E., Dworkin, J.P., Glavin, D.P., Elsila, J.E., Graham, H.V., Naraoka, H., Takano, Y., Tachibana, S., Karp, A.T., Grice, K., Holman, A.I., Freeman, K.H., Yurimoto, H., Nakamura, T., Noguchi, T., Okazaki, R., Yabuta, H., Sakamoto, K., Yada, T., Nishimura, M., Nakato, A., Miyazaki, A., Yogata, K., Abe, M., Okada, T., Usui, T., Yoshikawa, M., Saiki, T., Tanaka, Satoshi, Terui, F., Nakazawa, S., Watanabe, S., Tsuda, Y., Hamase, K., Fukushima, K., Aoki, D., Hashiguchi, M., Mita, H., Chikaraishi, Y., Ohkouchi, N., Ogawa, N.O., Sakai, S., Parker, E.T., McLain, H.L., Orthous-Daunay, F.-R., Vuitton, V., Wolters, C., Schmitt-Kopplin, P., Hertkorn, N., Thissen, R., Ruf, A., Isa, J., Oba, Y., Koga, T., Yoshimura, T., Araoka, D., Sugahara, H., Furusho, A., Furukawa, Y., Aoki, J., Kano, K., Nomura, S.M., Sasaki, K., Sato, H., Yoshikawa, T., Tanaka, Satoru, Morita, M.,

- Onose, M., Kabashima, F., Fujishima, K., Yamazaki, T., Kimura, Y., Eiler, J.M., 2023. Polycyclic aromatic hydrocarbons in samples of Ryugu formed in the interstellar medium. *Science* 382, 1411–1416. <https://doi.org/10.1126/science.adg6304>
- Zeng, X., Alain, K., Shao, Z., 2021. Microorganisms from deep-sea hydrothermal vents. *Mar. Life Sci. Technol.* 3, 204–230. <https://doi.org/10.1007/s42995-020-00086-4>